AD-A250 808

FINITE ELEMENT ANALYSIS OF LAMINATED COMPOSITE AXISYMMETRIC SOLIDS

VOL. I: THEORY AND APPLICATIONS

R.S. Sandhu, W.E. Wolfe, and R.A. Dandan
Department of Civil Engineering
The Ohio State University

DTIC
ELECTE
MAY 29 1992
S D

August 1991

Final Report for Period October 1987 - August 1988

92-14039

92 5 28 004

NOTICE

When Government drawings, specifications, or other data are used for any purpose other than in connection with a definitely Government-related procurement, the United States Government incurs no responsibility or any obligation whatsoever. The fact that the Government may have formulated or in any way supplied the said drawings, specifications, or other data, is not to be regarded by implication, or otherwise in any manner construed, as licensing the holder, or any other person or corporation; or as conveying any rights or permission to manufacture, use, or sell any patented invention that may in any way be related thereto.
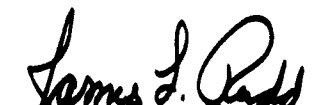
This report is releasable to the National Technical Information Service (NTIS). At NTIS, it will be available to the general public, including foreign nations.

This technical report has been reviewed and is approved for publication.

GEORGE P. SENDECKYJ, Project Engineer
Fatigue, Fracture and Reliability Group
Structural Integrity Branch

JOHN K. RYDER, Capt, USAF
Technical Manager
Fatigue, Fracture and Reliability Group
Structural Integrity Branch

FOR THE COMMANDER

JAMES L. RUDD, Chief
Structural Integrity Branch
Structures Division

If your address has changed, if you wish to be removed from our mailing list, or if the addressee is no longer employed by your organization, please notify WL/FIBEC, WPAFB, OH 45433-6553 to help us maintain a current mailing list.

Copies of this report should not be returned unless return is required by security considerations, contractual obligations, or notice on a specific document.

REPORT DOCUMENTATION PAGE

Form Approved
OMB No. 0704-0188

1a. REPORT SECURITY CLASSIFICATION	1b. RESTRICTIVE MARKINGS
Unclassified	None

2a. SECURITY CLASSIFICATION AUTHORITY	3. DISTRIBUTION/AVAILABILITY OF REPORT
	Approved for public release; distribution unlimited.
2b. DECLASSIFICATION/DOWNGRADING SCHEDULE	

4. PERFORMING ORGANIZATION REPORT NUMBER(S)	5. MONITORING ORGANIZATION REPORT NUMBER(S)
RF Project No. 764779/717297	WL-TR-91-3020, Vol. I

6a. NAME OF PERFORMING ORGANIZATION	6b. OFFICE SYMBOL (If applicable)	7a. NAME OF MONITORING ORGANIZATION
The Ohio State University Research Foundation	OSURF	Flight Dynamics Directorate (WL/FIBEC) Wright Laboratory

6c. ADDRESS (City, State, and ZIP Code)	7b. ADDRESS (City, State, and ZIP Code)
1960 Kenny Rd. Columbus, Ohio 43210-1063	Wright-Patterson Air Force Base Dayton, Ohio 45433-6553

8a. NAME OF FUNDING/SPONSORING ORGANIZATION	8b. OFFICE SYMBOL (If applicable)	9. PROCUREMENT INSTRUMENT IDENTIFICATION NUMBER
Flight Dynamics Directorate	WL/FIBEC	Contract No. F33615-85-C-3213

8c. ADDRESS (City, State, and ZIP Code)	10. SOURCE OF FUNDING NUMBERS			
	PROGRAM ELEMENT NO.	PROJECT NO.	TASK NO.	WORK UNIT ACCESSION NO.
Wright-Patterson Air Force Base Dayton, Ohio 45433-6553	61102F	2302	N1	02

11. TITLE (Include Security Classification)
Finite Element Analysis of Laminated Composite Axisymmetric Solids
Vol. I: Theory and Applications

12. PERSONAL AUTHOR(S)
R.S. Sandhu, W.E. Wolfe, and R.A. Dandan

13a. TYPE OF REPORT	13b. TIME COVERED	14. DATE OF REPORT (Year, Month, Day)	15. PAGE COUNT
Final	FROM 10/01/87 TO 8/30/88	1991, August	169

16. SUPPLEMENTARY NOTATION WL-TR-91-3020, Vol.II contains computer software. Distribution is limited to DOD. Non-DOD requests must be referred to WL/FIBEC and must include a Statement of Terms and Conditions--Release of AF-owned or developed computer software packages.

17.	COSATI CODES		18. SUBJECT TERMS (Continue on reverse if necessary and identify by block number)	
FIELD	GROUP	SUB-GROUP	Composite Laminated	Finite Element Method
			Delamination	Stress Analysis

19. ABSTRACT (Continue on reverse if necessary and identify by block number)

A finite element program is developed to analyze a composite laminate structure of axisymmetric geometry and loading. Circumferential displacement is considered in addition to the radial and axial. The fiber orientation may be oblique to the axis. Thus, each nodal point has three degrees of freedom and the procedure models the complete state of stress and strain.

The program is verified by application to cross-ply and angle-ply coupons. A segment of a large radius axisymmetric ring under uniform radial pressure is equivalent to a free-edge delamination coupon. The stress field from the axisymmetric analysis is compared with the results of a higher order finite element analysis of a free-edge delamination coupon. Additionally, the computer program has the capability to solve a variety of problems including tubular angle-ply specimens, nozzles, etc.

20. DISTRIBUTION/AVAILABILITY OF ABSTRACT	21. ABSTRACT SECURITY CLASSIFICATION
☒ UNCLASSIFIED/UNLIMITED ☐ SAME AS RPT ☐ DTIC USERS	Unclassified

22a. NAME OF RESPONSIBLE INDIVIDUAL	22b. TELEPHONE (Include Area Code)	22c. OFFICE SYMBOL
Dr. George Sendeckyj	513-255-6104	WL/FIBEC

FOREWORD

The research reported herein was supported by the Air Force System Command/ASD under Grant No.F33615-85-C-3213 to the Ohio State University. Dr. George P.Sendeckyj of Wright Laboratory, Flight Dynamics Directorate was the Program manager. The report covers part of the work done from July 1, 1987 to July 31, 1988. At the Ohio State University, the research was carried out under the supervision of the Principal Investigators Professors Ranbir S. Sandhu and William E. Wolfe, by Miss R.A. Dandan, Graduate Research Associate. This work includes and extends her research for the degree of Master of Science at the Ohio State University. The report is in two volumes. The first volume contains 'Theory and Applications' and the second describes the computer program and its usage.

iii

Accession For		
NTIS GRA&I	☑	
DTIC TAB	☐	
Unannounced	☐	
Justification		
By		
Distribution/		
Availability Codes		
Dist	Avail and/or Special	
A-1		

TABLE OF CONTENTS

LIST OF FIGURES

SECTION I

INTRODUCTION

Owing to the development and ever greater use of advanced composite materials, aerospace structures now evidence the most rapid evolution since the introduction of all metal aircraft. High strength and stiffness characterize composites. Such efficiency derives from the intrinsic strength of the constituent materials in composites. However, because of the greater complexity of their composition, composites demand much more complex structural evaluation than metals, and a need to have accurate stress analysis for design purpose is apparent.

Delamination is a critical failure mechanism for laminated composite materials. However, before delamination can be predicted, it is essential to develop analyses to accurately estimate the interlaminar stresses that cause delamination.

Over the past 2 decades considerable effort has been devoted to finite element stress analysis of structures made of composite materials. A two-dimensional analysis using

1

plane stress or plane strain assumptions have been used [1-5] to study the interlaminar shear strains at free edge. Three-dimensional finite element models have also been developed [6,7]. For the analysis of geometrically axisymmetric composite structures, a pseudo-three-dimensional analysis including three axisymmetric displacement degrees of freedom per node has been developed [8-10]. In this approach, the complete state of stress and strain is modeled.

Recently, Chang [11] developed a more sophisticated finite element model based on continuous displacement as well as continuous traction. This model can accurately predict the complete stress field of the free edge stress problem in composite laminate coupons. However, it is quite expensive in computational effort.

The Flight Dynamics Directorate had developed a model in which the laminated coupon subjected to uniform axial strain in longitudinal direction was visualized as a segment of a large radius axisymmetric ring under uniform radial pressure. The objective of the present research was to carefully document this work, improve the logic of the computer code to make it more efficient, and to extend its applicability to nonlinear material behavior.

A finite element computer program was developed for analysis of stresses and displacements in axisymmetric structures made of laminated composites. Fiber orientations at an angle with the axis were allowed. Three degrees of freedom for each nodal point permit modeling of the complete state of stress and strain. The model was validated by solving representative problems of cross-ply and angle-ply laminated coupons and comparing results with those obtained using the continuous traction element Q23 developed by Chang [11]. Section II contains the statement of the axisymmetric problem for linearly elastic composite materials. In Section III, the discretization by the finite element method is presented. Section IV contains application of the computer program developed and comparison of results with those obtained using Q23 finite element method. The procedure was developed specially for application to free-edge delamination coupons. However, it has the capability to model a variety of structures including laminated tubes, nozzles, etc. In the effort described in this report, the material was assumed to be linear elastic. Extension of the procedure to allow for nonlinear material behavior is currently in hand and will be the subject of another report.

SECTION II

ELASTIC AXISYMMETRICAL PROBLEM

FOR CONTINUOUS FIBER COMPOSITE MATERIALS

The equilibruim equations, strain displacement relations and constitutive relations for axisymmetric composite materials problem are listed in this section. Derivation of the stress-strain matrix in material, local and global coordinates is described.

2.1 EQUILIBRIUM EQUATIONS

The global coordinate system for axisymmetric analysis is a cylindrical system where r is the radial direction, T is the circumferential direction, Z is the axial direction and the corresponding displacement are u, v, w. The equilibrium equations in cylindrical coordinates are [24]:

$$\partial\sigma_r/\partial r + (1/r)\partial\sigma_{rT}/\partial T + \partial\sigma_{rz}/\partial z + (\sigma_r - \sigma_T)/r = -f_r$$

$$\partial\sigma_{rz}/\partial r + (1/r)\partial\sigma_{Tz}/\partial T + \partial\sigma_z/\partial z + \sigma_{rz}/r = -f_z$$

$$\partial\sigma_{rT}/\partial r + (1/r)\partial\sigma_T/\partial T + \partial\sigma_{Tz}/\partial z + 2\sigma_{rT}/r = -f_T$$

$$(2.1)$$

where f_r, f_z, f_T are components of body forces in r, z, T

4

directions respectively. For axisymmetric problems the stresses are independent of the tangential coordinate T. Therefore, the equilibrium equations reduce to:

$$\partial\sigma_r/\partial r \quad + \partial\sigma_{rz}/\partial z + (\sigma_r - \sigma_T)/r = -f_r$$

$$\partial\sigma_{rz}/\partial r \quad + \partial\sigma_z/\partial z + \quad \sigma_{rz}/r \qquad = -f_z \qquad\qquad (2.2)$$

$$\partial\sigma_{rT}/\partial r \quad + \partial\sigma_{Tz}/\partial z + 2\,\sigma_{rT}/r \quad = -f_T$$

2.2 STRAIN-DISPLACEMENT RELATIONS

The general strain-displacement relations in cylindrical coordinates are given by [24]:

$$e_r = \partial u/\partial r \qquad\qquad e_T = u/r + (1/r)(\partial v/\partial T)$$

$$e_z = \partial w/\partial z$$

$$2e_{rT} = (1/r)(\partial u/\partial T) + (\partial v/\partial r) - v/r \qquad\qquad (2.3)$$

$$2e_{rz} = \partial u/\partial z + \partial w/\partial r$$

$$2e_{zT} = \partial v/\partial z + (1/r)(\partial w/\partial T)$$

For axisymmetric analysis, the three components of displacement are all independent of T. Thus, the relationships given by (2.3) reduce to:

$$e_r = \partial u/\partial r \qquad , \qquad e_T = u/r$$

$$e_z = \partial w/\partial z \qquad , \qquad 2e_{rz} = \partial u/\partial z + \partial w/\partial r \qquad (2.4)$$

$$2e_{zT} = \partial v/\partial z \qquad , \qquad 2e_{rT} = \partial v/\partial r - v/r$$

5

2.3 STRESS-STRAIN RELATIONS FOR ORTHOTROPIC COMPOSITE MATERIALS

Composite structures made of oriented continuous fibers are usually constructed so that the high-strength, high-stiffness fibers are embedded in a weaker matrix material. Though the material is heterogeneous, it is often characterized as an equivalent homogeneous material for use in analysis [10], [12]. In the present analysis the material is assumed to be linear, homogeneous and orthotropic. Because of the material axis not being parallel to the global reference frame (Figure(1)), the stress-strain relations may appear to be anisotropic when written with reference to the global axes.

2.3.1 Stress-Strain Relationship in Material Coordinates

In the plane of fibers the material is orthotropic, and, therefore, in three-dimensional configuration, there are nine independent elastic constants. Let (1,2,3) be the material directions. Using 'reduced' vector representation for the symmetric stress and strain tensors, the stress-strain relationship can be written in matrix form as [12]:

$$\{\sigma\}_m = [C]_m \{\epsilon\}_m$$

Explicitly:
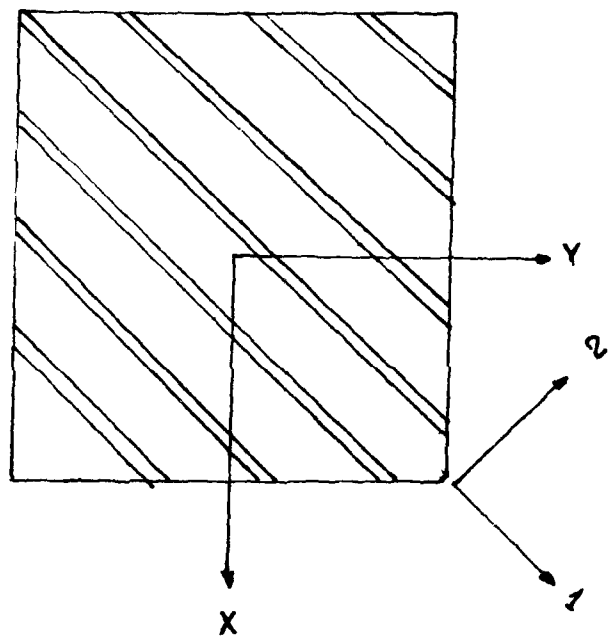
Figure 1: Oriented Fiber Composite Layer in the
          X-Y Coordinate Plane

$$
\begin{bmatrix} \sigma_{11} \\ \sigma_{22} \\ \sigma_{33} \\ \sigma_{32} \\ \sigma_{31} \\ \sigma_{12} \end{bmatrix} =
\begin{bmatrix}
C_{11} & C_{12} & C_{13} & 0 & 0 & 0 \\
C_{12} & C_{22} & C_{23} & 0 & 0 & 0 \\
C_{13} & C_{23} & C_{33} & 0 & 0 & 0 \\
0 & 0 & 0 & C_{44} & 0 & 0 \\
0 & 0 & 0 & 0 & C_{55} & 0 \\
0 & 0 & 0 & 0 & 0 & C_{66}
\end{bmatrix}
\begin{bmatrix} e_{11} \\ e_{22} \\ e_{33} \\ 2e_{32} \\ 2e_{31} \\ 2e_{12} \end{bmatrix}
$$

(2.5)

Where:

$C_{11} = E_{11}(1 - \mu_{23}\mu_{32})/D$

$C_{22} = E_{22}(1 - \mu_{31}\mu_{13})/D$

$C_{33} = E_{33}(1 - \mu_{12}\mu_{21})/D$

$C_{44} = G_{23} \qquad C_{55} = G_{13} \qquad C_{66} = G_{12}$ (2.6)

$C_{12} = (\mu_{21} + \mu_{31}\mu_{23})E_{11}/D = (\mu_{12} + \mu_{13}\mu_{32})E_{22}/D$

$C_{13} = (\mu_{31} + \mu_{21}\mu_{32})E_{11}/D = (\mu_{13} + \mu_{12}\mu_{23})E_{33}/D$

$C_{23} = (\mu_{32} + \mu_{12}\mu_{31})E_{22}/D = (\mu_{23} + \mu_{21}\mu_{13})E_{33}/D$

$D = 1 - \mu_{12}\mu_{21} - \mu_{23}\mu_{32} - \mu_{31}\mu_{13} - 2\mu_{21}\mu_{32}\mu_{13}$

and E_{ii} = Modulus of elasticity in the i direction i=1,2,3

G_{ij} = Shear modulus in the i-j plane, i,j=1,2,3

μ_{ij} = Poisson's ratio in the i-j plane i,j=1,2,3

2.3.2 Stress-Strain Relationship in Local Coordinates

In order to combine the standard behavior of various laminae to get the properties of the angle-ply laminate, it is necessay to rewrite the constitutive relations in a uniform system of coordinates. To do this one has to establish the relationships between stresses and strains in the material coordinate system with corresponding quantities in the local coordinate system.

The analysis presented herein is for an angle of rotation α of the fiber direction (1) as measured from the Z (axial) direction. Thus if β is the fiber orientation measured from the tangential direction, $\alpha = \beta - 90$. (Figure (2)). Let:

$$
\begin{bmatrix} \sigma_1 \\ \sigma_2 \\ \sigma_3 \\ \sigma_{32} \\ \sigma_{31} \\ \sigma_{12} \end{bmatrix} = [J] \begin{bmatrix} \sigma_z \\ \sigma_T \\ \sigma_{rz} \\ \sigma_{rT} \\ \sigma_{rz} \\ \sigma_{zT} \end{bmatrix} \quad ; \quad \begin{bmatrix} e_1 \\ e_2 \\ e_3 \\ 2e_{32} \\ 2e_{31} \\ 2e_{12} \end{bmatrix} = [T] \begin{bmatrix} e_z \\ e_T \\ e_r \\ 2e_{rT} \\ 2e_{rz} \\ 2e_{zT} \end{bmatrix} \quad (2.7)
$$
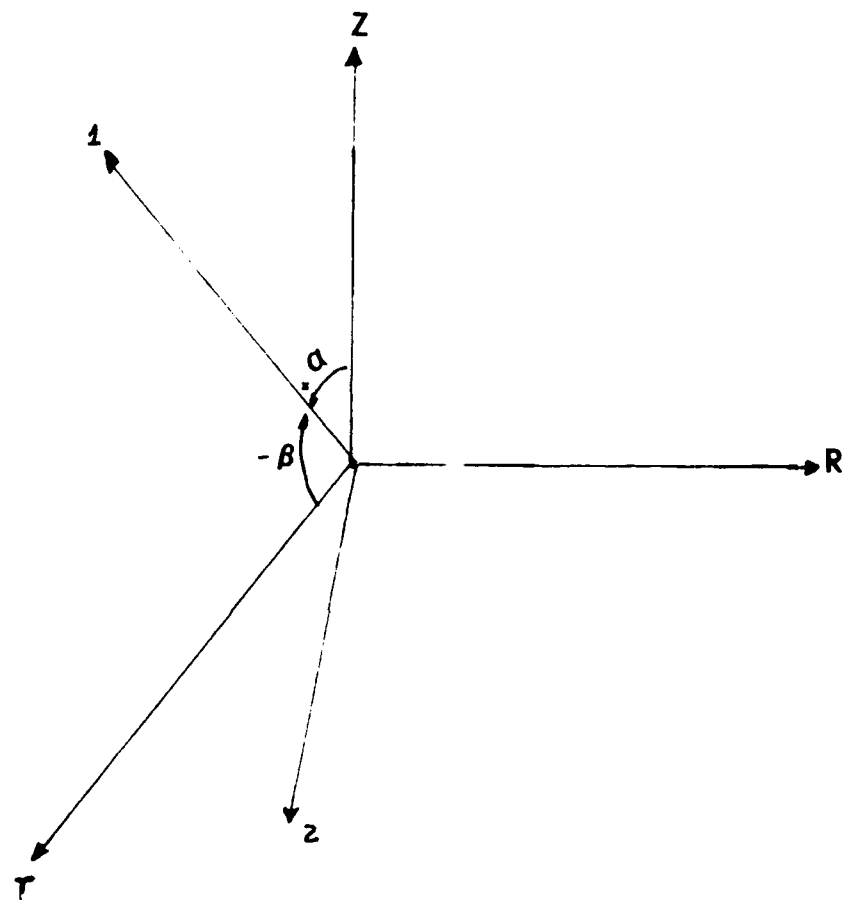
Figure 2: Local (R, T, Z) and Material

(1, 2, 3) Coordinates

or symbolically

$$\{\sigma\}_m = [J] \{\sigma\}_L \quad ; \quad \{\varepsilon\}_m = [T] \{\varepsilon\}_L$$

where [T], [J] are, respectively, the strain and the stress transformation matrix due to a rotation of the axis through an angle α and subscripts m and L refer to material and local coordinate systems respectively. Further, since strain energy is invariant due to rotation of axis we have:

$$[J]^{-1} = [T]^T$$

Let $\{t\}$ be the traction vector, and $\{n\}$ the normal at a certain point in the material , then by Cauchy's stress principle, $\{t\} = [\sigma] \{n\}$, where $[\sigma]$ is the stress matrix:

$$[\sigma] = \begin{bmatrix} \sigma_{11} & \sigma_{12} & \sigma_{13} \\ \sigma_{12} & \sigma_{22} & \sigma_{23} \\ \sigma_{31} & \sigma_{32} & \sigma_{33} \end{bmatrix} \tag{2.8}$$

Due to a rotation of axis about r, the new traction and normal vector are given as:

$$\{t\}_m = [L] \{t\}_L \qquad \{n\}_m = [L] \{n\}_L \tag{2.9}$$

Where [L] is the transformation matrix due to a rotation of

11

axis Z, T about r by an angle α. Explicitly:

$$[L] = \begin{bmatrix} m & n & 0 \\ -n & m & 0 \\ 0 & 0 & 1 \end{bmatrix} \qquad (2.10)$$

in which $m = \cos \alpha$, $n = \sin \alpha$.

The new stress matrix $[\sigma]_1$ in the local coordinates is then given by:

$$[\sigma]_1 = [L]^{-1} [\sigma] [L],$$

Comparing term by term and using the 'reduced' (vector) representation for stress, we get the stress transformation matrix relating stress in local coordinates to stress in material coordinates [18].

$$[J]^{-1} = [T]^T = \begin{bmatrix} m^2 & n^2 & 0 & 0 & 0 & -2mn \\ n^2 & m^2 & 0 & 0 & 0 & 2mn \\ 0 & 0 & 1 & 0 & 0 & 0 \\ 0 & 0 & 0 & m & n & 0 \\ 0 & 0 & 0 & -n & m & 0 \\ mn & -mn & 0 & 0 & 0 & m^2-n^2 \end{bmatrix}$$

$$(2.11)$$

The matrix [J] can be easily computed from $[J]^{-1}$. It corresponds to the transformation due to a rotation $-\alpha$ about r axis. Therefore, [J] can be found by replacing 'n' by '-n' in $[J]^{-1}$ i.e.,

$$
[J] = \begin{bmatrix}
m^2 & n^2 & 0 & 0 & 0 & 2mn \\
n^2 & m^2 & 0 & 0 & 0 & -2mn \\
0 & 0 & 1 & 0 & 0 & 0 \\
0 & 0 & 0 & m & -n & 0 \\
0 & 0 & 0 & n & m & 0 \\
-mn & mn & 0 & 0 & 0 & m^2-n^2
\end{bmatrix}
$$

$$(2.12)$$

The stress-strain relationship in local coordinates is then determined as follows:

We have, $\{\sigma\}_m = [C]_m \{\epsilon\}_m$

$\{\sigma\}_L = [T]^T \{\sigma\}_m,$ (2.13)

$\{\epsilon\}_m = [T] \{\epsilon\}_L$

then $\{\sigma\}_L = [T]^T [C]_m [T] \{\epsilon\}_L$ (2.14)

Therefore, the stress-strain relationship in local coordinates is given by:

$[C]_L = [T]^T [C]_m [T]$

Explicitly:

13

$$[C]_L = \begin{bmatrix} CC_{11} & CC_{12} & CC_{13} & 0 & 0 & CC_{16} \\ CC_{12} & CC_{22} & CC_{23} & 0 & 0 & CC_{26} \\ CC_{13} & CC_{23} & CC_{33} & 0 & 0 & CC_{36} \\ 0 & 0 & 0 & CC_{44} & CC_{45} & 0 \\ 0 & 0 & 0 & CC_{45} & CC_{55} & 0 \\ CC_{16} & CC_{26} & CC_{36} & 0 & 0 & CC_{66} \end{bmatrix}$$

$$(2.15)$$

Where:

$$CC_{11} = C_{11}m^4 + 2(C_{12} + 2C_{66})m^2n^2 + C_{22}n^4$$

$$CC_{12} = (C_{11} + C_{22} - 4C_{66})m^2n^2 + C_{12}(m^4 + n^4)$$

$$CC_{13} = C_{13}m^2 + C_{23}n^2$$

$$CC_{16} = -mn^3 C_{22} + m^3nC_{11} - mn(m^2 - n^2)(C_{12} + 2C_{66})$$

$$CC_{22} = C_{11}n^4 + 2(C_{12} + 2C_{66})m^2n^2 + C_{22}m^4$$

$$CC_{23} = C_{13}n^2 + C_{23}m^2$$

$$CC_{33} = C_{33}$$

$$CC_{26} = -nm^3 C_{22} + n^3mC_{11} + mn(m^2 - n^2)(C_{12} + 2C_{66})$$

$$CC_{36} = (C_{13} - C_{23})mn$$

$$CC_{44} = C_{44}m^2 + C_{55}n^2$$

$$CC_{45} = (C_{55} - C_{44})mn$$

$$CC_{55} = C_{55}m^2 + C_{44}n^2$$

$$CC_{66} = (C_{11} + C_{22} - 2C_{12})m^2n^2 + C_{66}(m^2 - n^2)^2$$

$$(2.16)$$

14

2.3.3 Stress-Strain Relationship in Global Coordinate

For the case of a ring in which the local and global axes do not coincide, it is necessary to transform the stress-strain relations derived in local system of axes to global coordinates. We note, however, that for cylindrical objects global and local axes, in general, coincide. T h e matrix relating stresses to strains after rotation of axis about the tangential axis is derived following the same approach used in the preceding section. Let:

$$(\sigma)_L = [J_1] \ (\sigma)_G$$

$$(\epsilon)_L = [T_1] \ (\epsilon)_G \qquad\qquad (2.17)$$

$$(t)_L = [L] \ (t)_G$$

$$(n)_L = [L] \ (n)_G$$

where the subscripts G, L denote the global and the local coordinates systems respectively, and

$$[L] = \begin{bmatrix} M & 0 & -N \\ 0 & 1 & 0 \\ N & 0 & M \end{bmatrix} \qquad (2.18)$$

in which M=cos α', N=sin α', and α' is the angle of rotation of r-Z plane about the tangential T axis. Then the inverse

15

of the stress transformation matrix relating stress in global coordinate to stress in local coordinates is:

$$[J_1]^{-1} = [T_1]^T = \begin{bmatrix} M^2 & 0 & N^2 & 0 & 2MN & 0 \\ 0 & 1 & 0 & 0 & 0 & 0 \\ N^2 & 0 & M & 0 & -2MN & 0 \\ 0 & 0 & 0 & M & 0 & -N \\ -MN & 0 & MN & 0 & M^2-N^2 & 0 \\ 0 & 0 & 0 & N & 0 & M \end{bmatrix}$$

(2.19)

The stress-strain matrix in the global coordinate is then computed as:

$$[C]_G = [T_1]_T \, [C]_L \, [T_1].$$

Explicitly:

$$[C]_G = \begin{bmatrix} DC_{11} & DC_{12} & DC_{13} & DC_{14} & DC_{15} & DC_{16} \\ DC_{12} & DC_{22} & DC_{23} & DC_{24} & DC_{25} & DC_{26} \\ DC_{13} & DC_{23} & DC_{33} & DC_{34} & DC_{35} & DC_{36} \\ DC_{41} & DC_{42} & DC_{43} & DC_{44} & DC_{45} & DC_{46} \\ DC_{15} & DC_{25} & DC_{35} & DC_{45} & DC_{55} & DC_{56} \\ DC_{16} & DC_{26} & DC_{36} & DC_{46} & DC_{56} & DC_{66} \end{bmatrix}$$

(2.20)

16

where:

$$DC_{11} = CC_{11} \, M^4 + 2 \, CC_{13} \, M^2N^2 + CC_{33} \, N^4 + 4M^2N^2 \, CC_{55}$$

$$DC_{12} = CC_{12} \, M^2 + CC_{23} \, N^2$$

$$DC_{13} = (CC_{11} + CC_{33} - 4CC_{55}) \, M^2N^2 + CC_{13} \, (M^4 + N^4)$$

$$DC_{14} = 2 \, M^2N^2 \, CC_{45} - M^2N \, CC_{16} - N3 \, CC_{36}$$

$$DC_{15} = -MN^3 \, CC_{11} + M^3N \, CC_{33} + MN(M^2-N^2) \, CC_{13} + (M^2-N^2)2MN \, CC_{55}$$

$$DC_{16} = MN^2 \, (2 \, CC_{45} + CC_{16}) + M^2N \, CC_{36}$$

$$DC_{22} = CC_{22}$$

$$DC_{23} = N^2 \, CC_{12} + M^2 \, CC_{23}$$

$$DC_{24} = -N \, CC_{26}$$

$$DC_{25} = -MN \, CC_{12} + MN \, CC_{23}$$

$$DC_{26} = M \, CC_{26}$$

$$DC_{33} = CC_{33} \, M^4 + 2 \, CC_{13} \, M^2N^2 + CC_{11} \, N^4 + 4M^2N^2 \, CC_{55}$$

$$DC_{34} = 2 \, M^2N \, CC_{45} - M^2N \, CC_{26} - N3 \, CC_{16}$$

$$DC_{35} = -MN^3 \, CC_{11} + M^3N \, CC_{33} - MN(M^2-N^2) \, CC_{13} - (M^2-N^2)2MN \, CC_{55}$$

$$DC_{36} = MN^2 \, (-2 \, CC_{45} + CC_{26}) + M^3 \, CC_{26}$$

$$DC_{44} = M^2 \, CC_{44} + N^2 \, CC_{66}$$

$$DC_{45} = MN^2 \, (CC_{16} - CC_{36}) + (M^2 - N^2)M \, CC_{45}$$

$$DC_{46} = MN \, CC_{44} - MN \, CC_{66}$$

$$DC_{55} = (M^2N^2)(CC_{11} - 2CC_{13} + CC_{33}) + (M^2 - N^2)^2 \, CC_{55}$$

$$DC_{56} = (M^2N - N^3) \, CC_{45} + M^2N \, (-CC_{16} + CC_{36})$$

$$DC_{66} = N^2 \, CC_{44} + M^2 \, CC_{66}$$

$$(2.21)$$

SECTION III

DISCRETIZATION BY THE FINITE ELEMENT METHOD

3.1 BASIC CONCEPTS:

The finite element method is a general technique for construction of approximate solutions to boundary value problems. The method essentially involves dividing the spatial domain of interest, R, into a finite number of nontrivial discrete elements, and using variational concepts to construct an approximation of the solution over the collection of finite elements.

Therefore, the principal ingredients of the finite element method for constructing approximate solutions of problems are:

1. The construction of a finite element mesh and selection of a set of piecewise-polynomial basis functions defined on the mesh satisfying the required continuity conditions. The elements are assumed to be interconnected at a discrete number of nodal points situated on their boundaries.

2. The construction of an approximation of the variational formulation of the problem, setting up of

element properties, assemblage of these into a system of algebraic equations with nodal values of the dependent variables or their derivatives up to a certain order as the unknown quantities.

3. Solution of the algebraic system.

3.2 FORMULATION

Sandhu and Pister [15,16] and Sandhu and Salaam [17] used a generalization of Mikhlin's basic variational theorem to extend its application to linear coupled initial boundary value problem. Specialization of an "extended" variational principle leads to the well-known potential energy theory which has been used in developing the finite element model described in this report. For elastostatics problem, assuming that the strains exactly satisfy the strain-displacement relationship, and the displacement field is continuous over the spatial region of interest R and satisfies the prescribed displacement boundary conditions on portion S_1 of the boundary ∂R of R, the potential energy is:

$$I(u) = <u_{i,j}, \ E_{ijkl} \ u_{k,l}>_R - 2<u_i, \ f_i>_R$$
$$- 2<u_i, t_i>_{S2} \qquad (3.1)$$

Here u_i, E_{ijkl}, f_i, t_i are components, respectively of the displacement vector, the isothermal elasticity tensor, body force vector, and the specified tractions on boundary S_2.

19

$< , >_R, < , >_{S2}$ denotes inner products of pairs of functions evaluated over the domain indicated by the subscript. S_1, S_2 are complementary subsets of ∂R.

Vanishing of the variation of $I(u)$ with respect to the displacement components u_i implies the satisfaction of equilibrium equations over R and on S_2. The finite element approximation consists of applying the theorem to the approximate functional evaluated by using the approximate values of the functions defined by the finite element interpolation scheme.

Taking the variation of the discretized form of the functional yields the system of algebraic equations:

$$[K]\{r\} = \{F\}$$

where:

    [K]:   The system stiffness matrix.

    {r}:   Nodal point displacement vector.

    {F}:   Nodal point load vector.

3.3   INTERPOLATION FUNCTIONS FOR THE MODIFIED BILINEAR ISOPARAMETRIC QUADRILATERAL ELEMENT QM4

3.3.1 Bilinear Interpolation Function for Isoparametric Quadrilateral Element

The element used in the analysis is an arbitrary quadrilateral. The displacements are bilinearly interpolated over each element. The interpolation functions are expressed as:

$$N_1 = 1/4 \ (1-s)(1-t)$$
$$N_2 = 1/4 \ (1+s)(1-t) \qquad\qquad (3.2)$$
$$N_3 = 1/4 \ (1+s)(1+t)$$
$$N_4 = 1/4 \ (1-s)(1+t)$$

where s,t is a set of coordinates such that the corners of the quadrilateral are (-1,-1), (-1,1), (1,1), (1,-1).

3.3.2 Modified Bilinear Isoparametric Element

Selective reduced integration was introduced by Taylor et al., [19] for evaluation of the stiffness matrix for bending problems. Salaam [18] reported remarkable improvement in numerical results for some problems where selective reduced integration had been used. This was physically explained [19] as resulting from the excessive

transverse shear strain energy contribution when using isoparametric elements. As a remedy for this problem, a constant shear strain was imposed on the element by assigning the shear strain associated with the center of the element to the entire element. The modified (constant shear) element so obtained was labelled as QM4 and was used in the finite element code developed in this research program.

SECTION IV

APPLICATION TO DELAMINATION SPECIMENS

4.1 INTRODUCTION

Although the computer program is capable of obtaining approximate stresses and deformations in any axisymmetrical laminated solid, the primary motivation of the development was to obtain an approximation of stress fields in a free-edge delamination coupon. The program was validated through application to a four-ply symmetric laminate. Results were compared to numerical solutions obtained using a continuous traction finite element formulation [11]. The computer program was also used to solve for stresses and deformations in a 22-layer symmetric angle-ply laminate.

4.2 MATHEMATICAL MODEL

The straight coupon subjected to a uniform inplane strain in the longitudinal direction is viewed as a short segment of a large radius ring subjected to a radial pressure. Figure (3) shows the correspondence between a ring segment and a short straight coupon. For a sufficiently large radius of the ring, a uniform inner pressure will
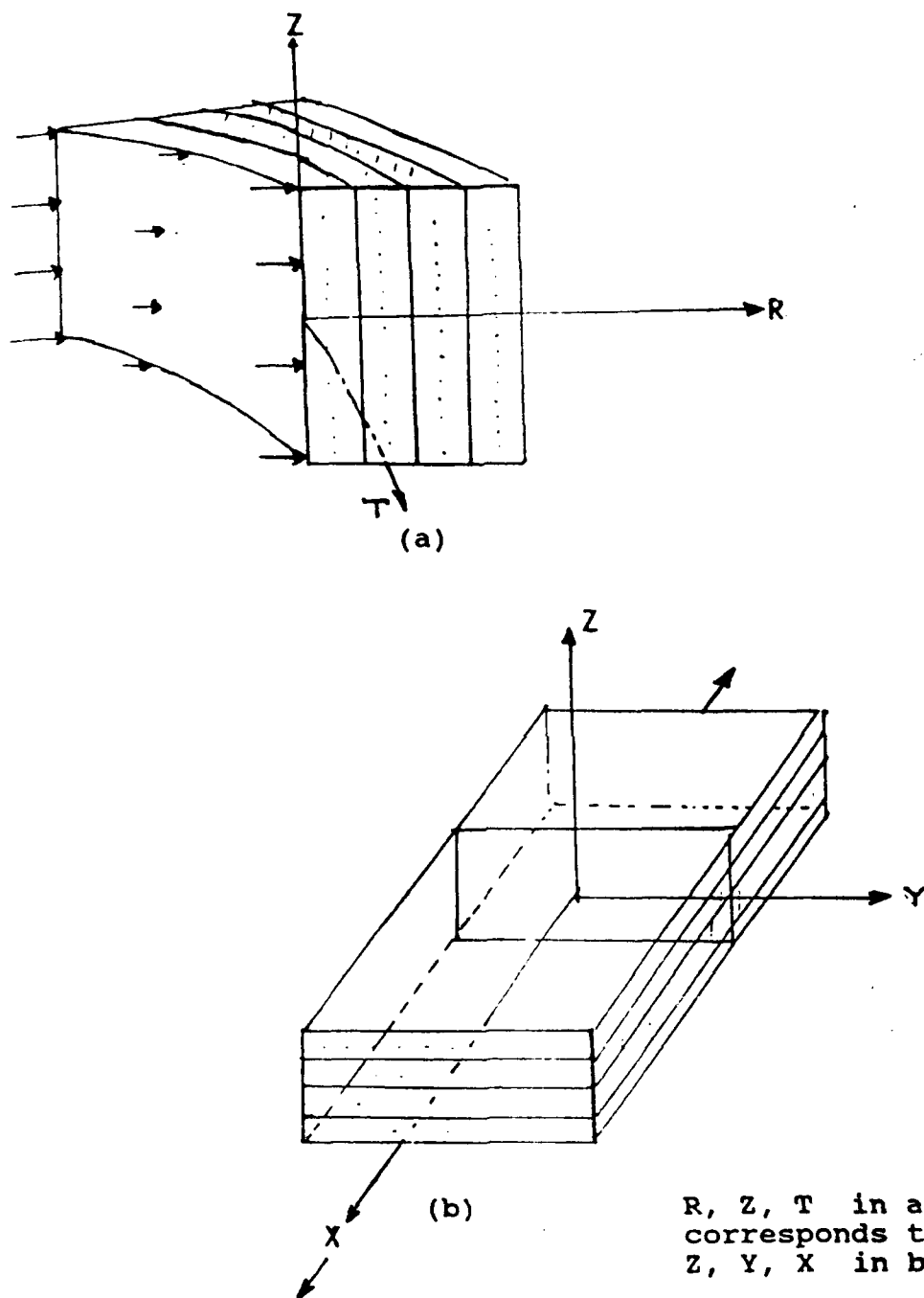
Figure 3: Correspondence Between Ring Specimen a)
and Strip Specimen b)

R, Z, T   in a)
corresponds to
Z, Y, X   in b)

yield a reasonably uniform tangential strain over all elements of a section. Also, for large radius the magnitude of the radial internal pressure will be small in comparison with the other stresses in the ring and, therefore, will not be of much influence in determining failure.

To insure accuracy of results, different values of the inner radius were tried. It was found that for a radius equal to 10^4 times the thickness of the specimen, the tangential strain was uniform, up to a four-digit accuracy, over all elements of the section. Figure (4) shows through-thickness distribution of T-strain near the free-edge for radii 10^4, 10^3 and 10^2 times the thickness.

In general, axisymmetric loading of a composite ring will cause circumferential displacement due to the composite material behavior. Thus, when the hoop is loaded axisymmetrically with internal pressure, a circumferential strain is generated in addition to the radial deformation and shear strain over planes parallel t the axis [10]. Therefore, to allow the complete state of stress and strain to be modeled, three displacement degrees of freedom, independent of the circumferential coordinate, need to be associated with each node: u, axial; v, circumferential; w, radial. Two computer programs were, therefore, developed.

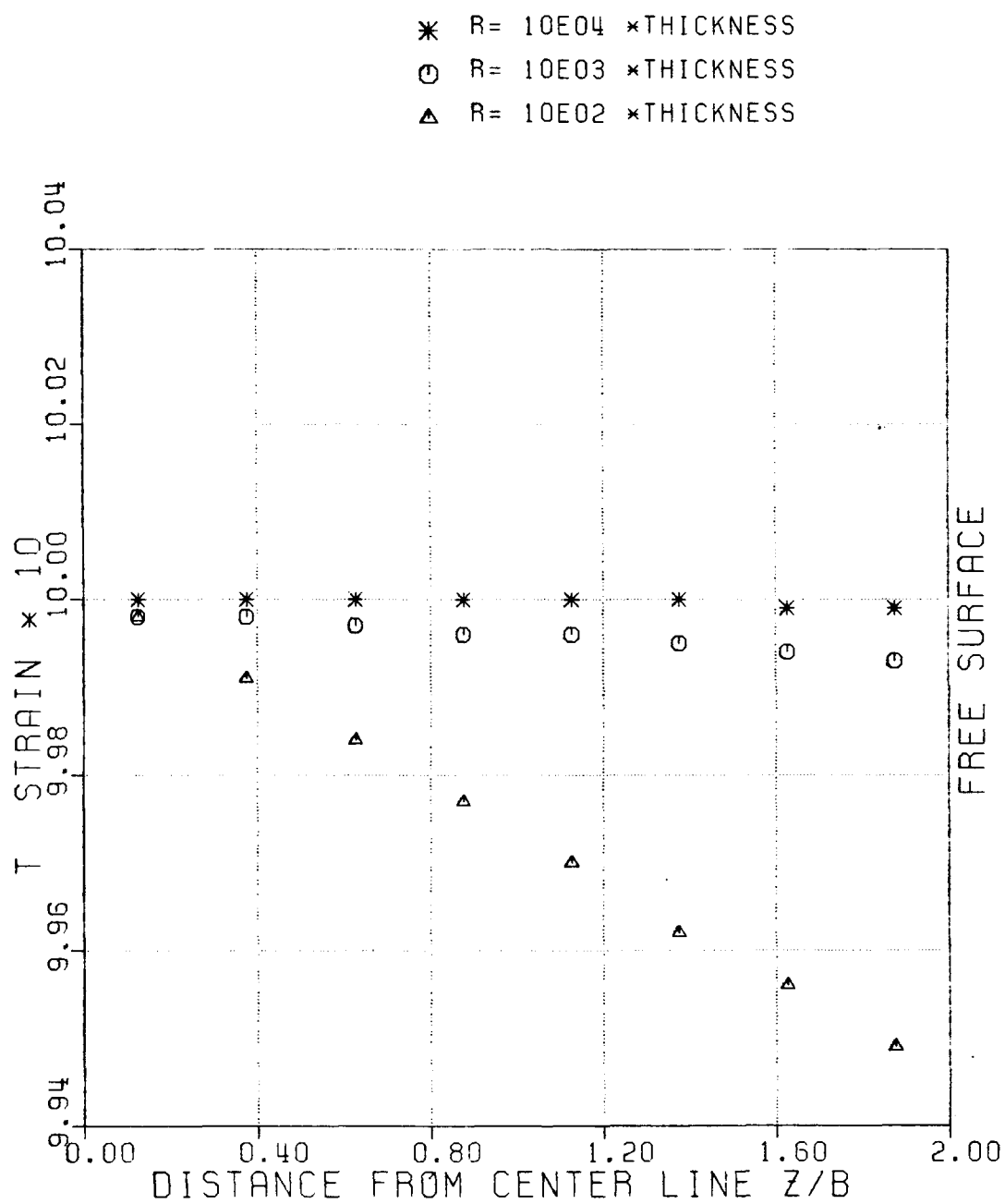**Figure 4:** Through-Thickness Distribution of T-Strain of [45/-45]$_s$ Laminate for Different Ring Radii

26

One allowed for all the three displacement degrees of freedom and the other allowed only the radial and axial displacements. In the two-dimensional analysis, rT and zT-strains are assumed zero while the corresponding stresses can have nonzero values, depending upon the material properties and fiber directions.

4.3 FOUR-PLY LAMINATES

4.3.1 Geometry, Material Properties and Finite Element Mesh

Ring specimens with fiber orientation $[0/90]_s$ and $[45/-45]_s$ under uniform internal pressure were considered in the present analysis. The relation between laminate width and thickness was 2b = 16h, as in references [11], [23]. Each ply was idealized as a homogeneous, elastic orthotropic material with the following properties [11]:

$$E_{11} = 20 * 10^6 \text{ psi}$$
$$E_{22} = E_{33} = 2.1 * 10^6 \text{ psi}$$
$$G_{12} = G_{13} = G_{23} = 0.85 * 10^6 \text{ psi}$$
$$\mu_{12} = \mu_{13} = \mu_{23} = 0.21$$

The subscripts 1,2,3 correspond to material coordinates in the longitudinal, transverse and thickness directions respectively. Each physical layer of thickness h was subdivided into sublayers, the total number of sublayers is

denoted by N. The mesh used was refined near the free edge in order to obtain more reliable results in regions where steeply varying stresses are expected. A 288 (N=16) element model, as shown in Figure (5), was used to discretize a typical half section of the ring. This corresponds to a 144-element model for a quadrant as used with continuous traction Q23 element in [11]. The r, z, T axes in the model correspond to the z, y, x axes in the cartesian representation of the coupon. The edge z=b is the free-edge and R=0, R=4h respectively are the bottom and top surface of the specimen. The value R_i, shown in Figure (5), denotes the distance from the central plane of section to the center of the ith sublayer. R_1 is the closest to the midplane of the specimen and R_8 is closest to the top surface.

The internal pressure applied was 1108 (psi) and 290.53 (psi) for the cross-ply and the angle-ply laminate, respectively. This pressure yields a unit average axial strain, corresponding to the uniform axial strain applied in the continuous traction Q23 analysis [11].

28
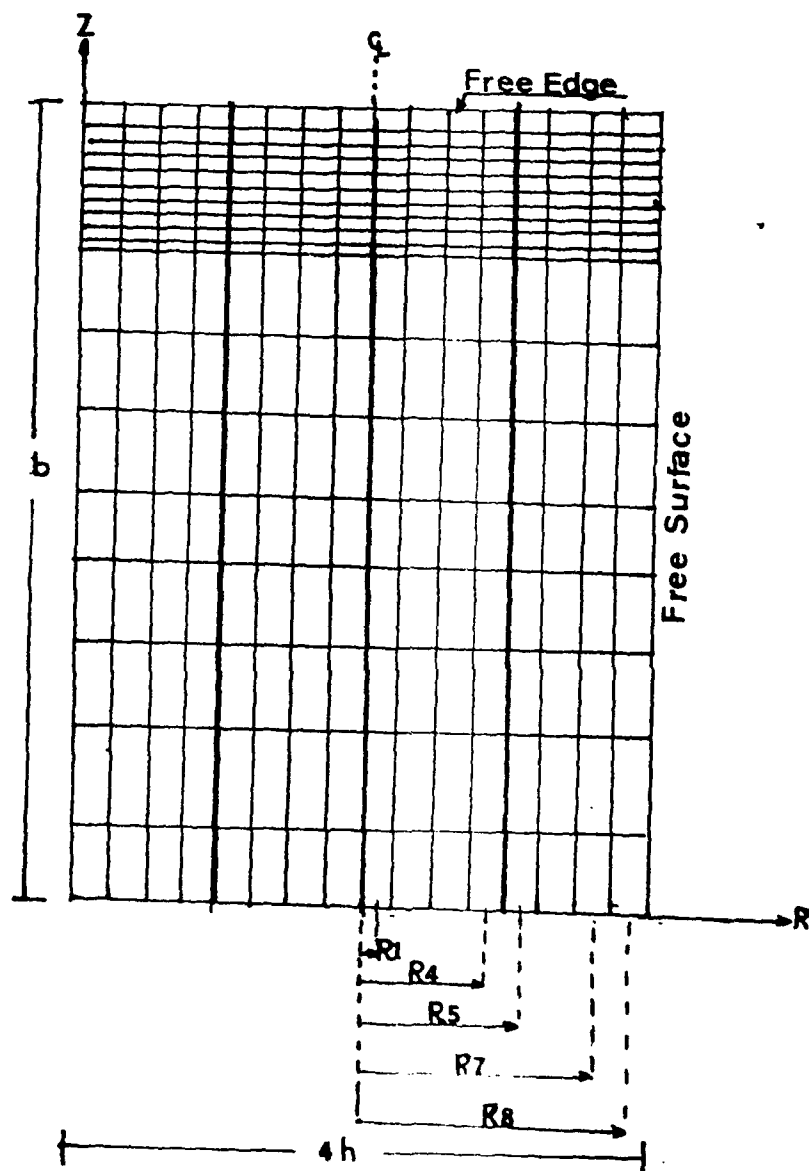
Radius = 10^4 * Thickness

Figure 5: 288 Element Mesh (16x18)

4.3.2 Cross-Ply Laminates

The cross-ply laminate was analyzed using both the two degree-of-freedom computer program as well as the pseudo-three-dimensional approach and the results compared. For cross-ply laminates, the transverse Tr and Tz stresses were negligible compared to the other stresses in the pseudo-three-dimensional analysis and were nearly zero in the two-dimensional analysis. Further, the four stress components σ_r, σ_z, σ_T, σ_{rz} were only slightly affected by the introduction of the third degree of freedom. Figures (6), (7) show the distribution of R-stress along R1 and Rz-stress along R4 for the cross-ply laminate. The figures indicate excellent agreement between results obtained using three degrees of freedom for each node and those obtained using two degrees of freedom for each node. These sections were selected for the comparison as representatives. Similar agreement was also obtained for stress distributions at other sections.

Because of the symmetry in the laminate about the Z=0 axis, only half the section was considered. Numerical results based on two-dimensional axisymmetric analysis using QM4 element were compared with results based on the continuous traction Q23 element described in [11]. The same mesh size was used in both the analyses. The numerical
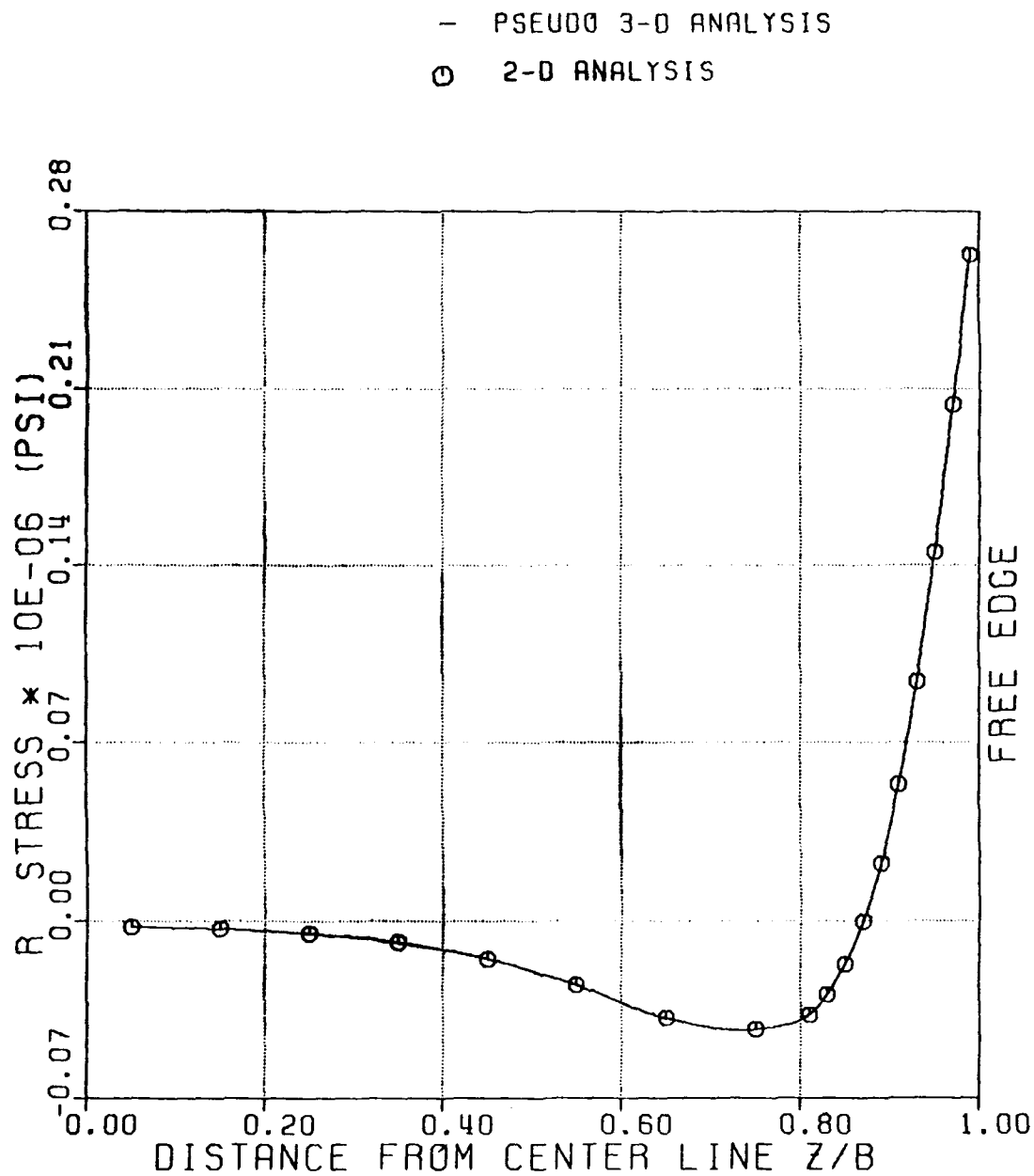
30

Figure 6: Distribution of R-Stress Along R1 of
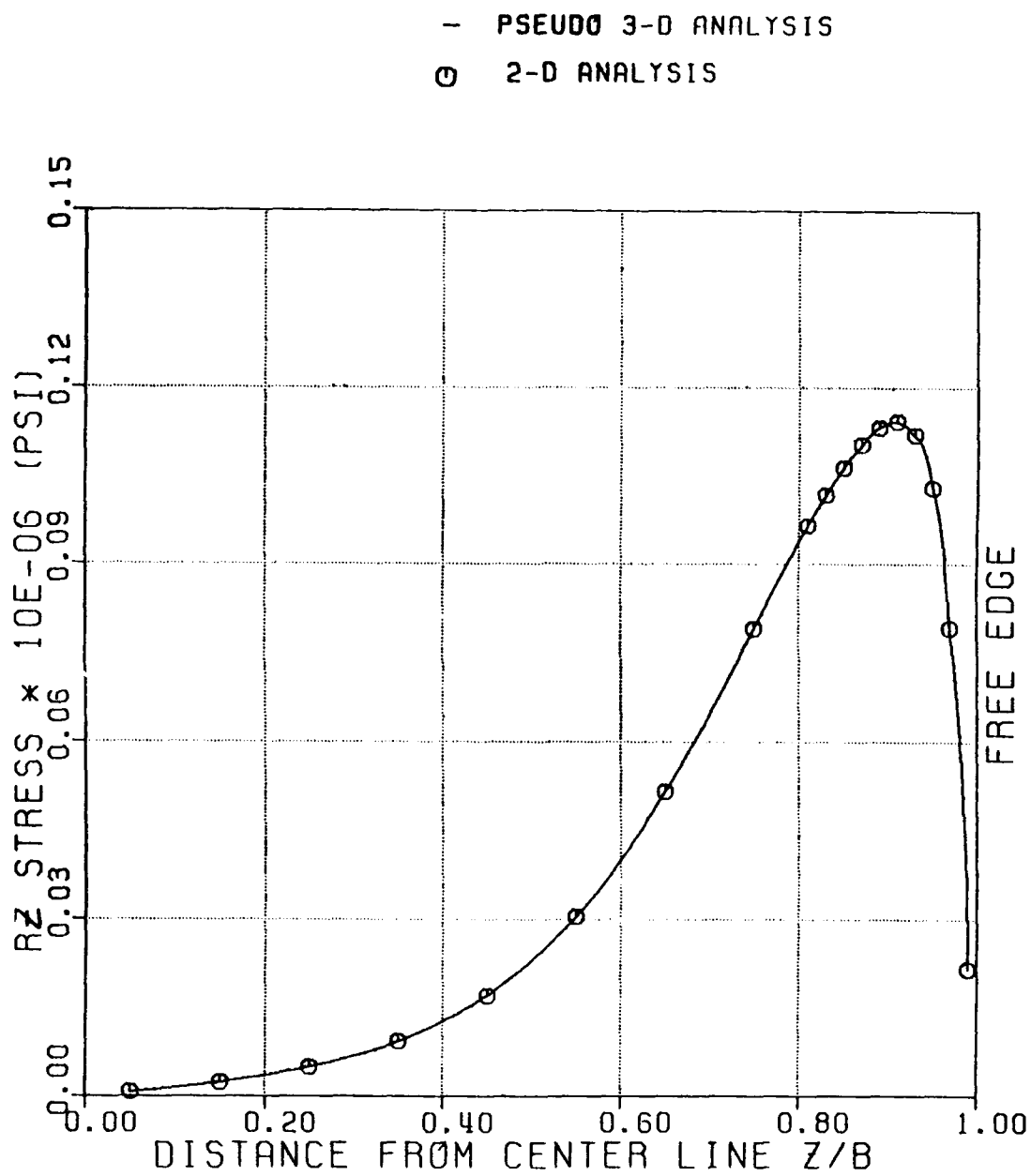
[0/90]$_s$ Laminate: 2-D and Pseudo 3-D Analysis

31

Figure 7: Distribution of Rz-Stress Along R4 of

[0/90]$_s$ Laminate: 2-D and Pseudo 3-D Analysis

32

result using Q23 [11] has shown good agreement with Pagano's analytical solution [23] which is based on a generalization of Reissner's theory. Figures (8) through (23) compare stress fields at specific locations for the cross-ply laminates using Q23 and the axisymmetric analysis.

Distribution of R-stress along the center of the first sublayer beyond the central plane (at R1) of the $[0/90]_S$ is shown in Figure (8). Solutions obtained from the axisymmetric analysis practically coincide with Q23 element solution over the entire width of the laminate. The distribution of stresses indicates a sharp rise near the free edge which agrees with Pagano's solution [11],[23]. Figures (9), (10) show the distribution of R-stress at center of the last sublayer of 0° ply (at R4) and the first sublayer of the 90° ply (at R5) respectively. At the interface of the 0 and 90 degree plies, a stress singularity is expected at the free edge due to the discontinuity in elastic properties. The stress distributions, however, are only obtained at the centers of adjacent elements and can only be compared there. It is noted that the stress value near the free-edge obtained using axisymmetric analysis overestimated the stress at R4 and underestimated it at R5 as compared with Q23 solution.
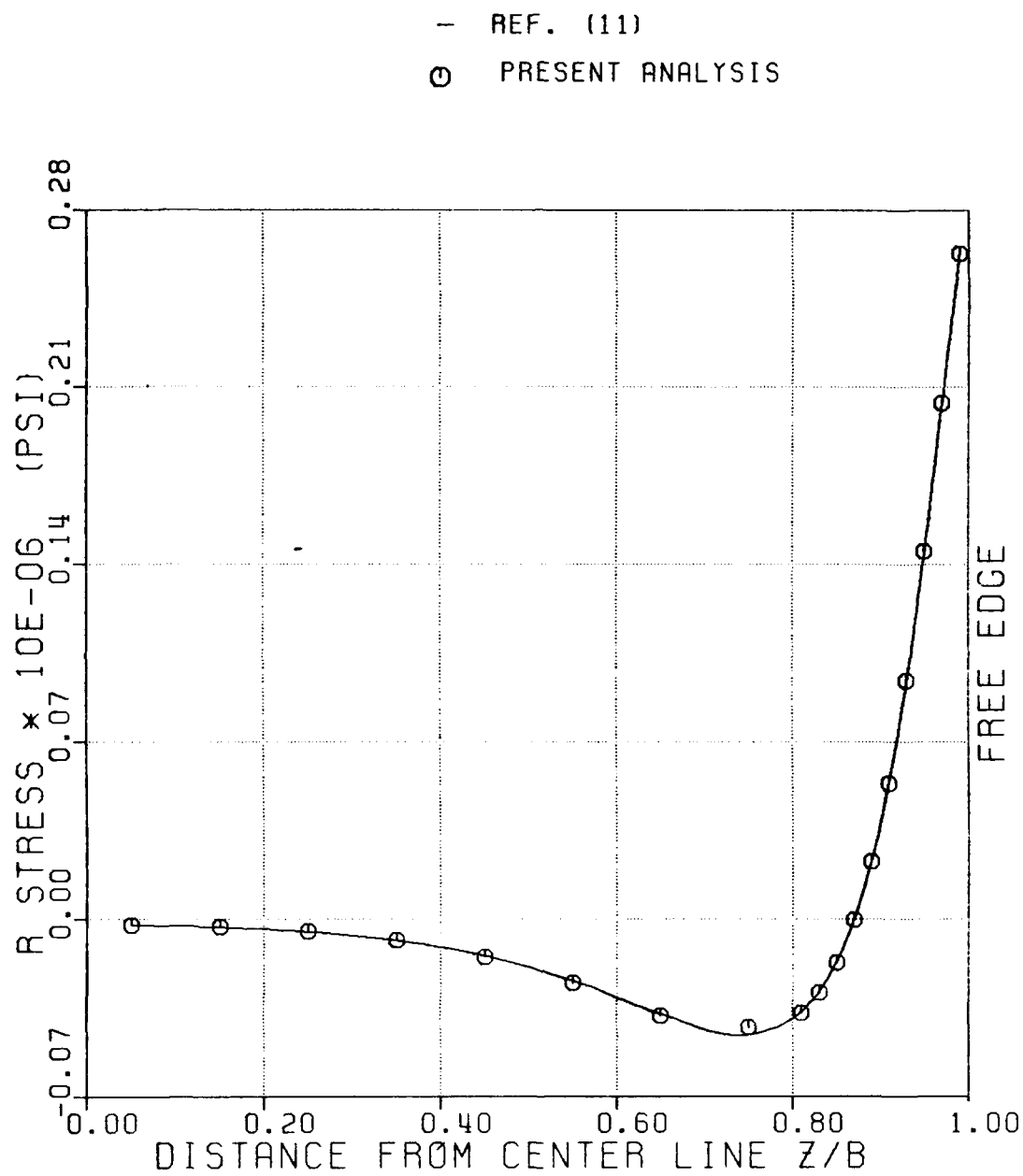
Figure 8: Distribution of R-Stress Along R1
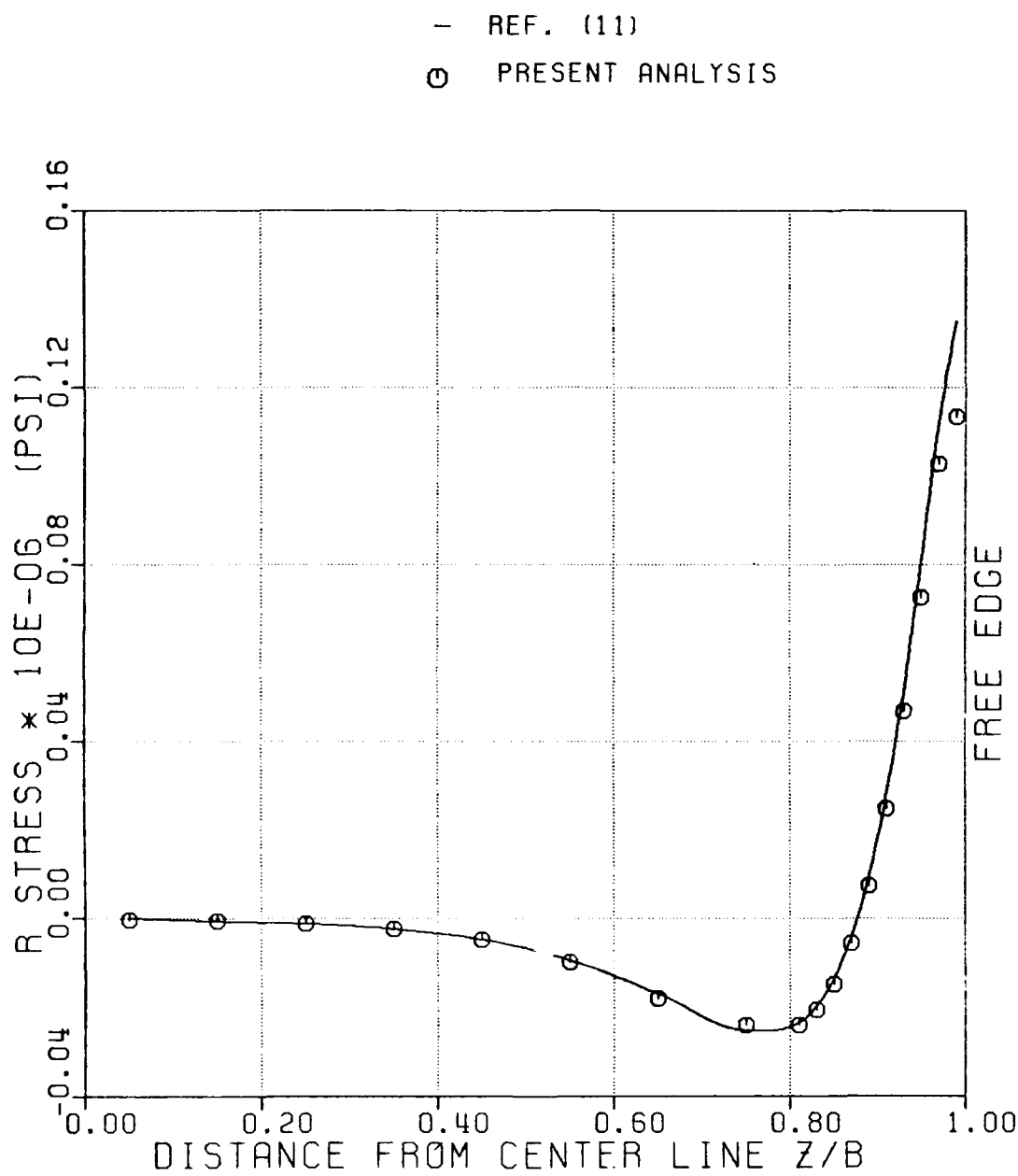
of $[0/90]_s$ Laminate.

Figure 10: Distribution of R-Stress Along R5
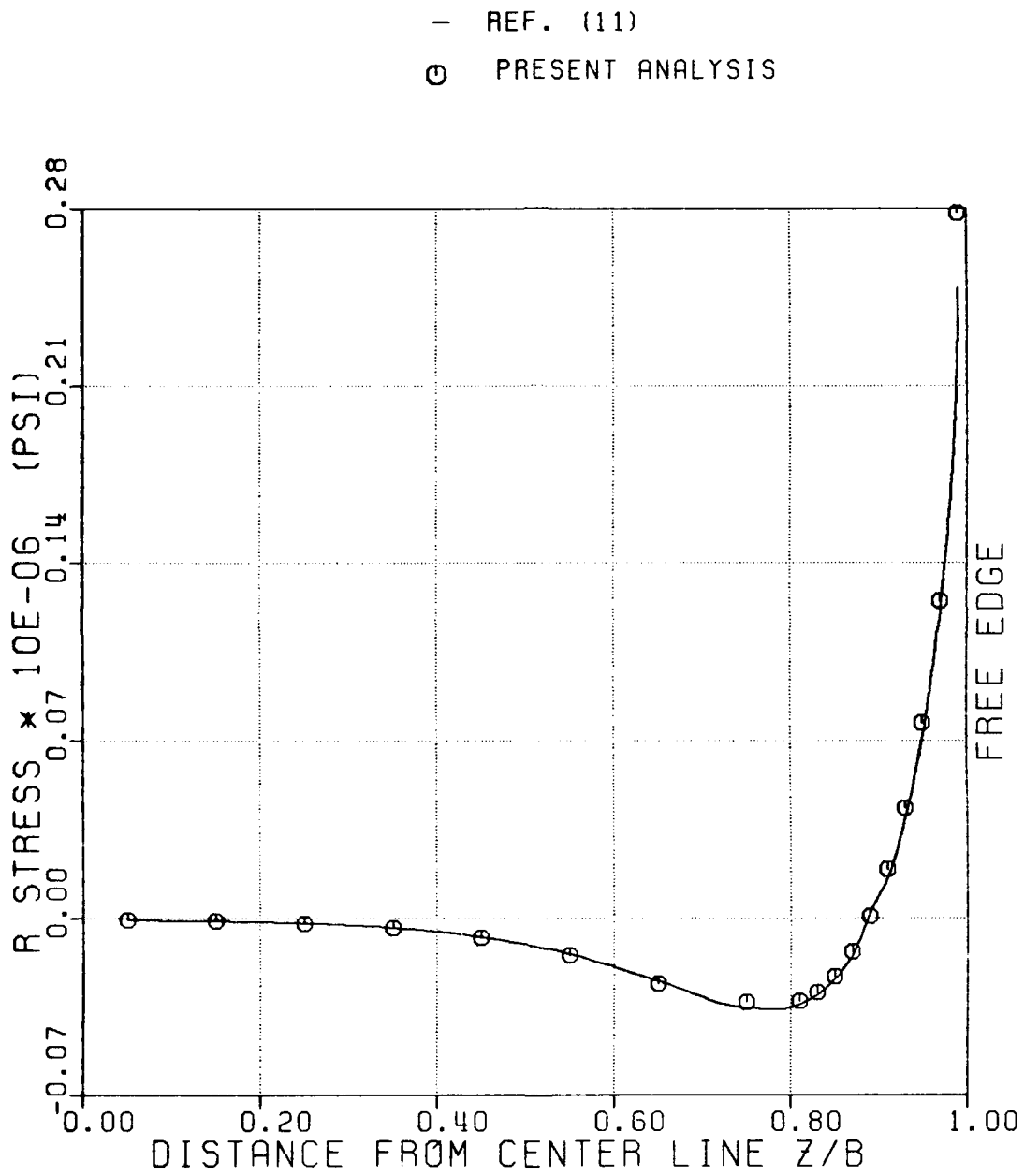
of [0/90]$_s$ Laminate.

36

Figure 9: Distribution of R-Stress Along R4

of [0/90]_s Laminate.

35

A discrepancy in the distribution of R-stress, for the two procedures, at the center of the last (nearest to the surface) sublayer (R8) and the sublayer near to it is observed in Figures (11) and (12). This could possibly be because, in the present procedure, the traction-free boundary condition is not enforced. The difference in stresses is less severe away from the free surface as shown in the distribution of R-stress at R7 (Figure (11)) than that at R8 (Figure (12)).

Figure (13) shows through-the-thickness distribution of R-stress near the free edge (at $Z/B = 0.99$) of the laminate. In the vicinity of the interface, a difference in the solution of continuous-traction element and the axisymmetric analysis exists. It was felt that this could be due to the finite element mesh not being fine enough to approximate the steeply varying stresses associated with abrupt change of material properties. To explore this further, the effect of mesh refinement was studied. This is described later in this section.

Values of Rz-stress along the center of the first sublayer beyond the center plane of the laminate (along R1), along R4 and along R5 are shown in Figures (14,15,16) respectively. The result showed satisfactory agreement with
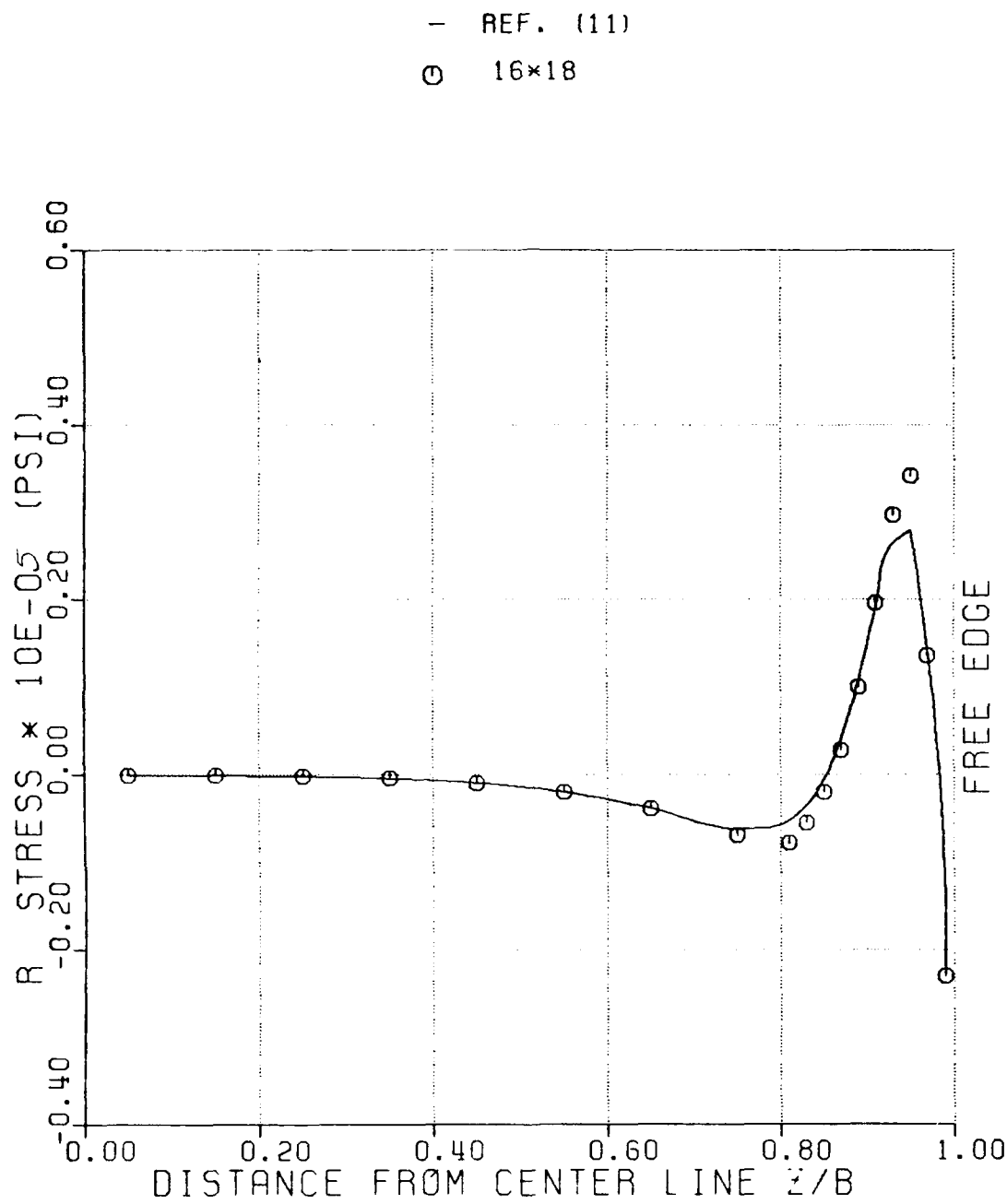
37

Figure 11: Distribution of R-Stress Along R7

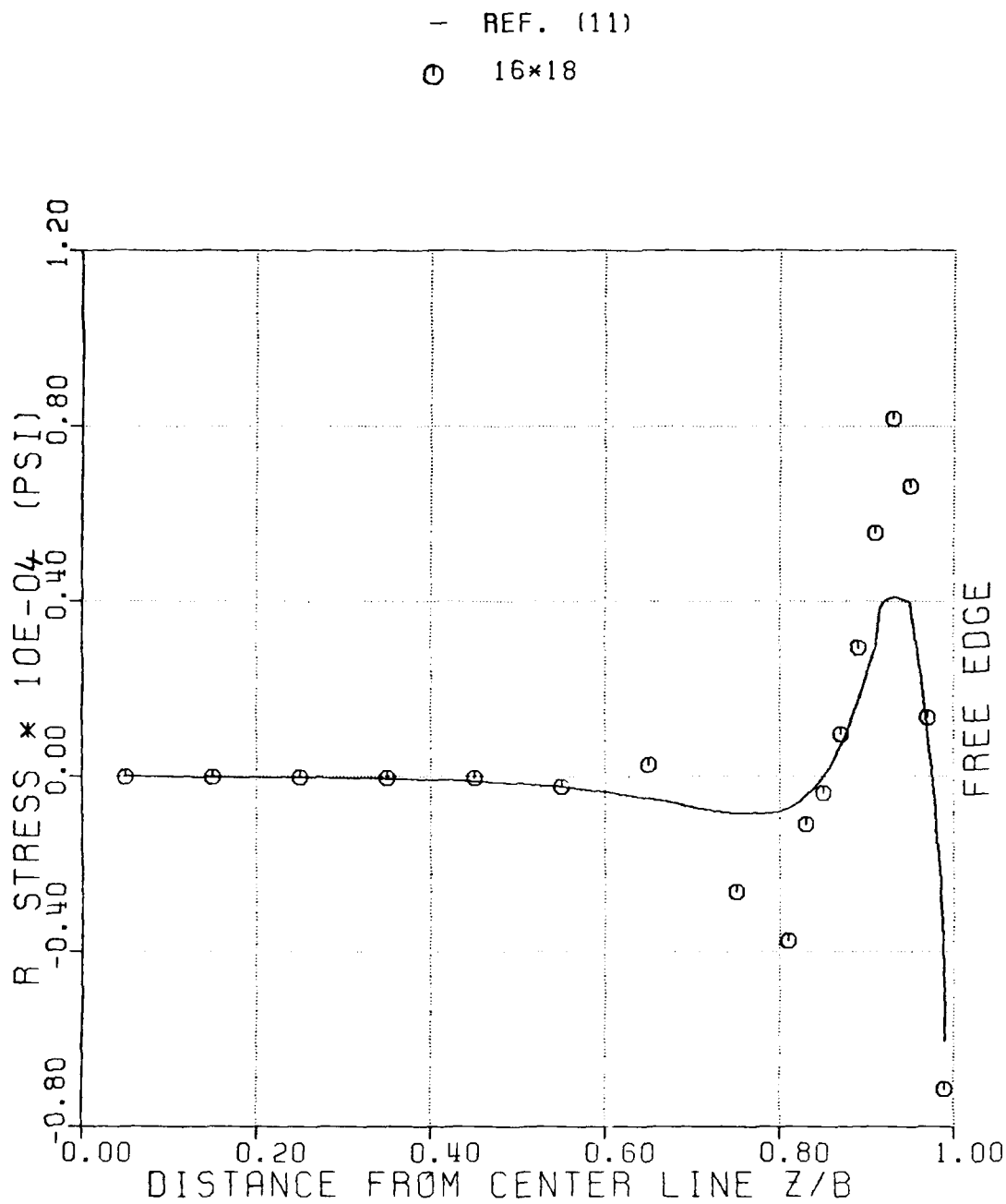of [0/90]$_s$ Laminate.

- REF. (11)
⊖ 16×18

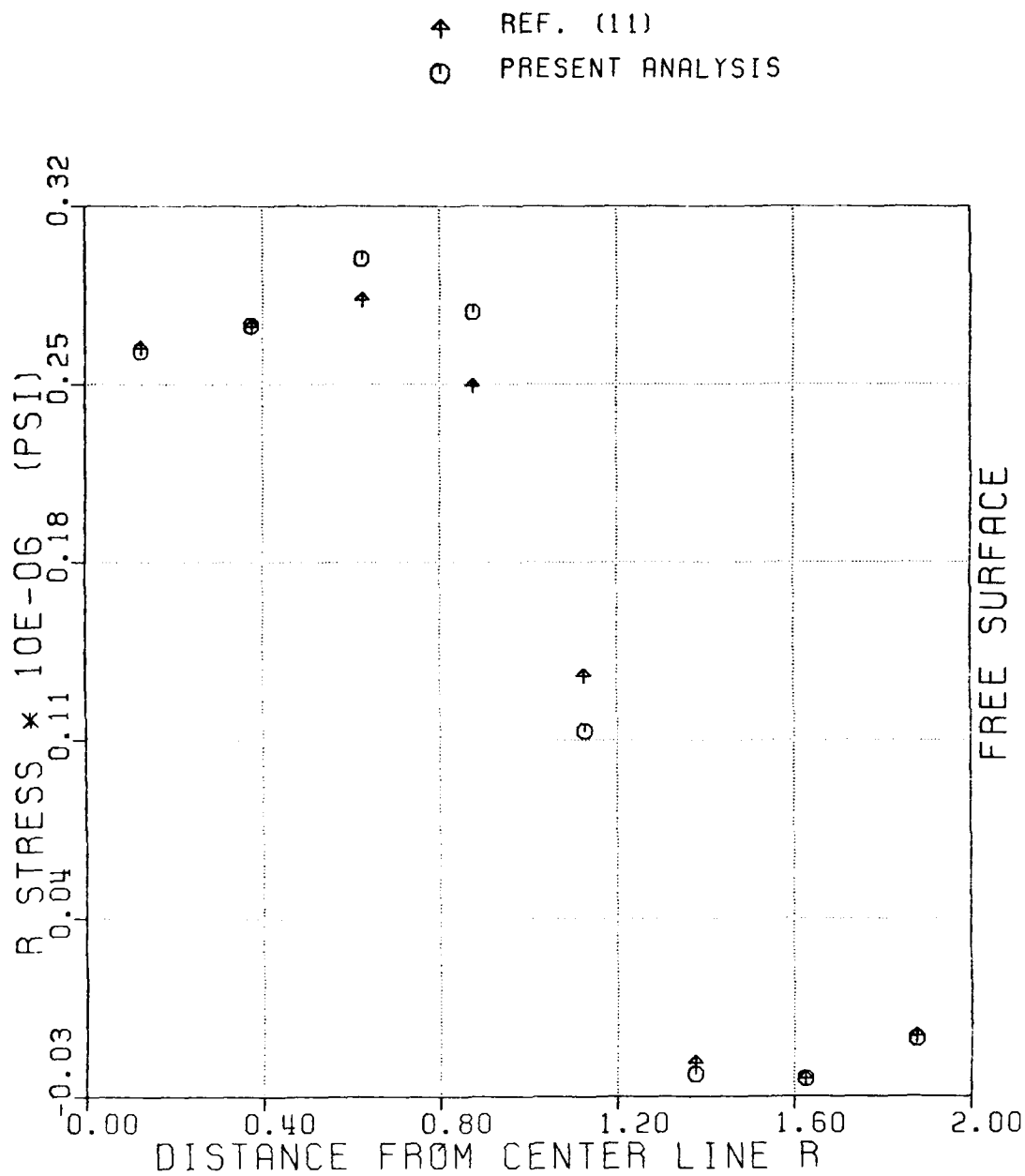Figure 12: Distribution of R-Stress Along R8

of [0/90]$_s$ Laminate.

39

Figure 13: Through-thickness Distribution of R-Stress near Free Edge (Z/B = 0.99) of [0/90]$_s$ Laminate.

40

those obtained using Q23 element. However, a discrepancy is observed near the free edge in Figure (16). This is apparently because the continuous traction Q23 element exactly satisfies the traction-free boundary condition, while axisymmetric displacement formulation does not. A more refined mesh near the free edge is likely to give more satisfactory result. This was investigated and is described later in this section.

Figures (17) and (18) show the distribution of Rz-stress along R7 and along the center of the last sublayer (at R8). Contrary to the distribution of R-stress at these locations, the RZ-stress distributions are in good agreement with those obtained from Q23 element.

Through-the-thickness distribution of Rz-stress near free edge (at Z/b =0.99) is shown in Figure (19). The results show significant difference with those for the Q23 analysis specially near the interface of 0°/90° layers.

Distribution of Z-stress along R1, R4 and R8 are shown in Figures (20, 21, 22) respectively. The results along R1 and R8 obtained using the axisymmetric analysis agreed well with the Q23 element solution across the entire width of the laminate. However, a difference in stress distribution along R4 is observed near the free edge where a steeply varying
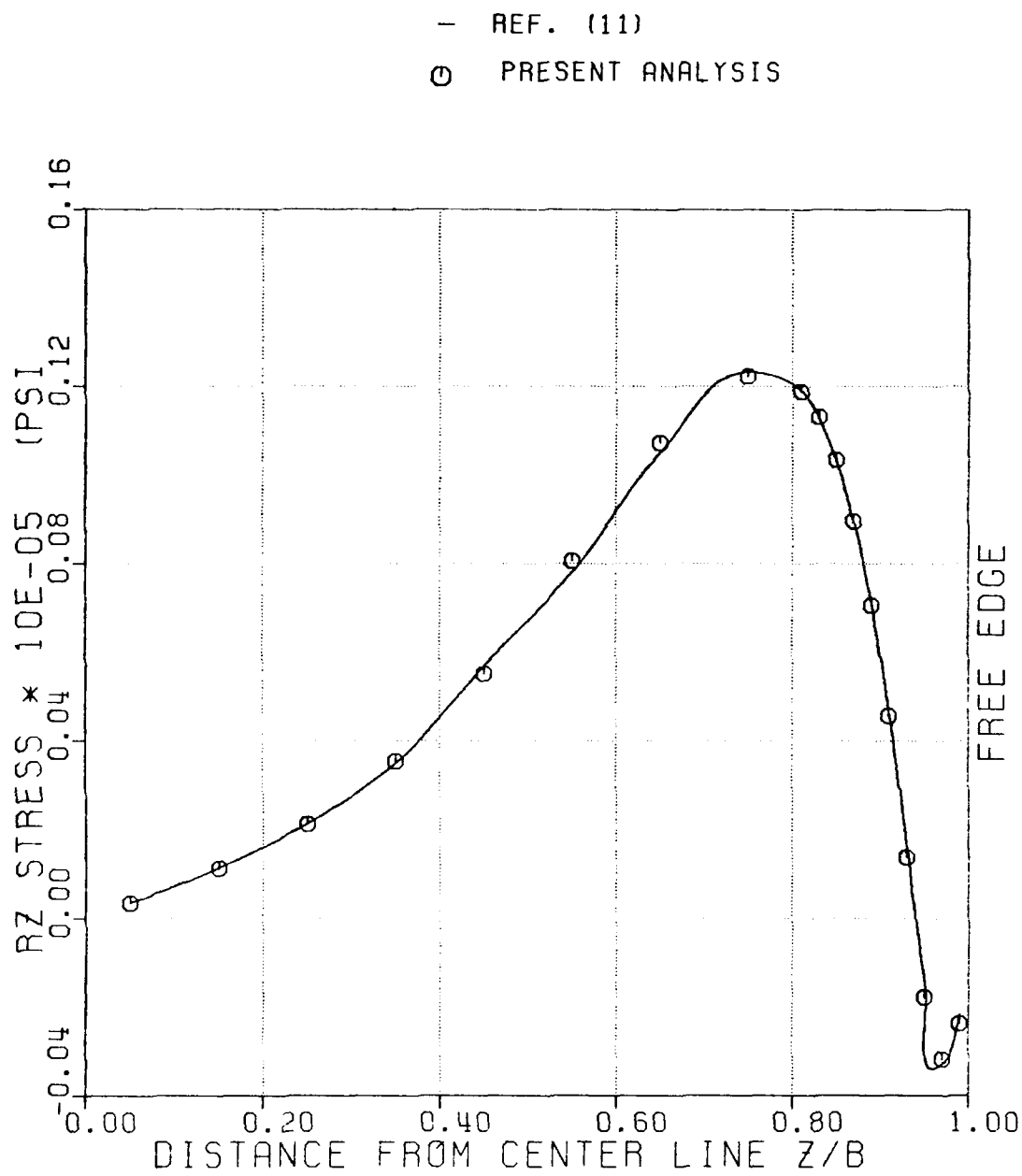
41

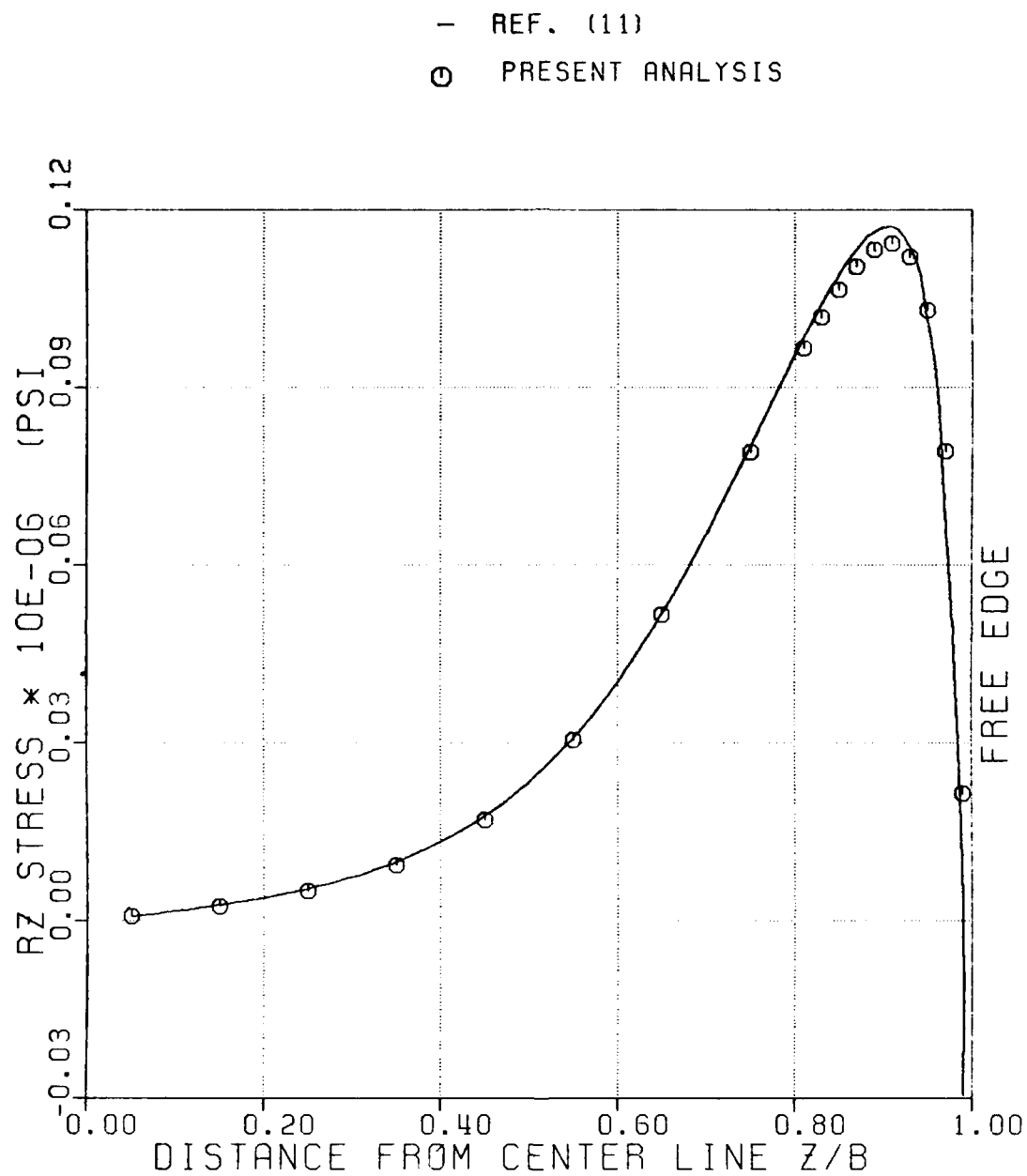Figure 14: Distribution of RZ-Stress Along R1

of $[0/90]_s$ Laminate.

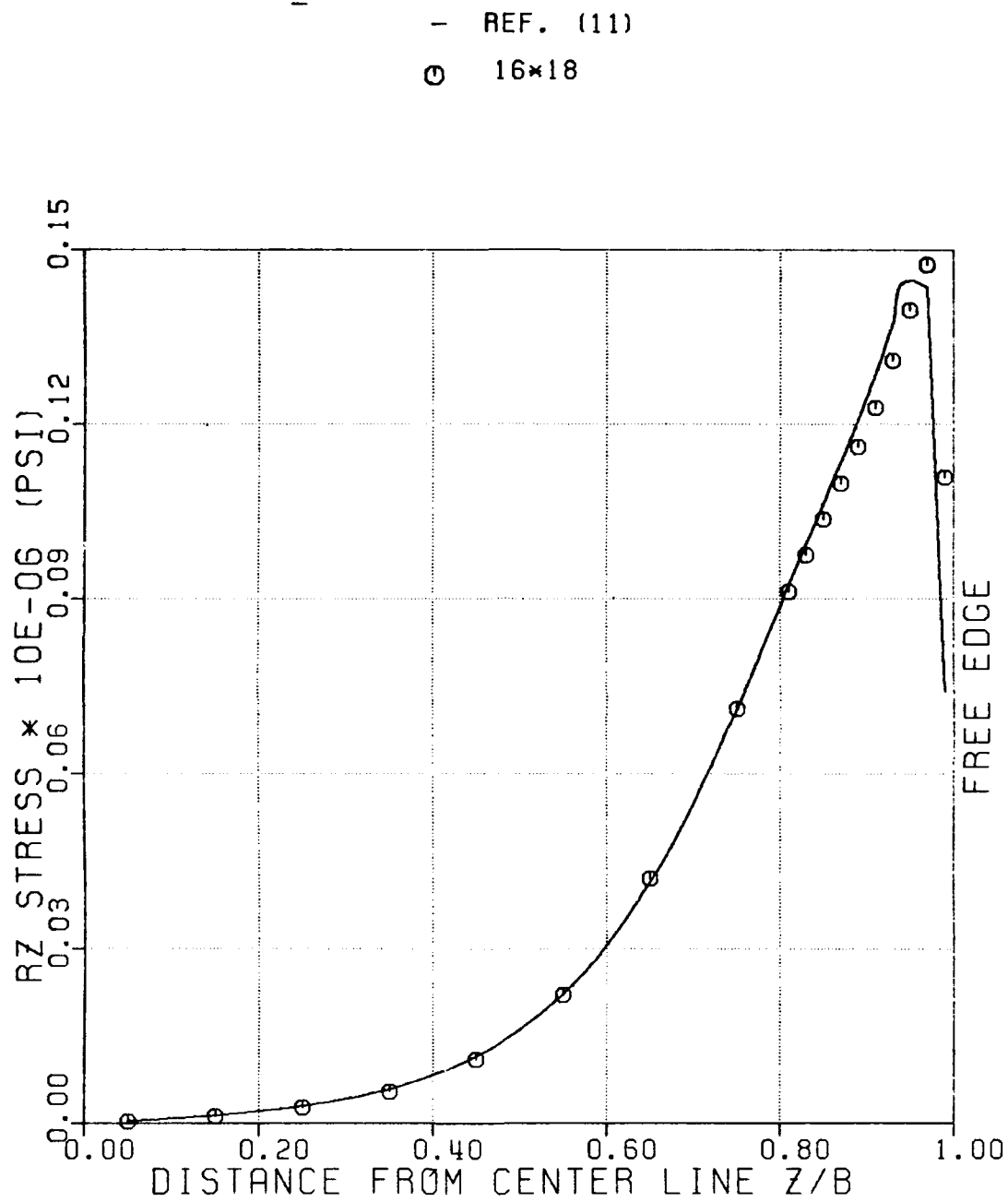Figure 15: Distribution of RZ-Stress Along R4
of [0/90]$_s$ Laminate.

43

Figure 16: Distribution of RZ-Stress Along R5
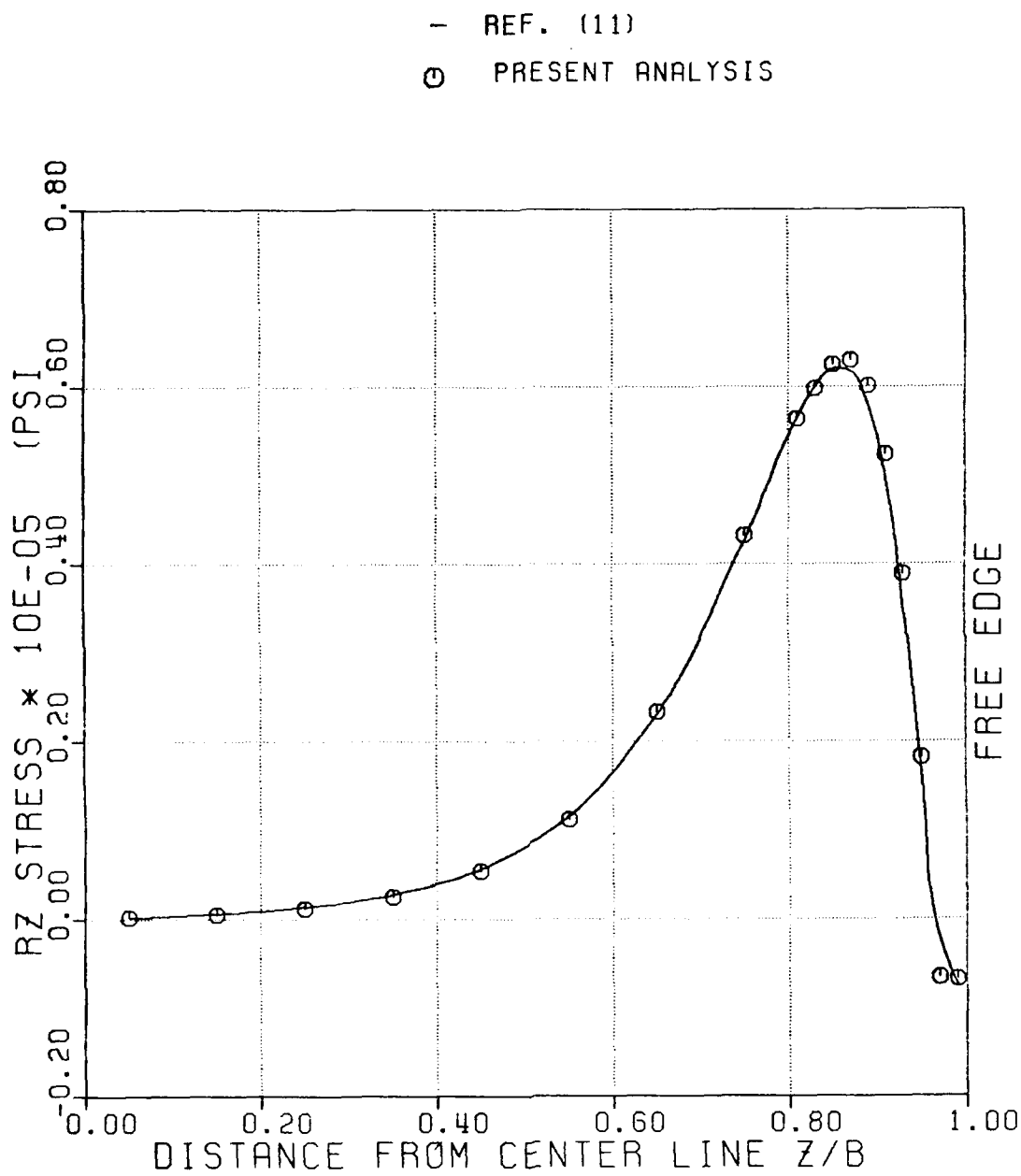of $[0/90]_s$ Laminate.

44

Figure 17: Distribution of RZ-Stress Along R7
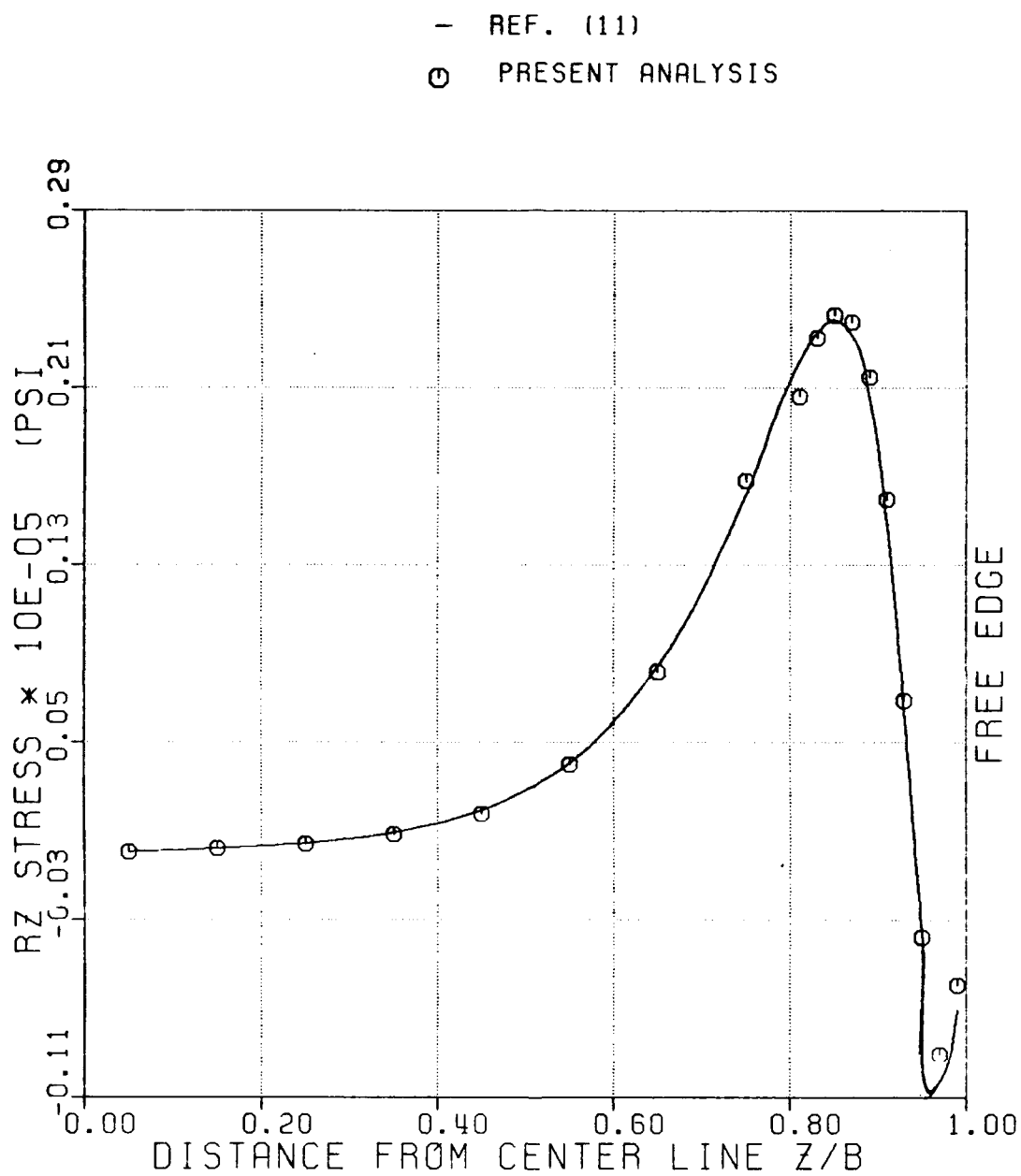
of [0/90]$_s$ Laminate.

45

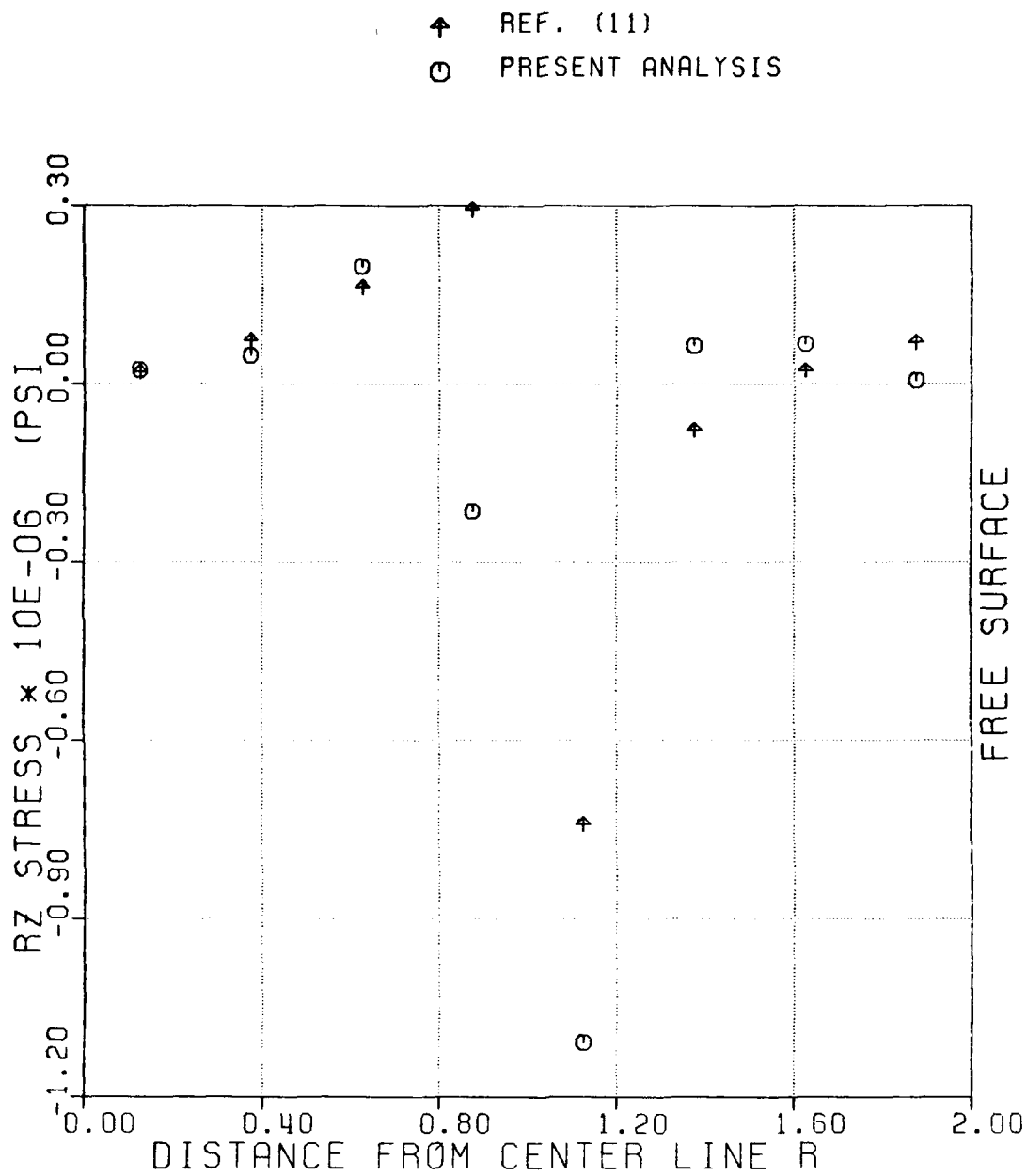Figure 18: Distribution of RZ-Stress Along R8

of [0/90]$_s$ Laminate.

46

Figure 19: Through-Thickness Distribution of
RZ-Stress near Free Edge (Z/B=.39)
of [0/90]ₛ Laminate.
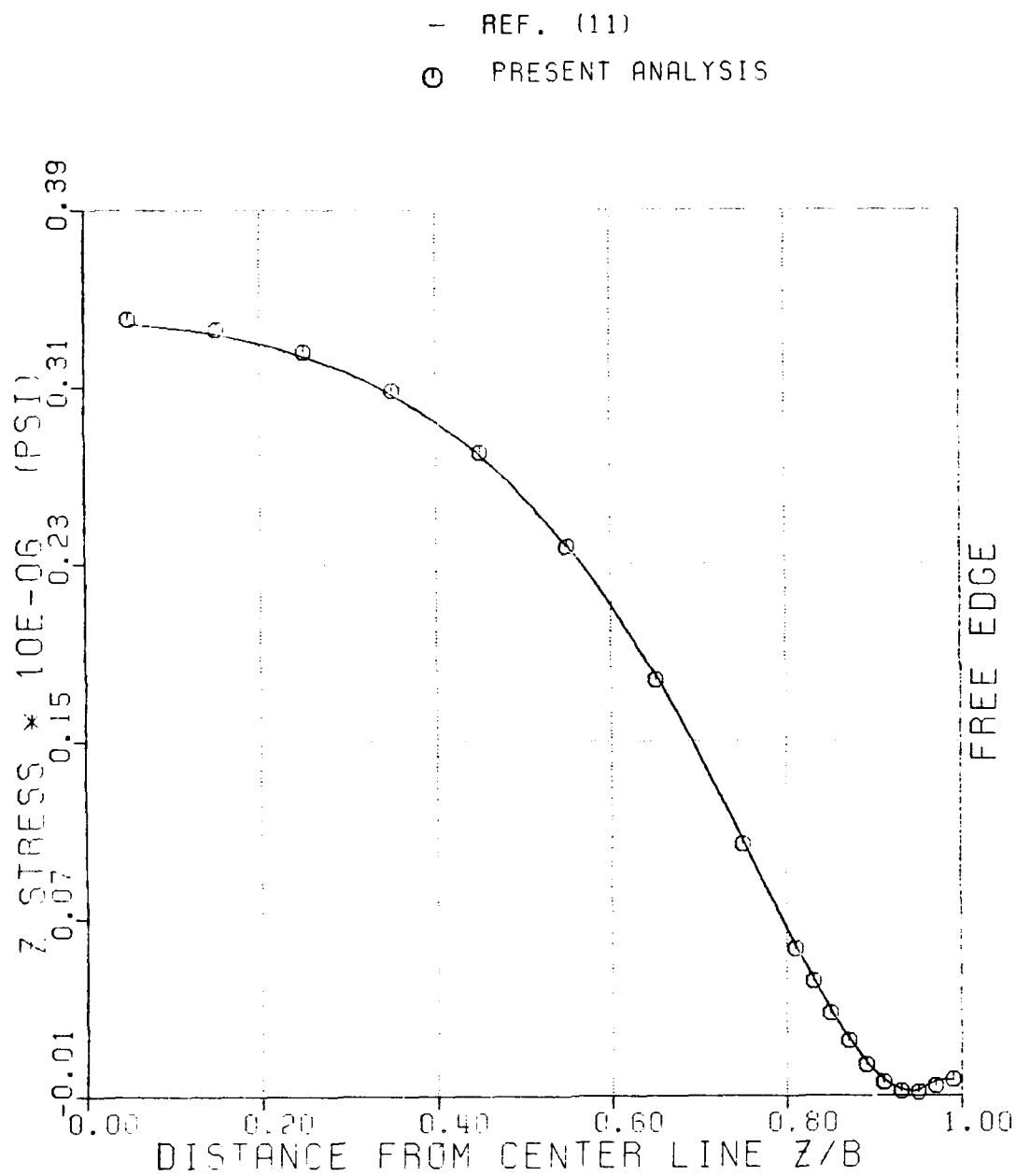
47

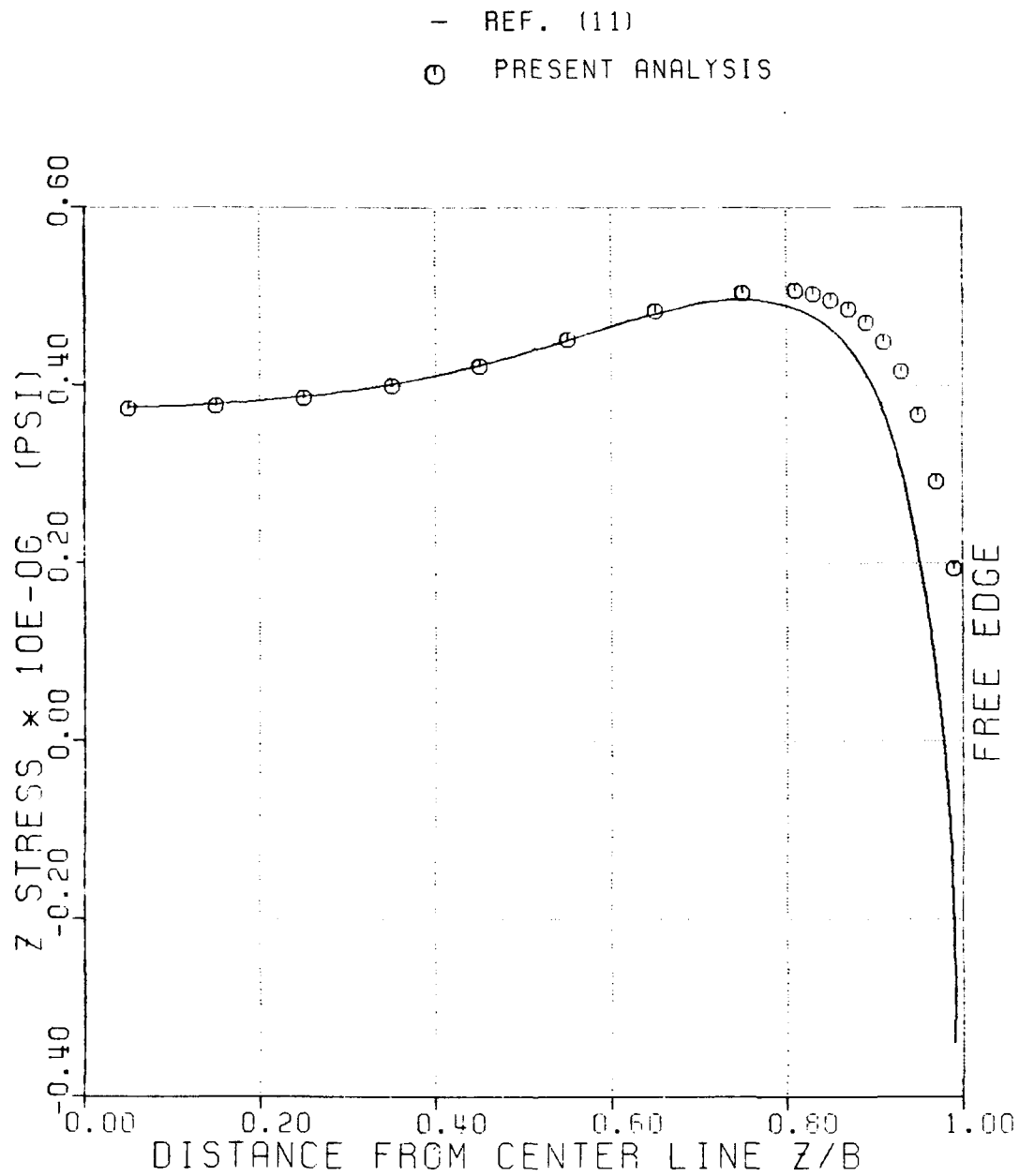Figure 20: Distribution of Z-Stress Along R1

of $[0/90]_s$ Laminate.

Figure 21: Distribution of Z-Stress Along R4 of [0/90]ₛ Laminate.

49
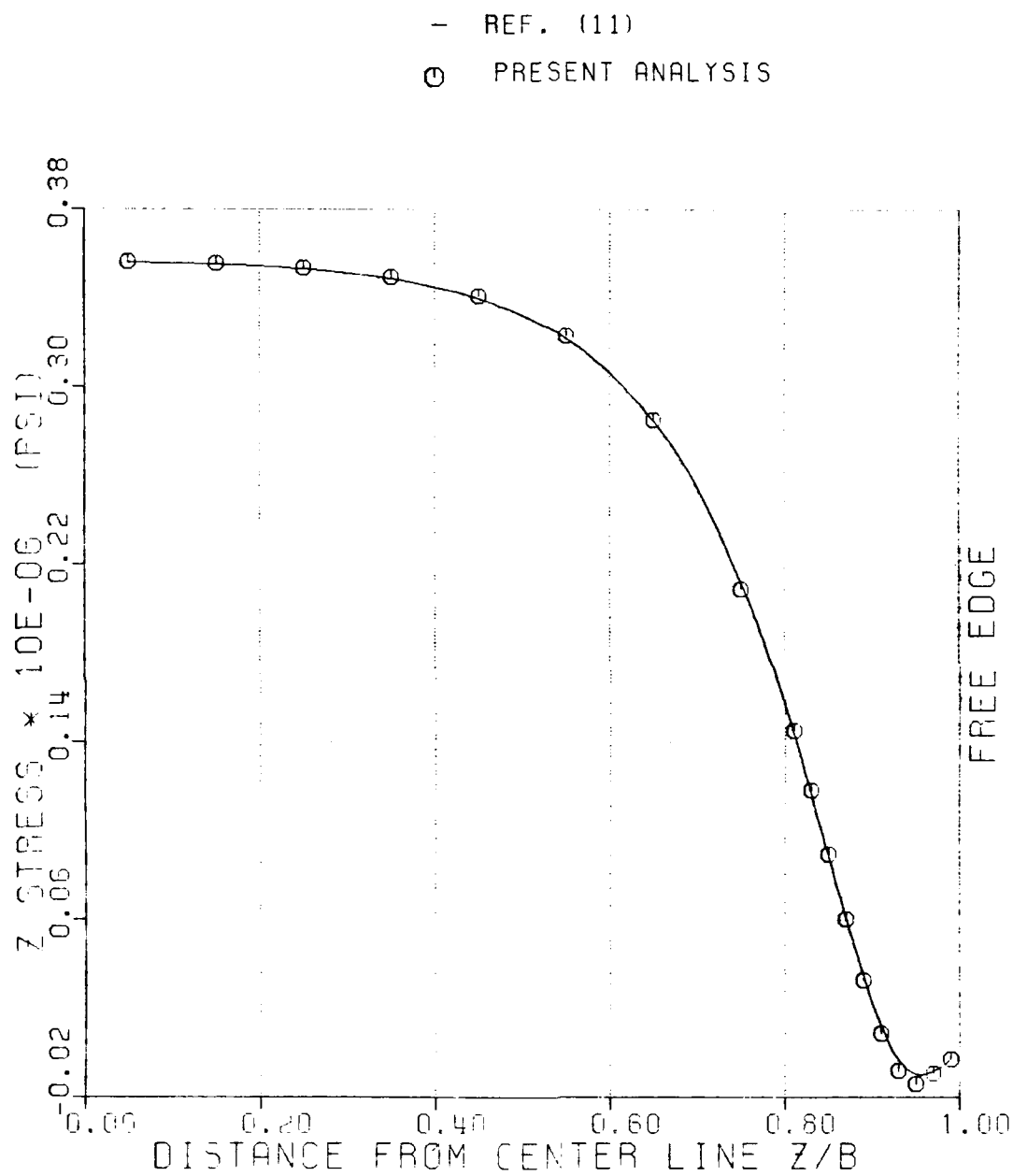
Figure 22: Distribution of Z-Stress Along R8

of [0/90]ₛ Laminate.

stress exists. Figure (23) shows the distribution of T-stress along R8. The figure indicates satisfactory agreement between the axisymmetric analysis and the Q23 element solution.

4.3.3 Angle-Ply Laminate

A ring specimen with fiber orientation $[45/-45]_s$ under uniform internal pressure was analyzed. Using the two axisymmetric analysis approaches, it was found that the introduction of the circumferential degree of freedom was necessary for modeling the complete state of strain and stress. The distribution of Z-stress along R1 and Rz-stress along R4, Figures (24) and (25) respectively, indicate that the two-dimensional analysis gave negligible stresses as compared to results obtained using the pseudo three-dimensional analysis. The Tr-stress had values of the order 10^6 psi in the pseudo three-dimensional analysis, comparable to the z, rz and r-stress components, while they were zero in the two-dimensional axisymmetric analysis. Figure (26) shows the distribution of Tz-stress along R1 and indicates that the two-dimensional analysis gave a practically constant variation of stress and did not satisfy the stress-free boundary condition at the free edge while the pseudo-three dimensional analysis did.
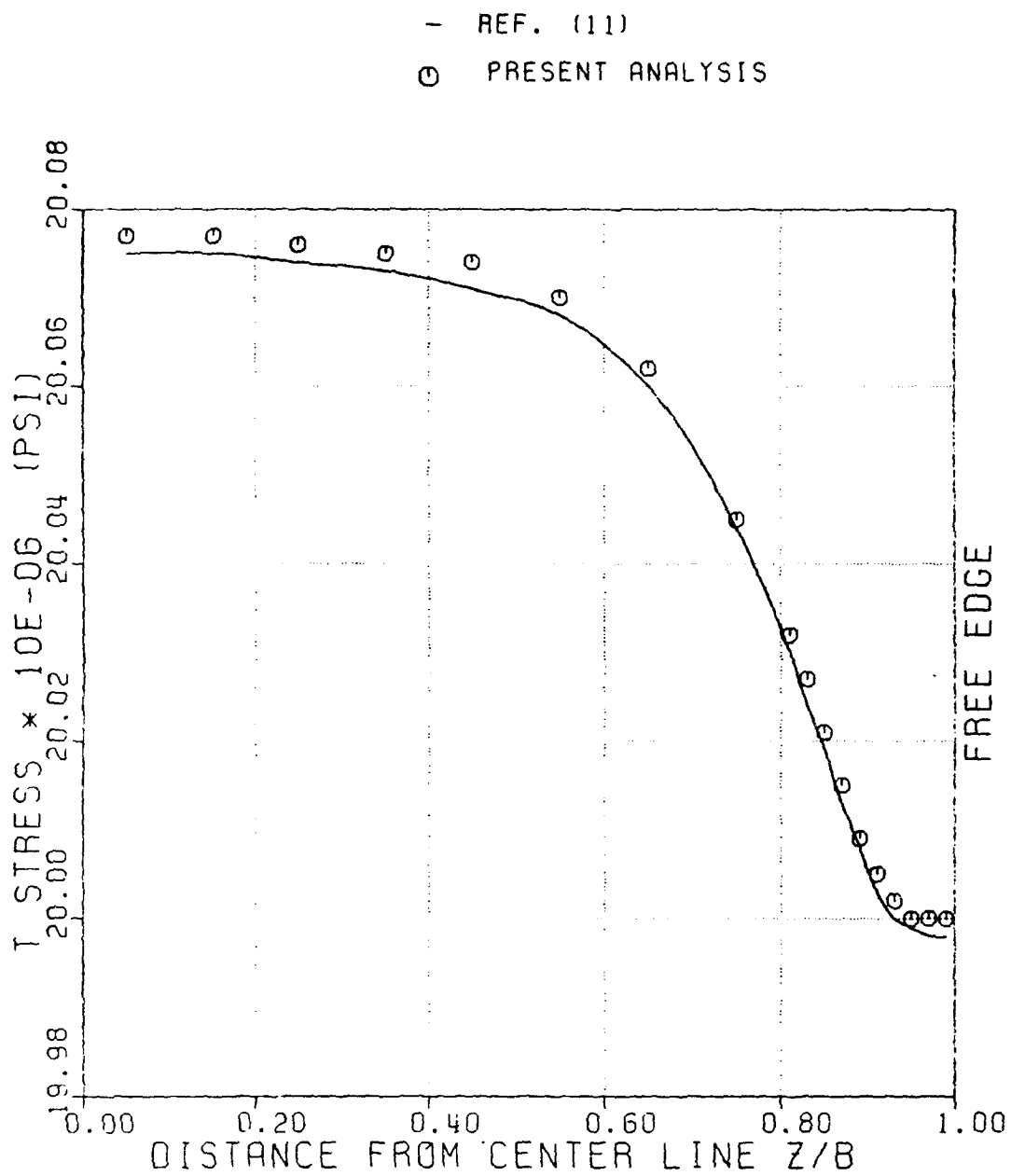
Figure 23: Distribution of T-Stress Along R8
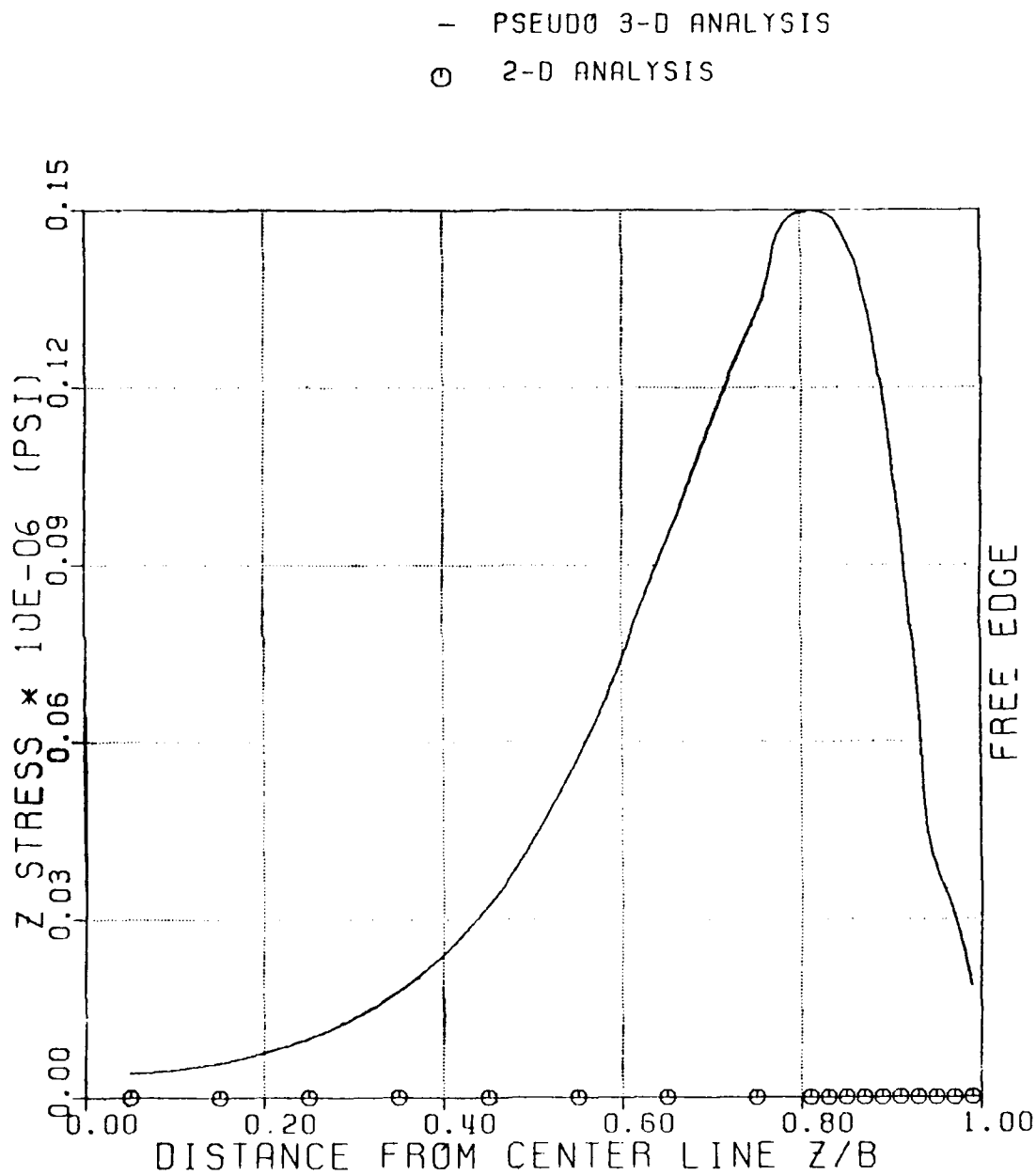
of [0/90]$_S$ Laminate.

52

Figure 24: Distribution of Z-Stress Along R1 of

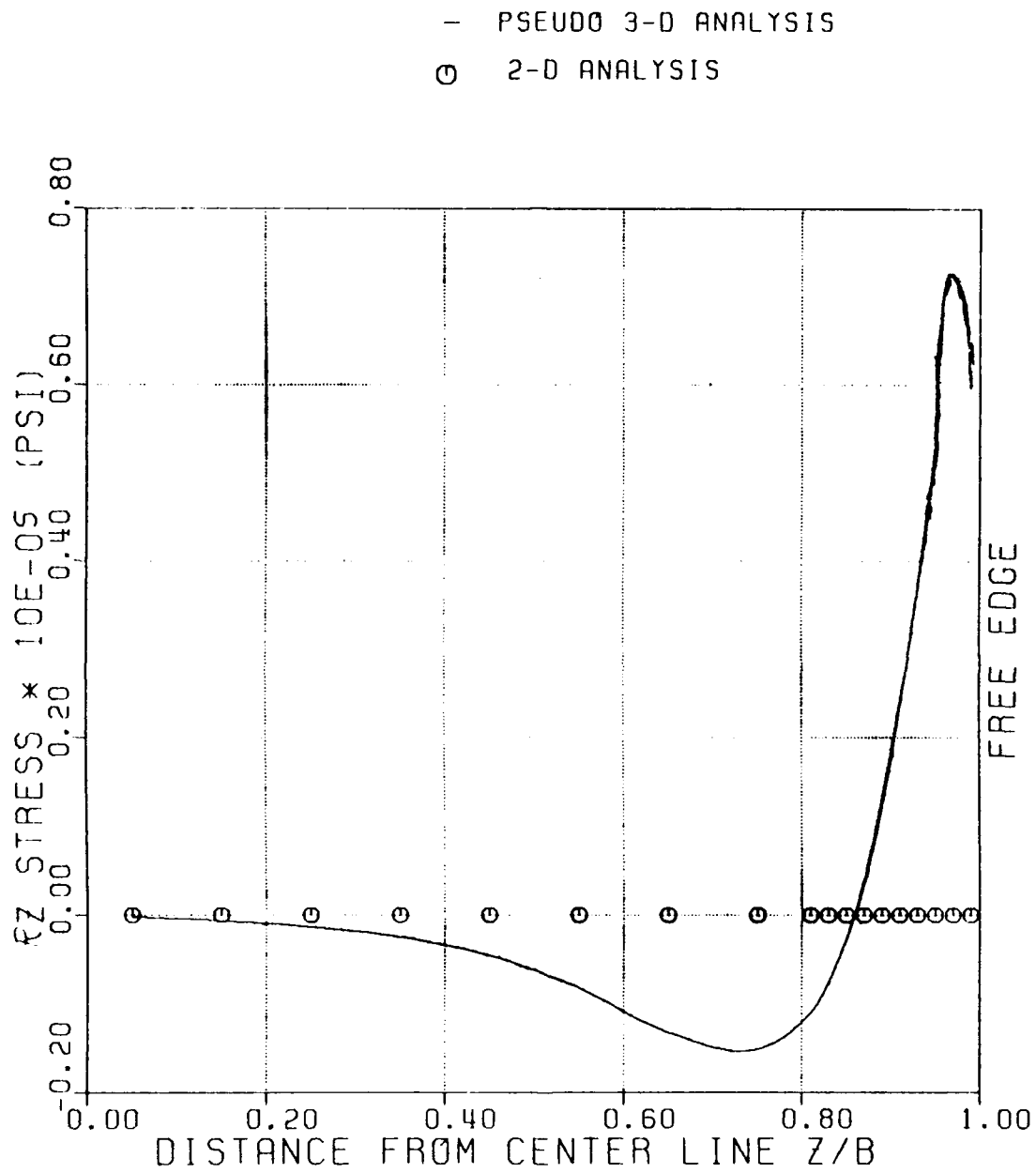[45/-45]$_s$ Laminate: 2-D and Pseudo 3-D Analysis

53

Figure 25: Distribution of Rz-Stress Along R4 of

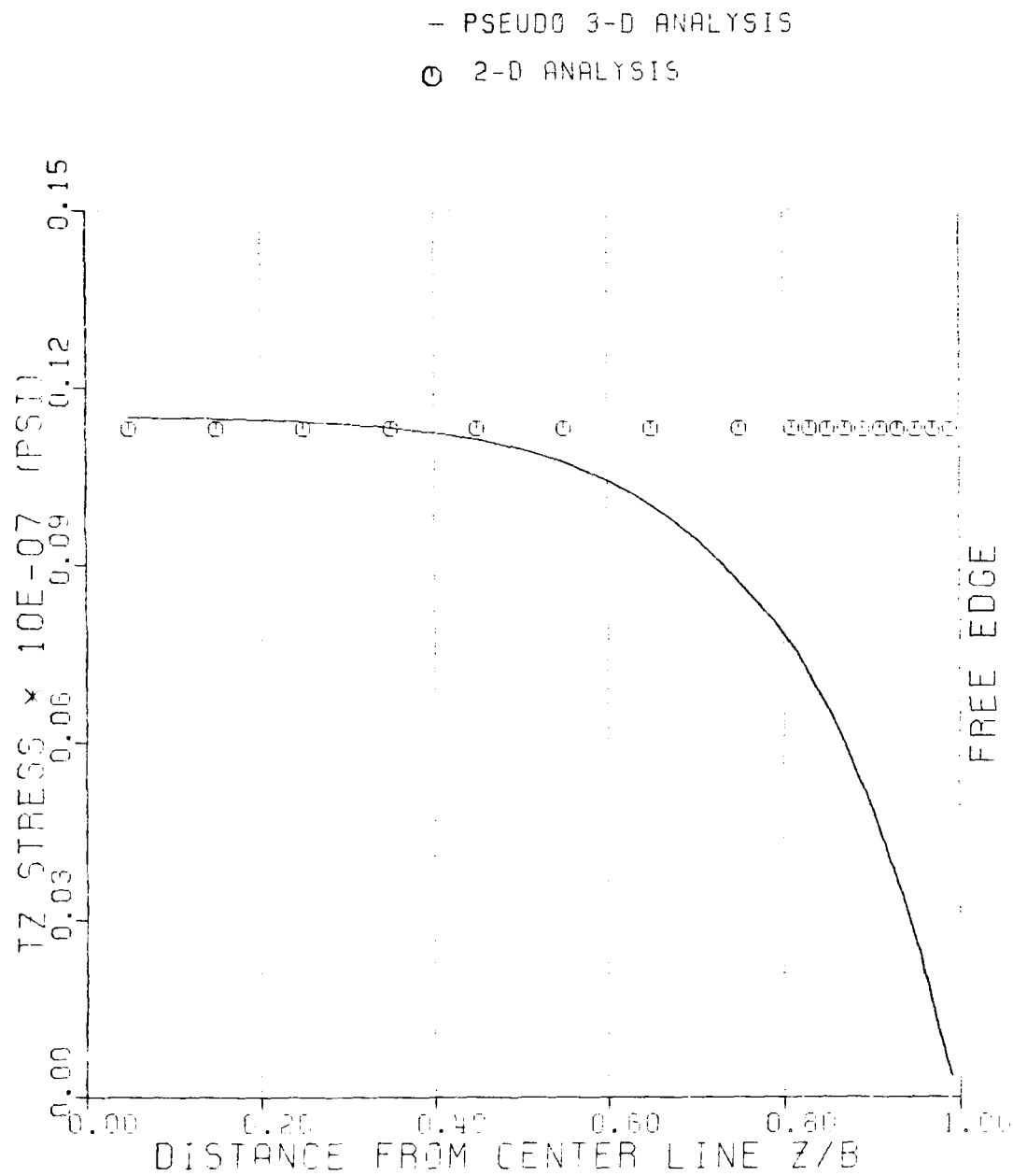$[45/-45]_s$ Laminate: 2-D and Pseudo 3-D Analysis

54

Figure 26: Distribution of Tz-Stress Along R1 of

$[45/-45]_s$ Laminate: 2-D and Pseudo 3-D Analysis

55

For angle-ply laminate, in contrast to the case of the cross-ply laminates with material axes parallel to the tangential plane, the symmetry about the Z = 0 plane does not exist. Both half-section and full-section of the ring specimen were analyzed using the same mesh and results were compared. Figures (27) and (28) show the distribution of Tz-stress and Z-stress along R1 for full and half section analysis. Even though the results agree near the free surface, the stresses near midsurface were quite different. Therefore, for analysis of angle-ply laminates, discretization of the full section is necessary.

Results for the pseudo-three-dimensional analysis were compared with the numerical solution obtained using Q23 element [11]. The same mesh size was used in both procedures. Figures (29) through (44) compare stress fields at specific locations for the $[45/-45]_s$ laminate using the Q23 and the present axisymmetric analysis. The mesh used was refined near the free edge. Each physical layer was subdivided into sublayers, the total number of sublayers is denoted by N. Full section was used for the axisymmetric analysis, corresponding to 288 (16x18), (N=16) mesh for half the section of the ring (i.e., the total number of elements used was 576). Figures (29), (30) and (31) show the distribution of Tz-stress along R1, R4 and R8 respectively. The results along R1 and R8 obtained using axisymmetric
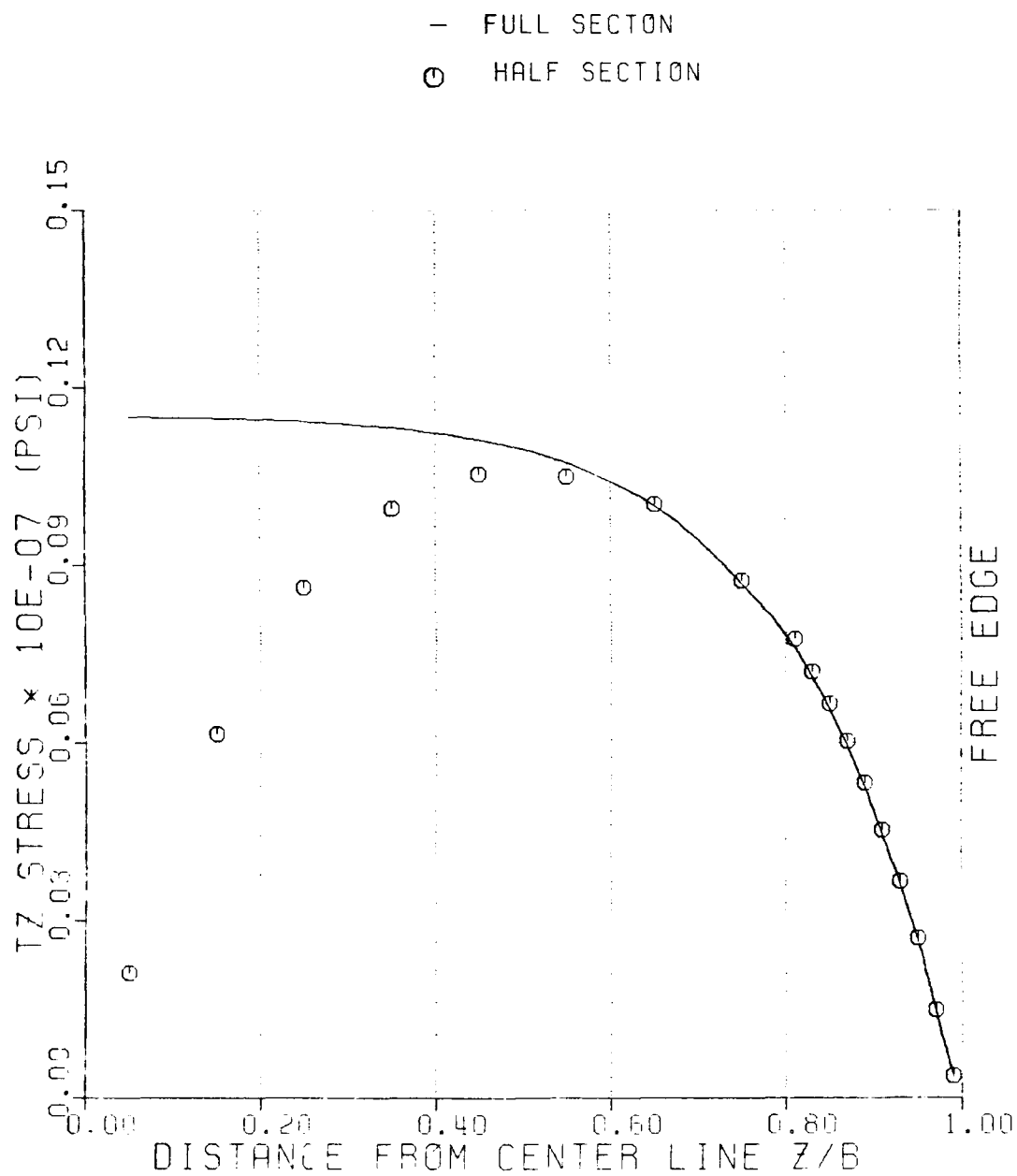
Figure 27: Distribution of Tz-Stress Along R1 of
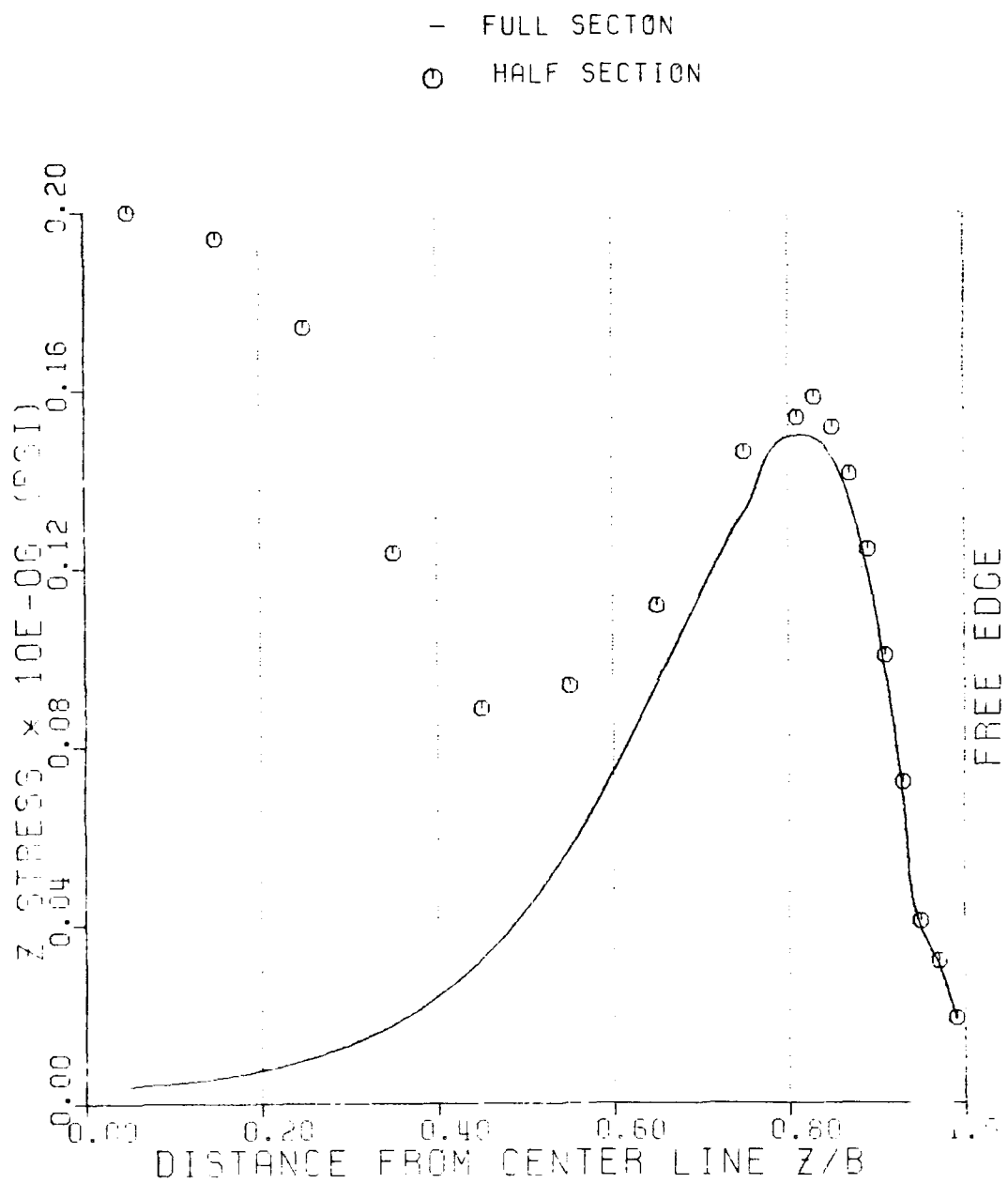[45/-45]$_s$: Full and Half Section Analysis

57

Figure 28: Distribution of Z-Stress Along R1 of
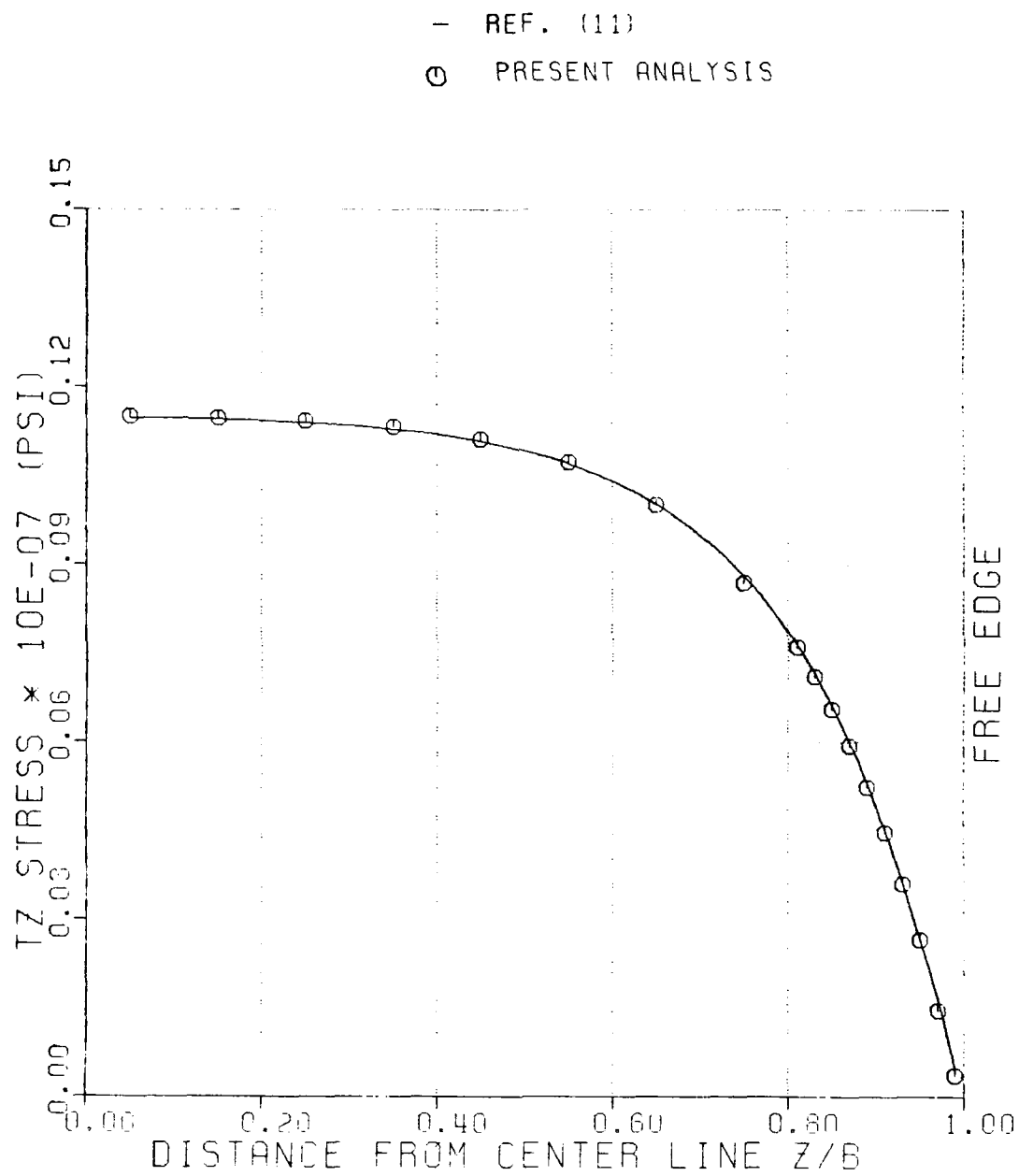
[45/-45]$_s$: Full and Half Section Analysis

58

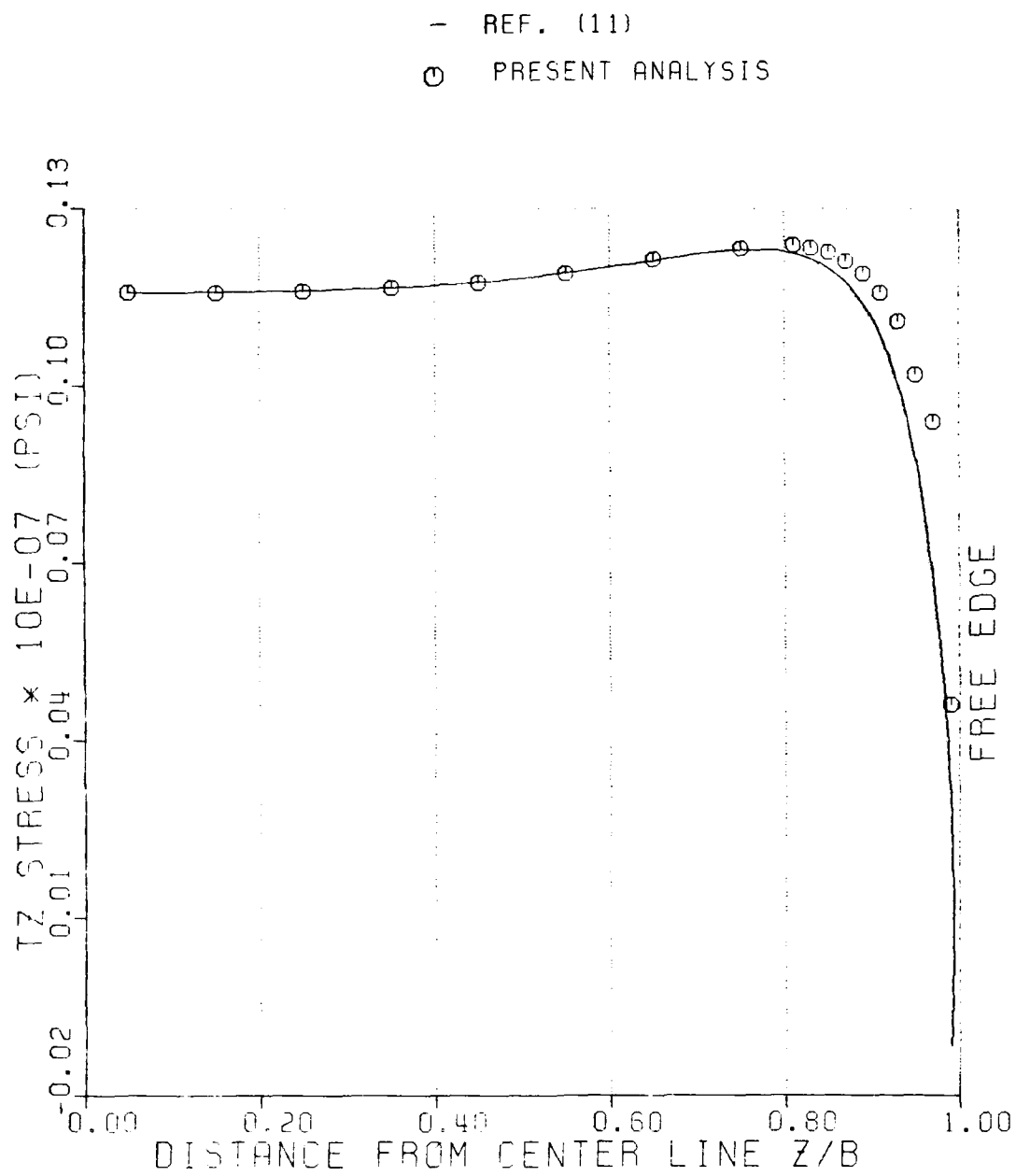Figure 29: Distribution of Tz-Stress Along R1

of [45/-45]$_s$ Laminate.

Figure 30: Distribution of Tz-Stress Along R4
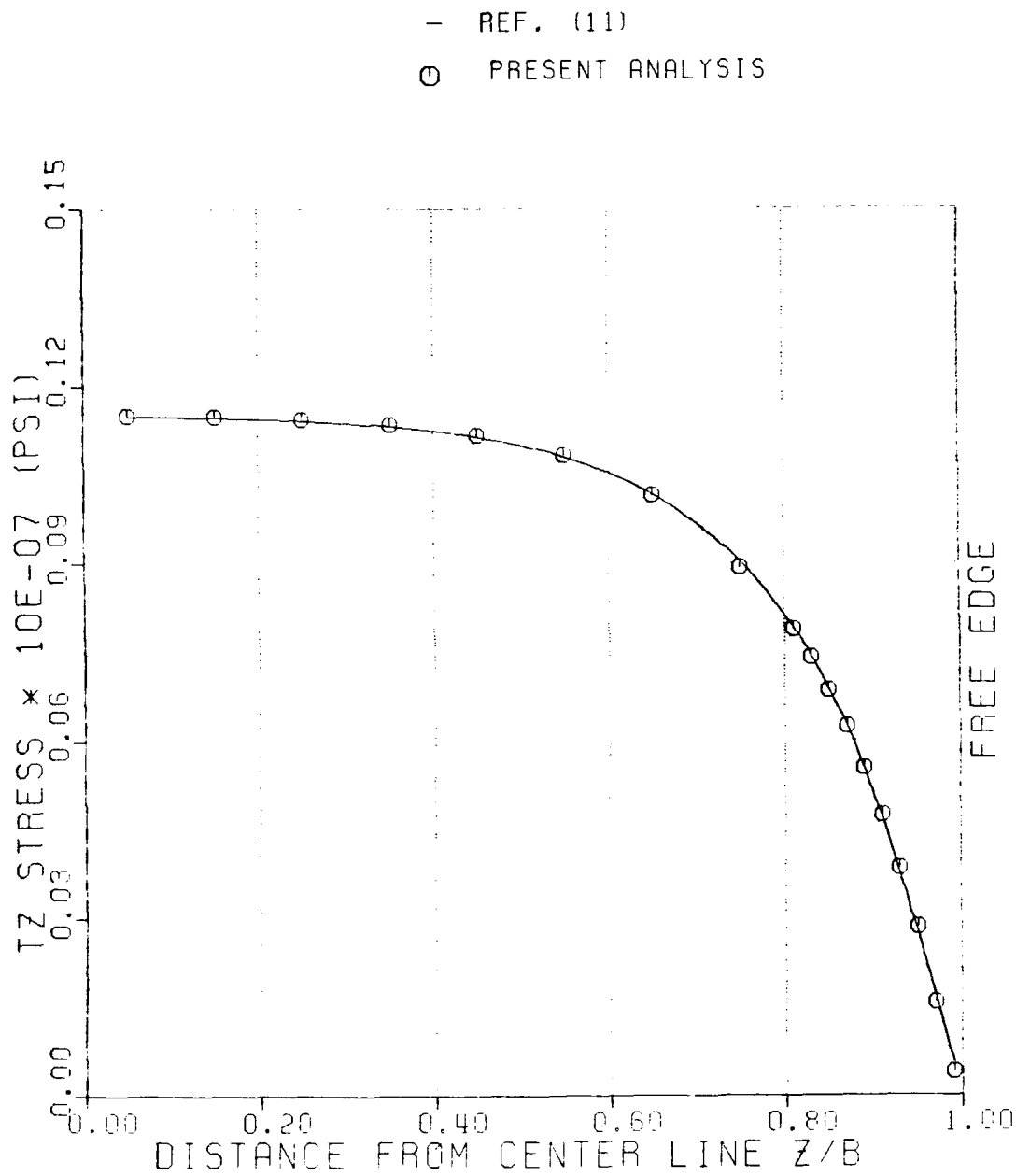
of [45/-45]$_s$ Laminate

60

Figure 31: Distribution of Tz-Stress Along R8
of $[45/-45]_s$ Laminate

61

analysis agreed well with Q23 element solution across the entire width of the laminate. The distribution of other stress components along R1 were also in satisfactory agreement with Q23 element solution. A difference in the stress distribution along R4 is observed near the free edge where a steeply varying stress exists.

A comparison of the TR-shear stress distribution along R4 (Figure (32)) indicated that the axisymmetric analysis solution had sharp rise toward the free edge similar to Q23 solution. Satisfactory agreement was observed between these two solutions for stress across the width except at the free-edge boundary where axisymmetric analysis overestimated the stress values as compared to Q23. Figure (33) shows the distribution of TR-stress along R8. The results agreed well except near the free edge. This could be due to the finite element mesh not being fine enough to approximate the steeply varying stress near the free corner. Figure (34) shows through-thickness distribution of TR-stress near the free edge (at Z/B=0.99). Singular behavior of TR-stress which is highly localized near the interface of 45/-45 layers is noticeable. The axisymmetric analysis gave higher value of stresses than the Q23 element in the vicinity of the interface. Distribution of R-stress along R4 is shown in
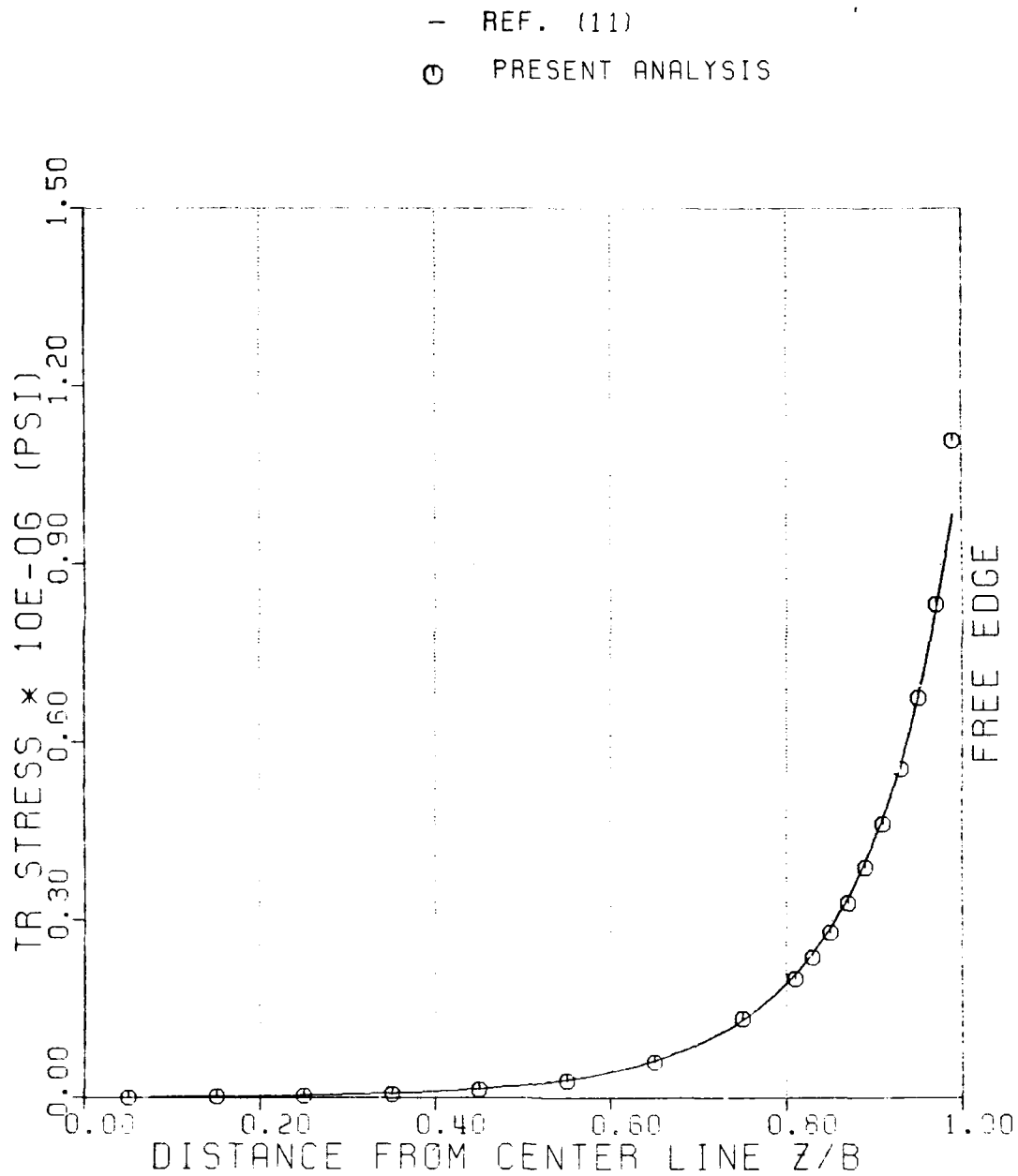
Figure 32: Distribution of TR-Stress Along R4
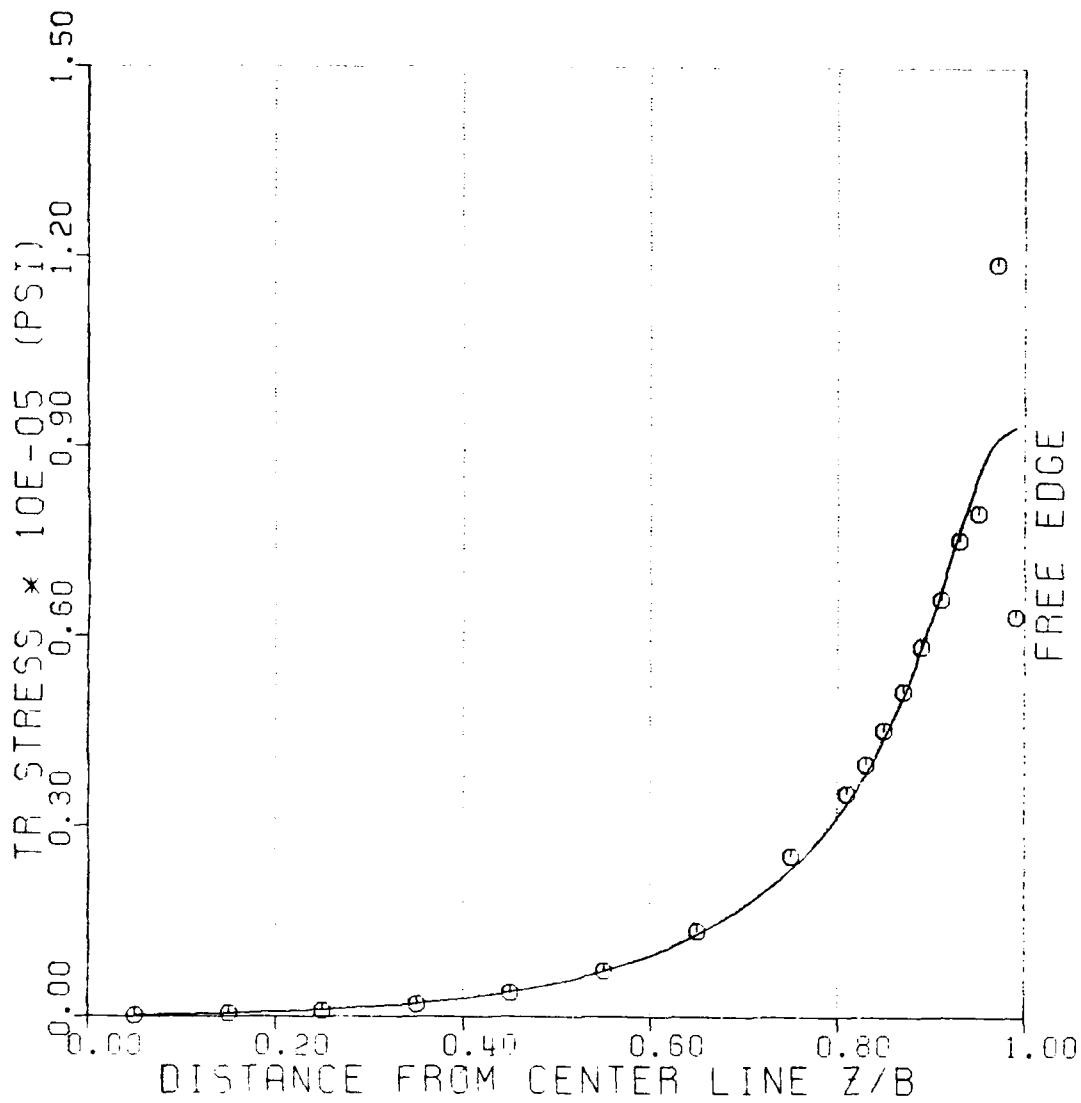
of $[45/-45]_s$ Laminate

63

Figure 33: Distribution of TR-Stress Along R8

of [45/-45]$_s$ Laminate

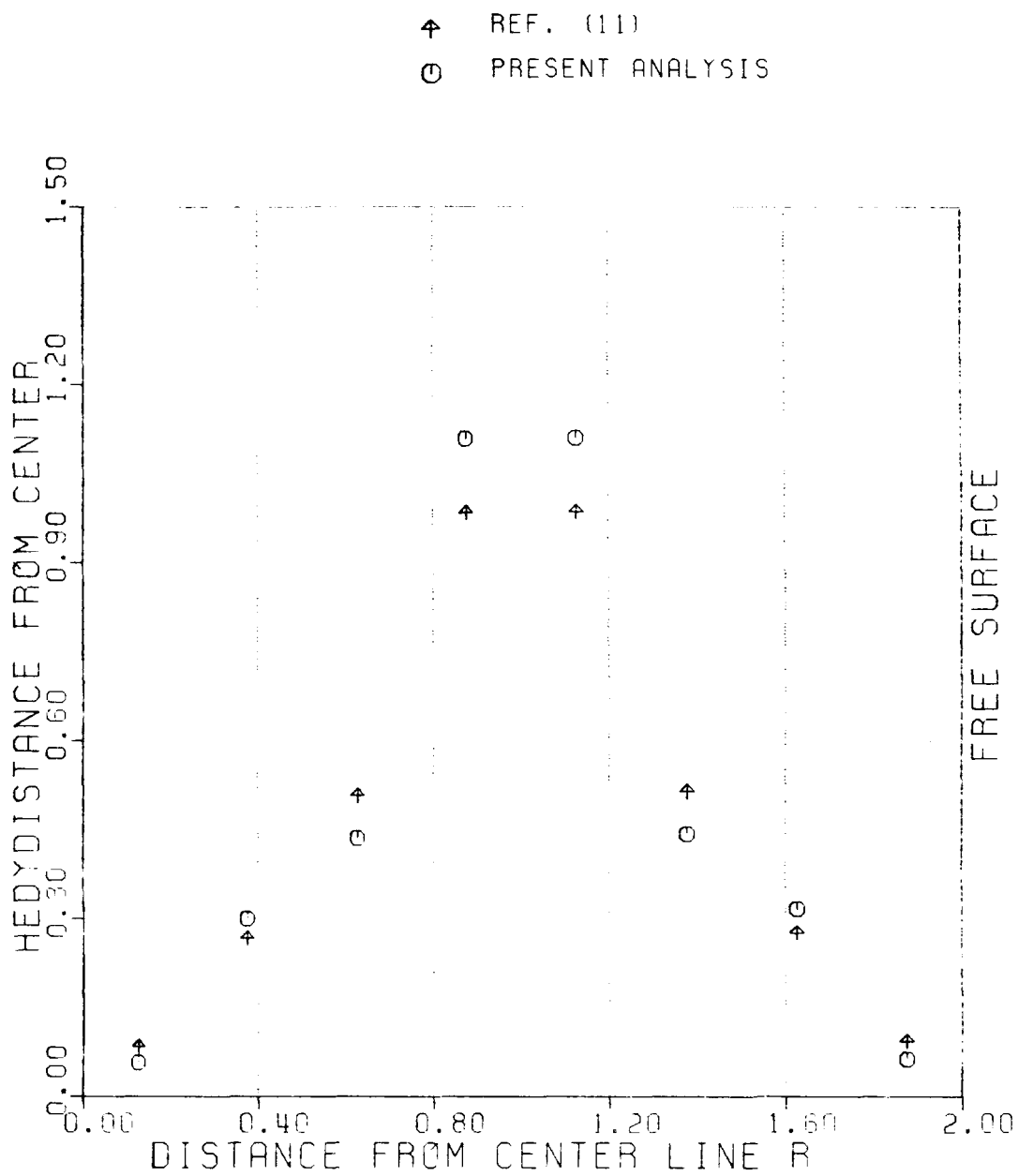Figure 34: Through-Thickness Distribution of TR-
Stress Near Free edge (Z/B=0.99) of
[45/-45]$_s$ Laminate. Q23 and axisymmetric

Figure (35). The results showed reasonable agreement with those obtained using Q23 element. Through-thickness distribution of R-stress near the free edge (Figure (36)) shows a steeply varying stress distribution in the vicinity of the interface of 45/-45 layers.

Figure (37) shows the distribution of Rz-stress along k4. A very close agreement was generally observed between solutions except at the last value near the free edge where a steeply varying stress exists. Figure (38) shows through-thickness distribution of Rz-stress at Z/B=0.99. A steeply varying stress distribution associated with abrupt change of material properties is also observed in the vicinity of the interface of 45/-45 layers. However, the axisymmetric analysis gave a lower, as compared to Q23 analysis, estimate of the stresses near the interface. A discrepancy in the distribution of Z-stress along R4 and R8, between the two procedures, near the free edge is observed in Figures (39) and (40).

Distribution of T-stress along R8 is shown in Figure (41). Contrary to the T-strain distribution, the T-stress distribution is not uniform along a sublayer. This is because it depends on r, z, Tz and T-strains. Figures (42-44) show the distributions of r, z, and Tz-strains near the free surface of the coupon.
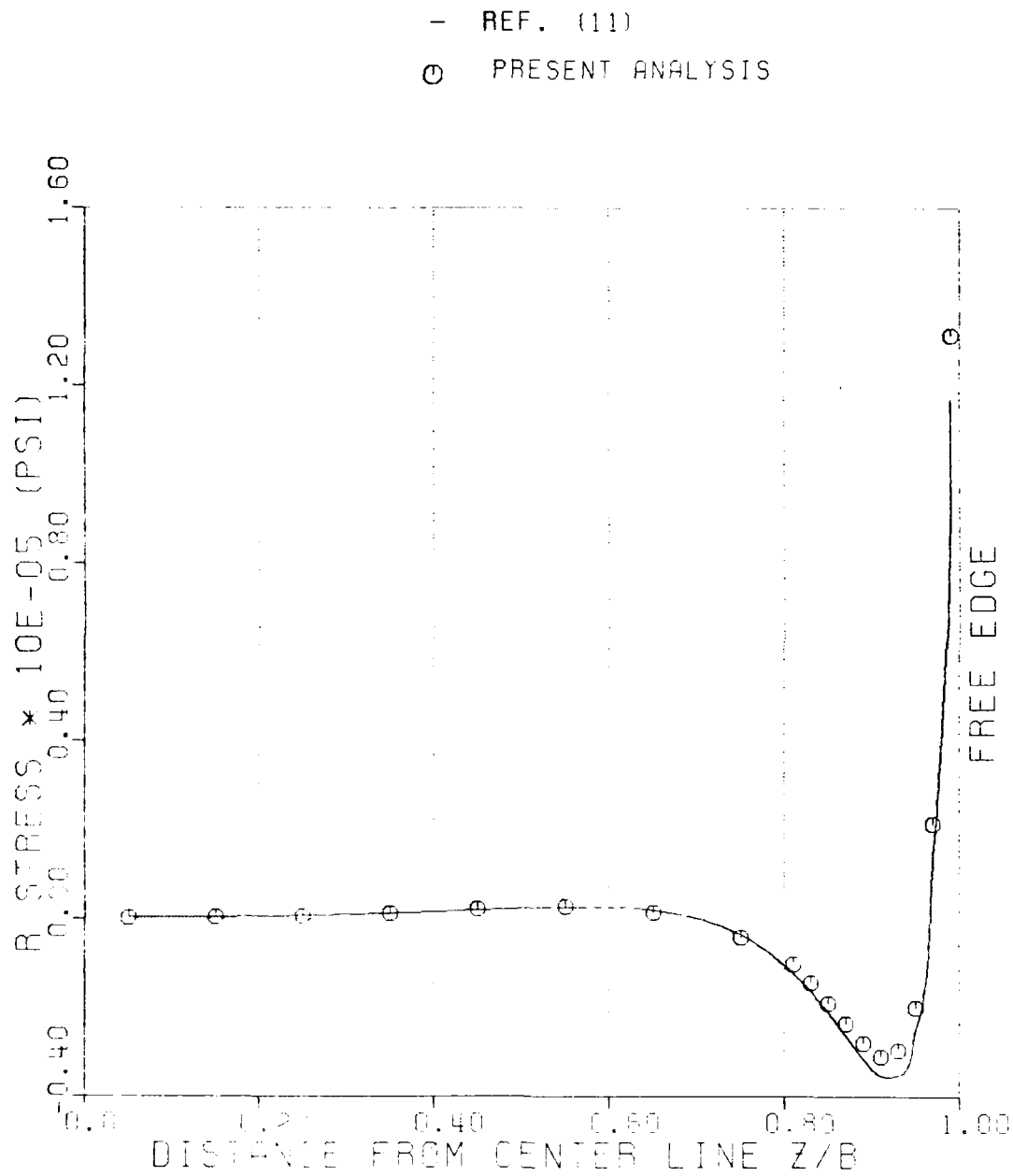
66

Figure 35: Distribution of R-Stress Along R4

of [45/-45]$_s$ Laminate

Figure 36: Through-Thickness Distribution of
R-Stress Near Free edge (Z/B=0.99)
of [45/-45]$_s$ Laminate

68
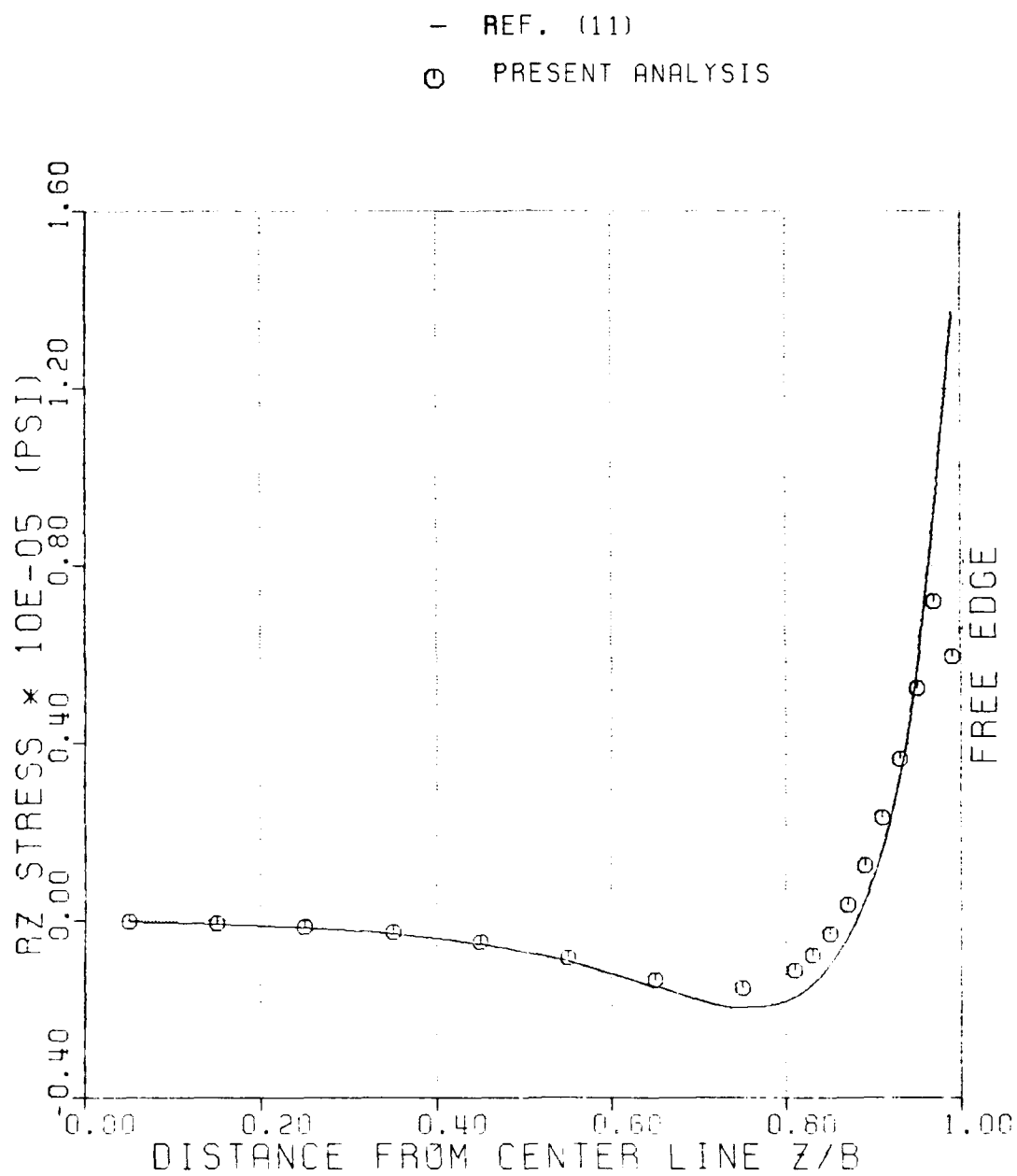
Figure 37: Distribution of Rz-Stress Along R4

of $[45/-45]_s$ Laminate

69
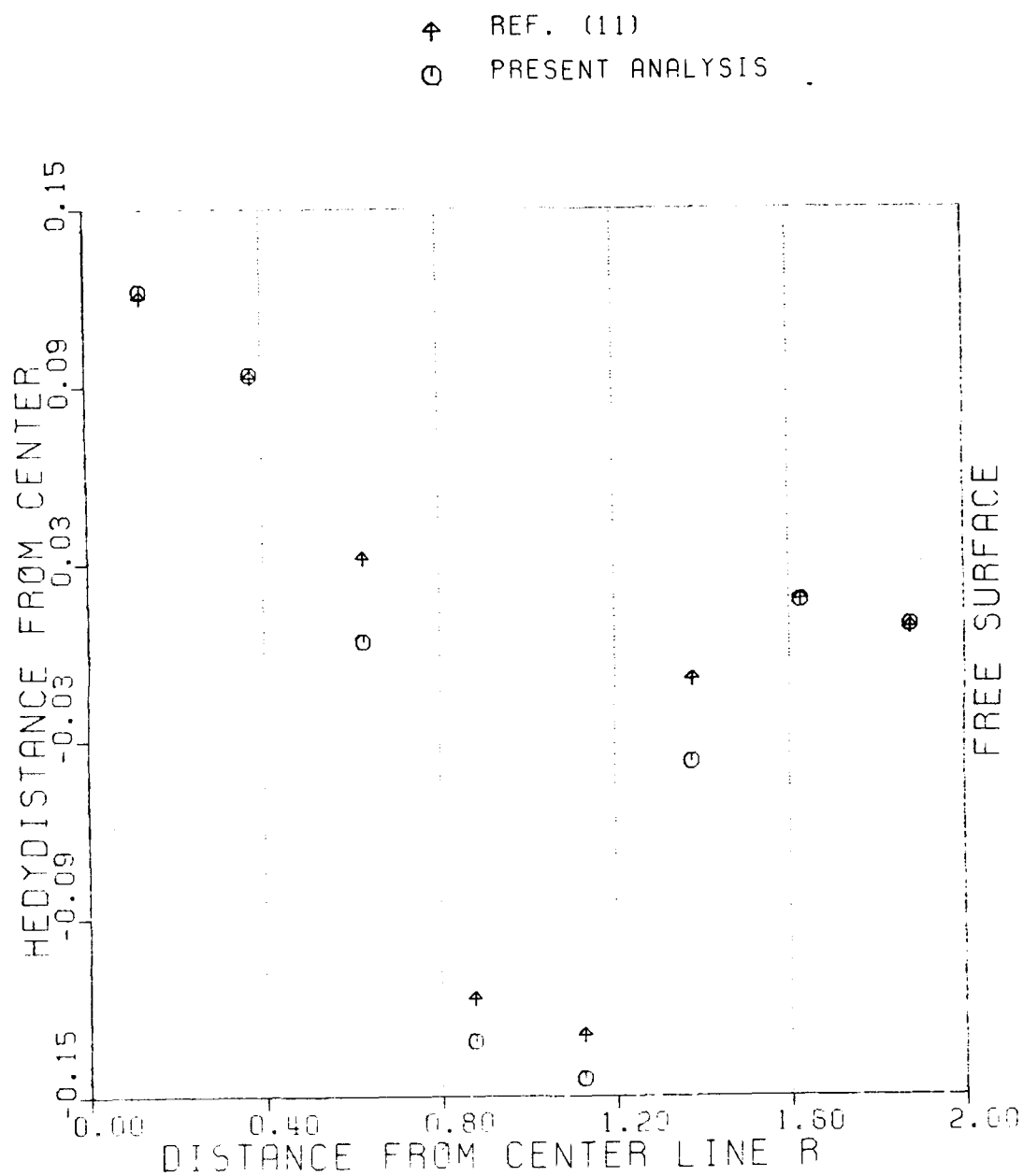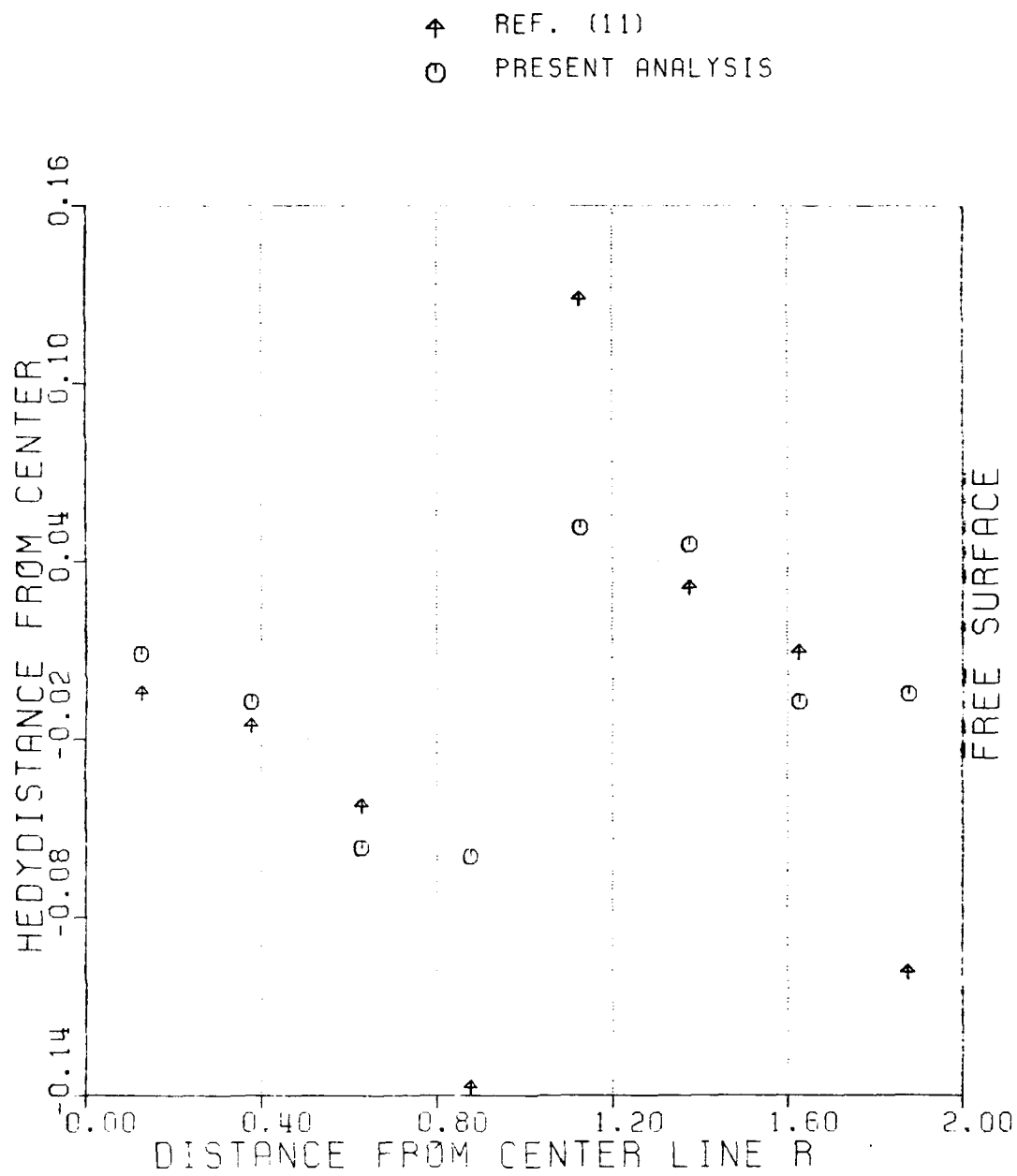
Figure 38: Through-Thickness Distribution of Rz-
Stress Near Free edge (Z/B=0.99)
of [45/-45]$_s$ Laminate

70
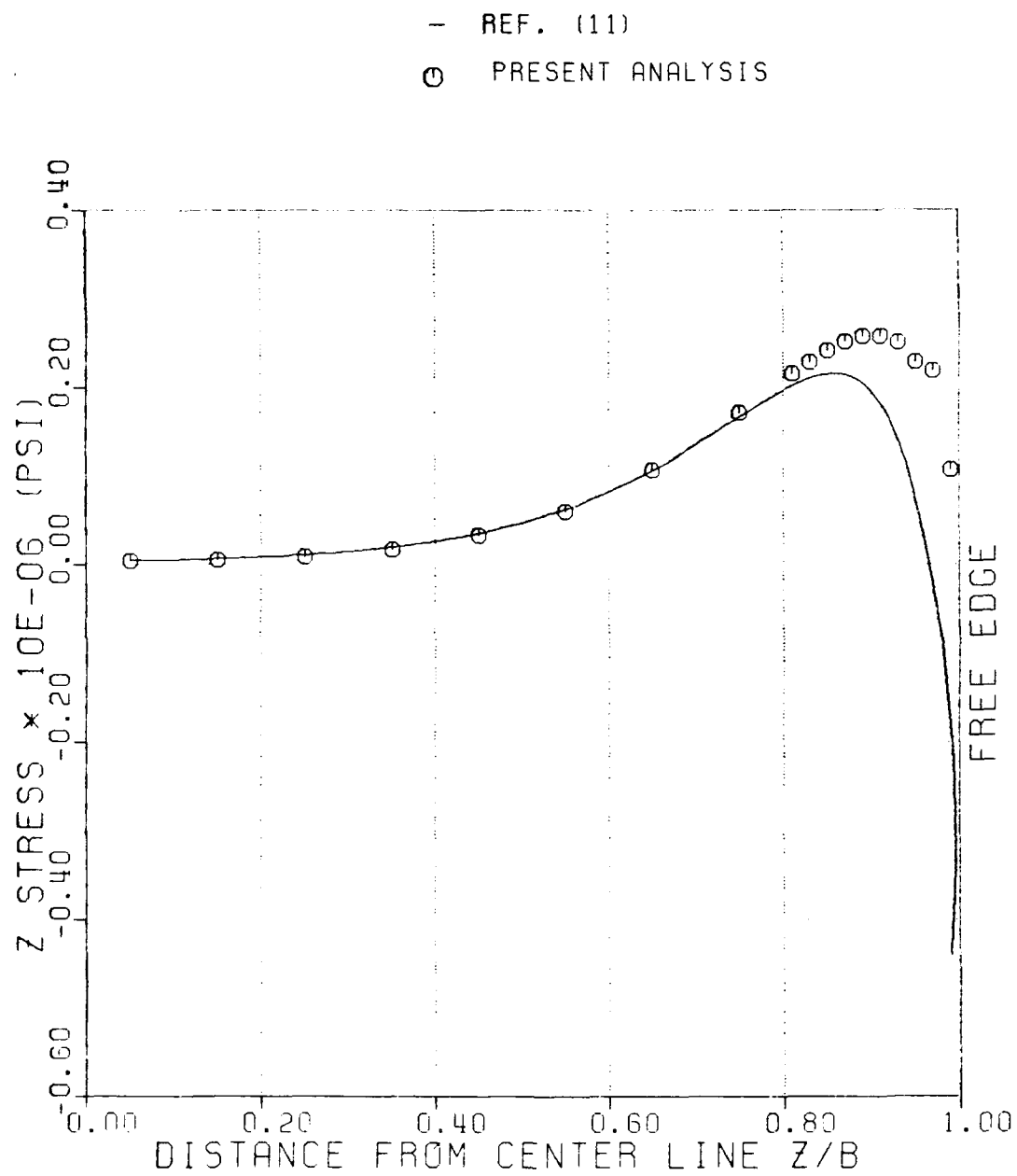
Figure 39: Distribution of Z-Stress Along R4

of [45/-45]$_s$ Laminate

Figure 40: Distribution of Z-Stress Along R8

of [45/-45]$_s$ Laminate

72

Figure 41: Distribution of T-Stress Along R8

of $[45/-45]_s$ Laminate

73

* PRESENT ANALYSIS

Figure 42: Distribution of R-Strain Along R8

of [45/-45]$_s$ Laminate

74

* PRESENT ANALYSIS

Figure 43: Distribution of Z-Strain Along R8

of [45/-45]$_s$ Laminate

75

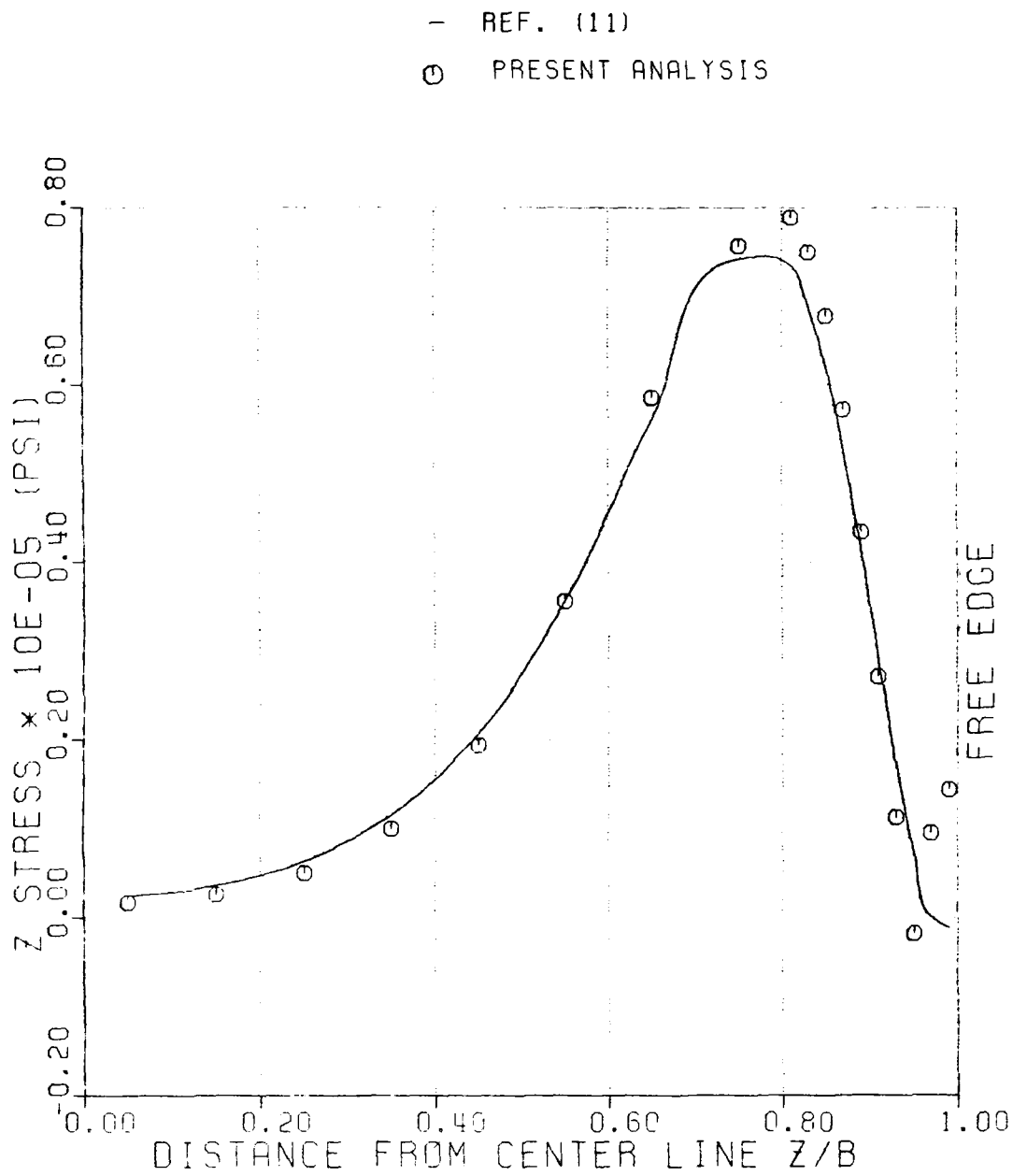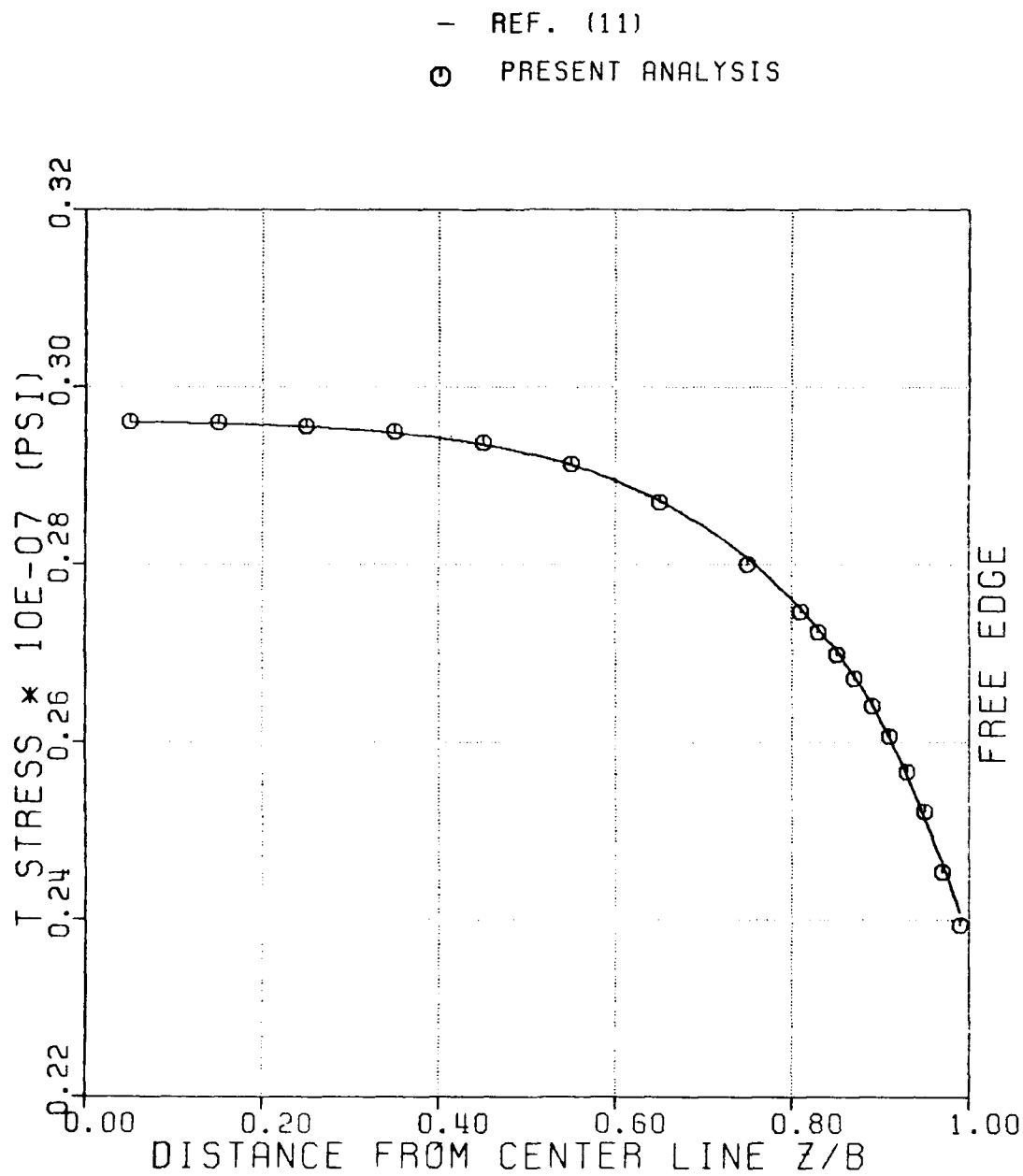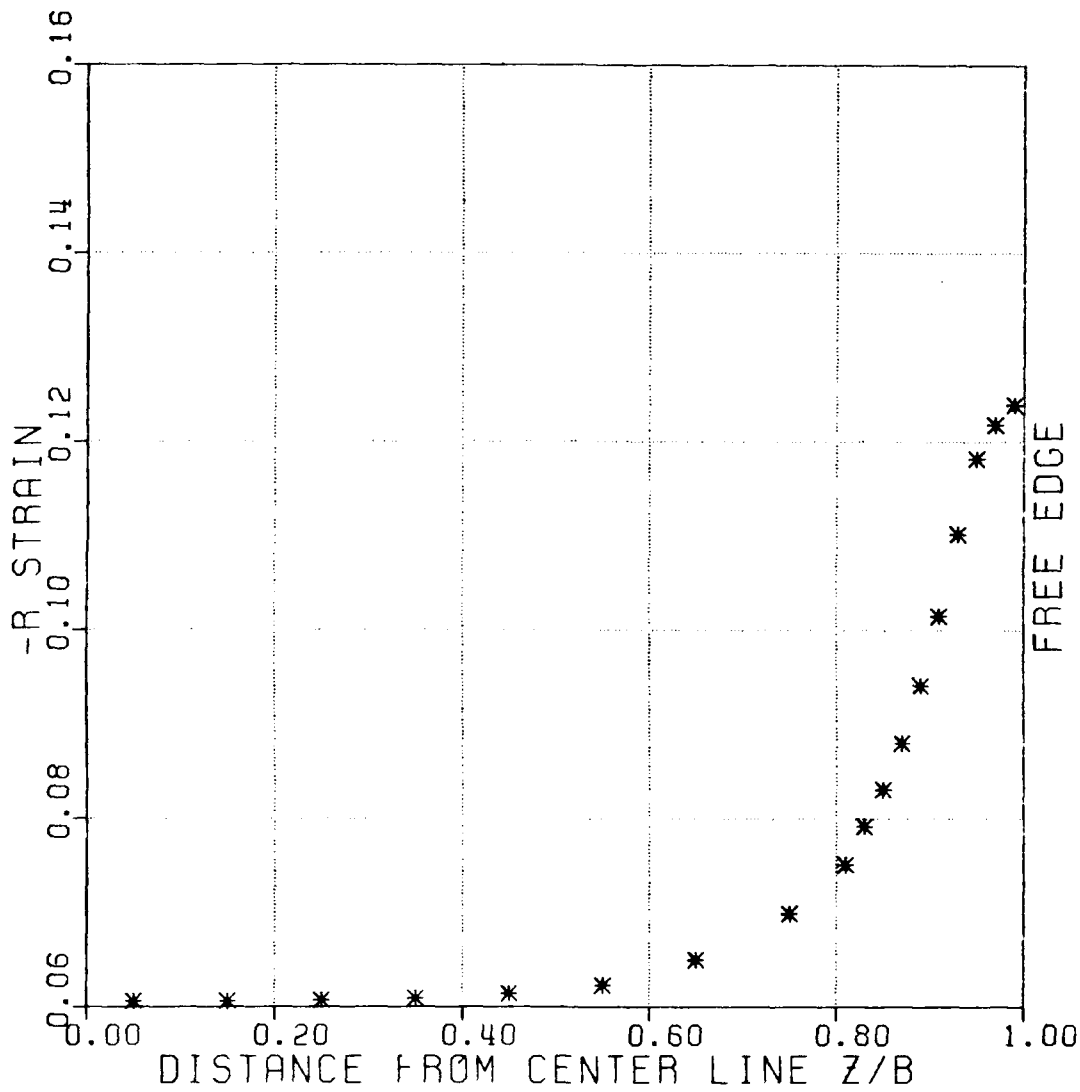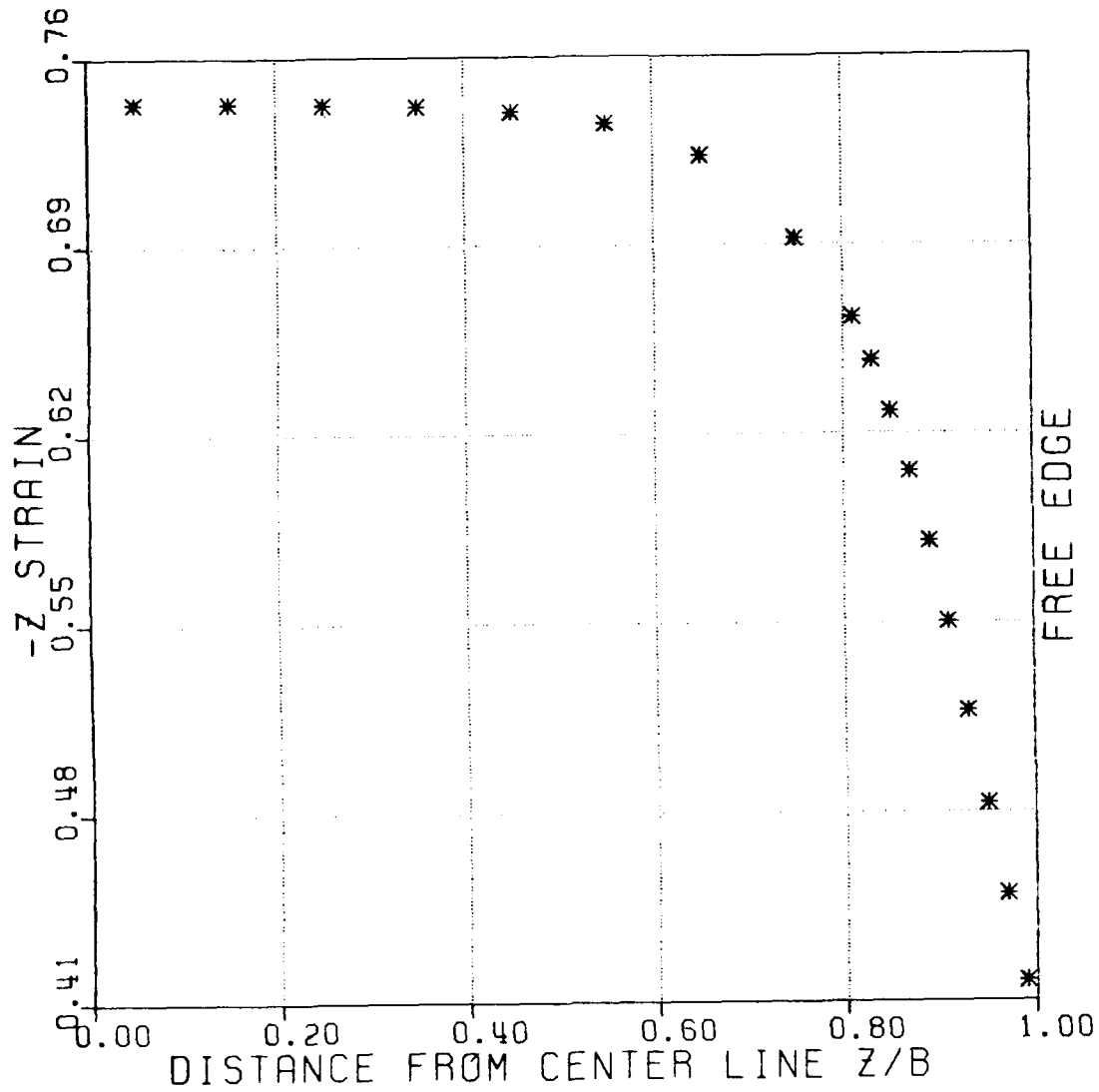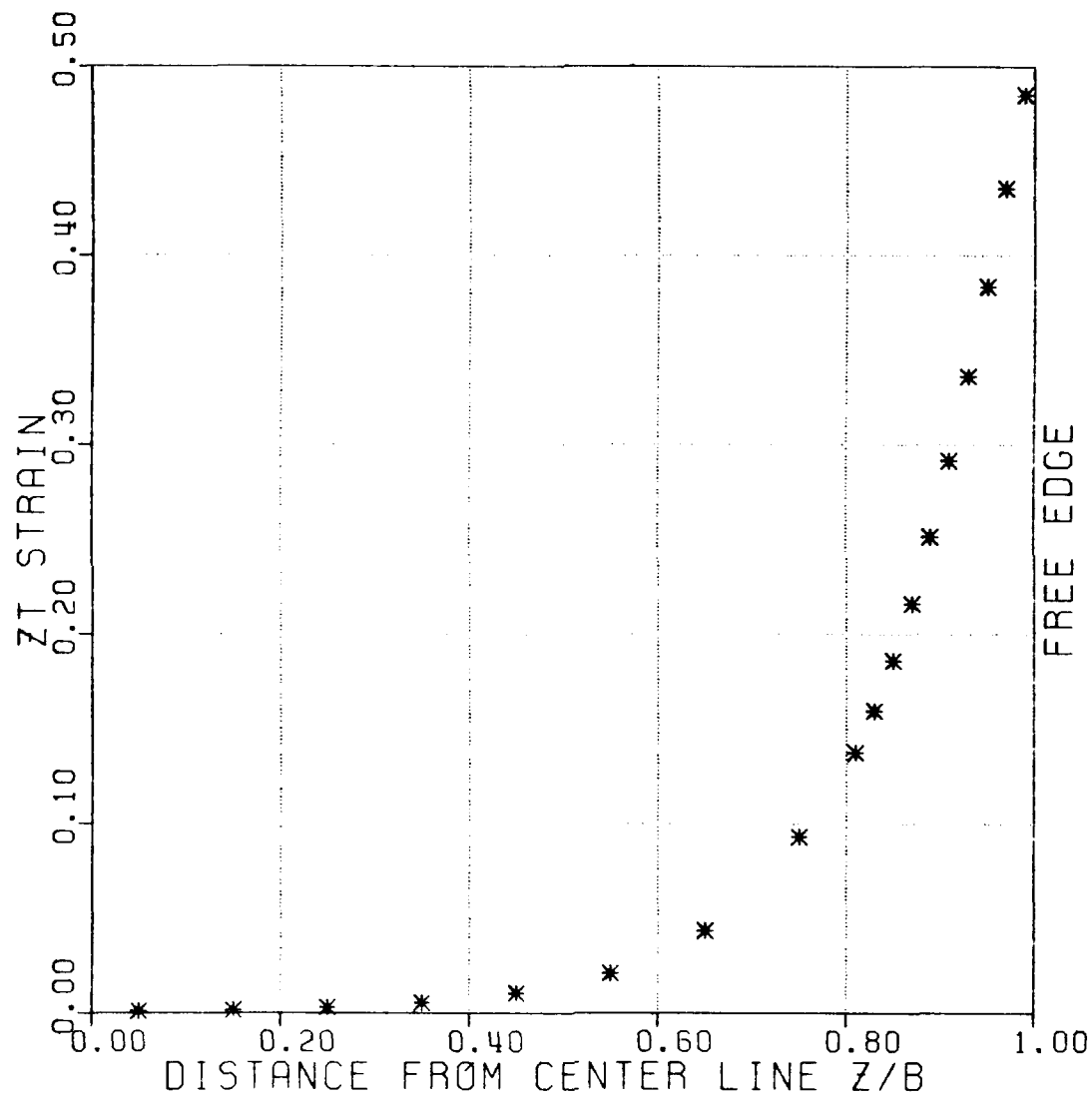Figure 44: Distribution of TZ-Strain Along R8

of [45/-45]$_s$ Laminate

76

4.3.4 Effect Of Mesh Refinement

Analysis of the four-ply laminate was done in this study using a 288-element model for half section analysis, locally refined near the free edge in the Z-direction. To study the effect of local mesh refinement near the free edge on the solutions, comparisons were made for the stress distributions in the four-ply laminate specimen between results from a uniform 160-element model shown in Figure (45) and those from a locally refined 288-element model. The 288-element, Figure (4), model was obtained by dividing the two elements closest to the free edge in the 160-element model into 10 elements along the Z-direction. Refinement for both the cross-ply and the angle-ply specimens were studied.

Figure (46) shows the distribution of R-stress along R5 near the interface of 0/90 layers. It is clear that the singular stress behavior near the free-edge was reproduced more closely by the 288-element model and did not show well in the results based on the 160-element mesh. Therefore, a finite element mesh refined in regions of steeply varying stresses is necessary.

Further refinement in the Z-direction was considered in order to study the effect of mesh refinement on some stress distributions where poor results were observed. A more
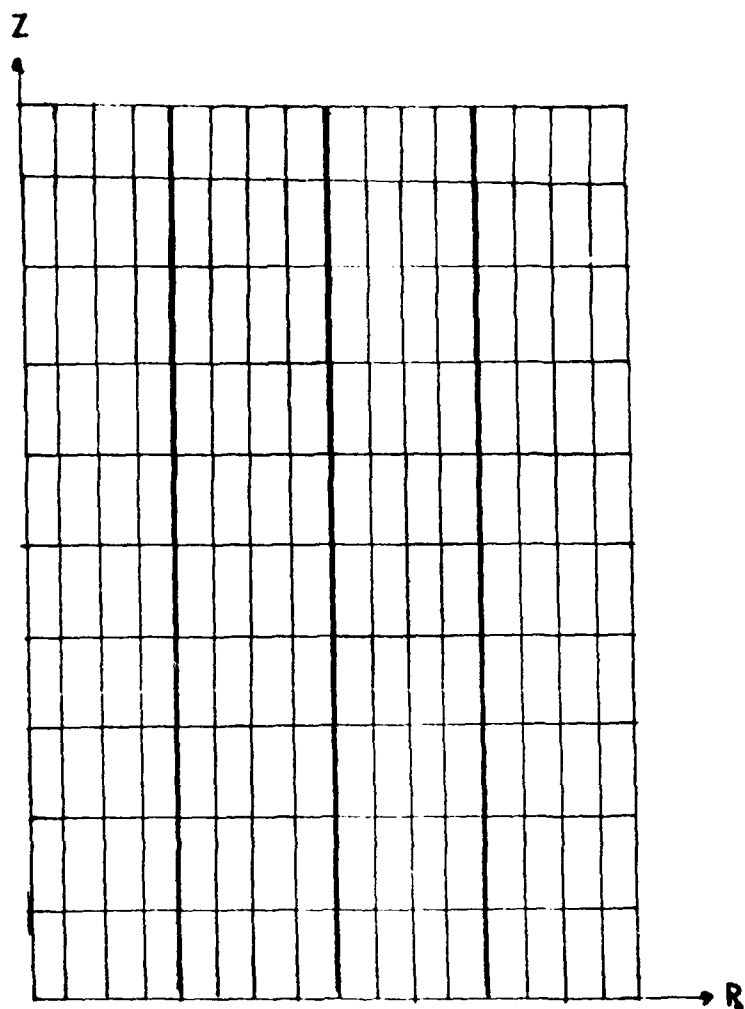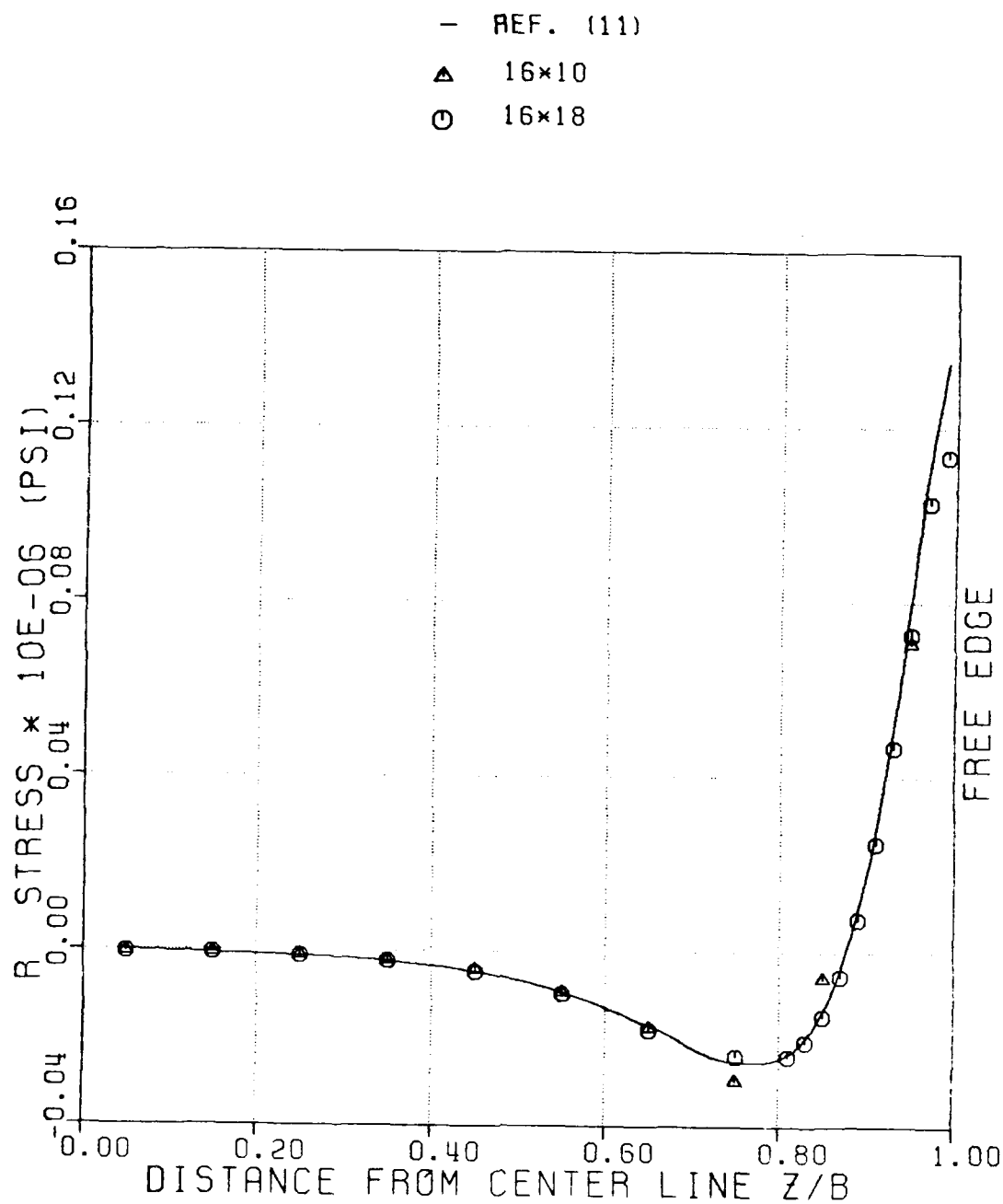
Z

R

Figure 45: 160 Element Model (16x10)

Figure 46: Effect of Mesh Refinement on Distribution
of R-Stress Along R5 of [0/90]$_s$ Laminate

79

refined mesh, 416 elements (16x26) for half section analysis, obtained by further dividing the two elements closest to the free edge in the 288-element model (16x18) into 10 elements, was used. Results from the axisymmetric analysis were compared with the Q23 element solutions obtained using the original mesh size which corresponds to the (16x18) elements model. Figure (47) indicates the improvement in the distribution of Rz-stress along R5 specially near the free edge where the traction-free boundary condition was better reproduced by the finer mesh. The distribution of Z-stress along R4 is shown in Figure (48). Refinement did not make any noticeable difference to the distribution. The only improvement was that values of stresses closer to the free edge were available. Figures (49), (50) show the distribution of R-stress at R7 and R8. Refinement of the mesh near the free edge did not have much influence on the calculated values of the stress components. The oscillatory variation in the stress component near the free edge is present in all the analyses.

The effect of mesh refinement on the distribution of Tz, Rz and Z-stresses along R4 of [45/-45]$_s$ laminates is shown in Figures (51), (52) and (53) respectively. The refined mesh near the free edge was necessary to represent the steeply varying stresses in this vicinity (i.e., near

Figure 47: Effect of Mesh Refinement on Distribution of RZ-Stress Along R5 of [0/90]$_s$ Laminate

Figure 48: Effect of Mesh Refinement on Distribution

of Z-Stress Along R4 of [0/90]$_s$ Laminate

82

Figure 49: Effect of Mesh Refinement on Distribution of R-Stress Along R7 of [0/90]$_s$ Laminate

83

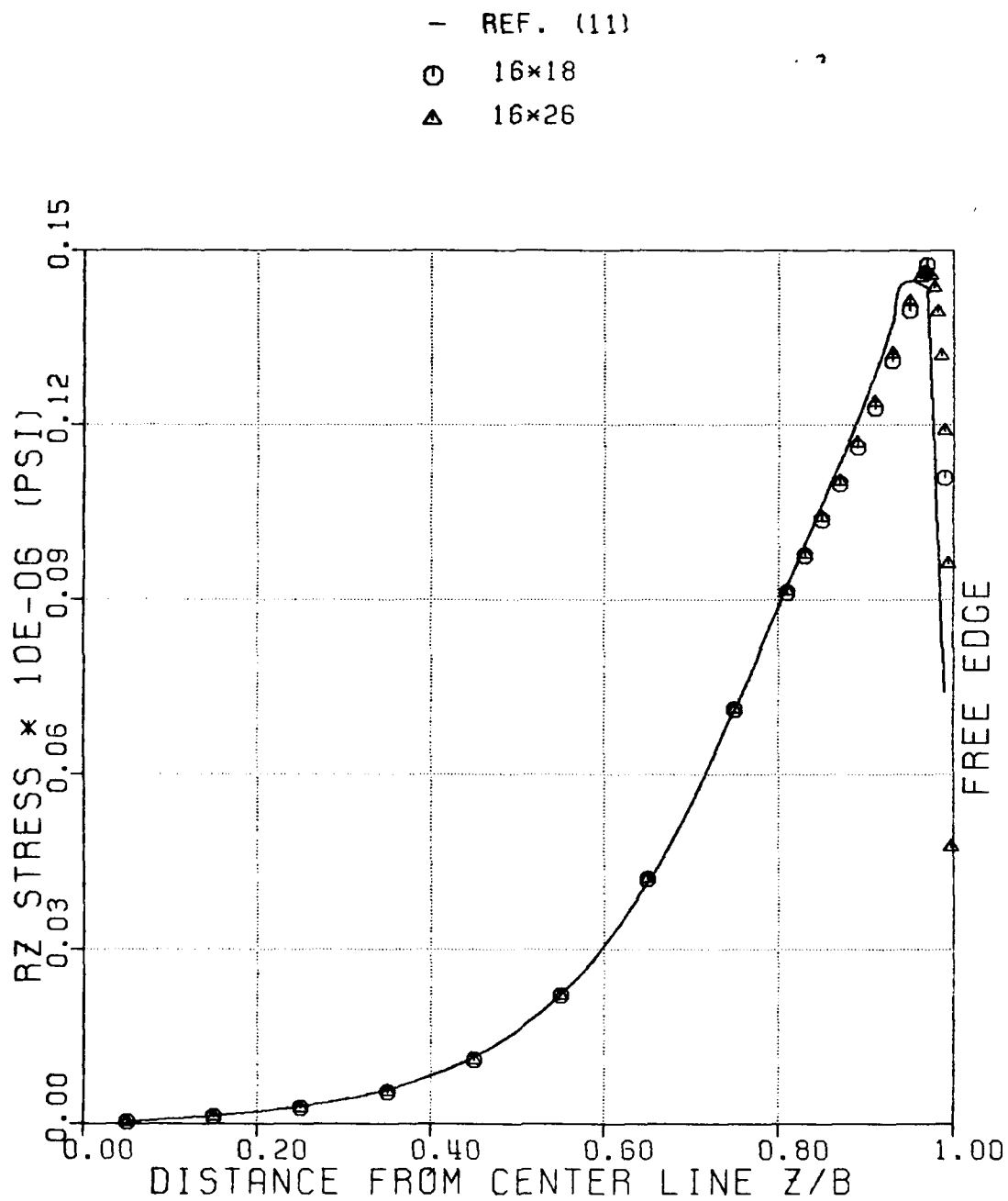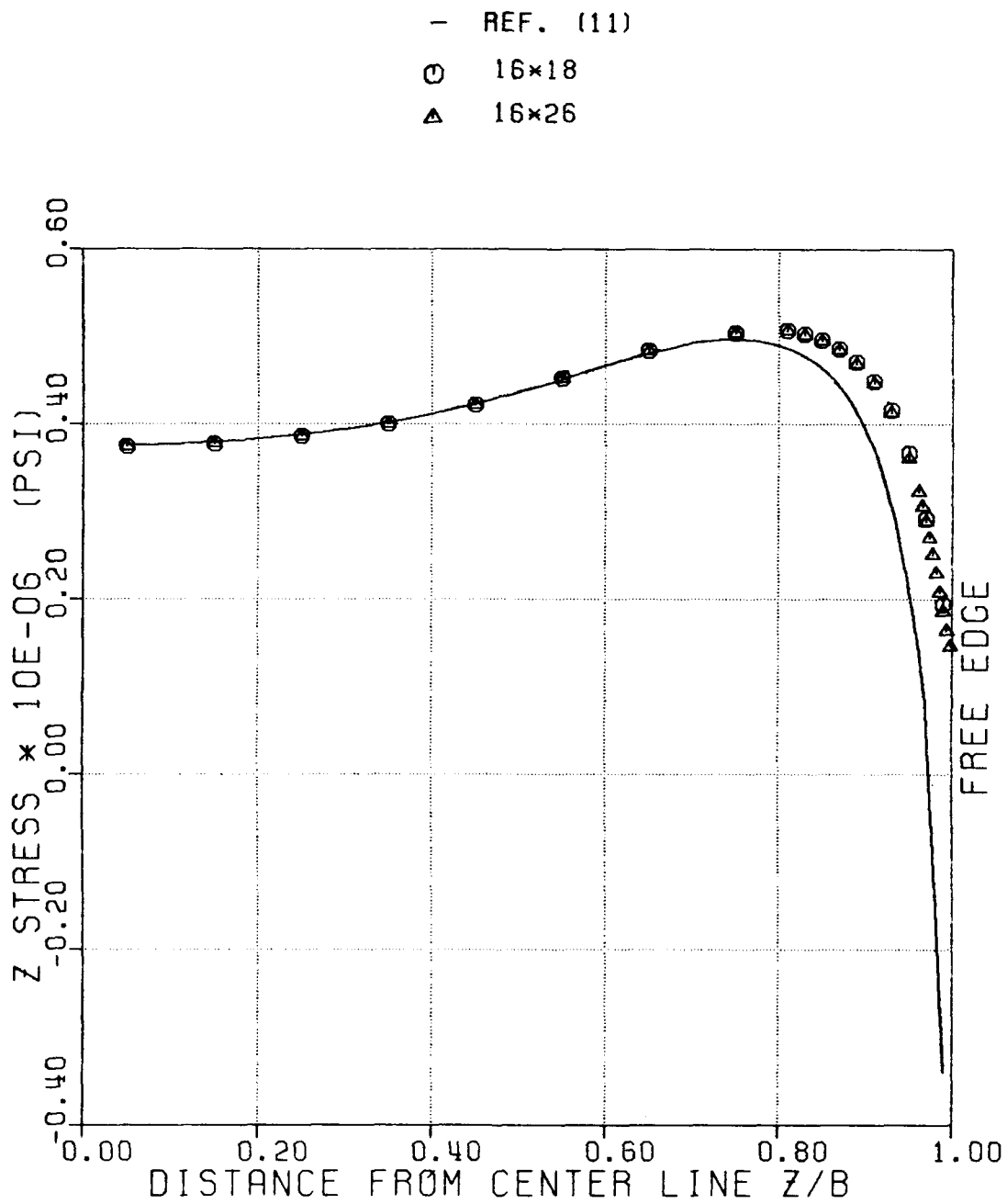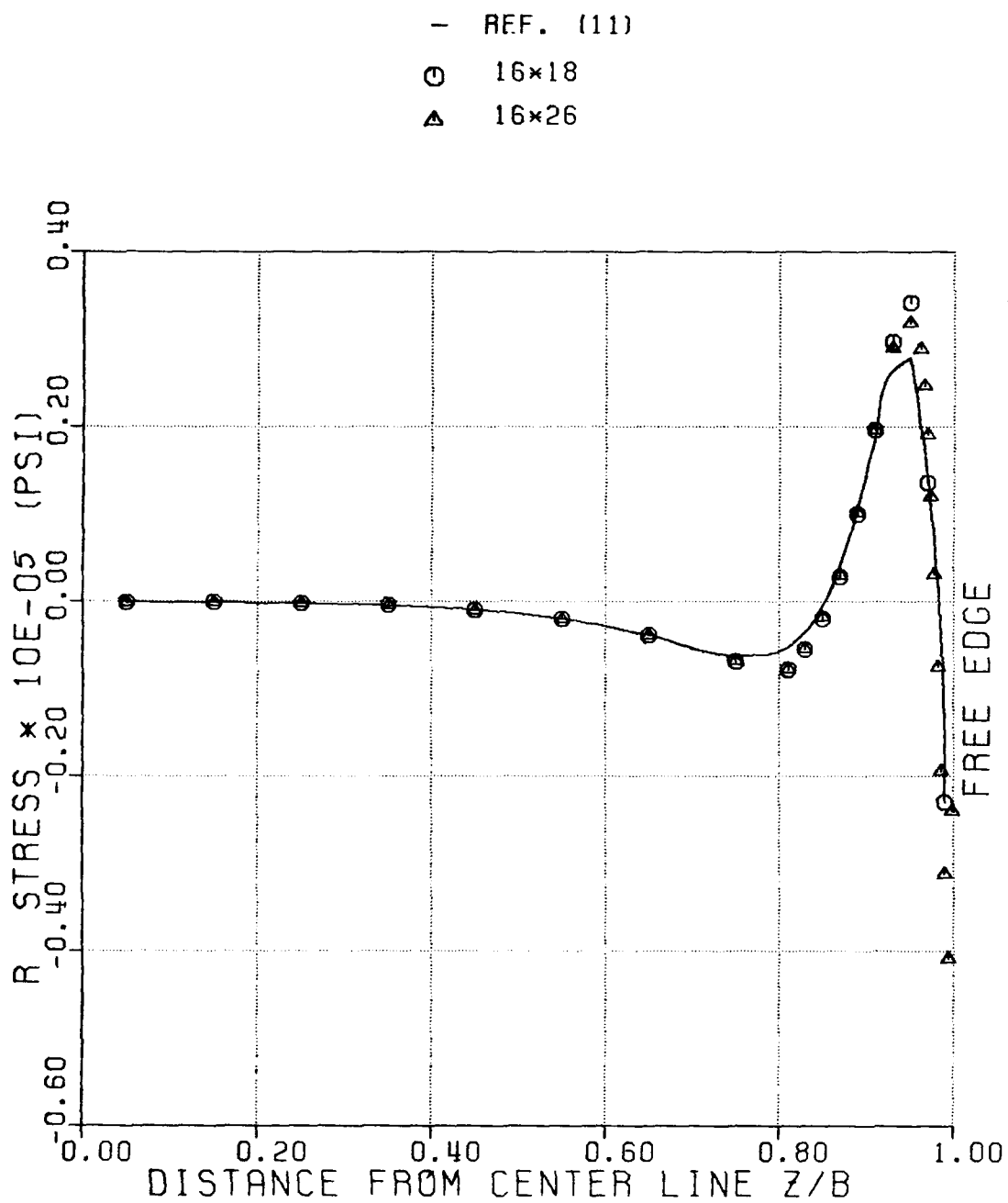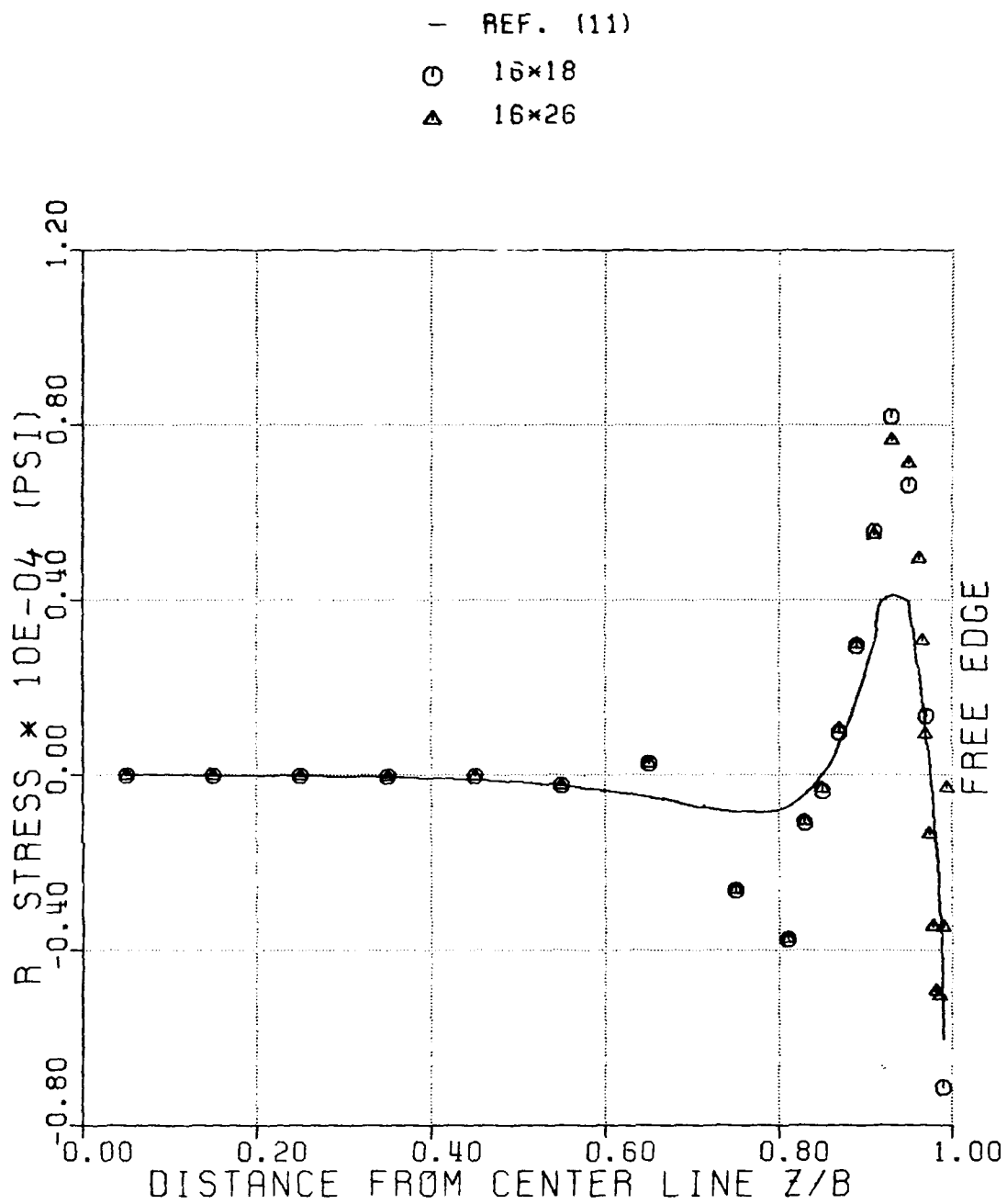Figure 50: Effect of Mesh Refinement on Distribution
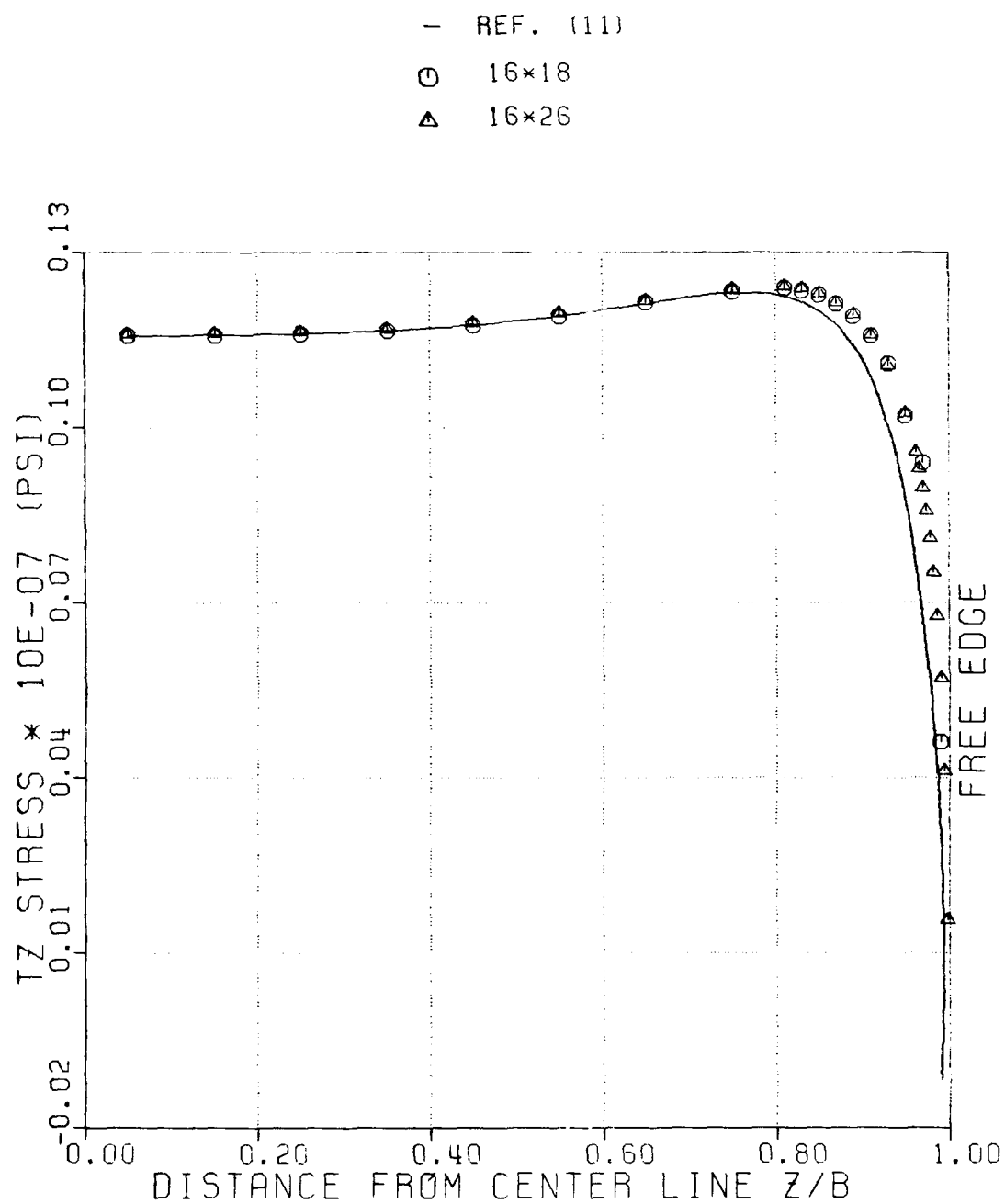
of R-Stress Along R8 of [0/90]$_s$ Laminate

Figure 51: Effect of Mesh Refinement on Distribution of TZ-Stress Along R4 of [45/-45]$_s$ Laminate
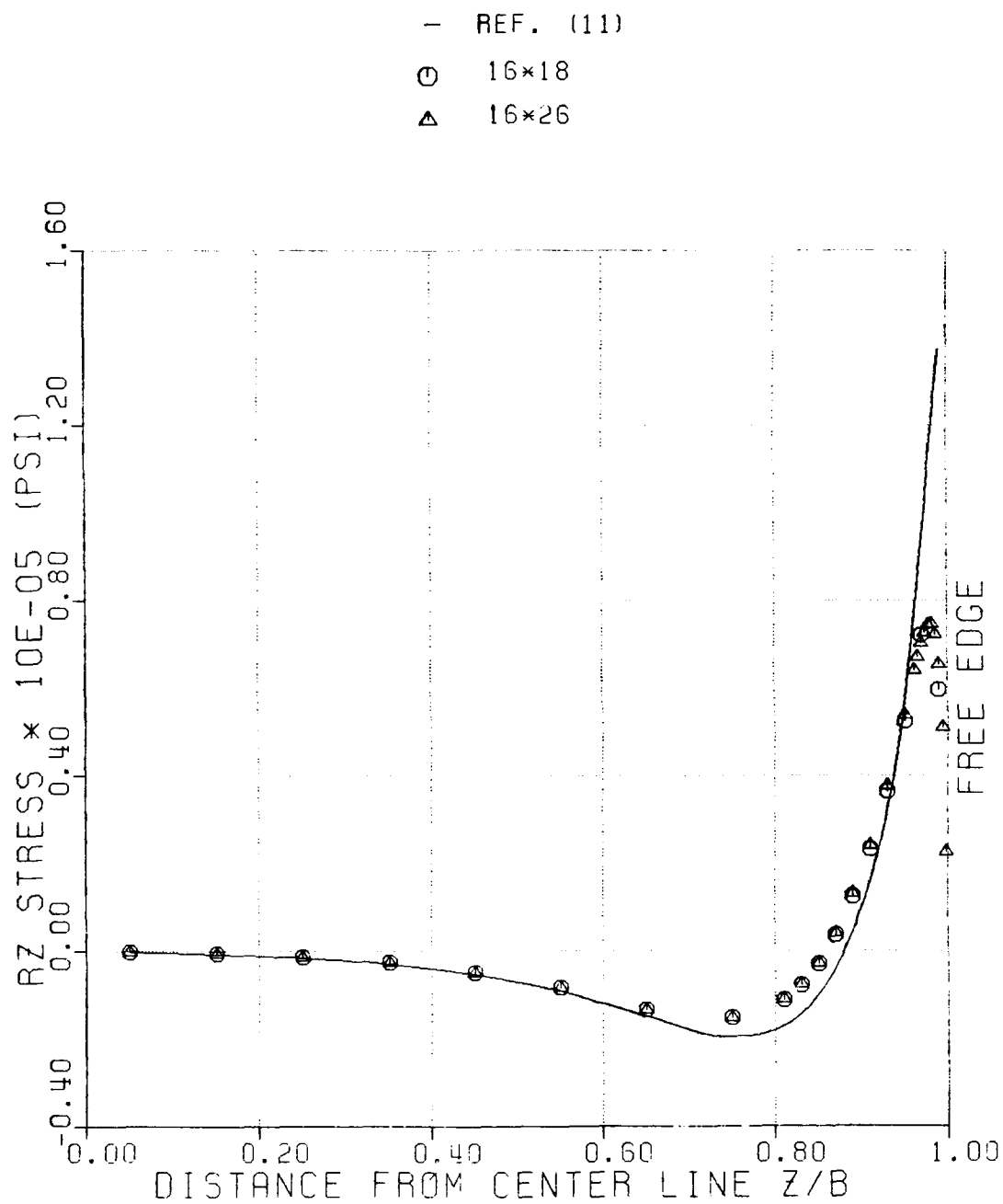
85

Figure 52: Effect of Mesh Refinement on Distribution
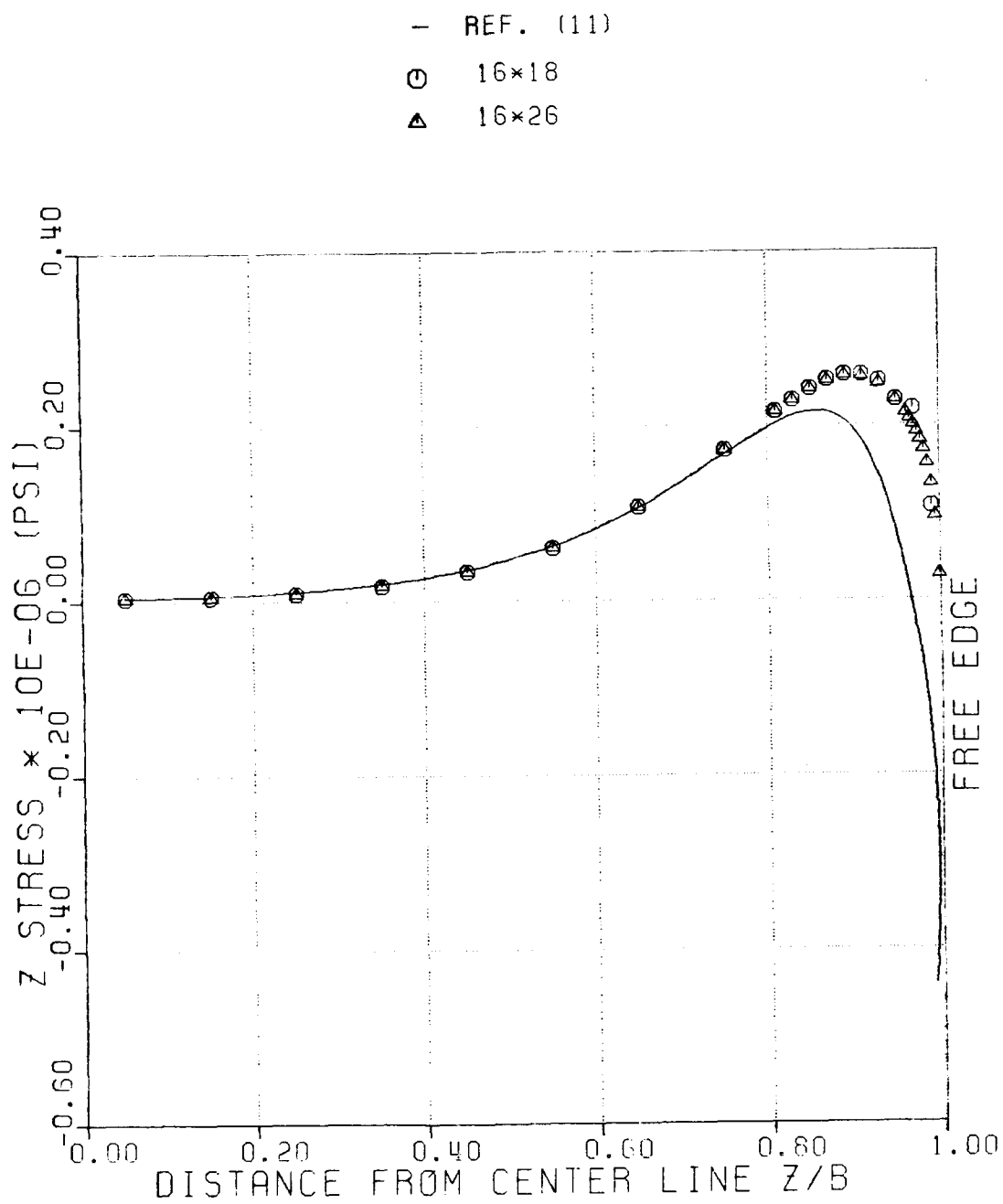of RZ-Stress Along R4 of [45/-45]$_s$ Laminate

Figure 53: Effect of Mesh Refinement on Distribution of Z-Stress Along R4 of [45/-45]$_s$ Laminate

87

the interface of 45/-45 layers and near free edge). The figures indicate that the stress values obtained using the refined mesh approached the traction-free boundary condition.

Figure (54) shows the effect of mesh refinement near the free edge of TR-stress along R8. The stresses varied steeply near the corner of the laminate and the singular stress behavior was reproduced somewhat better by the refined mesh.

The effect of refinement in the r-direction was also studied. Figures (55), (56) show the distribution of R-stress along R7 and R8 of the cross-ply laminate for N=48 (each physical layer was subdivided into twelve uniform sublayers), and they indicate that the result of the refined mesh, N=48 gave better results then those obtained for N=16. The values at R7 were nearly coincident with the results of the Q23 analysis. At R8 there was considerable improvement but an oscillation of stresses existed near Z/B = 0.6 to 0.8.

The effect of mesh refinement in the r-direction on through-thickness distribution of stresses near the free edge for N=32, (each physical layer was subdivided into 8 sublayers) and N=16 is described in Figures (57) through
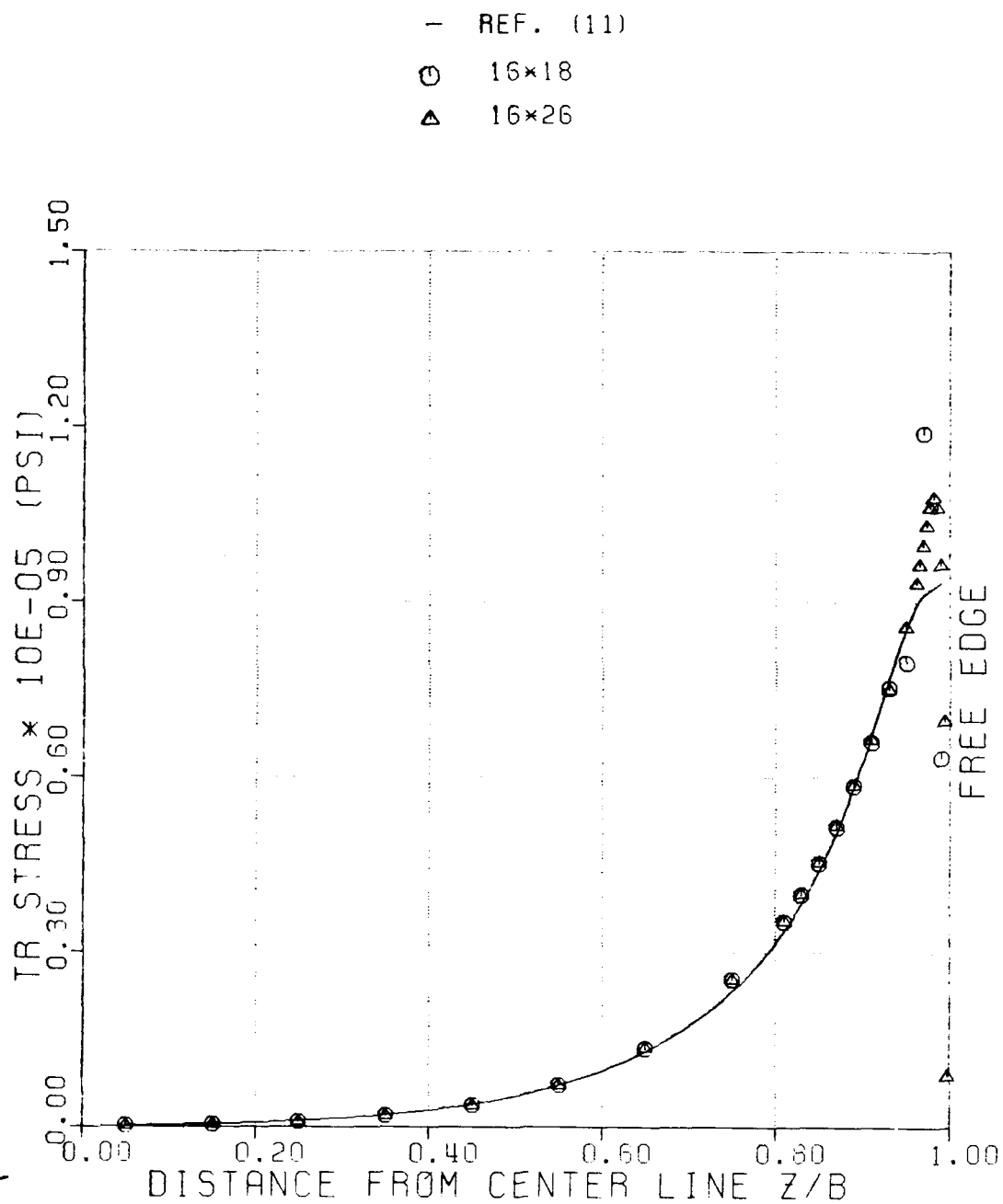
88

Figure 54: Effect of Mesh Refinement on Distribution of TR-Stress Along R8 of [45/-45]$_s$ Laminate
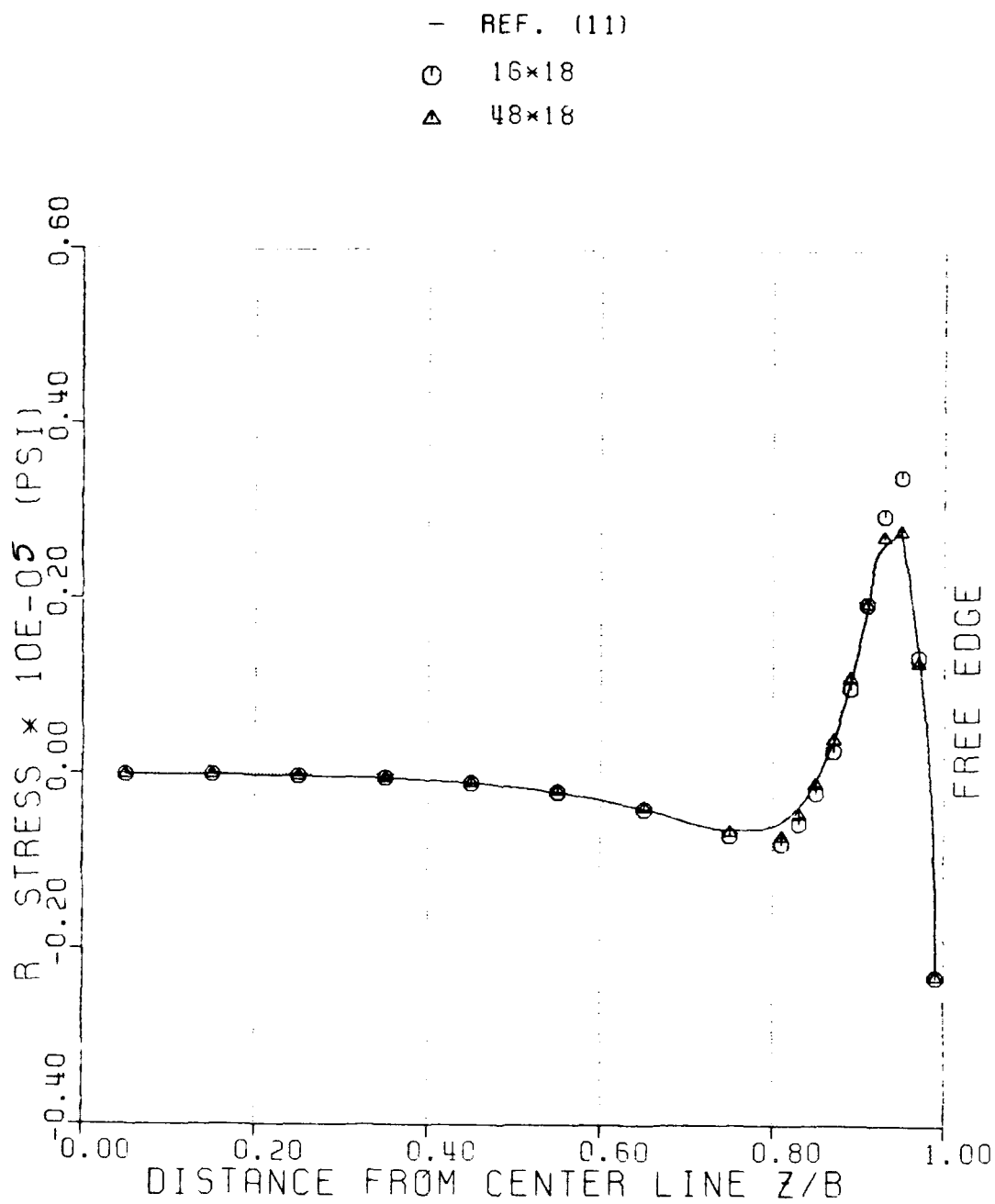
Figure 55: Effect of Mesh Refinement in R-Direction
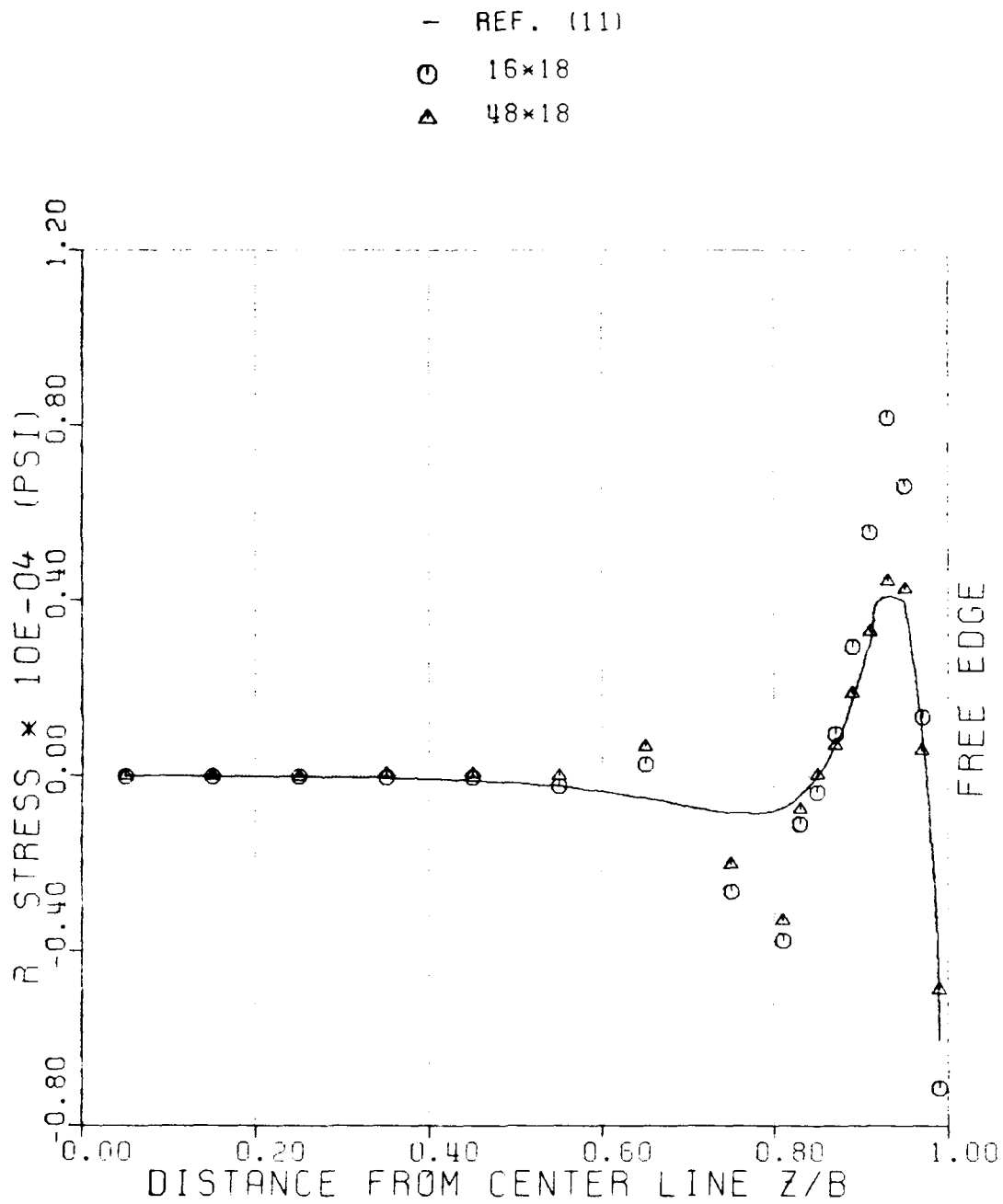on Distribution of R-Stress Along R7
of [0/90]$_s$ Laminate.

Figure 56: Effect of Mesh Refinement in R-Direction on Distribution of R-Stress Along R8 of [0/90]$_s$ Laminate.

(61). The continuous-traction analysis gave values of the stress field at the interface of the layers. For the axisymmetric analysis, an estimate of the stress field at the interface of lamina was made by interpolating from the stress field computed at the centers of the sublayers. Cubic spline functions were used.

Figures (57), (58) show through-thickness distribution of R and Rz-stresses at Z/B=0.99 of cross-ply laminate. The steeply varying stresses near the interface of the 0/90 laminate and the stress free condition at the free surface were more closely reproduced by the refined mesh. The percentage difference in the values of the stresses, at the interface of 0/90 laminate, using the present analysis and using the Q23 element were 10% and 46% for R-stress and Rz-stress respectively.

Figures (59), (60) and (61) show through-thickness distribution of TR, R and Rz-stresses near the free edge of [45/-45]$_s$ laminate. The figures indicate a difference in results between the axisymmetric analysis and the Q23 element solution near interface of 45/-45 layers. However, the refined mesh gave satisfactory results near the free surface where a traction-free condition exists. At the interface of the 45/-45 layers, the interpolated values obtained using spline fitting of the axisymmetric analysis

Figure 57: Effect of Mesh Refinement in R-Direction on Through-Thickness Distribution of R-Stress at Z/B = 0.99 of [0/90]$_s$ Laminate

Figure 58: Effect of Mesh Refinement in R-Direction
on Through-Thickness Distribution of
Rz-Stress at Z/B = 0.99 of [0/90]$_s$

Figure 59: Effect of Mesh Refinement in R-Direction
on Through-Thickness Distribution of
TR-Stress at Z/B = 0.99 of [45/-45]$_s$

Figure 60: Effect of Mesh Refinement in R-Direction
on Through-Thickness Distribution of
R-Stress at Z/B = 0.99 of [45/-45]ₛ

96

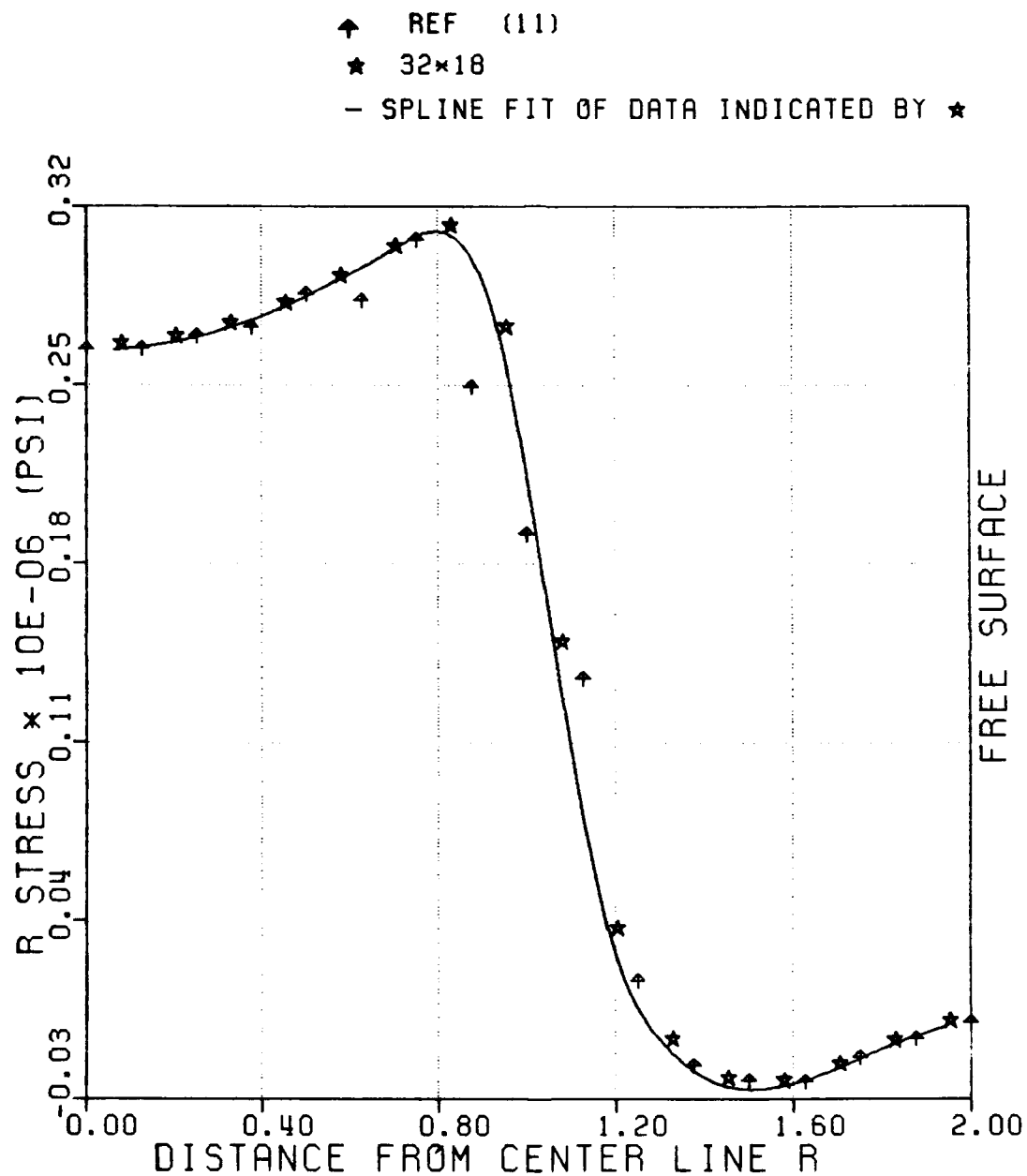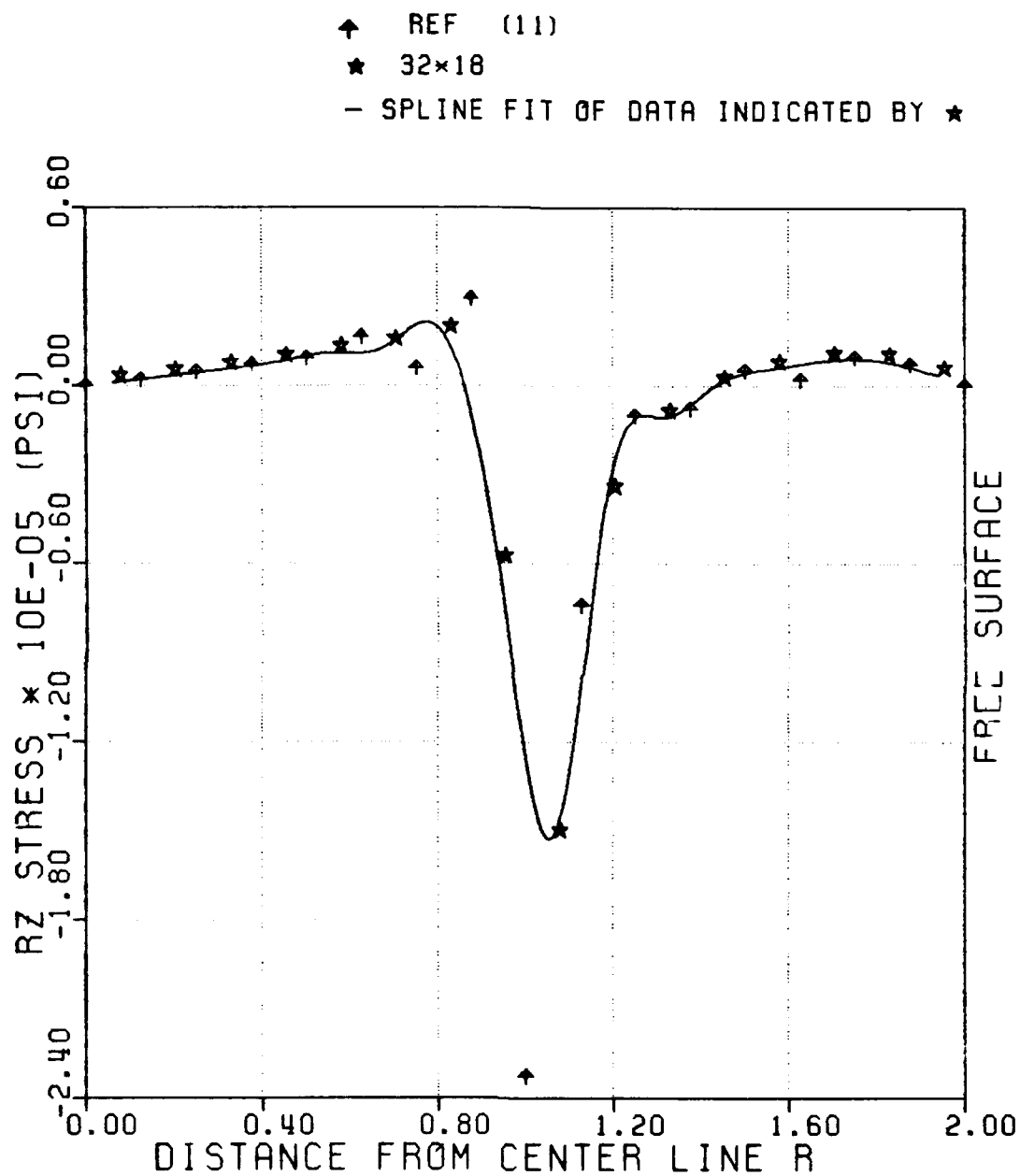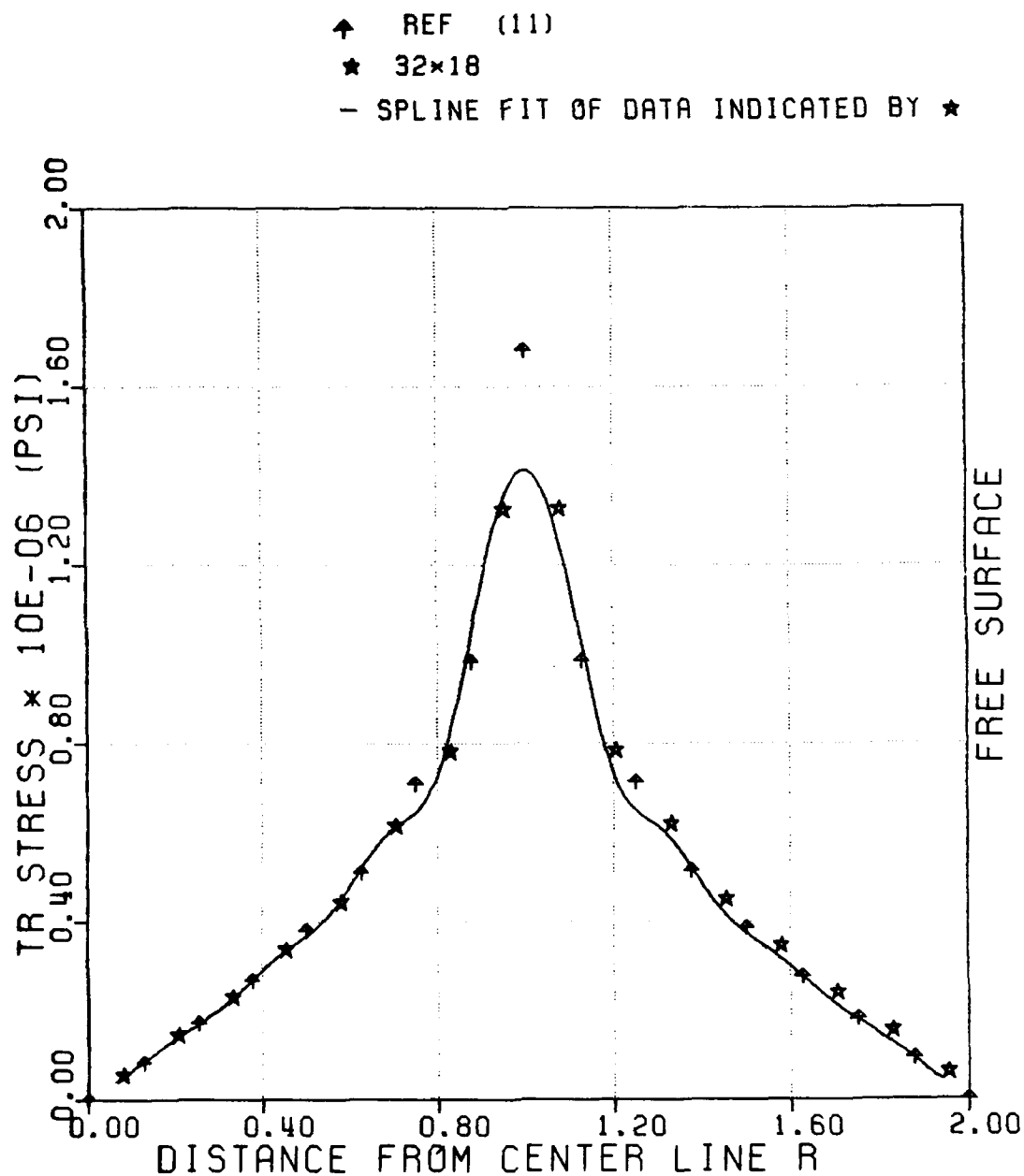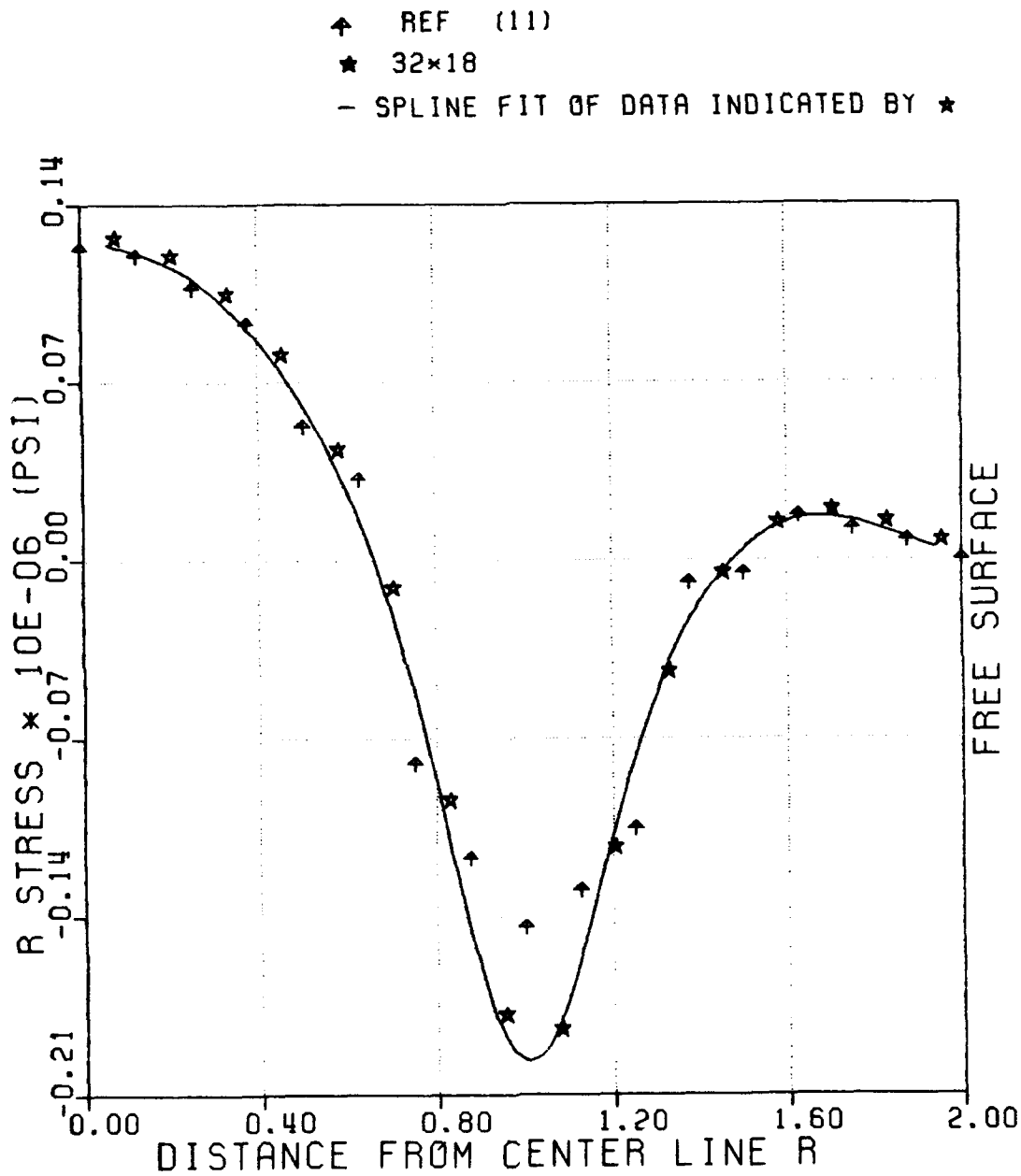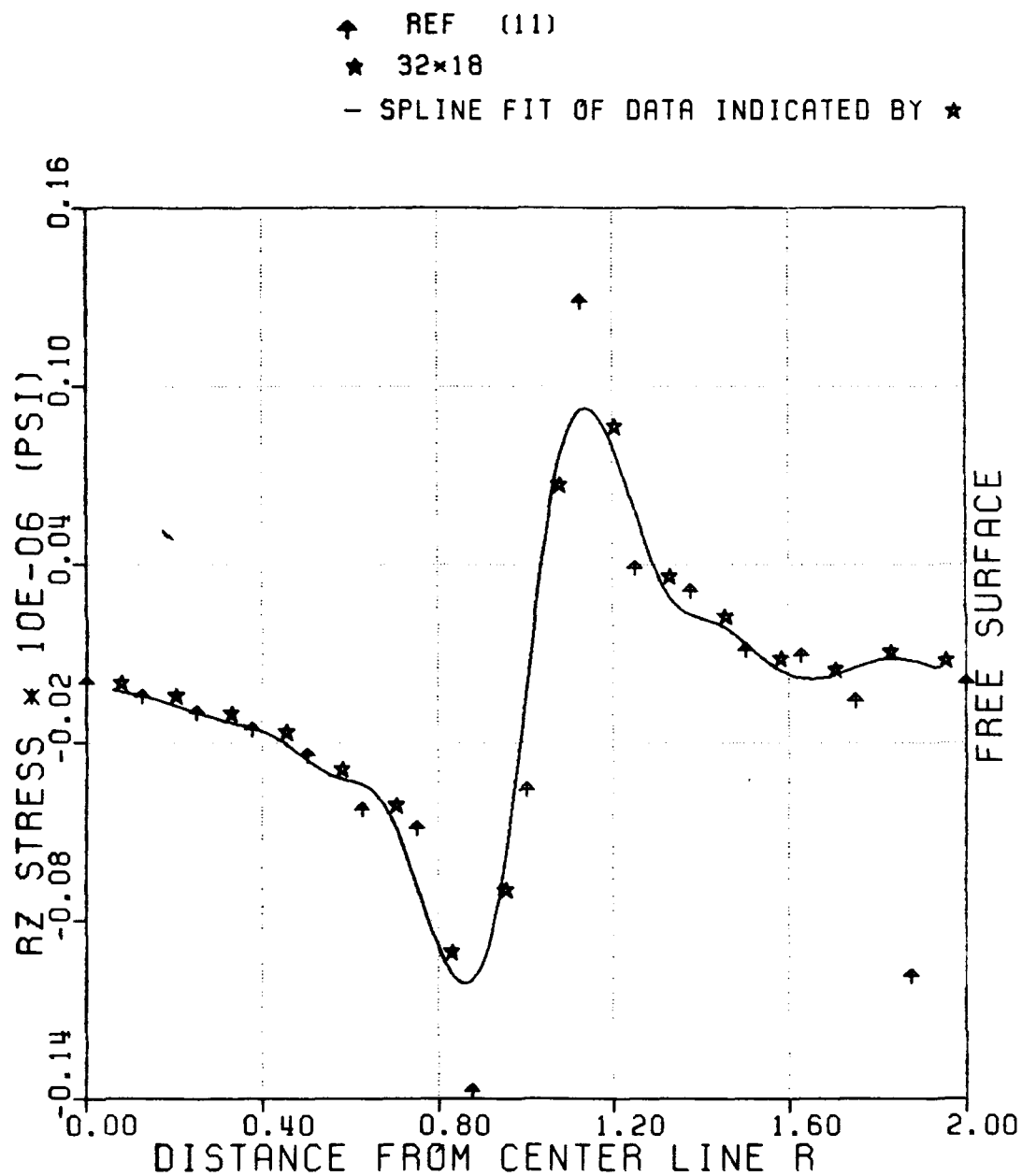Figure 61: Effect of Mesh Refinement in R-Direction on Through-Thickness Distribution of Rz-Stress at Z/B = 0.99 of $[45/-45]_s$

results differed by 16%, 26%, 10%, as compared to approximate stress value obtained using the Q23 analysis, for TR, R, and Rz stress components respectively.

Another interpolating scheme, used in order to estimate the stress field at the interface in Figures (57) through (61) was studied. Cubic spline functions were used except for the two stress values near the interface where quadratic functions were used. The two quadratic curves were assumed to have equal and opposite curvature. In this case, the interpolating polynomials had continuous first and second derivatives except at the interface where there is a discontinuity in stress gradients. Figures (62), (63) show through-thickness distribution of R and Rz-stresses at Z/B=0.99 for cross-ply laminate. Using the interpolating scheme described above, the percentage difference, at the interface of 0/90 layers, of R-stress values for the axisymmetric analysis compared with that from the Q23 element analysis increased from 10% to 16% while that of Rz-stress decreased from 46% to 28%, as compared to the spline fit interpolation. Figures (64), (65), (66), show, respectively, through-thickness distribution of Tr, R, Rz-stresses near the free edge. The percent error, at the interface of 45/-45 layers decreased from 16% to 2% for Tr-stress and from 10% to 9% for Rz-stress but increased from

98

Figure 62: Interpolation of Stresses at Interface: R-
Stress Through-Thickness distribution at
Z/B = 0.99 of [0/90]$_s$ (Combination of
Cubic and Quadratic Interpolating Function)

Figure 63: Interpolation of Stresses at Interface:
RZ-Stress Through-Thickness distribution
at Z/B = 0.99 of [0/90]$_s$ (Combination of
Cubic and Quadratic Interpolating Function)

100

Figure 64: Interpolation of Stresses at Interface:
TR-Stress Through-Thickness distribution
at $Z/B = 0.99$ of $[45/-45]_s$ (Combination of
Cubic and Quadratic Interpolating Function)

101

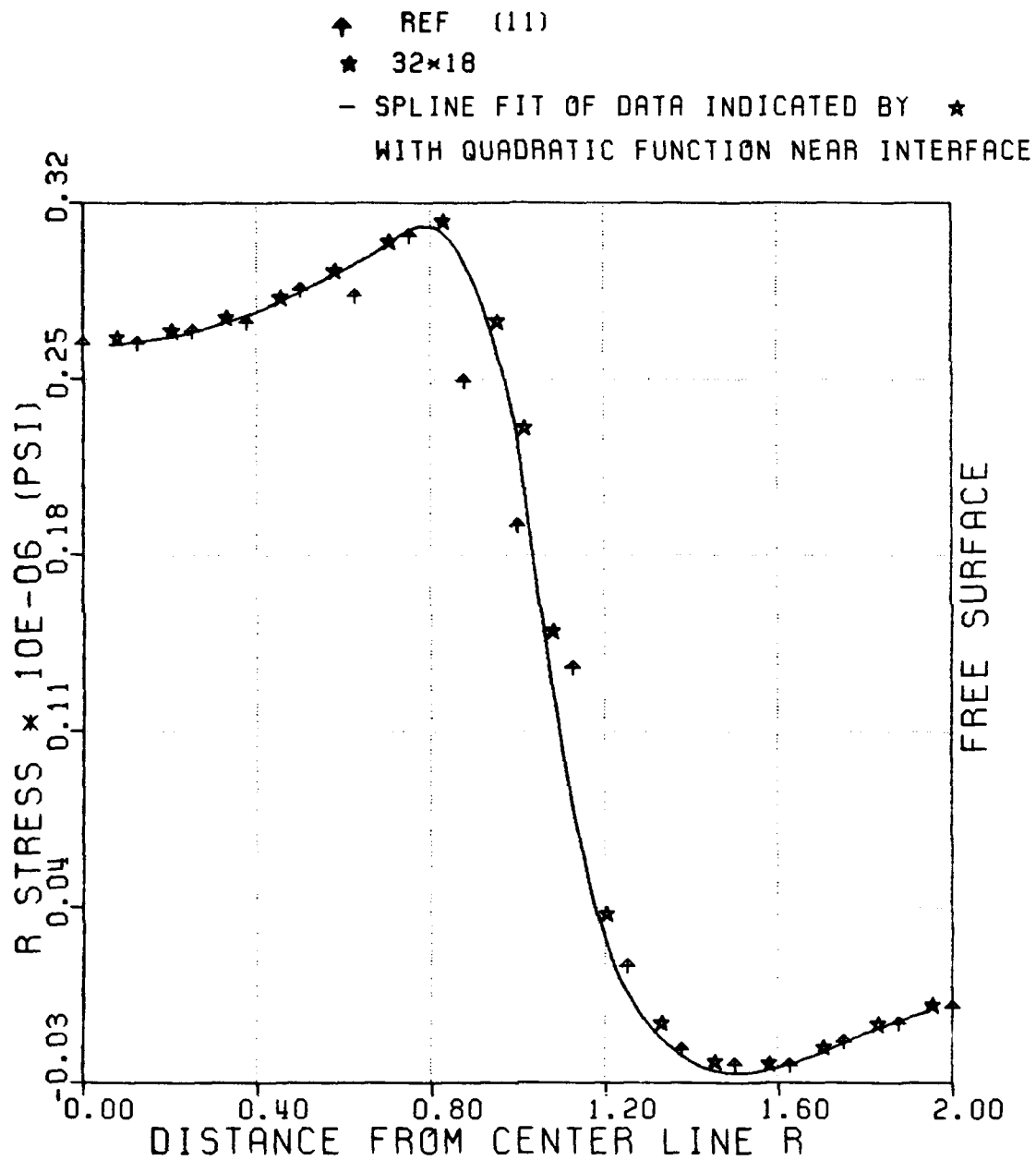Figure 65: Interpolation of Stresses at Interface: R-Stress Through-Thickness distribution at Z/B = 0.99 of [45/-45]$_s$ (Combination of Cubic and Quadratic Interpolating Function)
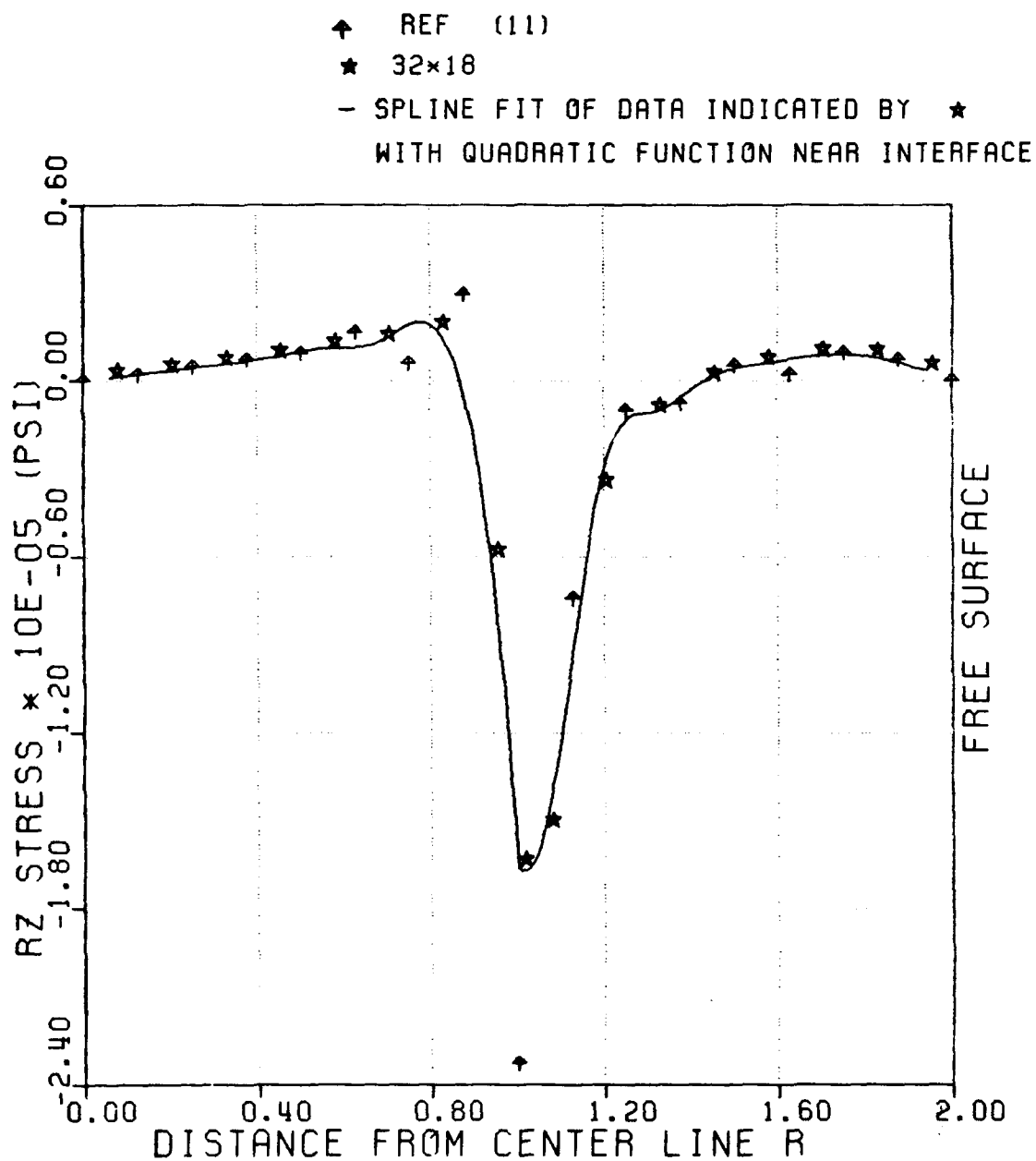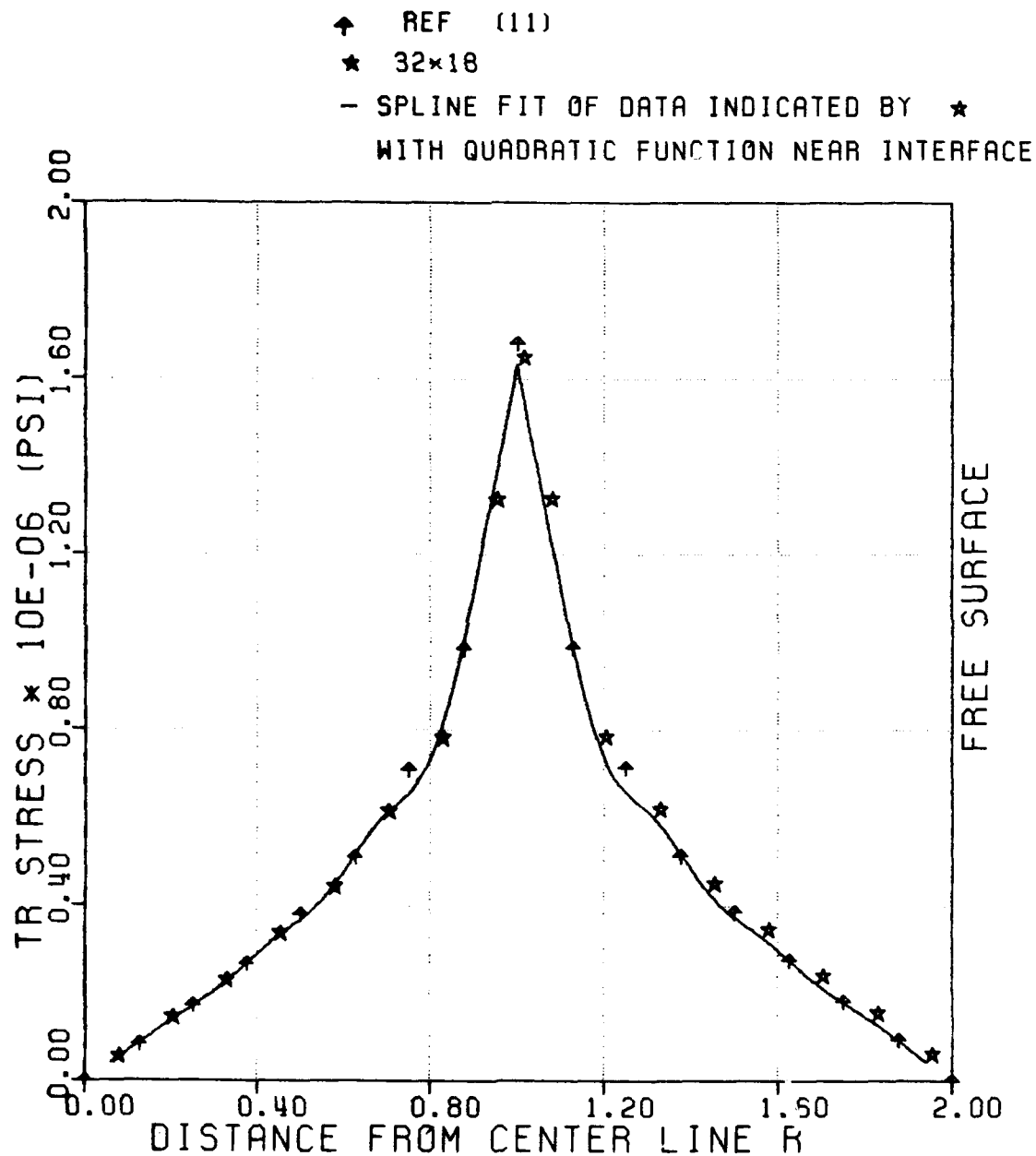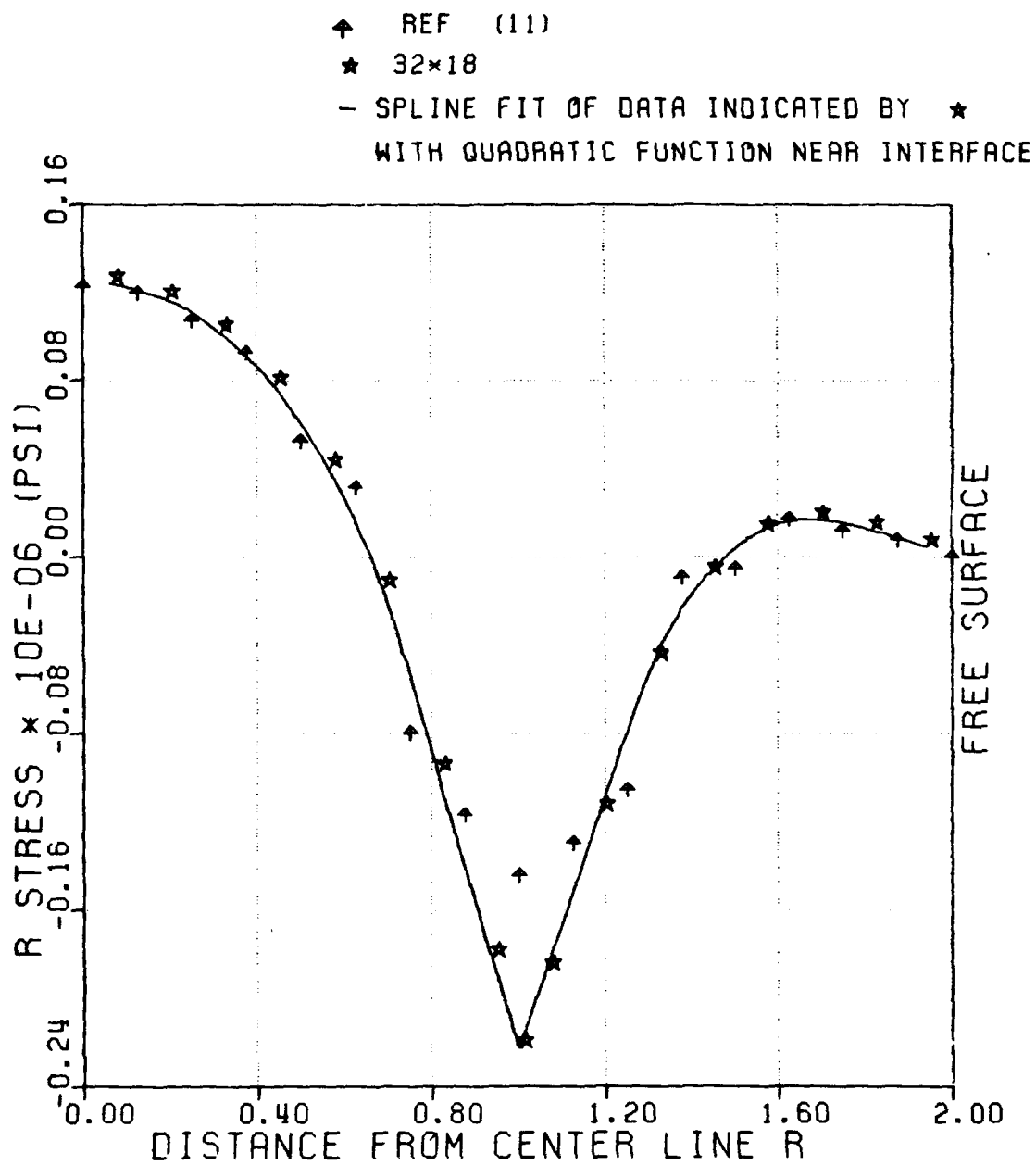
Figure 66: Interpolation of Stresses at Interface:
RZ-Stress Through-Thickness distribution
at Z/B = 0.99 of [45/-45]$_s$ (Combination of
Cubic and Quadratic Interpolating Function)

103

26% to 35% for R-stress, as compared with the spline fit interpolation.

A third scheme consisted of a two-step curve fitting procedure. The stress values on each side of the interface were obtained by extrapolating from a spline fit to all the points other than the interface. The two curves had zero curvature at the interface and gave different values of the stress at the interface. The actual stress at the interface was then assumed to be the average of the two interpolated values. Having found the stress at the interface, a spline fit of data was carried out. The results showed that there was not much difference in the interpolated stress value as compared to the previous interpolation scheme. Figures (67), (68) show the distribution of Rz-stress for the cross-ply laminate and TR-stress for the angle ply laminate, respectively, for this scheme.

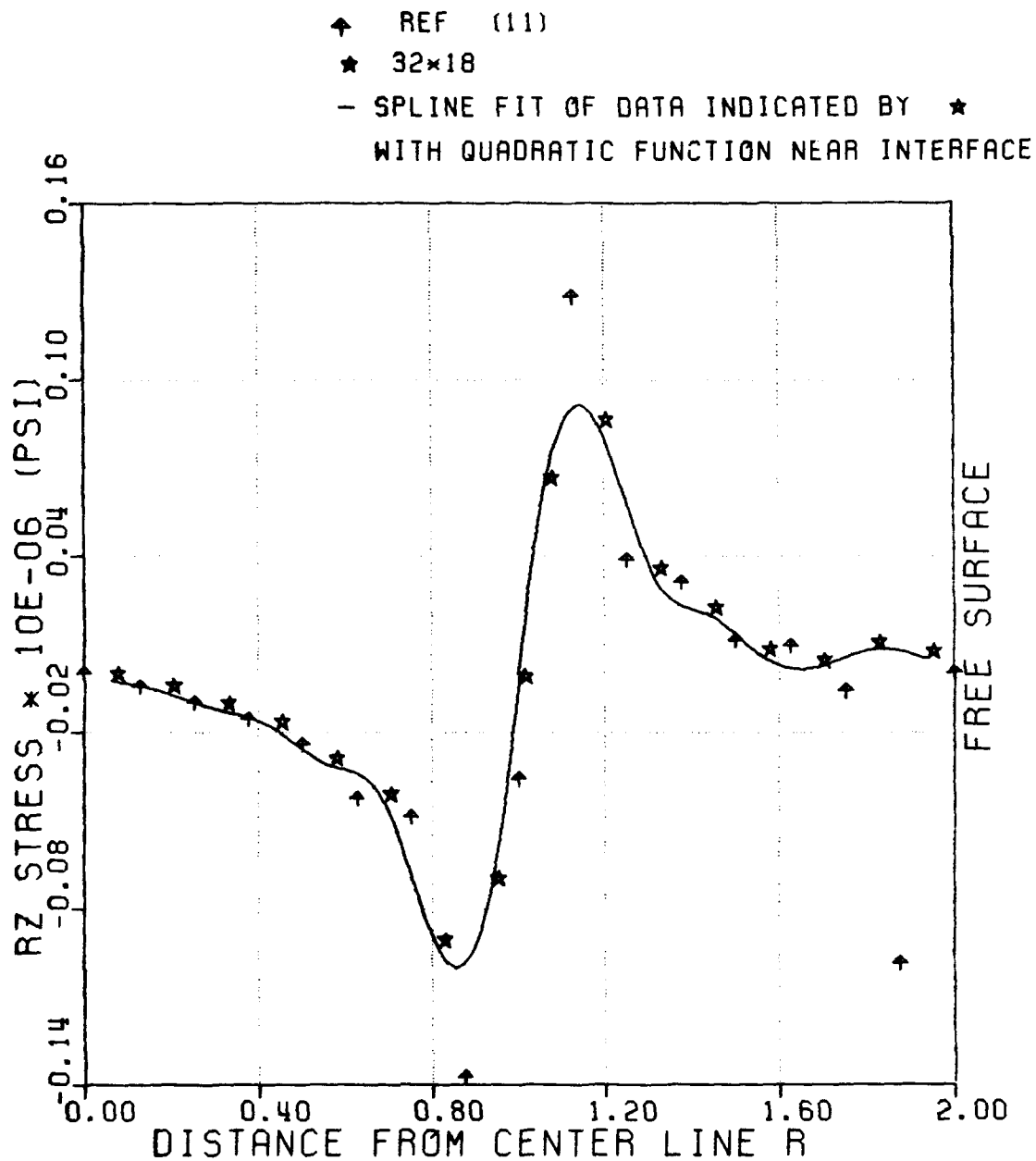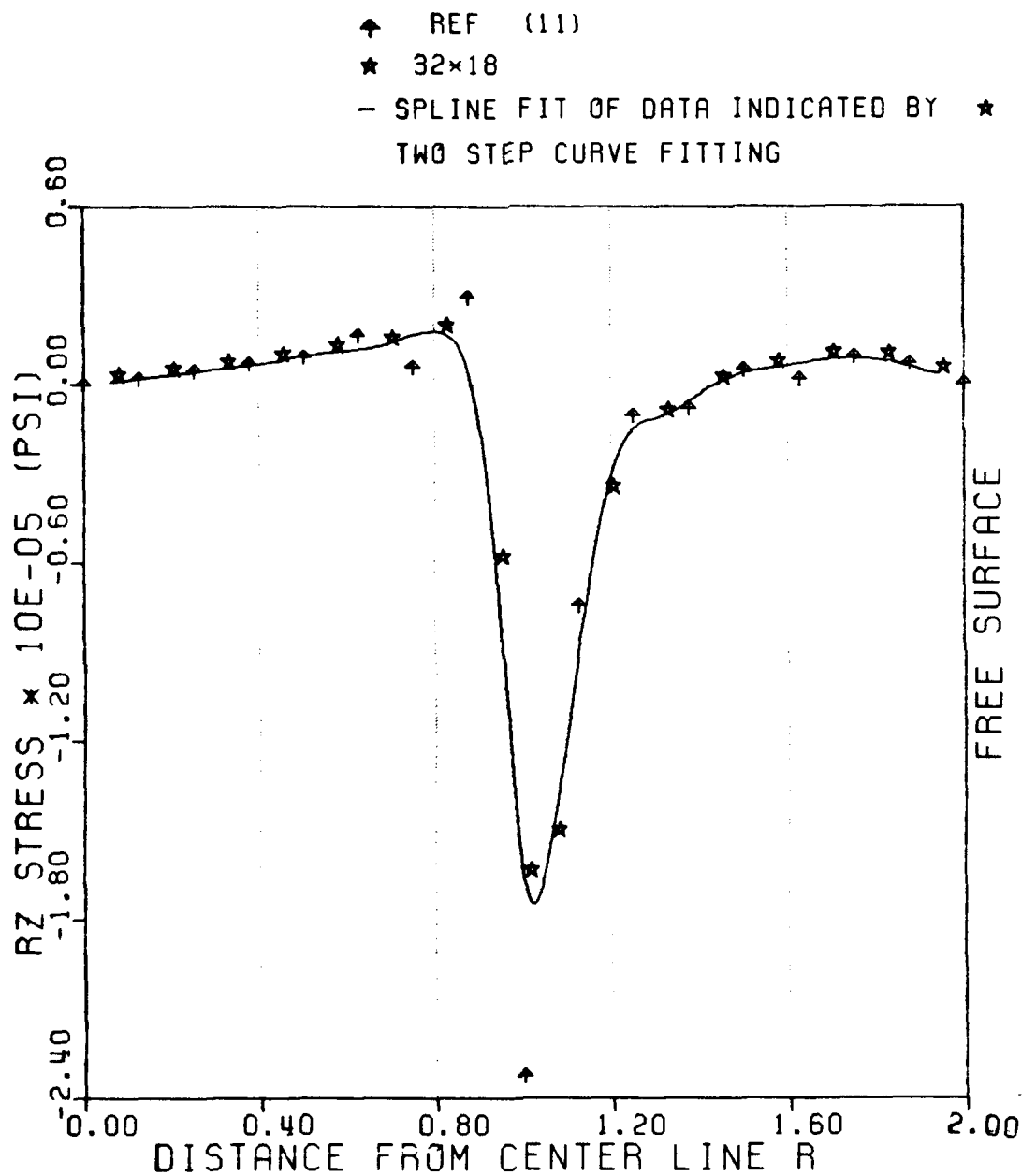Figure 67: Interpolation of Stresses at Interface: RZ-Stress Through-Thickness distribution at Z/B = 0.99 of [0/90]$_s$ (Two-Step Curve Fitting)
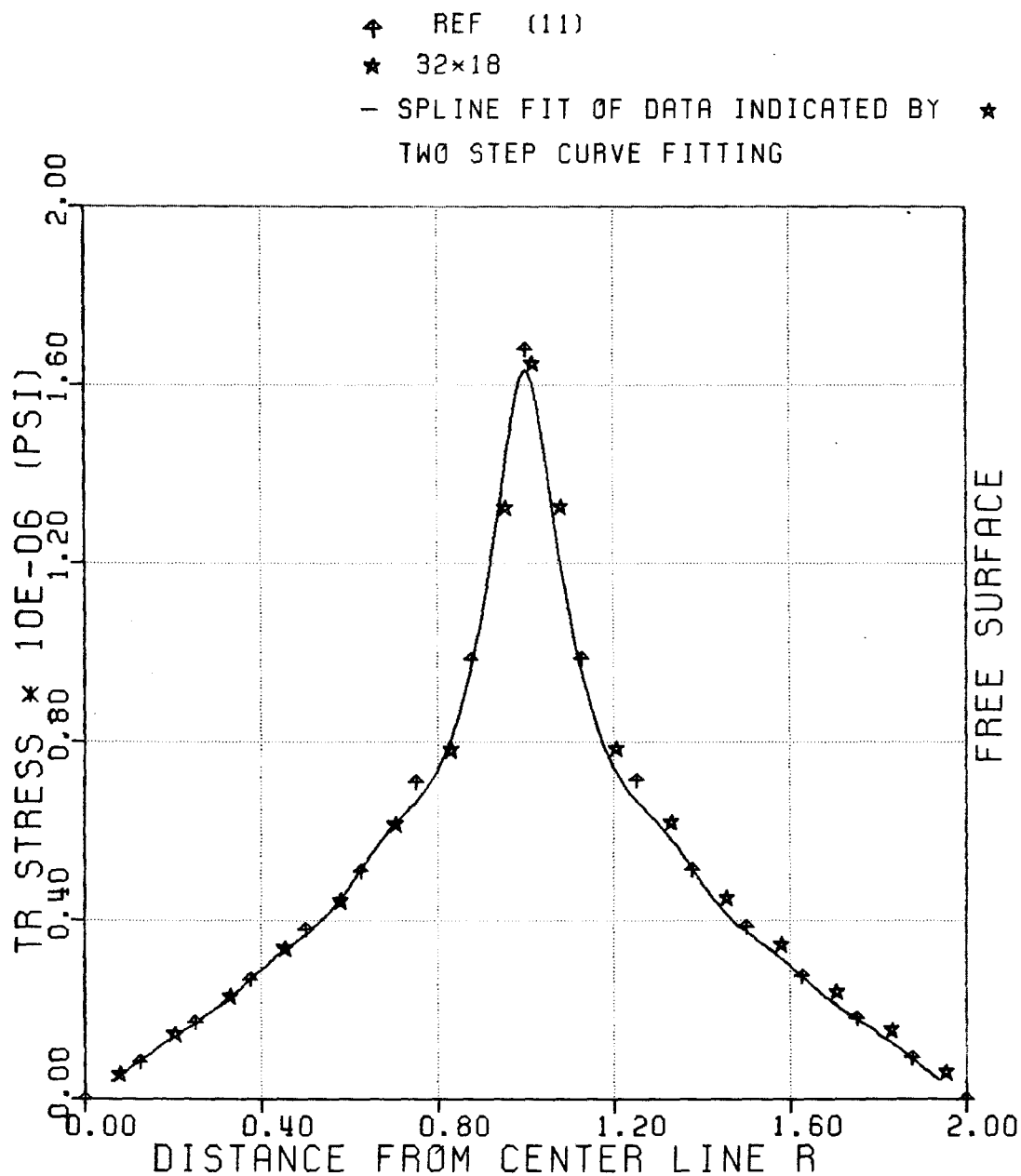
105

Figure 68: Interpolation of Stresses at Interface:
TR-Stress Through-Thickness distribution
at Z/B = 0.99 of [45/-45]$_s$ (Two-Step Curve
Fitting)

4.4 TWENTY-TWO ANGLE PLY LAMINATE

4.4.1 Geometry, Material Properties and Finite Element Mesh

A ring specimen with fiber orientation $[(25.5/-25.5)_5/90]_s$ was used in the present investigation. The laminate width and ply thickness were 1.0 in and 0.00505 in respectively. The material properties were [11]:

$$E_{11} = 19.26 * 10^6 \text{ psi}$$

$$E_{22} = E_{33} = 1.32 * 10^6 \text{ psi}$$

$$G_{12} = G_{13} = G_{23} = 0.83 * 10^6 \text{ psi}$$

$$\mu_{12} = \mu_{13} = \mu_{23} = 0.35$$

Each ply was modeled by a single element through its thickness $(N = 22)$. The mesh used was more refined near the free-edge. Full section was used for the axisymmetric analysis, corresponding to 308 (22x14) mesh as shown in Figure (69), for half-section discretization of the ring. This corresponds to 154-element model for a quadrant as used with the continuous traction Q23 element in [11]. The value R_i, shown in Figure (69), denotes the distance from the central plane of section to the center of the ith layer. R_1 is the closest to the midplane of the specimen and corresponds to the 90-degree ply, R_{11} is closest to the top surface and corresponds to the 25.5-degree ply. The internal pressure applied was 0.00987687 (psi) which yields an average axial strain equal to that applied in Q23 element analysis $(0.95414 * 10^{-5})$.
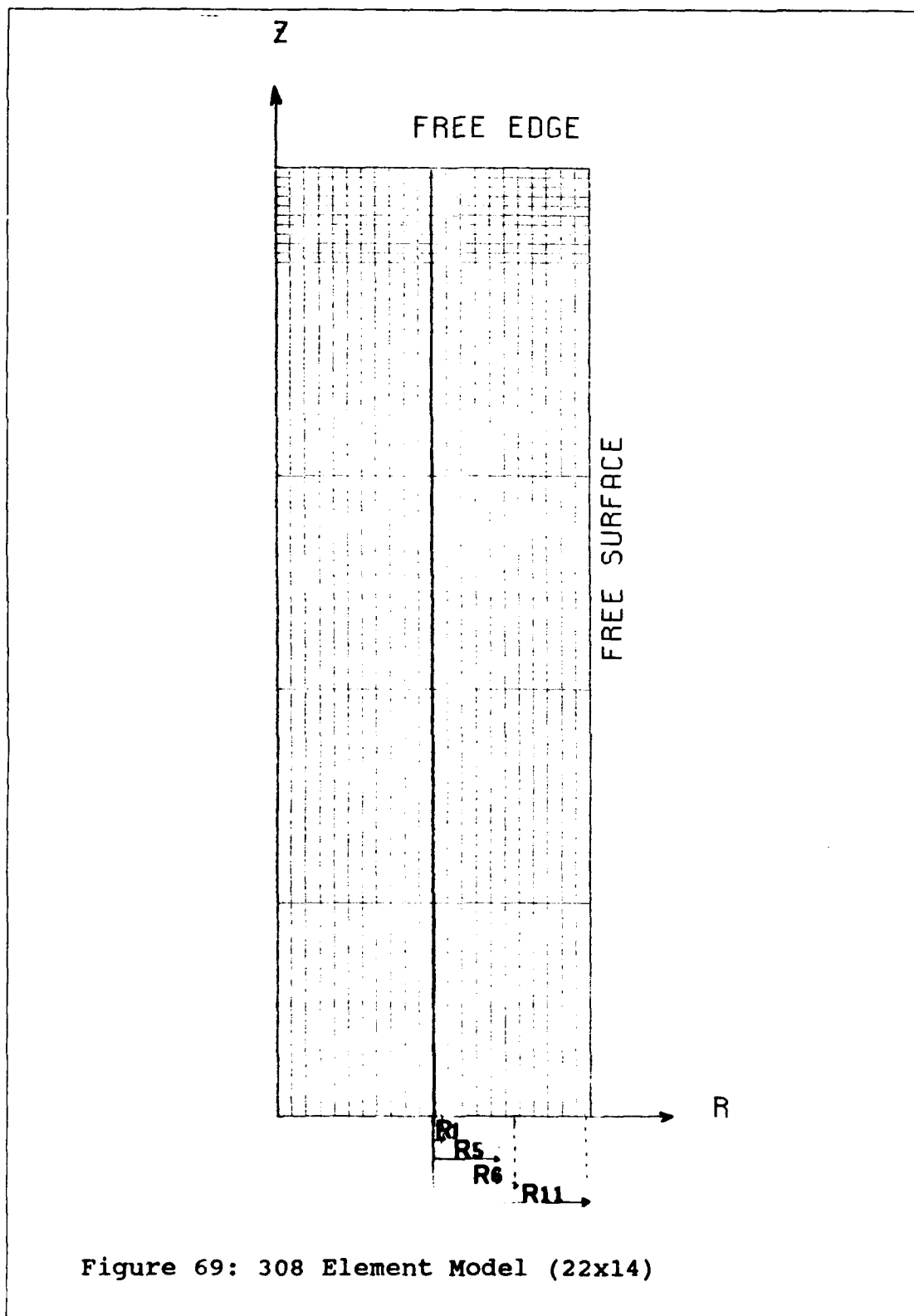
Figure 69: 308 Element Model (22x14)

4.4.2 <u>Numerical Results</u>

Numerical results based on the pseudo-three dimensional axisymmetric analysis using QM4 element were compared with results based on the continuous traction Q23 element described in [11]. The same mesh size was used in both the analysis. Figures (70) through (85) show comparison of stress fields at specific locations for the multi-ply laminate using the Q23 element and the axisymmetric analysis.

Figures (70), (71), (72) and (73) show the distribution of z-stress along R1, R5, R6 and R11 respectively. Satisfactory agreement was observed between the axisymmetric analysis and the Q23 element solution except at $Z/B = 0.56$ to 0.89 in Figures (70) and (73). This could be due to the finite element mesh not being fine enough in this region. The effect of mesh refinement is described later in this section. The figures also indicate that the stress values obtained using the axisymmetric analysis approach the traction-free boundary condition at the free edge.

A comparison of Rz-stress distribution along R1, R5 and R6 (Figures (74), (75) and (76) respectively) indicated that the results obtained using axisymmetric analysis agreed well with Q23 element solution across the entire width of the

Figure 70: Distribution of Z-Stress Along R1 of

$[(25.5/-25.5)_5/90]_s$ Laminate

110

Figure 71: Distribution of Z-Stress Along R5 of

[(25.5/-25.5)$_5$/90]$_s$ Laminate

111

— REF. (11)

⊙ PRESENT ANALYSIS

Figure 72: Distribution of Z-Stress Along R6 of

$[(25.5/-25.5)_5/90]_s$ Laminate

112

Figure 73: Distribution of Z-Stress Along R11 of

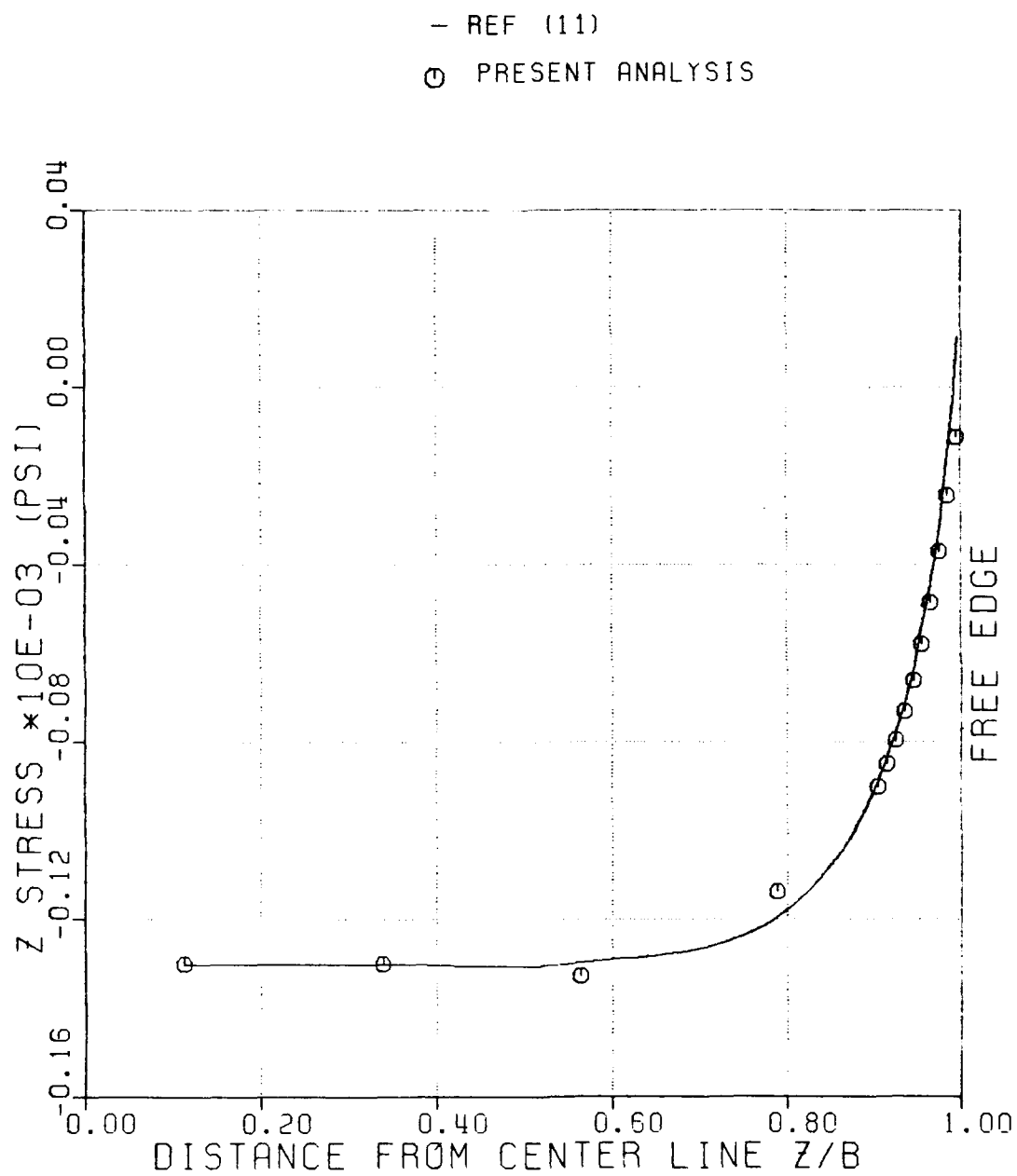$[(25.5/-25.5)_5/90]_s$ **Laminate**

113

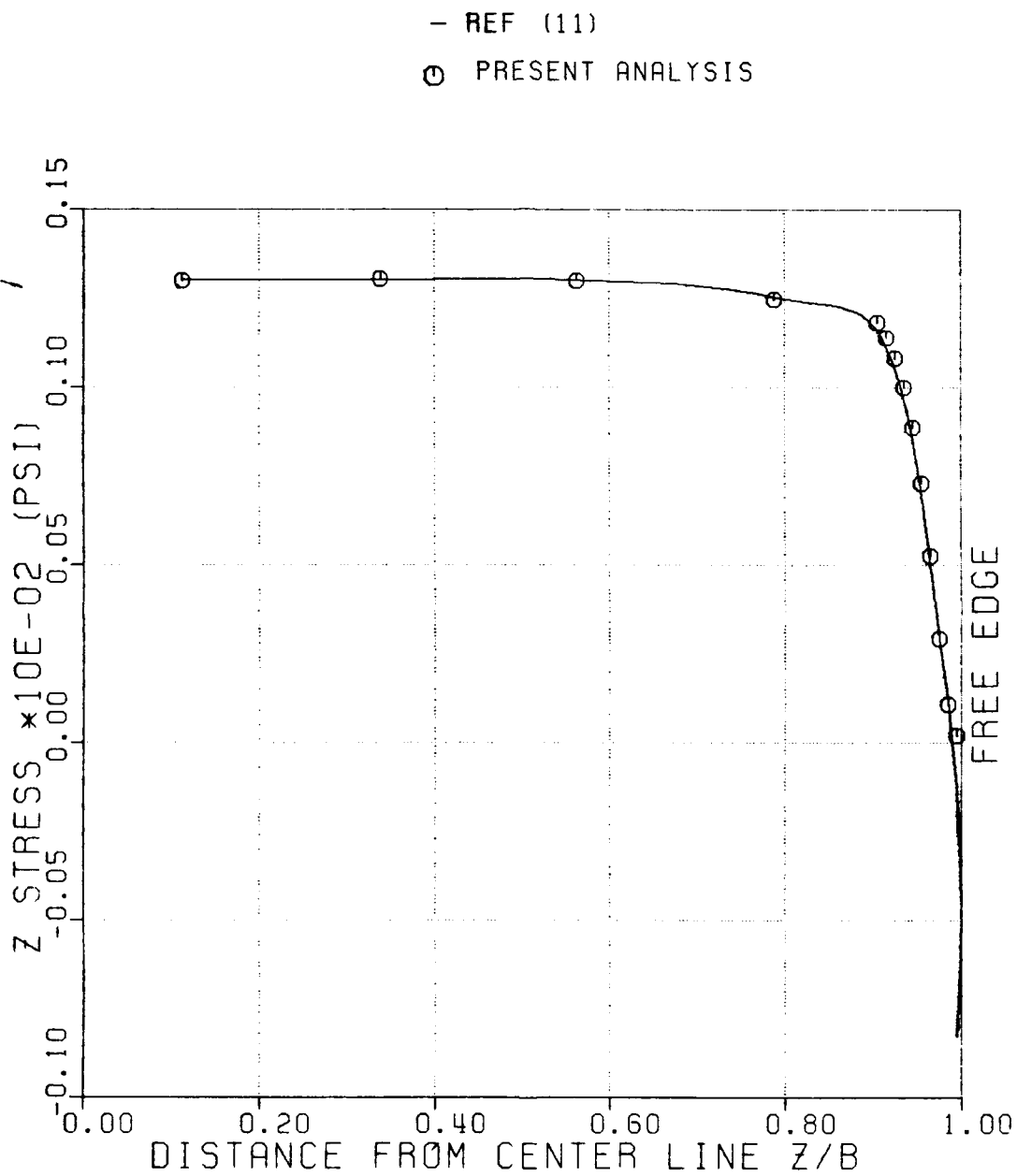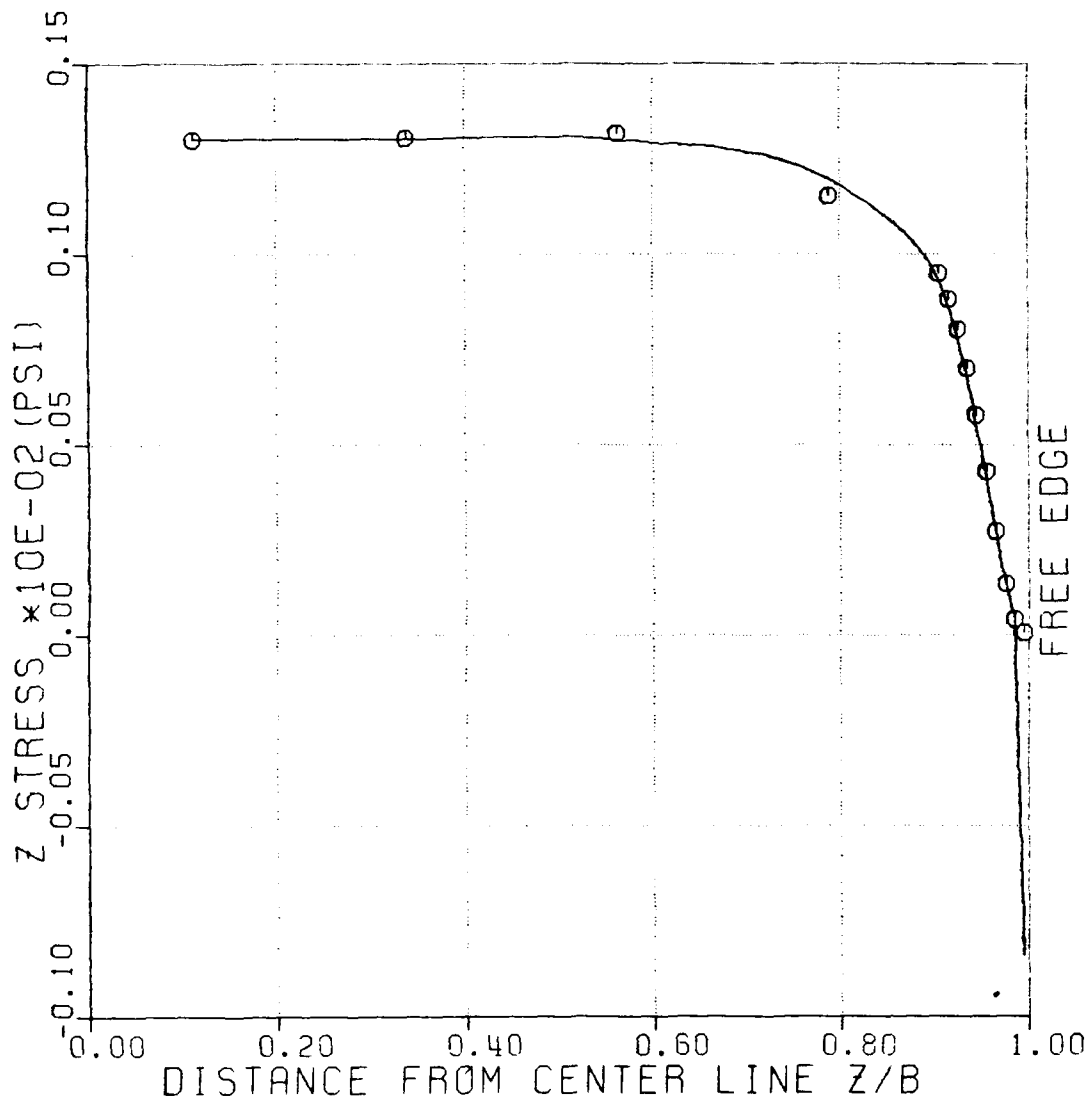Figure 74: Distribution of RZ-Stress Along R1 of
$[(25.5/-25.5)_5/90]_s$ Laminate

114

Figure 75: Distribution of RZ-Stress Along R5 of

$[(25.5/-25.5)_5/90]_s$ Laminate

115

Figure 76: Distribution of RZ-Stress Along R6 of

$[(25.5/-25.5)_5/90]_s$ Laminate

116

laminate except in the region of Z/B = 0.56 to 0.79 where apparently the mesh was not fine enough to approximate the steeply varying stress. Figure (77) shows the distribution of Rz-stress at R11, center of the layer nearest to the surface. A discrepancy in results was observed.

Figures (78), (79), (80) and (81) show the distribution of Tz-stress at R1, R5, R6 and R11 respectively. A close agreement was observed between the Q23 element and the axisymmetric solution except near the free edge where a steeply varying stress exists. Distribution of T-stress along R1 is shown in Figure (82). The figure indicates satisfactory agreement between the axisymmetric analysis and the Q23 element solution.

Figures (83),(84), (85) show, respectively, through-thickness distribution of R, Rz and TR-stresses at Z/B=0.995. A difference in results at some locations was observed between the two analyses for the Rz and TR-stresses. The R-stress values at centers of elements were underestimated throughout. Considering that the coarseness of mesh could be contributing to the discrepancy and to study convergence of results effect of mesh refinement in both the R and the Z-direction was considered.
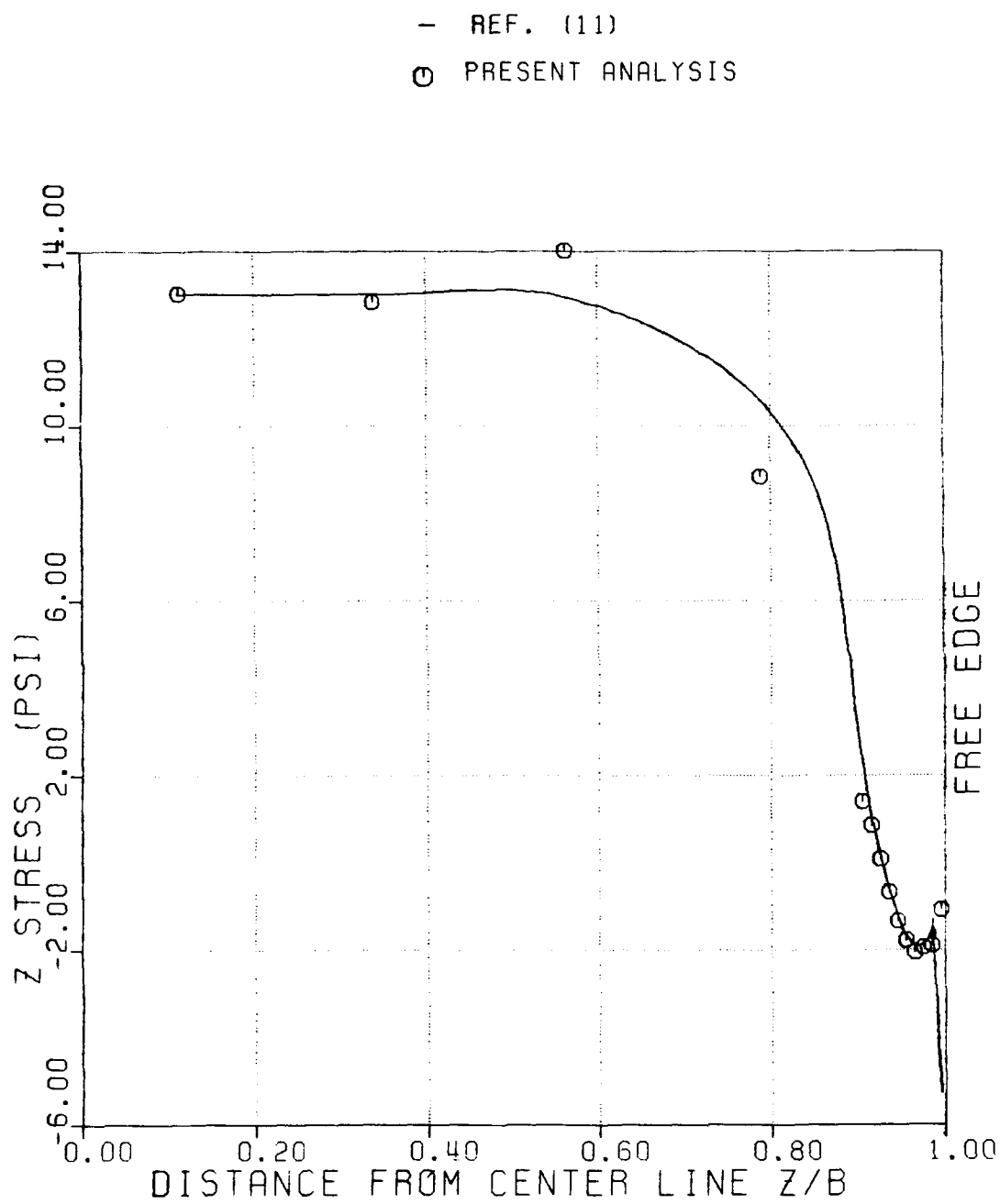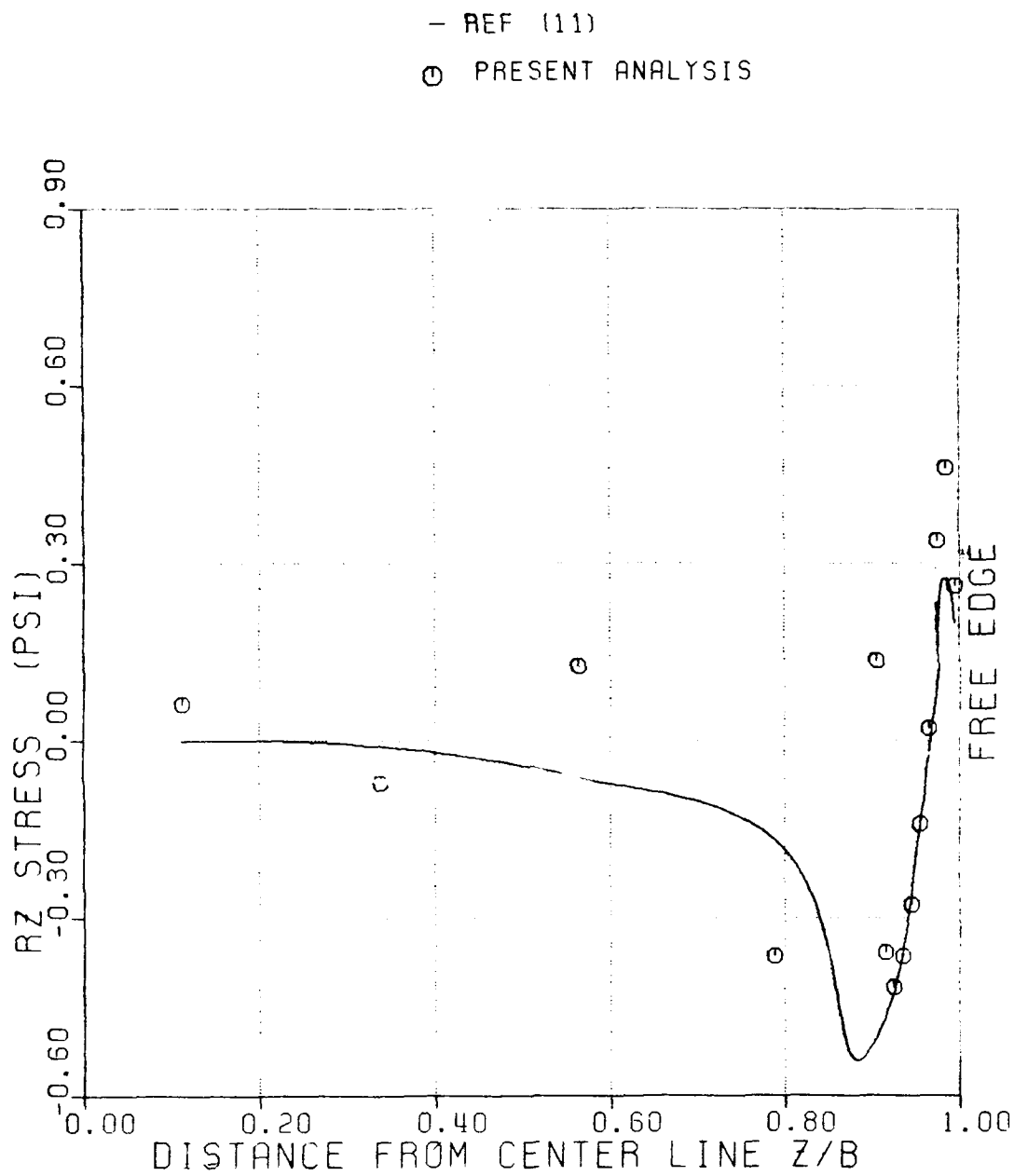
Figure 77: Distribution of RZ-Stress Along R11 of
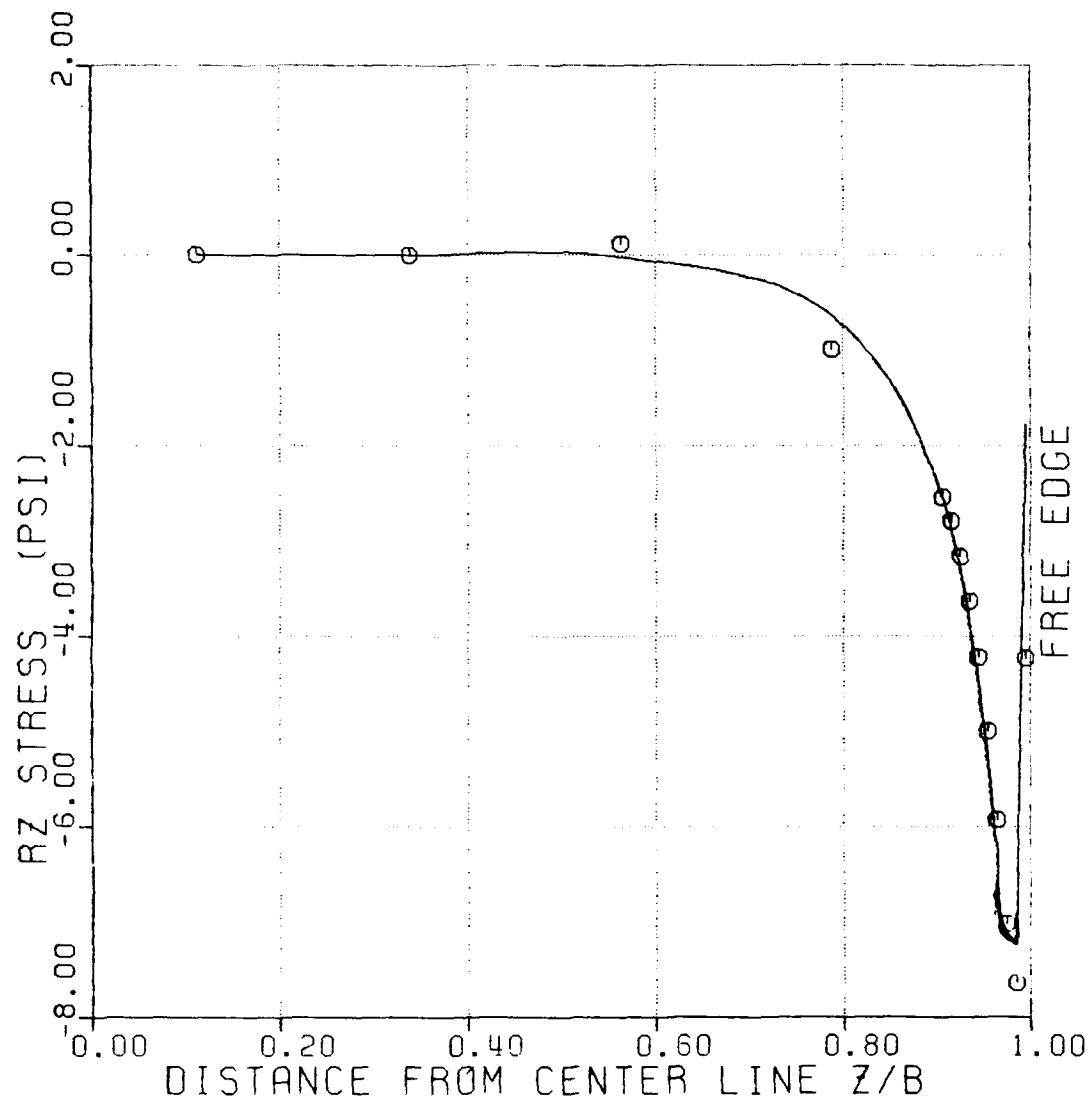
[(25.5/-25.5)₅/90]ₛ Laminate
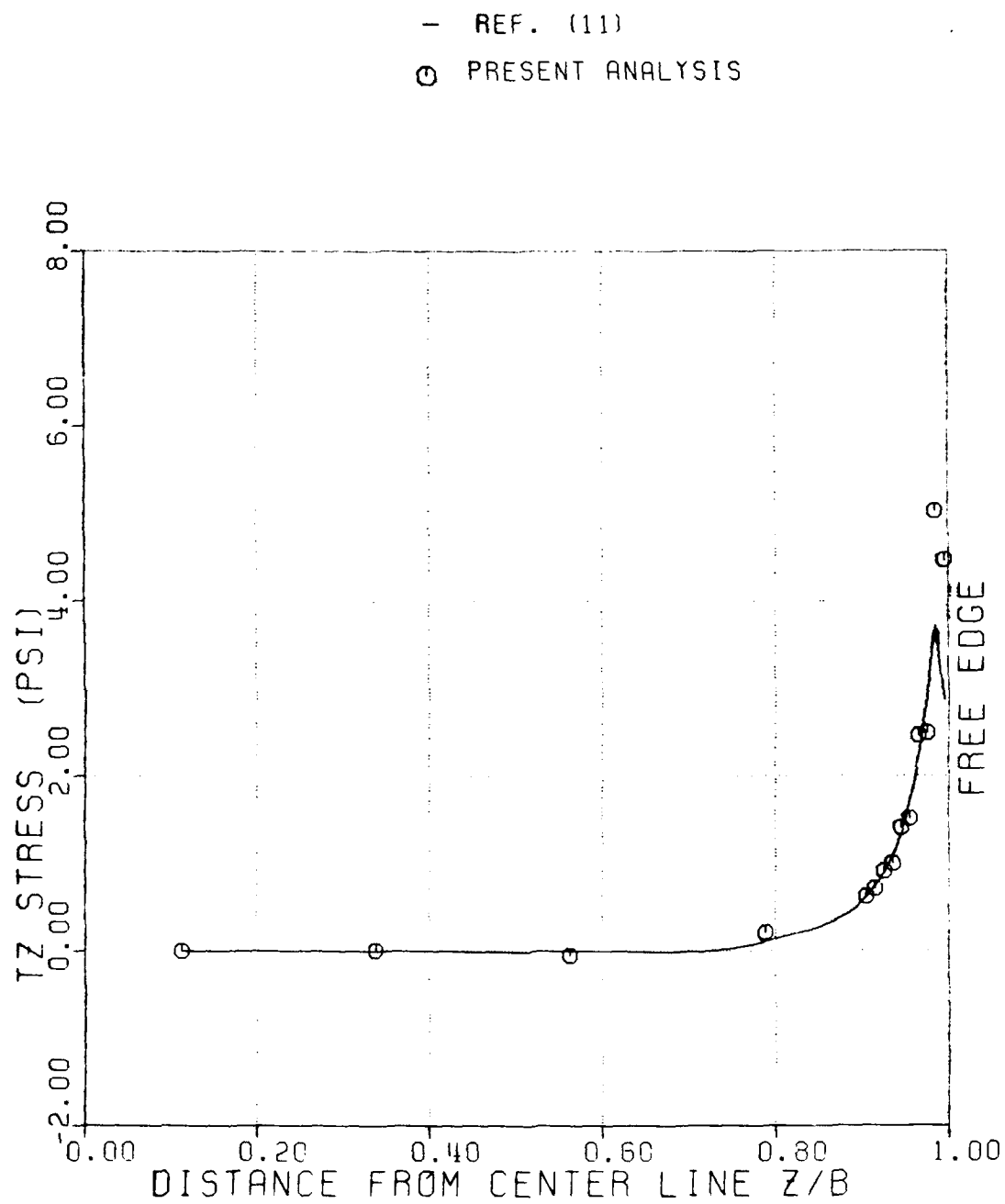
Figure 78: Distribution of TZ-Stress Along R1 of
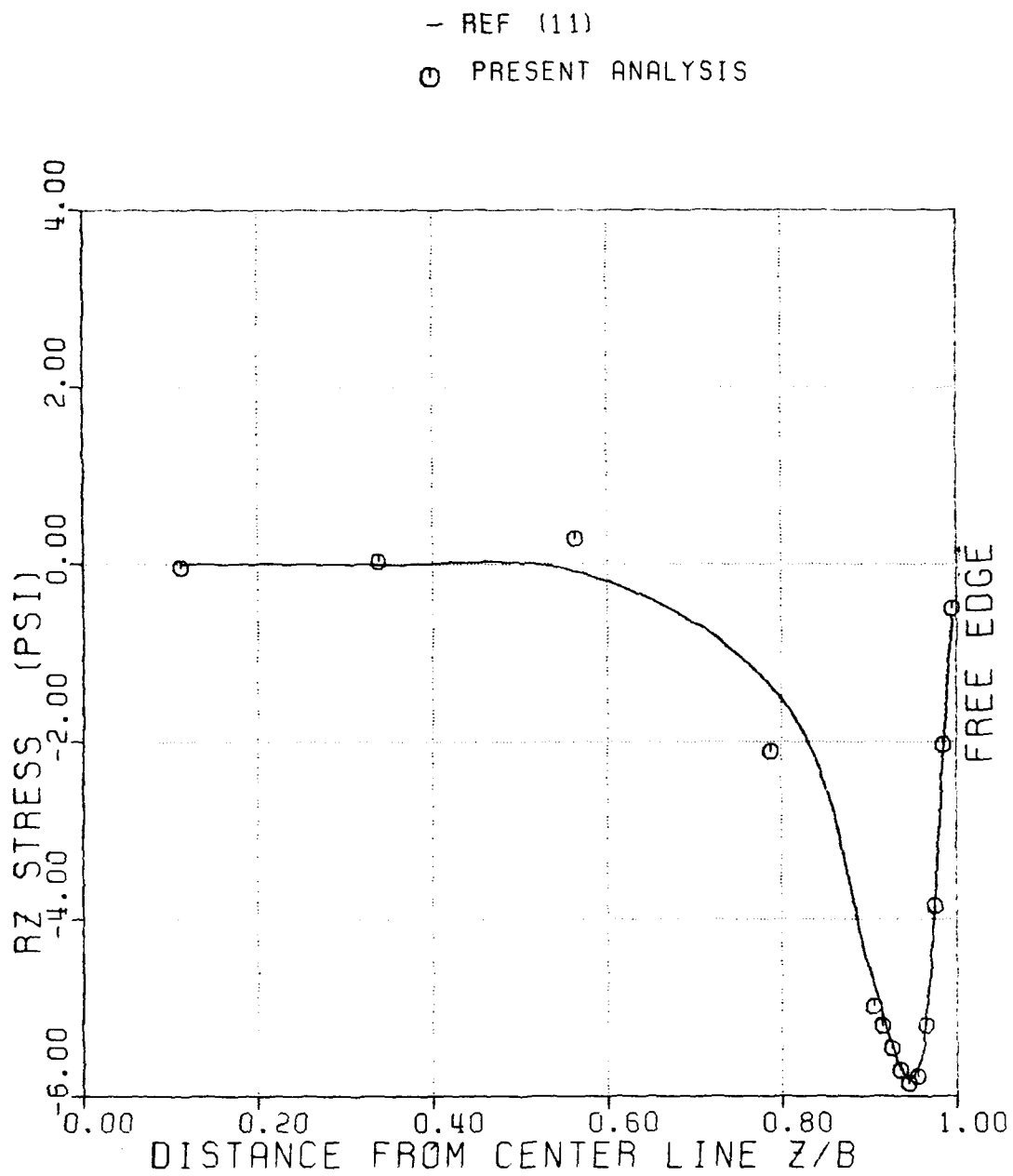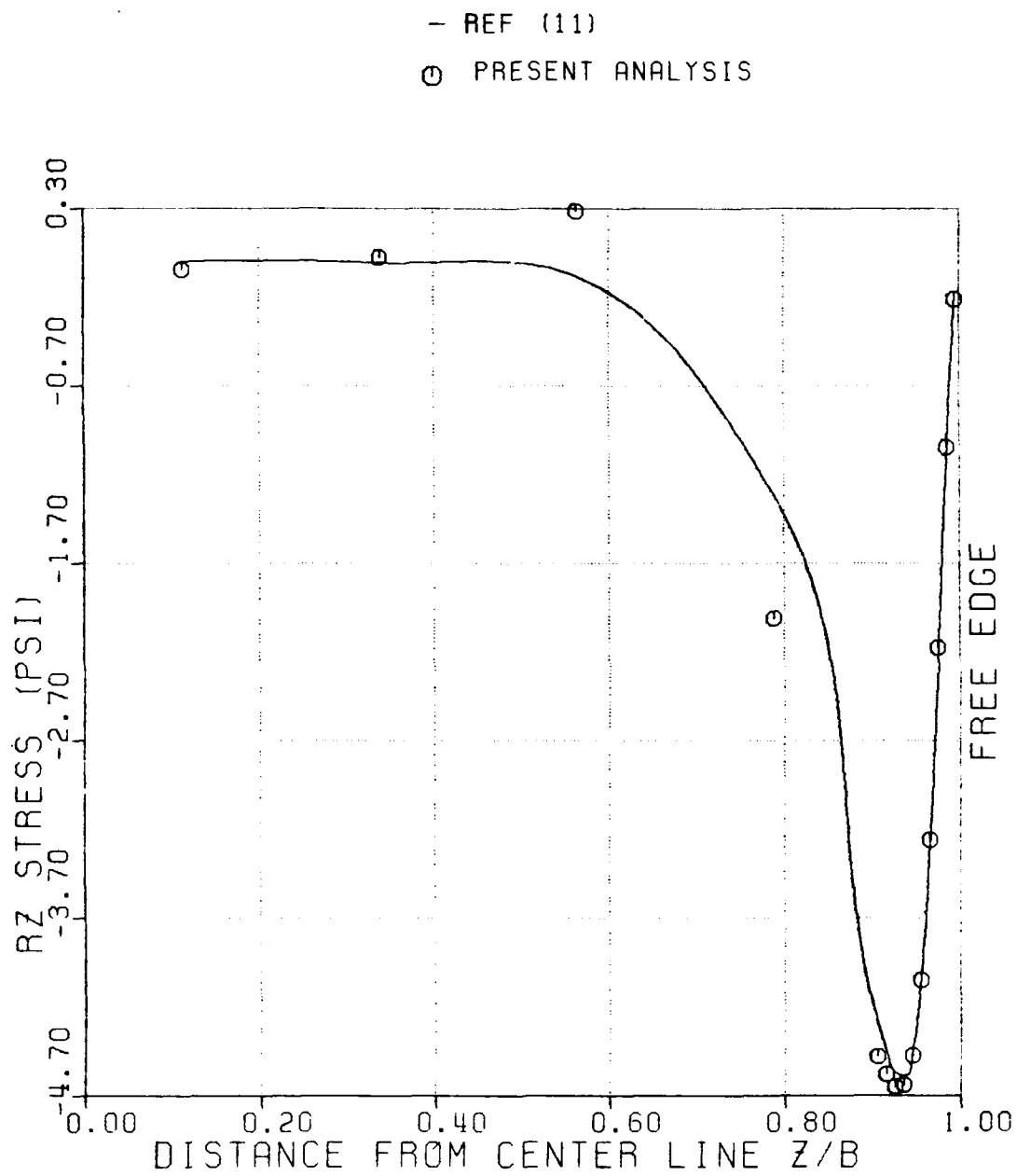
$[(25.5/-25.5)_5/90]_s$ Laminate

119
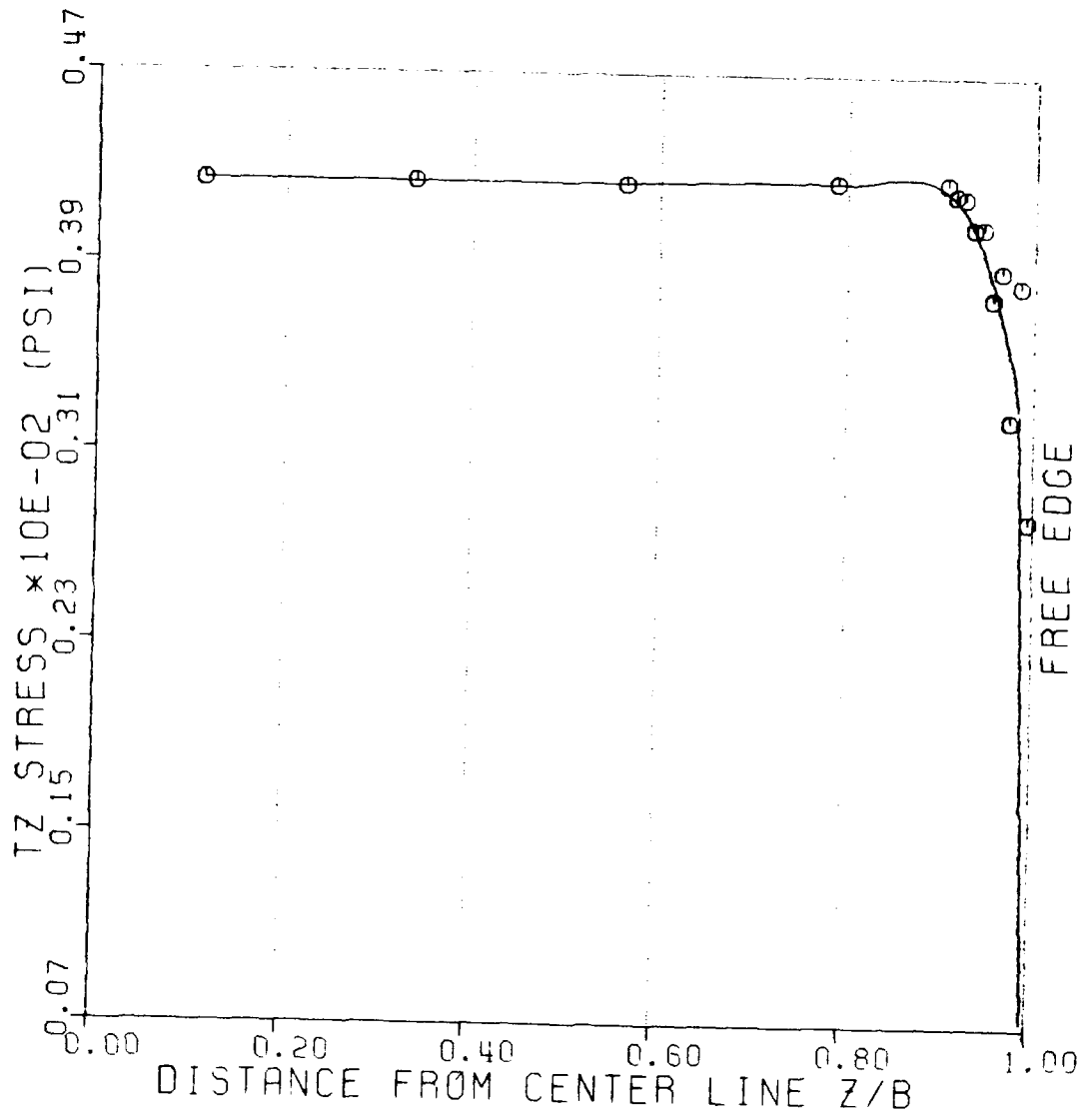
Figure 79: Distribution of TZ-Stress Along R5 of

$[(25.5/-25.5)_5/90]_s$ Laminate

120
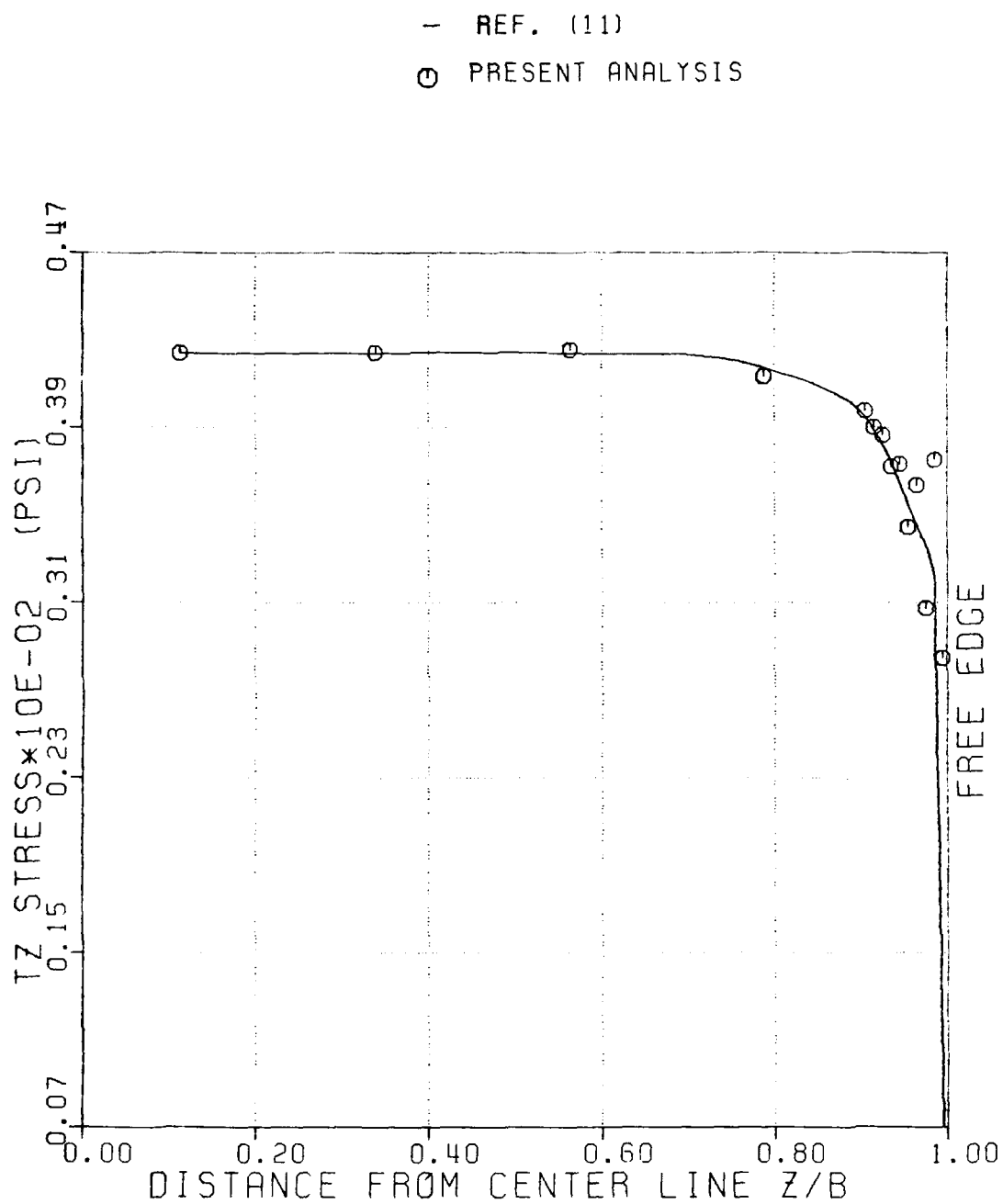
Figure 80: Distribution of TZ-Stress Along R6 of

$[(25.5/-25.5)_5/90]_s$ Laminate

121
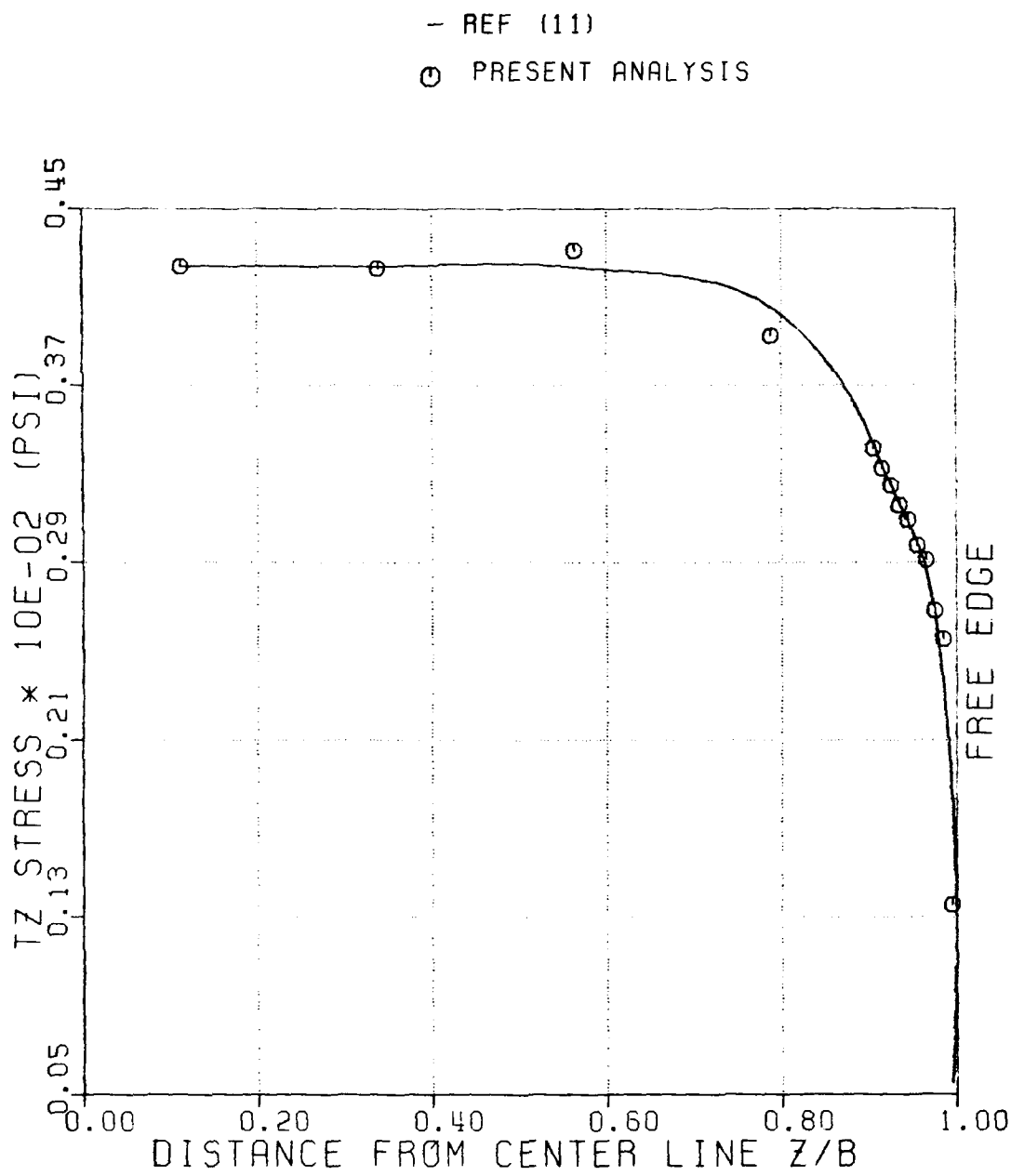
Figure 81: Distribution of TZ-Stress Along R11 of

$[(25.5/-25.5)_5/90]_s$ Laminate

122
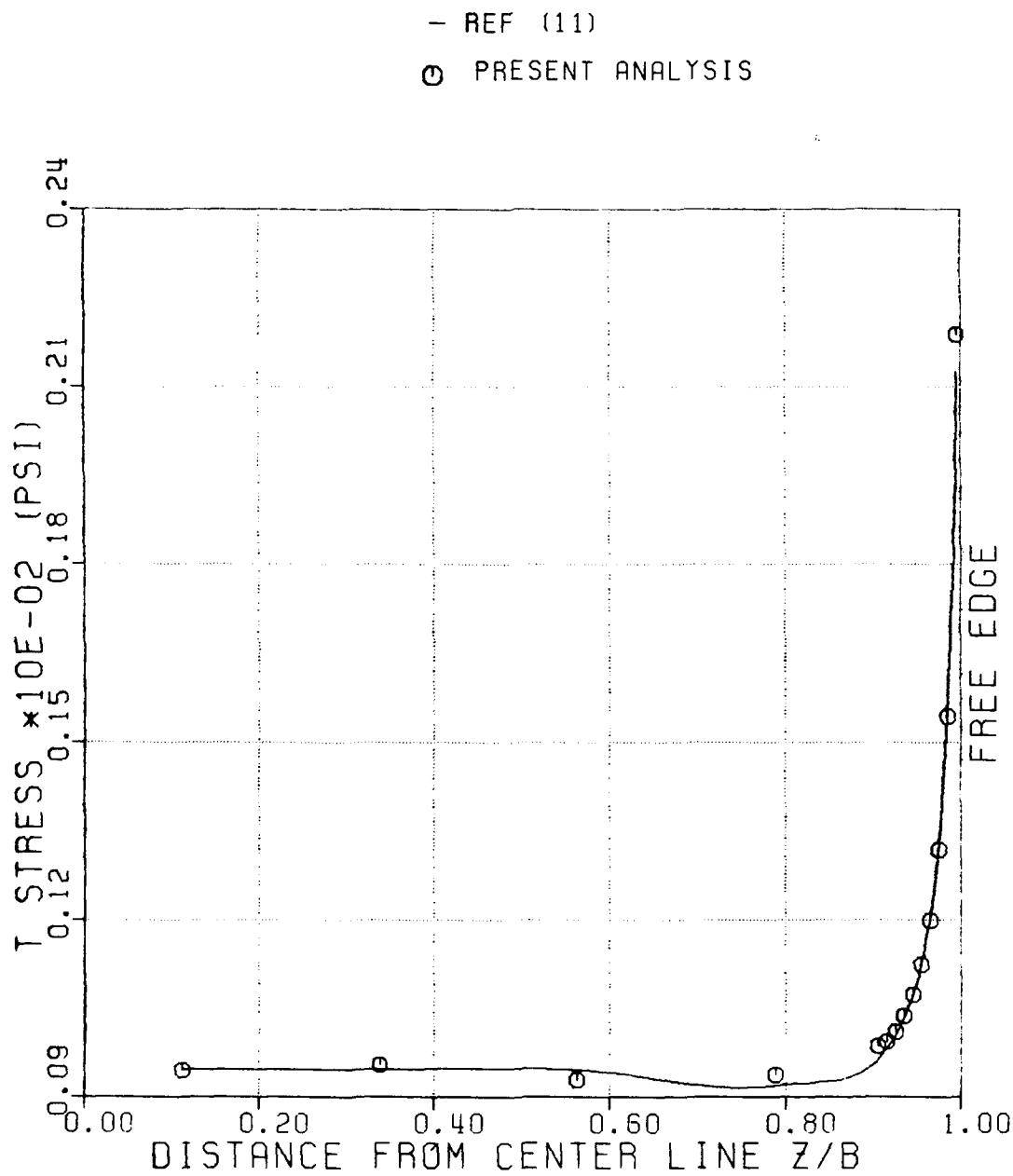
Figure 82: Distribution of T-Stress Along R1 of

$[(25.5/-25.5)_5/90]_s$ **Laminate**

123
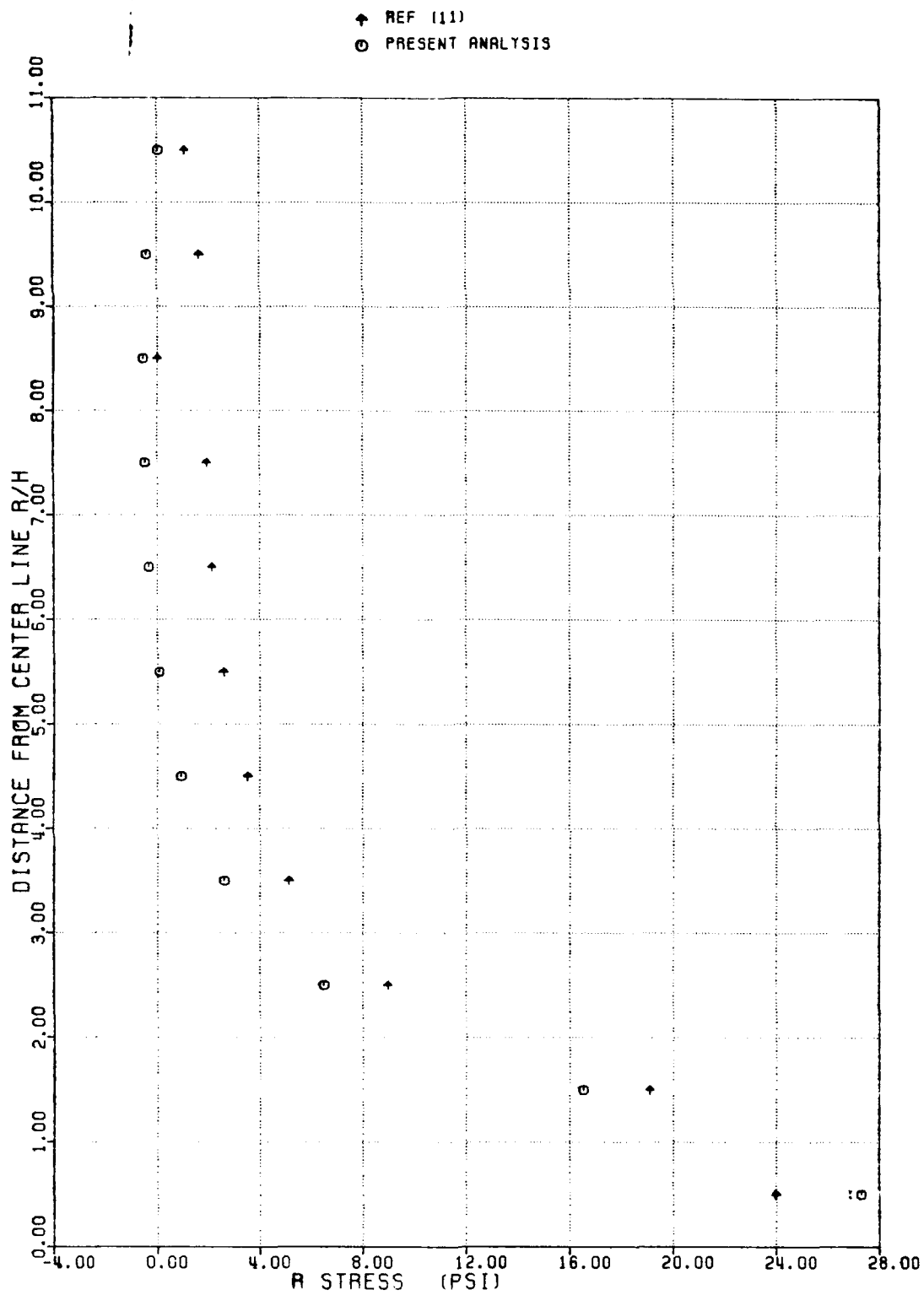
Figure 83: Through-Thickness Distribution of R-Stress Near Free edge (Z/B=0.995) of $[(25.5/-25.5)_5/90]_s$ Laminate
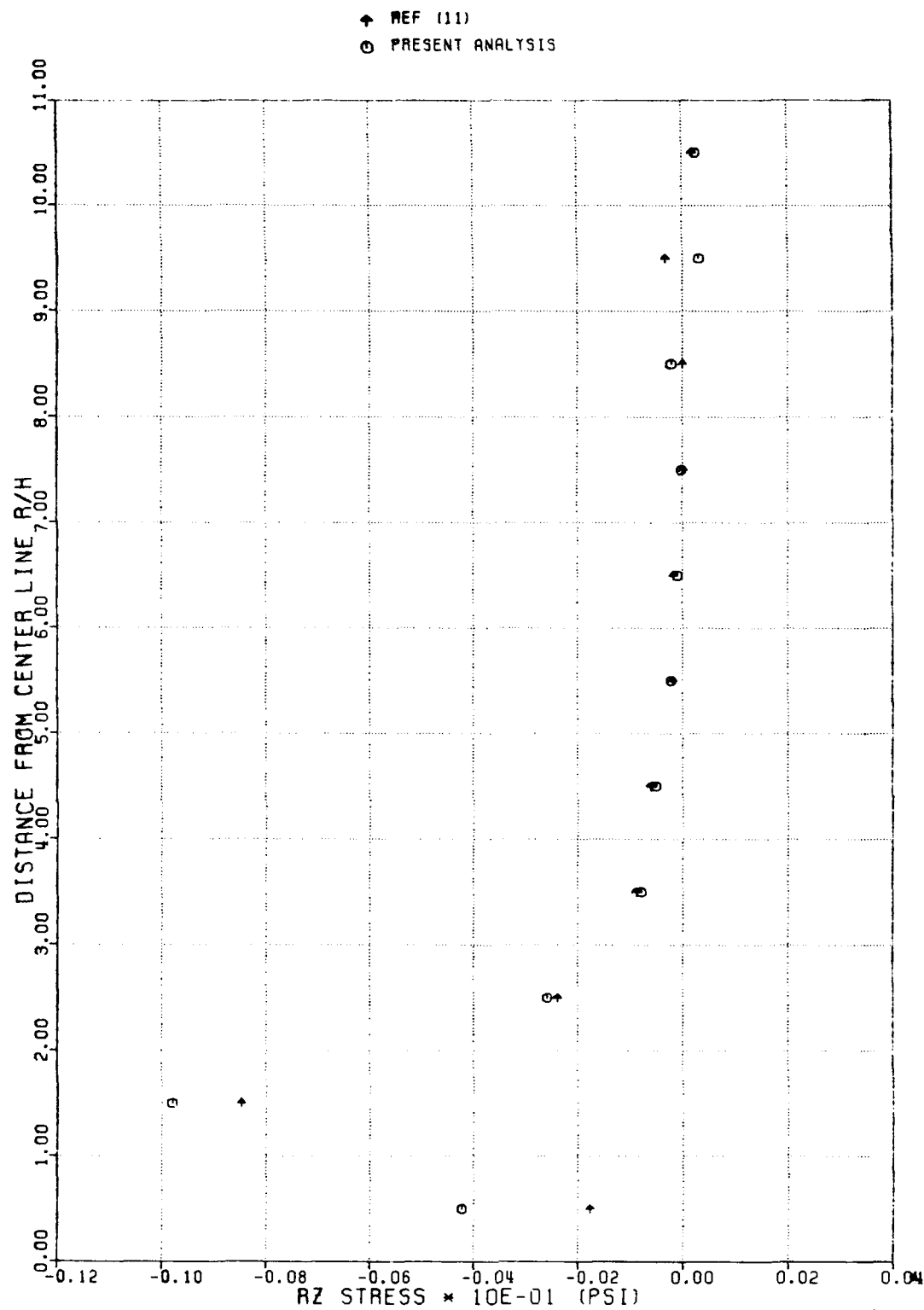
Figure 84: Through-Thickness Distribution of Rz-Stress Near Free edge (Z/B=0.995) of [(25.5/-25.5)₅/90]ₛ Laminate
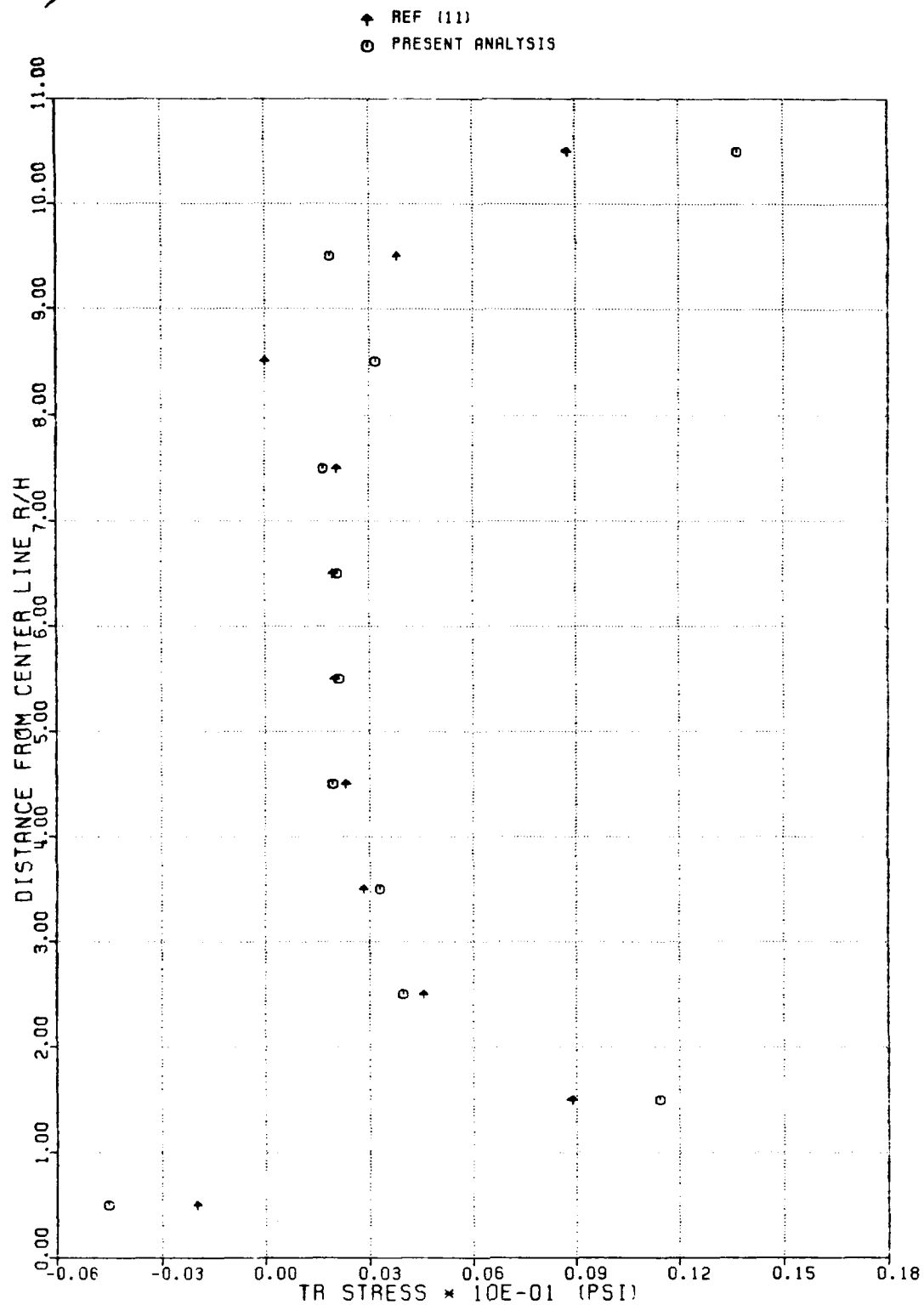
Figure 85: Through-Thickness Distribution of TR-
Stress Near Free edge (Z/B=0.995)
of [(25.5/-25.5)₅/90]ₛ Laminate

126

4.4.3 Effect of Mesh Refinement

Mesh refinement in the R-direction as well as in the Z-direction near the free edge was considered. Full section was used for the axisymmetric analysis. The mesh, corresponding to 726 (22x33) as shown in Figure (86) for half section discretization, was used to study refinement effect near the free edge. The mesh was obtained by dividing the two elements closest to the free edge in the 308-element model into 10 elements and also by refining in the region of $Z/B = 0.4$ to 0.8. results from the axisymmetric analysis were compared with the Q23 solutions obtained using the original mesh size which corresponds to the 308-element model.

Figures (87), (88), (89), and (90) show the distribution of Z-stress along R1, R5, R6, and R11 respectively. The figures indicate improvement in the distribution of Z-stress specially in the region of $Z/B = 0.56$ to 0.8 and near the free edge where the traction-free boundary condition was better reproduced by the finer mesh.

The effect of mesh refinement on Rz-stress distribution along R1, R5, R6 and R11 is shown in Figures (91), (92), (93) and (94) respectively. The refined mesh in the region of $Z/B = 0.6$ to 0.8 was necessary to represent the stress
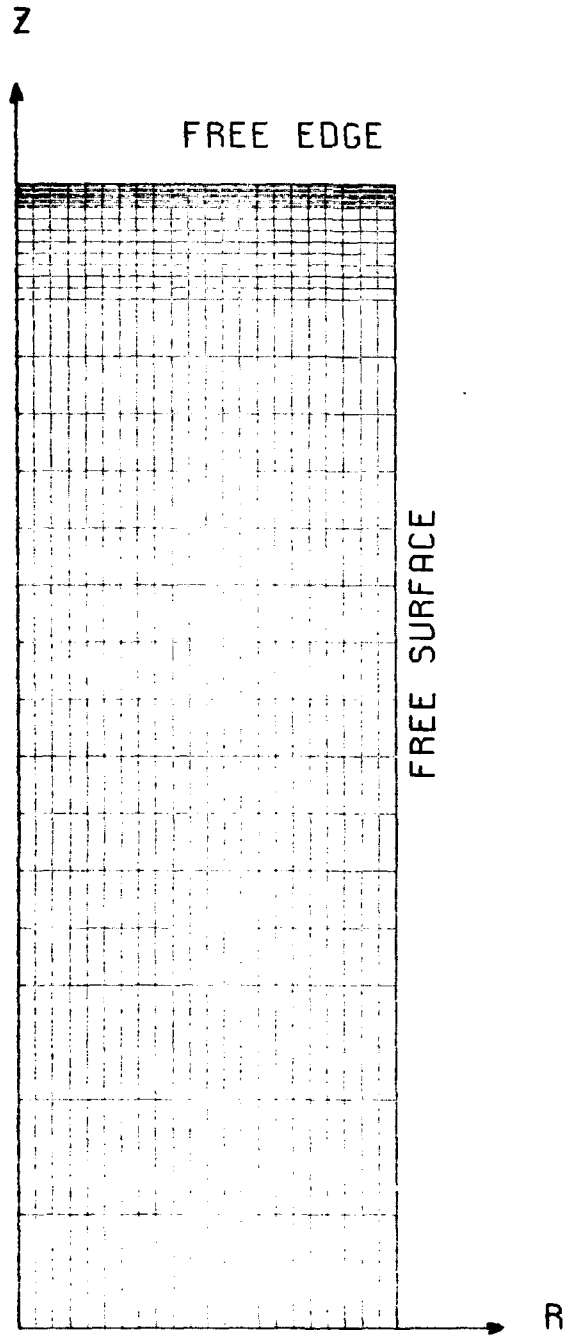
Figure 86: 726 Element Model (22x33)

Figure 87: Effect of Mesh Refinement on Distribution of Z-Stress Along R1 of [(25/-25)$_5$/90]$_s$ Laminate

129

Z STRESS *10E-02 (PSI)

0.15
0.10
0.05
0.00
-0.05
-0.10

FREE EDGE

0.00   0.20   0.40   0.60   0.80   1.00

DISTANCE FROM CENTER LINE Z/B

Figure 88: Effect of Mesh Refinement on Distribution of Z-Stress Along R5 of $[(25/-25)_5/90]_s$ Laminate

130

Figure 89: Effect of Mesh Refinement on Distribution of Z-Stress Along R6 of $[(25/-25)_5/90]_s$ Laminate

131

Figure 90: Effect of Mesh Refinement on Distribution of Z-Stress Along R11 of $[(25/-25)_5/90]_s$ Laminate

132

Figure 91: Effect of Mesh Refinement on Distribution of RZ-Stress Along R1 of $[(25/-25)_5/90]_s$ Laminate

133

Figure 92: **Effect of Mesh Refinement on Distribution of RZ-Stress Along R5 of [(25/-25)$_5$/90]$_s$ Laminate**

134

Figure 93: Effect of Mesh Refinement on Distribution of RZ-Stress Along R6 of $[(25/-25)_5/90]_s$ Laminate

Figure 94: Effect of Mesh Refinement on Distribution of RZ-Stress Along R11 of $[(25/-25)_5/90]_s$ Laminate

variation in this region even though a difference in the axisymmetric analysis and the Q23 element solution was still observed in Figures (92-94). The distribution of Rz-stress along R11 (Figure (94)) shows that the stresses varies steeply near the corner of the laminate and the singular stress behavior was reproduced somewhat better by the refined mesh.

Figures (95), (96), (97) show the effect of mesh refinement on Tz-stress distribution along R1, R5, and R6. A difference in results between the Q23 element solution and the axisymmetric analysis near the free edge was still observed. Figures (98) shows the distribution of Tz-stress along R11 and indicates that the results obtained using the refined mesh agreed well with the Q23 element solution.

The effect of mesh refinement in the R-direction on through-thickness distribution of stresses near the free edge was also studied. Each physical layer was subdivided into two sublayers, which correspond to (44x14) element model for half section discretization. For the axisymmetric analysis, an estimate of the stress field at the interfaces of the lamina was made by interpolating from the stress field computed at the adjacent centers of the sublayers. Cubic spline functions were used. Results were compared with
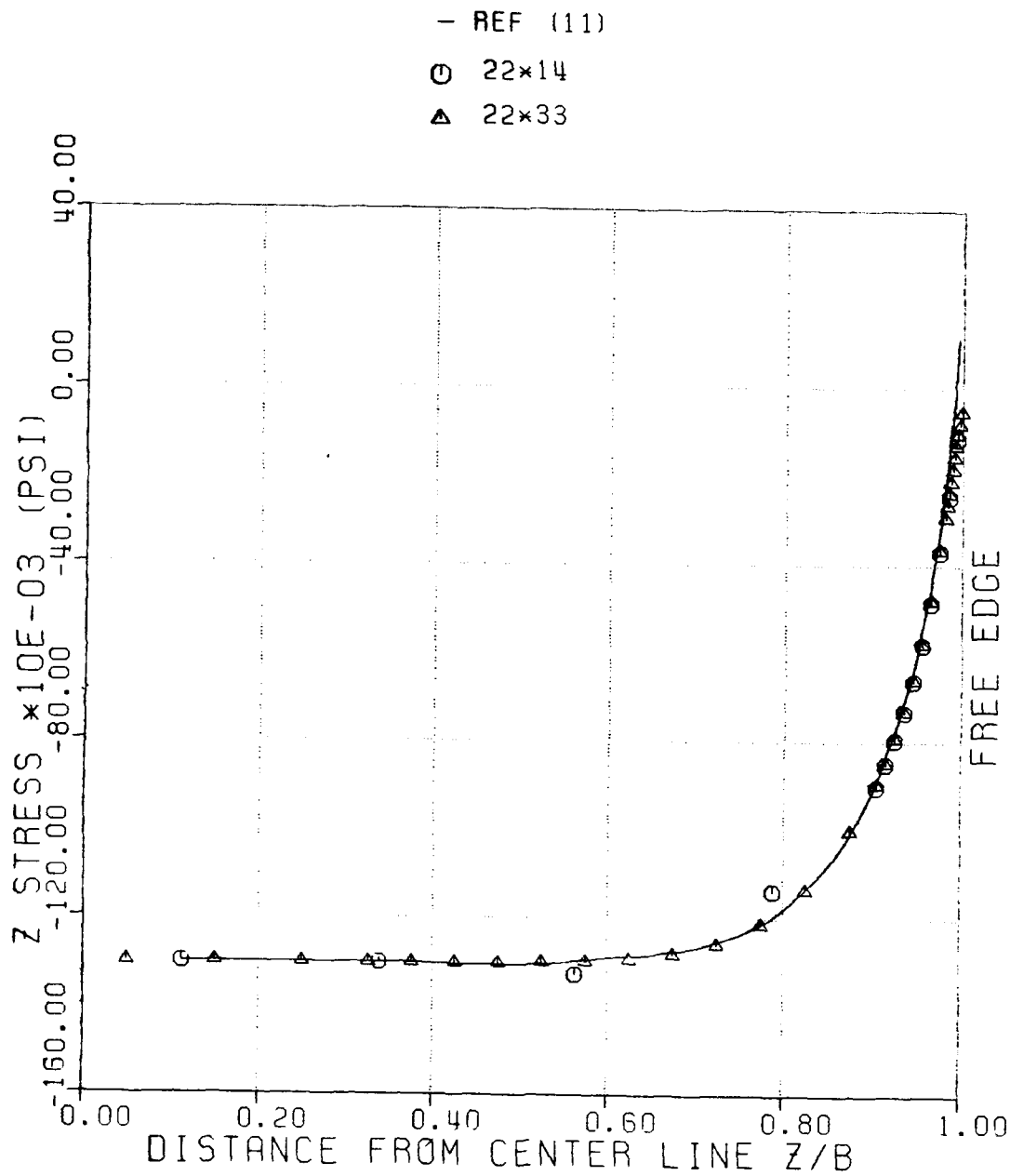
Figure 95: Effect of Mesh Refinement on Distribution of TZ-Stress Along R1 of $[(25/-25)_5/90]_s$ Laminate

138

Figure 96: Effect of Mesh Refinement on Distribution of TZ-Stress Along R5 of [(25/-25)$_5$/90]$_s$ Laminate
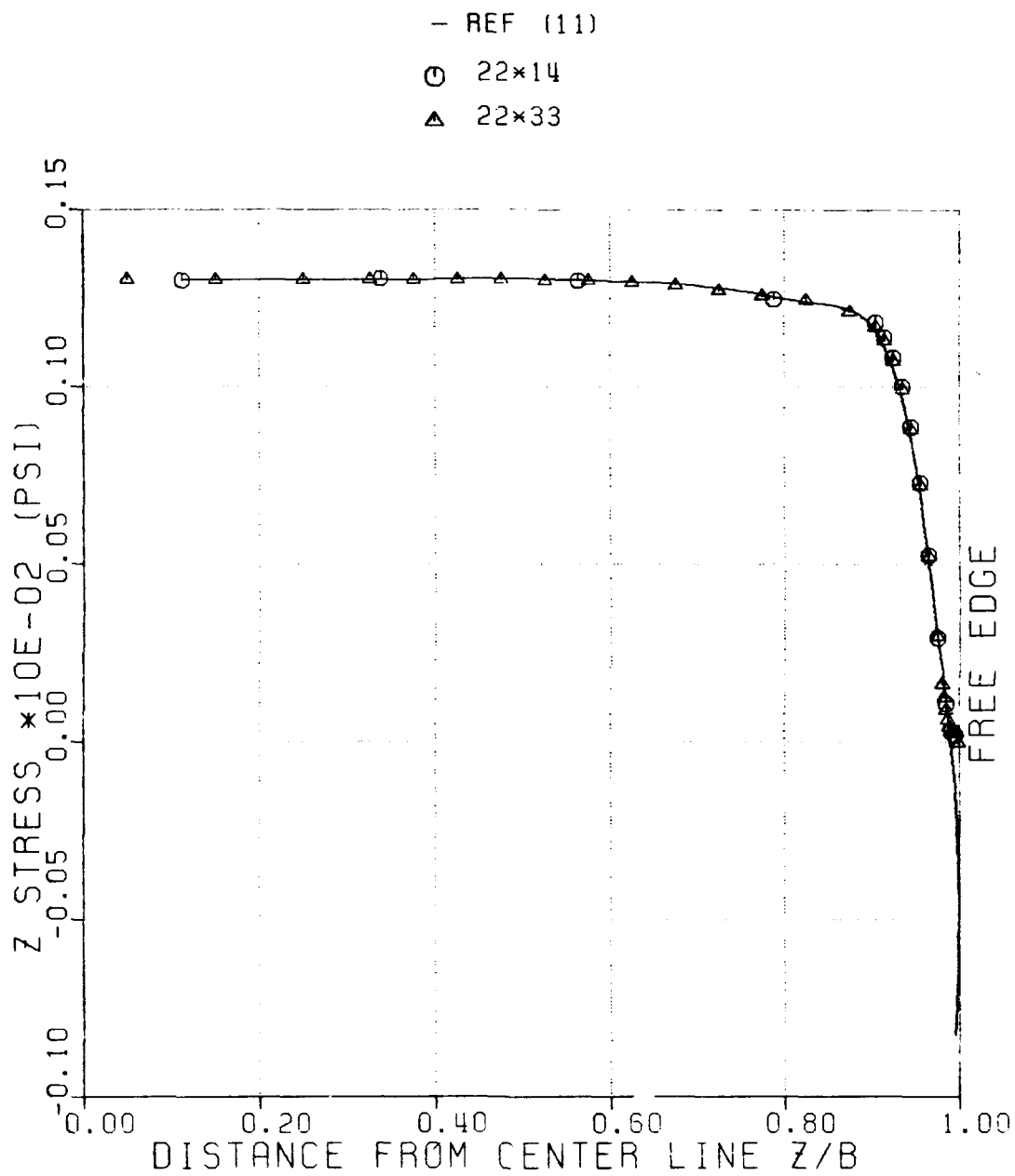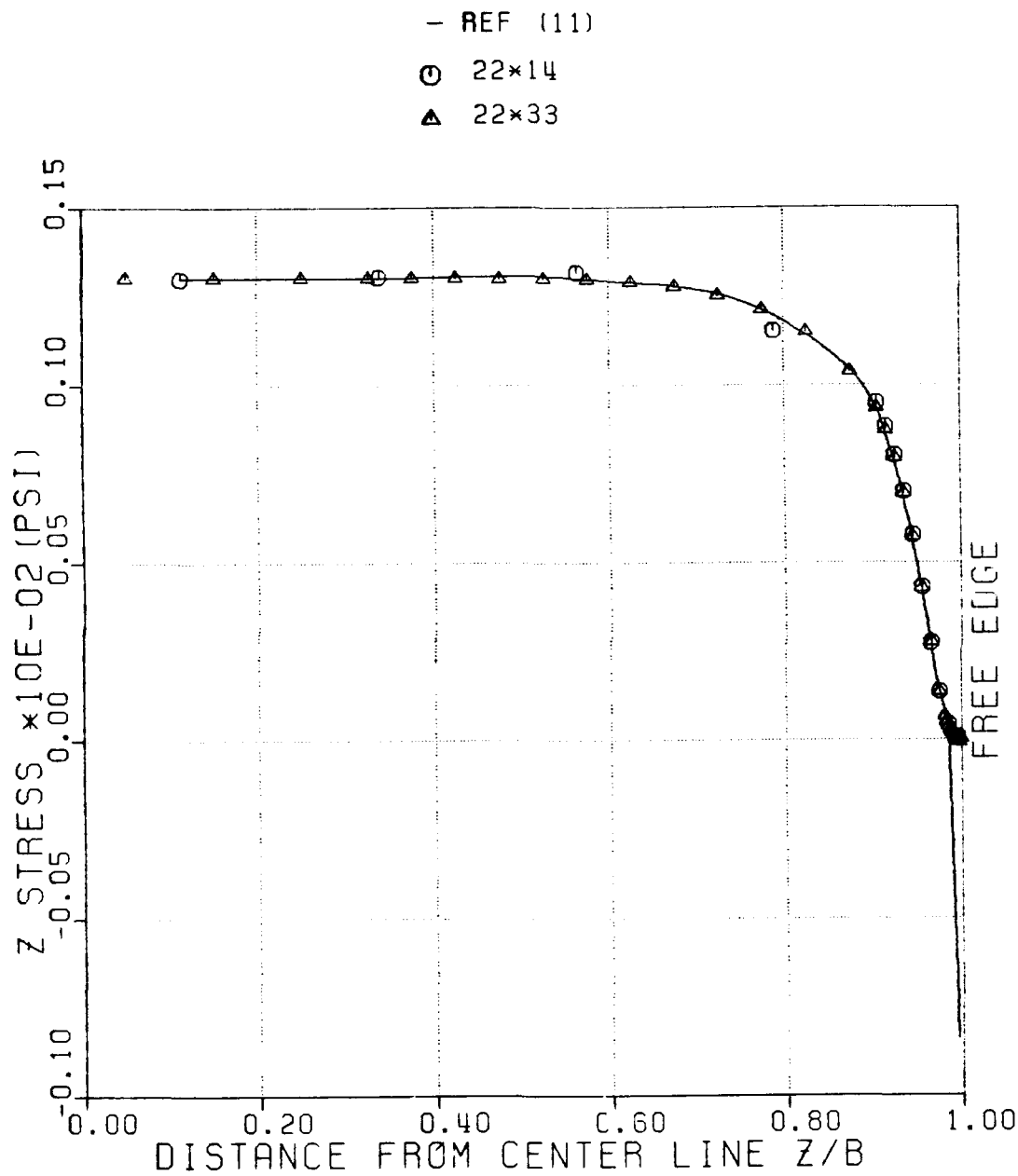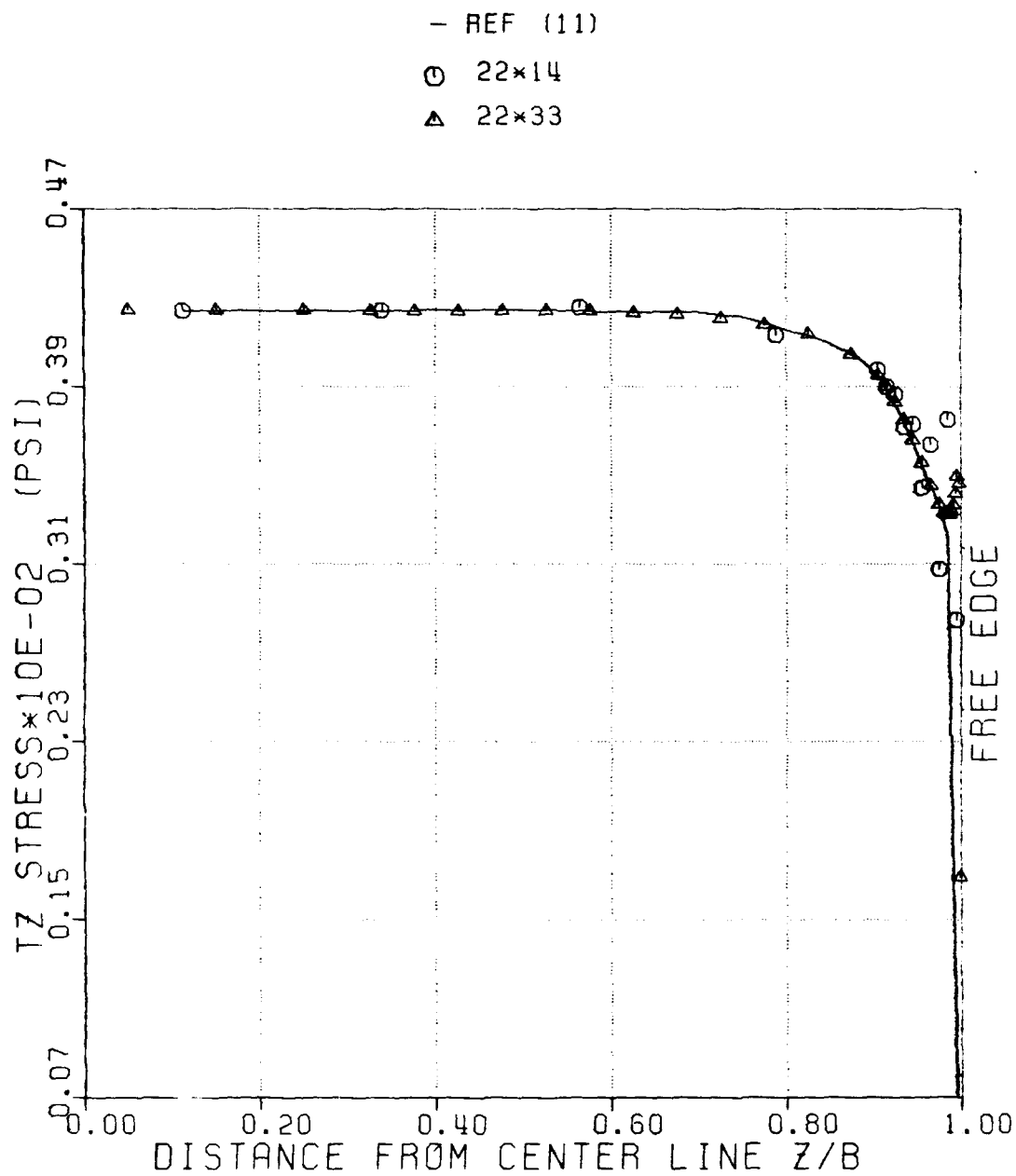
Figure 97: Effect of Mesh Refinement on Distribution
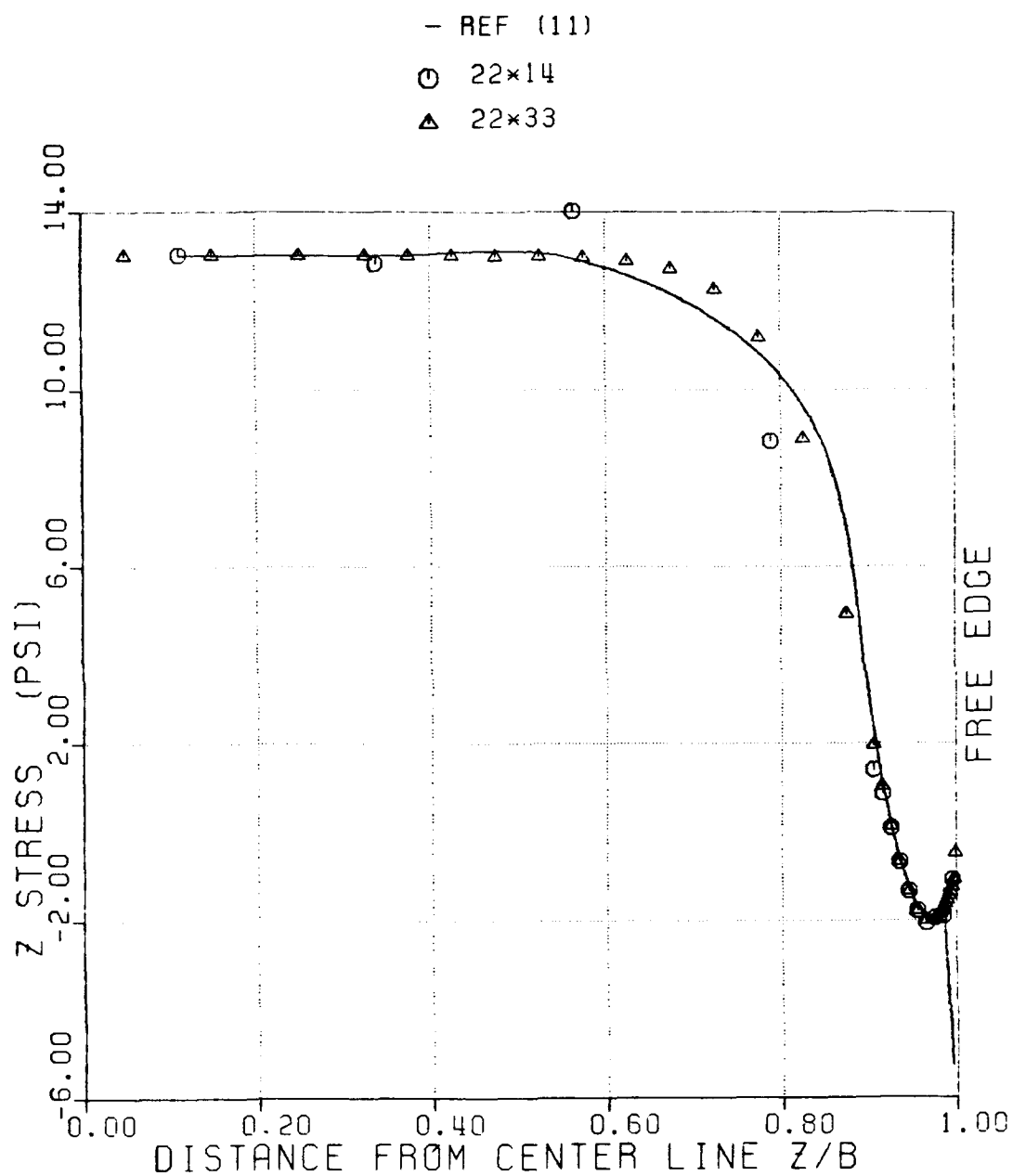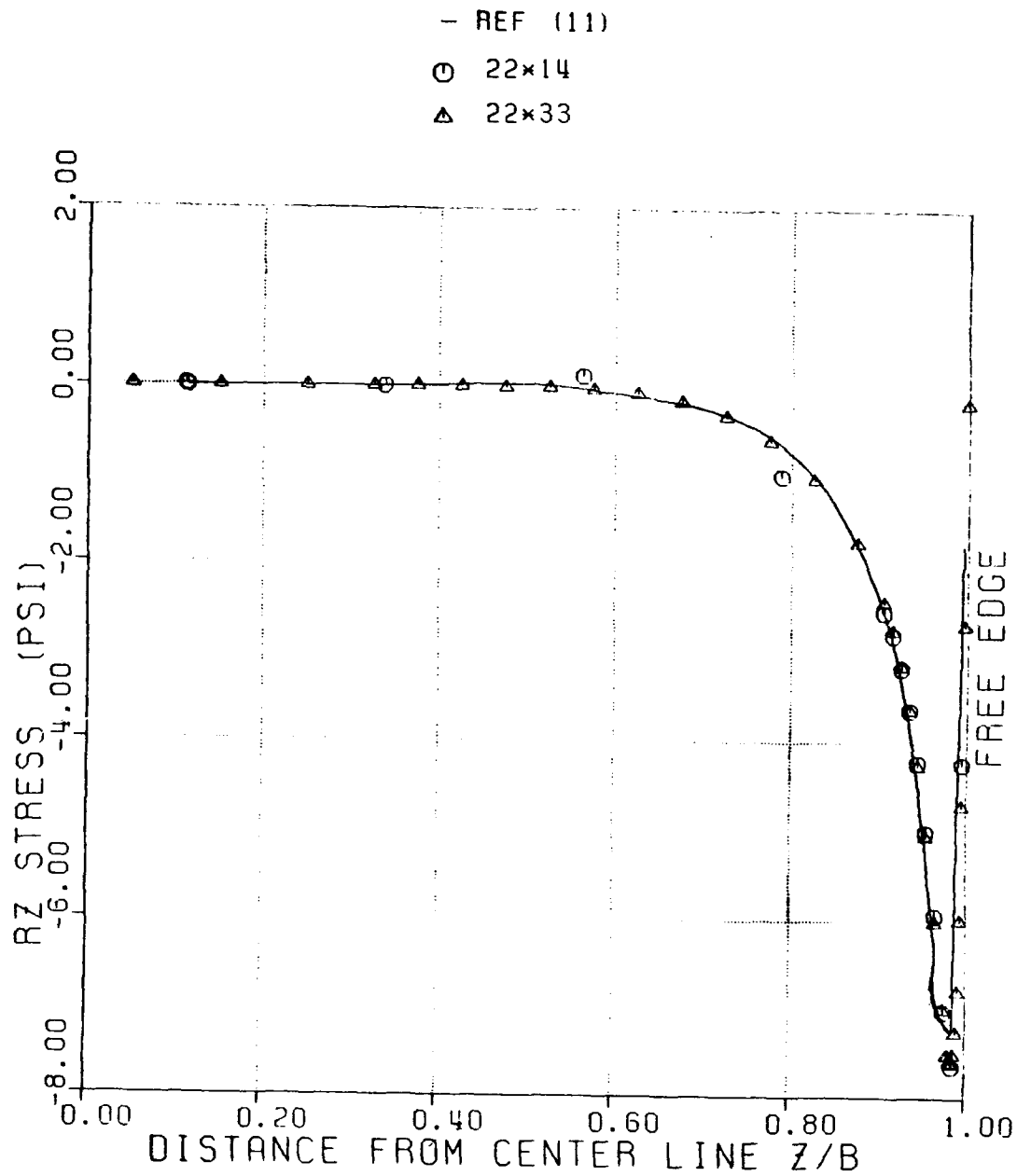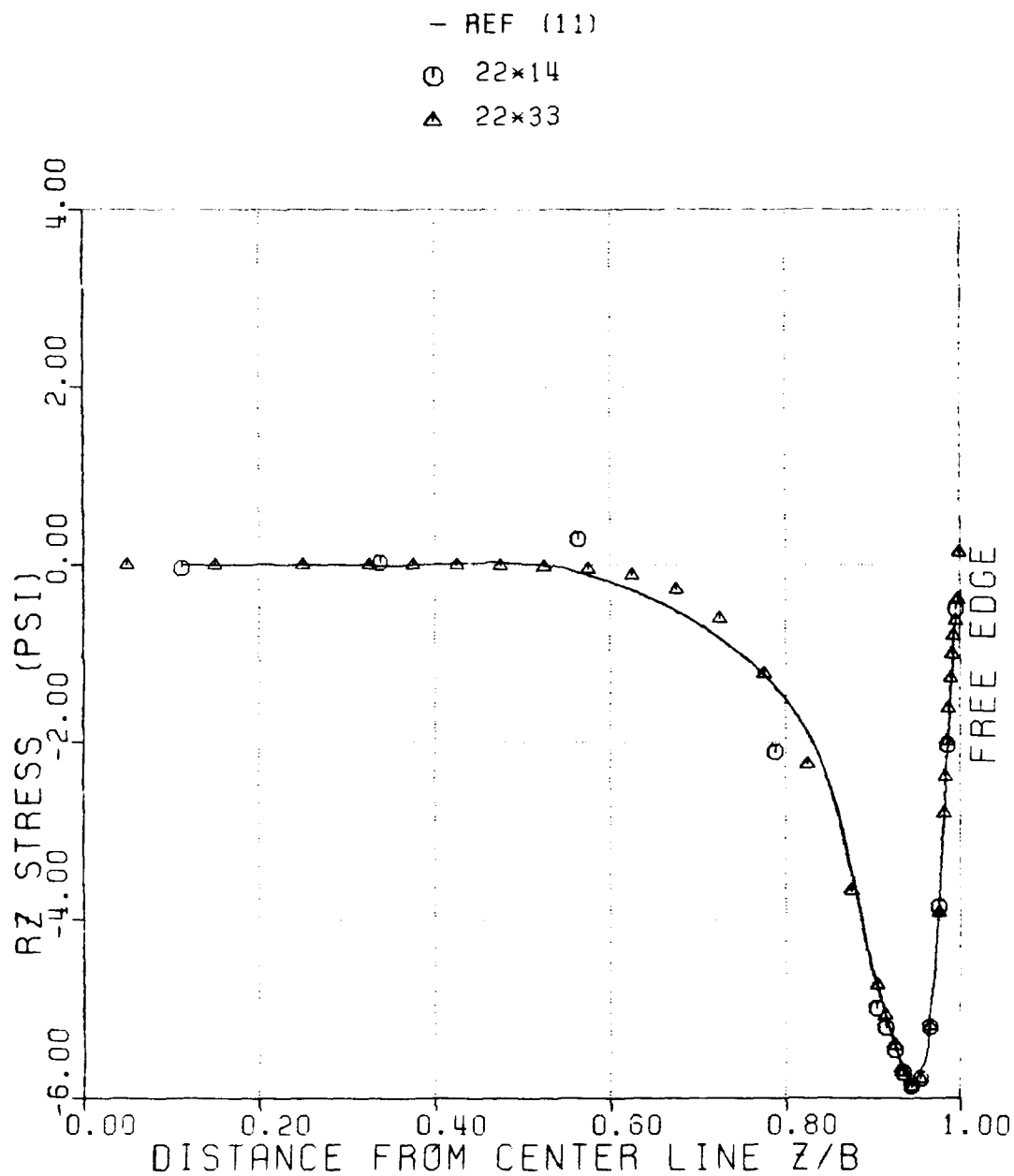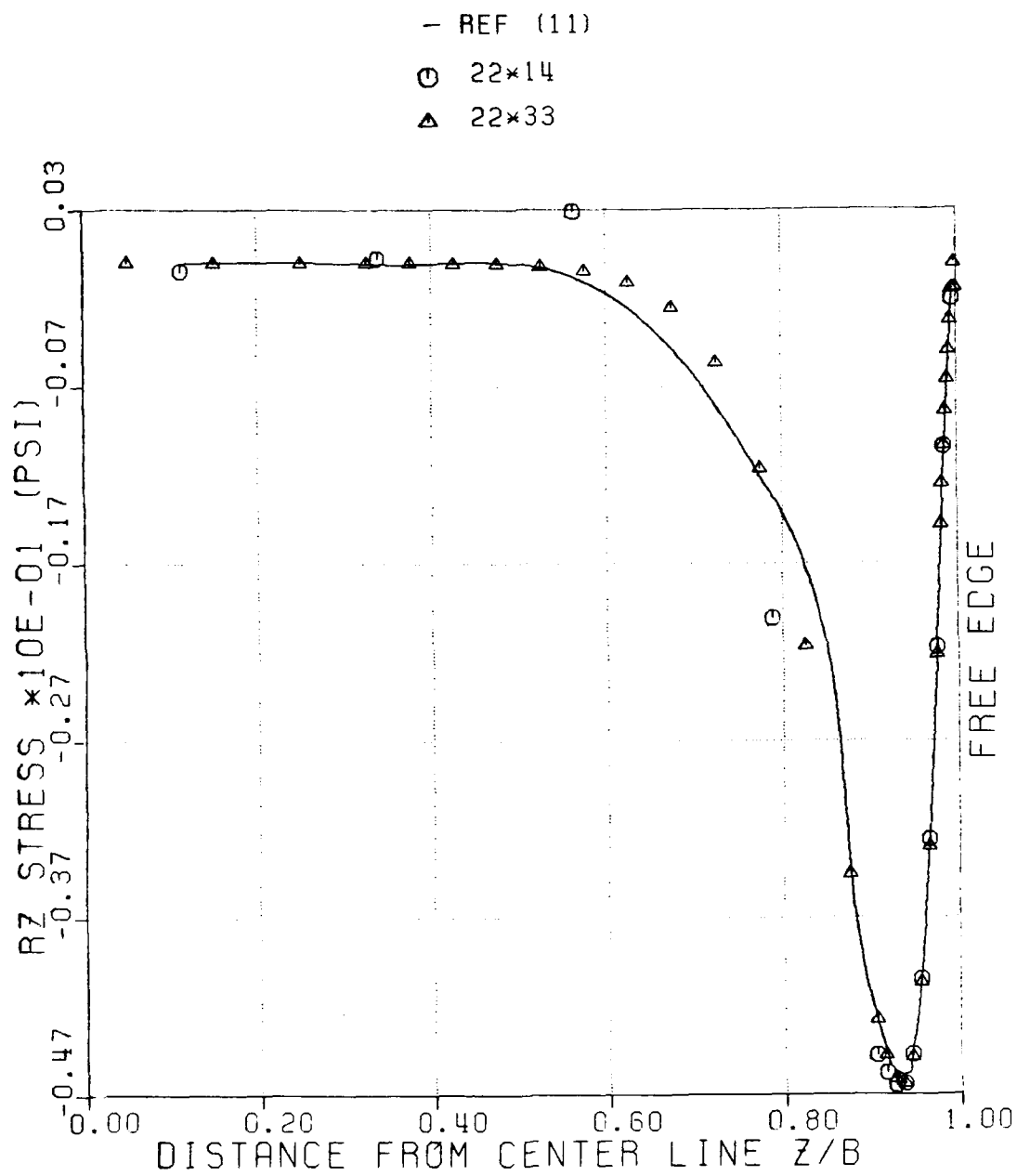   of TZ-Stress Along R6 of $[(25/-25)_5/90]_s$
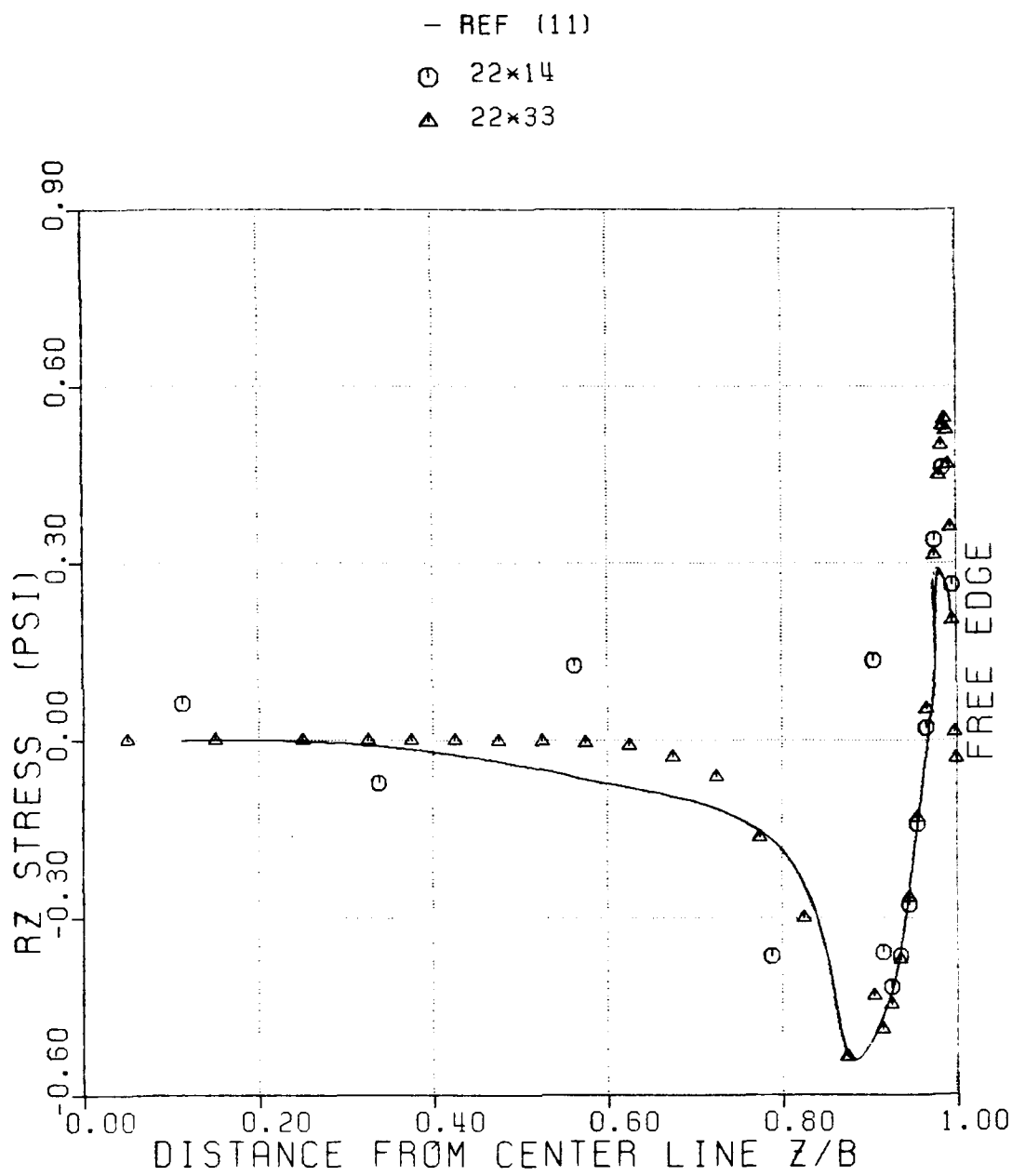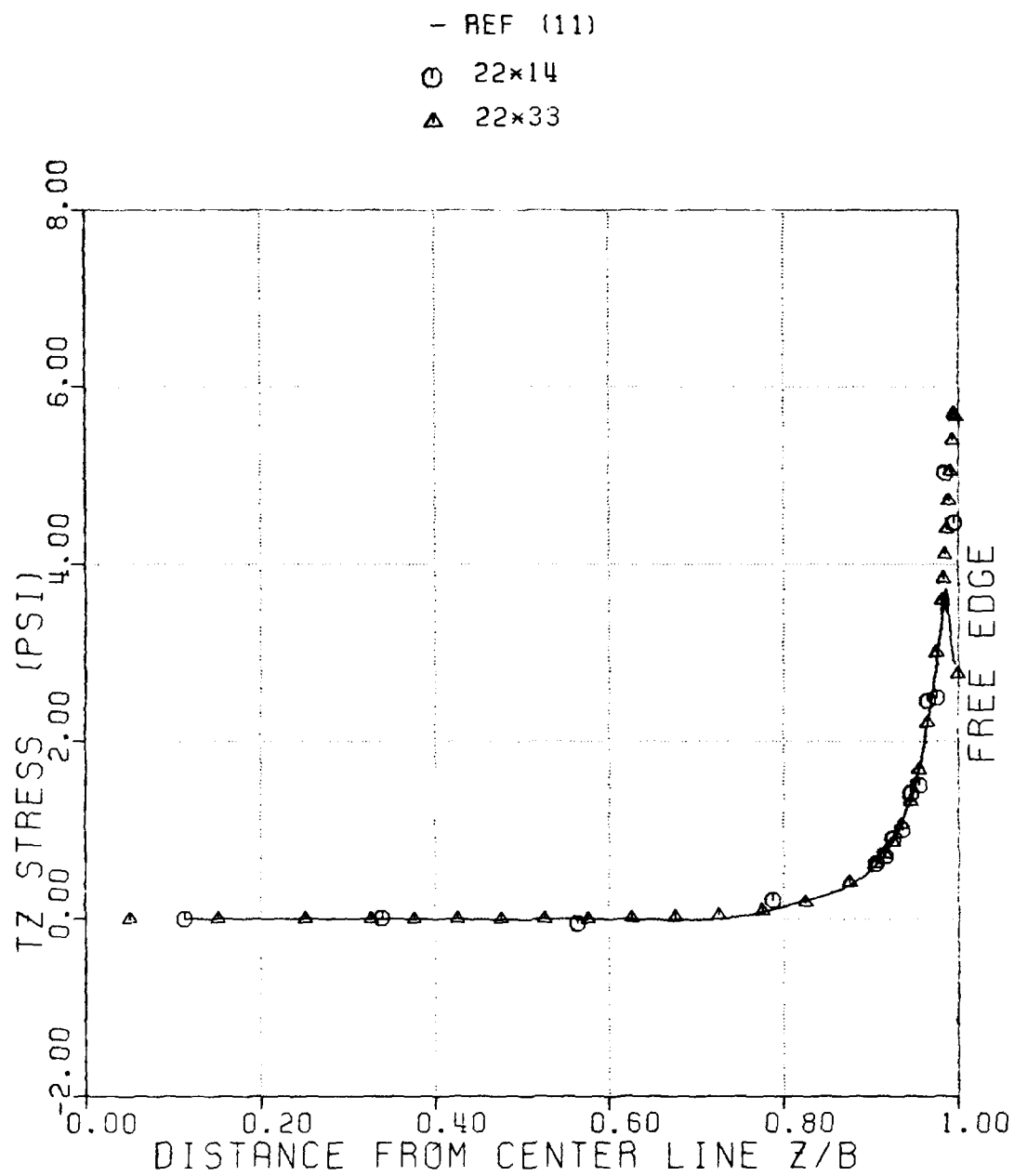   Laminate

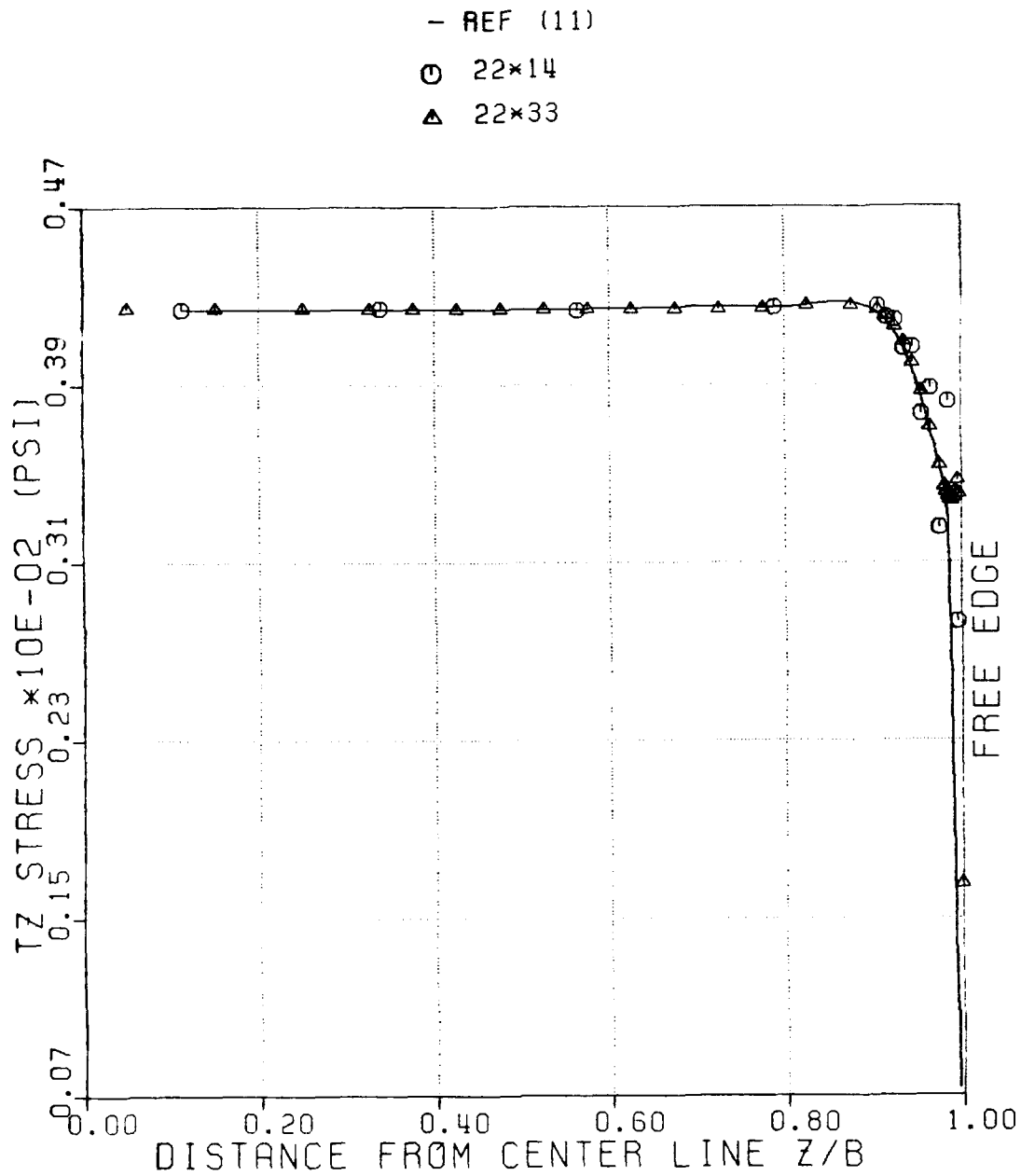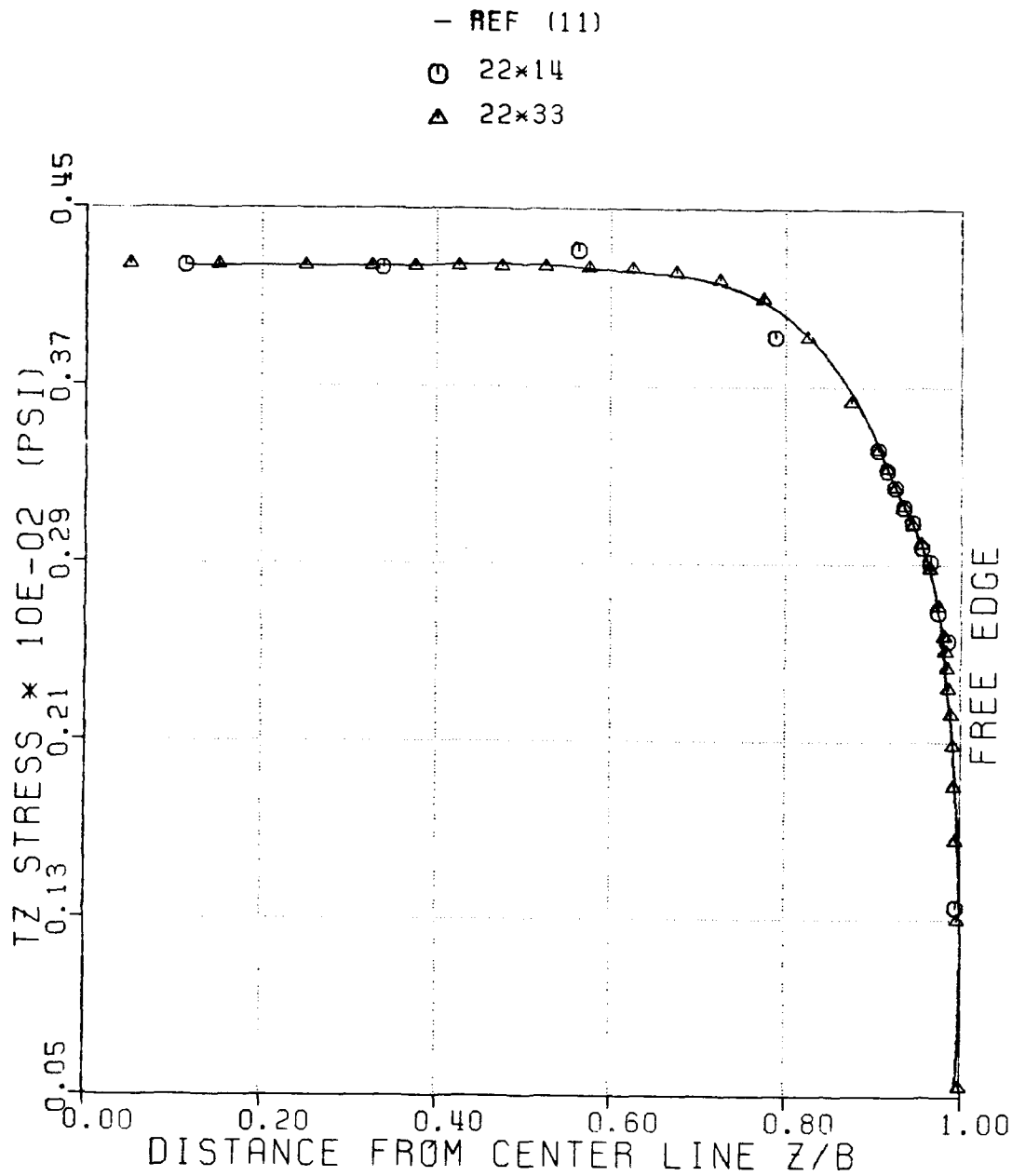**Figure 98: Effect of Mesh Refinement on Distribution of TZ-Stress Along R11 of [(25/-25)$_5$/90]$_s$ Laminate**

141

the Q23 element solution which gave values of the stress fields at the interfaces. Figure (99) shows through-thickness distribution of R-stress at Z/B= 0.995. The Q23 element solution showed an oscillatory pattern of stress which was not seen in the spline fit of the axisymmetric analysis. Figure (100) shows through-thickness distribution of Rz-stress at Z/B = 0.995. The figure indicates satisfactory agreement between the axisymmetric analysis and the Q23 element solution except at the interface of the 90-degree layer and the angle-ply layer where a singular stress behavior is observed. Figure (101) shows through-thickness distribution of Tr-stress near the free edge. The refined mesh showed an oscillatory pattern of stress which agreed with the Q23 solution. At the interfaces of the layers, the interpolated value, obtained using spline fitting of the axisymmetric analysis results differed by up to 16% as compared to the approximate stress values obtained using the Q23 analysis. However, this discrepancy could be largely due to the spline fit which insures continuity of slopes and curvatures. For the laminate considered, the TR-stress component may (and Q23 analysis confirms this) have discontinuity in gradients at the interfaces.
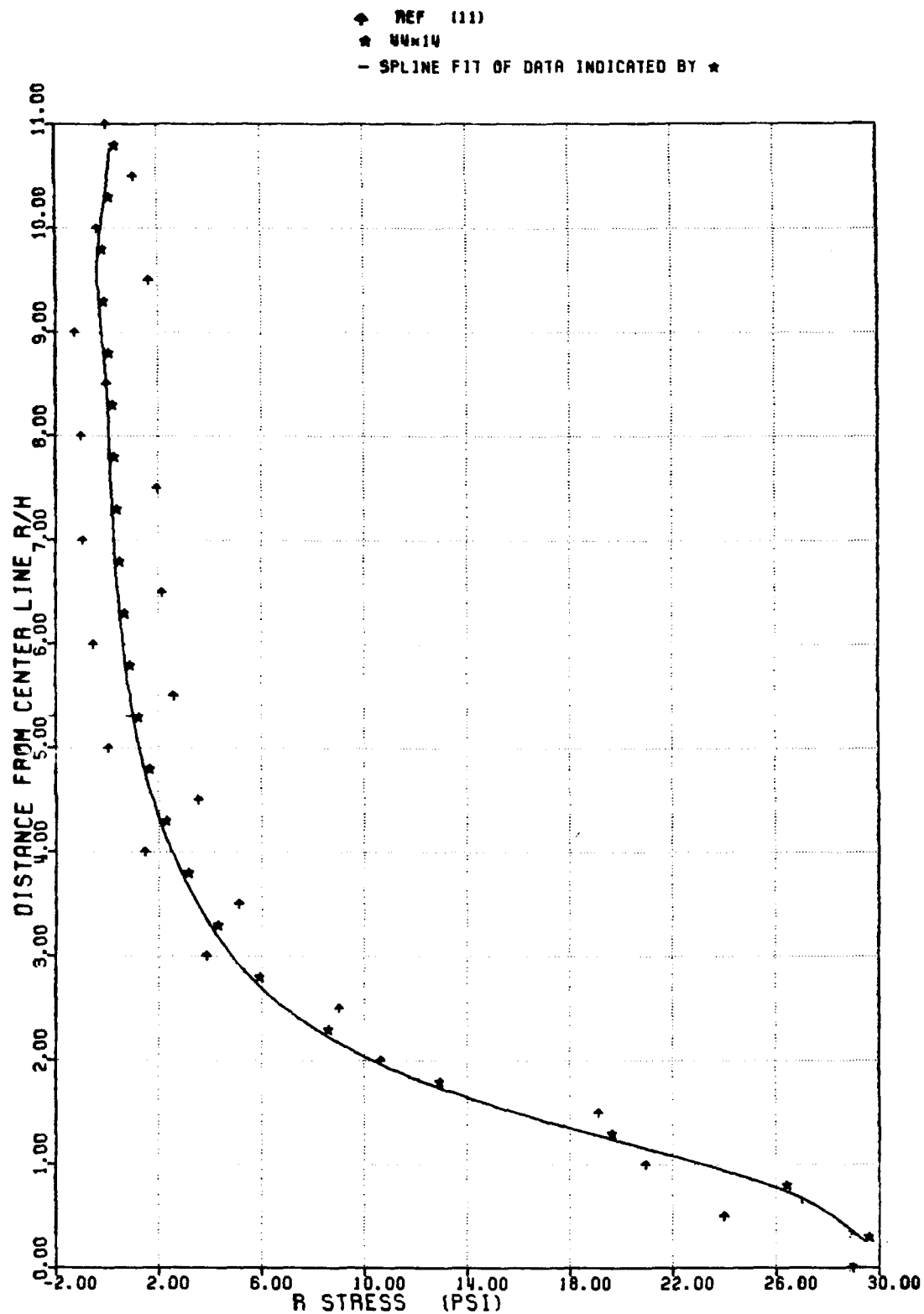
Figure 99: Effect of Mesh Refinement in R-Direction
on Through-Thickness Distribution of
R-Stress at Z/B = 0.995 of $[(25/-25)_5/90]_s$

143
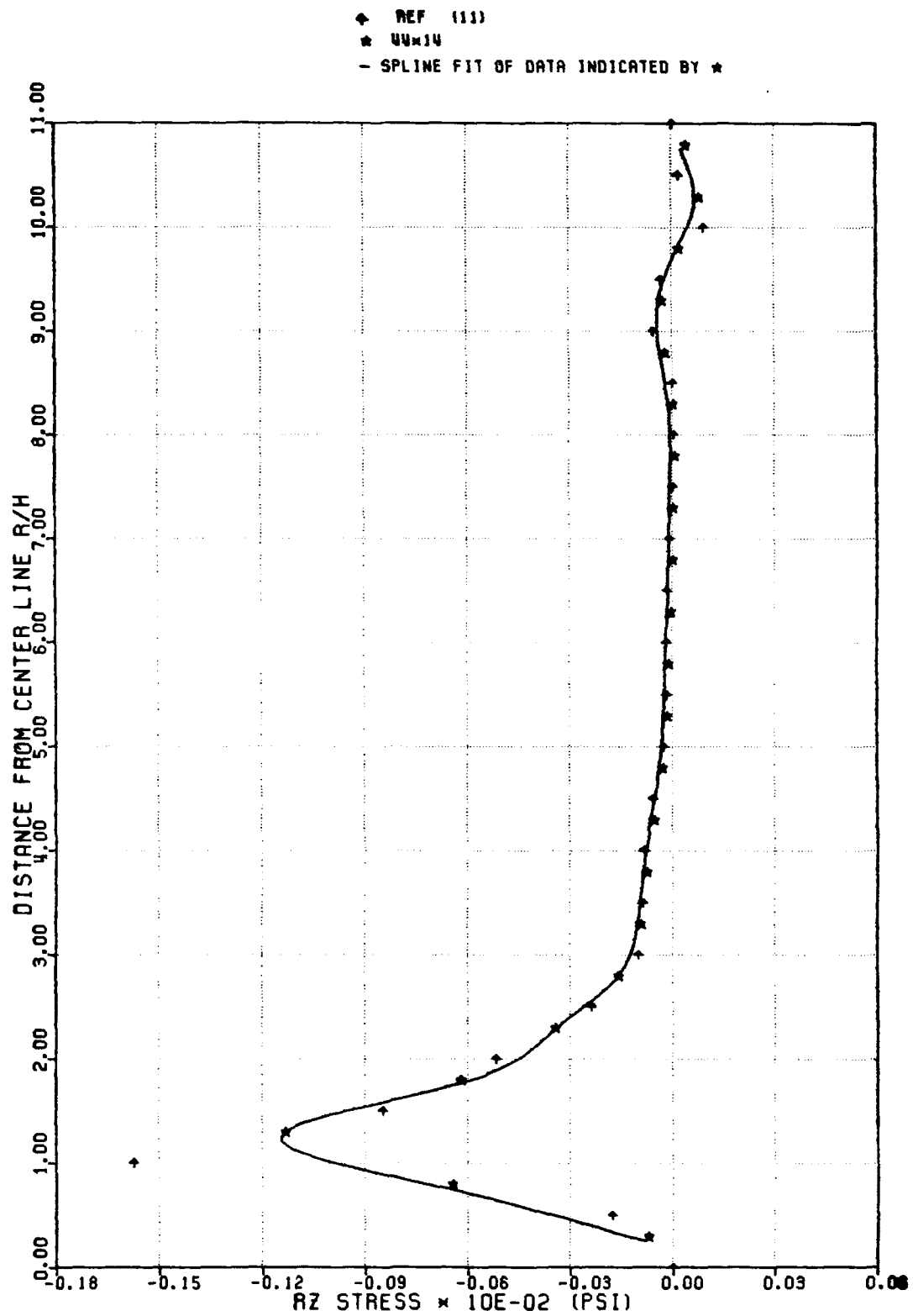
Figure 100: Effect of Mesh Refinement in R-Direction on Through-Thickness Distribution of RZ-Stress at Z/B = 0.995 of $[(25/-25)_5/90]_s$

144
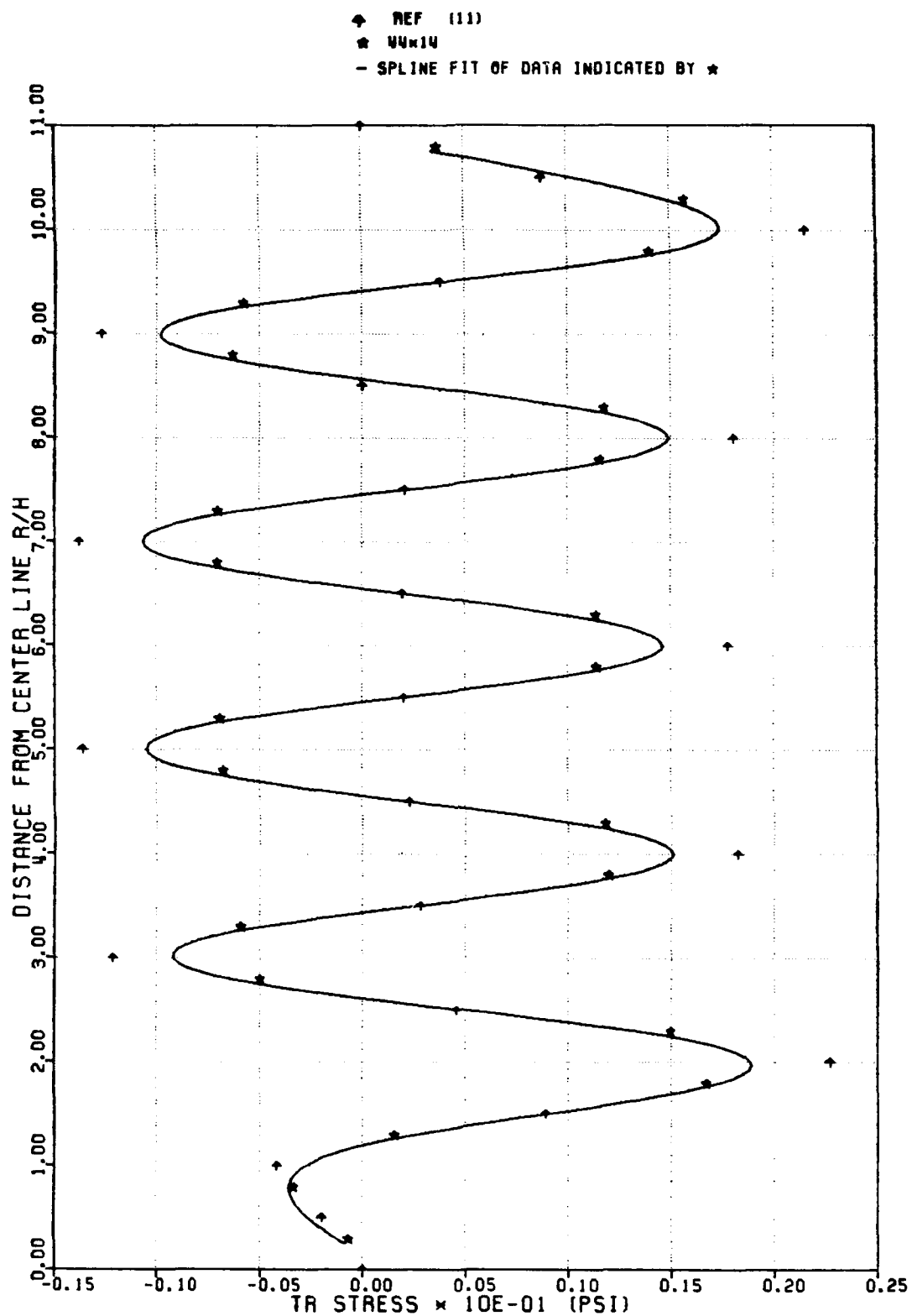
Figure 101: Effect of Mesh Refinement in R-Direction on Through-Thickness Distribution of TR-Stress at Z/B = 0.995 of $[(25/-25)_5/90]_s$

SECTION V

DISCUSSION

The problem of linear elastic stress analysis of a composite structure of axisymmetric geometry and loading has been investigated and computer programs developed based on finite element discretization using the modified bilinear quadrilateral elements with selectively reduced integration. Allowing for the tangential degree of freedom, the analysis is applicable to angle ply laminates. The axisymmetric analysis procedure can be used to model behavior of cross-ply as well as angle-ply coupons subjected to uniform axial strain. For a sufficiently large diameter, a ring specimen subjected to internal pressure is equivalent to an endless straight free edge coupon subjected to an essentially uniform inplane extension. Therefore, the main advantage of the ring specimen, compared with other finite element models, is that it is completely free of end constraints, thereby modeling the free edge delamination coupons somewhat better.

In the cross-ply laminate analysis, numerical results calculated from the axisymmetric stress analysis generally agreed well with the continuous traction Q23 element except near the free surface. This is because the continuous traction Q23 element allows traction-free boundary conditions to be specified in a pointwise sense while the present analysis does not. The study also revealed that the pattern of mesh refinement had significant effect on the estimate of the stress distribution in the vicinity of the free surface and the traction-free edge.

For the angle-ply laminate problem, a pseudo-three dimensional analysis specifying geometry and displacements as axisymmetric but including displacements in all three coordinates directions is necessary. Further, discretization of the full section is necessary for the analysis of angle-ply laminate since symmetry about the $Z = 0$ plane does not exist. Numerical results from the axisymmetric analysis agreed well with continuous traction Q23 element except near the free edge. Mesh refinement in the vicinity of the free edge indicated that the traction-free boundary condition was more closely approximated by the refined mesh. It was found that for a good estimate of the stress field, a mesh refined in the vicinity of the free edge as well as near the free surface should be used.

In the multi-ply laminate analysis, numerical results obtained using the pseudo-three dimensional axisymmetric analysis agreed well with the Q23 element solution except at the free edge and at the interfaces of the layers. A mesh refined in the vicinity of the free-edge and in the thickness direction had significant effect on the estimate of the stress field.

The computational procedure developed is efficient in terms of computation time for the analysis of axisymmetric composite structures with axisymmetric loading. In particular, for the free-edge delamination problem, the procedure is much less expensive than the continuous traction Q23 element [11]. For the same mesh of the four-ply laminate problem, the CPU time, on an IBM 3081 mainframe computer, using the present analysis was 25 seconds for the two-dimensional analysis (323 nodal points), and 4 minutes for the pseudo-three-dimensional analysis (629 nodal points) and full section discretization, as compared to 40 minutes using the continuous traction Q23 element (485 nodal points). For the 22-ply laminate problem, the CPU time using the present analysis was, respectively, 4 minutes 40 seconds, 9 minutes 41 seconds, 12 minutes and 31 minutes 45 seconds for a mesh corresponding to (22x14) (667 nodal points), (44x14) (1305 nodal points), (22x33) (1541 nodal points) and (44x33) (3015 nodal points) for half section

discretization. The CPU time using the continuous traction element was 45 minutes 38 seconds for a mesh of (14x22) (513 nodal points). The code is applicable to general axisymmetric laminated systems.

SECTION VI

REFERENCES

1. G. Isakson and A. Levy, 'Finite element analysis of interlaminar shear in fibrous composites,' J. Comp. Mat., Vol. 5, 273,1971.

2. A.S.D. Wang and F.W. Crossman, 'Some new results on edge effect in symmetric composite laminates,' J. Comp. Mat., Vol. 11, 92, 1977.

3. A.S.D. Wang and F.W. Crossman, 'Calculation of edge stresses in multilayer laminates by substructuring,' J. Comp. Mat., Vol. 12, 76, 1978.

4. C.W. Pryor, Jr. and R.M. Baker, 'A finite element analysis including transverse shear effects for application to laminated Plates,' AIAA J., Vol. 9, 12, 1971.

5. I.A. Raju, and J.H. Crews, 'Interlaminar stress singularities at a straight free edge in composite laminates,' Comp. and Struct., Vol. 14, No 1-2, 21, 1981.

6. R.M. Baker, F. Lin and J.R. Dana, 'Three-dimensional finite element analysis of laminated composites,' Comp. and Struct., Vol. 2, 1013, 1972.

7. E.F. Rybicki, 'Approximate three-dimensional solution for symmetric laminate under inplane loading,' J. Comp. Mat., Vol. 4, 354, 1971.

8. R.R. Riaao and A.A. Vicario, 'A finite element analysis of laminated anisotropic tubes,' J. Comp. Mat., Vol. 4, 344, 1970.

9. D.O. Stalnaker, R.H. Kennedy and J.L. Ford, 'Interlaminar shear strain in a two-ply balanced cord-rubber composite,' Experimental Mech., Vol. 20, 87, 1980.

10. H.P. Patel and R.H. Kennedy, 'Nonlinear finite element analysis for composite structures of axisymmetric geometry and loading,' Comp. and Struct., Vol. 15, 79, 1982.

11. C.C. Chang, <u>Finite element analysis of laminated composite free edge delamination specimens</u>, Ph.D. Dissertaion, Ohio State University, Columbus, Ohio, 1988.

12. J.R. Vinson and R.L. Sierakowski, <u>The behavior of structures composed of composite materials,</u> Martinus Nijhoff, 1986.

13. N.J. Pagano, 'Stress fields in composite laminates,' Int. J. Solids and Struct., Vol. 14, 385, 1978.

14. S. Timoshenko and J.N. Goodier, <u>Theory of Elasticity</u>, McGraw Hill, 1951.

15. R.S. Sandhu and K.S. Pister, 'A variational principle for linear coupled field problems in continuum mechanics,' Int. J. of Engrg. Sci., Vol. 8, 989, 1970.

16. R.S. Sandhu and K.S. Pister, 'A variational prininciple for boundary value and initial boundary problems in continuum mechanics,' Int. J. Solids and Struct., Vol. 7, 639, 1971.

17. R.S. Sandhu and U. Salaam, 'Variational formulation of linear problems with nonhomogeneous boundary conditions and internal discontinuities,' Comp. Meth. App. Mech. and Engrg., Vol. 7, 75, 1975.

18. U. Salaam and R.S. Sandhu, 'A finite element Galerkin formulation and its numerical performance,' Int. J. Numer. Methods. Engrg., Vol 10, 1077, 1976.

19. R.L. Taylor, E.L. Wilson and W.P. Doherty, 'Stress analysis of axisymmetric solids utilizing higher order quadrilateral finite element,' SESM Report 69-3, Dept. of Civil Engrg., University of California at Berkeley, Berkeley, California, 1969.